The Mechanism of Enzyme-catalyzed Ergothioneine Degradation

Inauguraldissertation

zur Erlangung der Würde eines Doktors der Philosophie
vorgelegt der
Philosophisch-Naturwissenschaftlichen Fakultät
der Universität Basel

von

Alice Maurer

aus Deutschland

Basel, 2020

Genehmigt von der Philosophisch-Naturwissenschaftlichen Fakultät

auf Antrag von

Prof. Dr. Florian Seebeck

Prof. Dr. Michael Müller

Basel, den 15.09.2020

Prof. Dr. Martin Spiess

Dekan der Philosophisch-Naturwissenschaftlichen Fakultät

Abstract

The sulfur containing histidine derivative ergothioneine is a ubiquitous natural product. Research on its biosynthesis and degradation can elucidate the complex biological and molecular function of this small molecular weight compound. The biosynthesis of ergothioneine is well established, yet little is known about its degradation. The first step of ergothioneine degradation is catalyzed by the enzyme ergothionase, which will be the focus of this thesis.

Ergothionase catalyzes the 1,2-elimination of trimethylamine from ergothioneine to yield thiourocanic acid. In this work, kinetic and structural investigations elucidate the mechanism of ergothionase. Based on the identification of catalytic residues, we are able to portray ergothionase producing organisms and found that they are mainly gut bacteria. This finding is in particular interesting because ergothioneine as food-additive is generally regarded as safe, whereas the ergothionase-mediated degrading of ergothioneine yields to trimethylamine, which is toxic.

Furthermore, we characterized two unknown lyases. One of these new lyases employs a similar mechanism as ergothionase but uses an oxidized substrate derivative. Whereas, the other new lyase catalyzes the elimination of trimethylamine from trimethylhistidine (TMH) and has distinctive differences in the active site compared to ergothionase. The function and position of the catalytic acid in the active site of TMH-lyase suggest a mechanistic variation of the thought to be well-known 4-methylideneimidazol-5-one (MIO) dependent aromatic amino acid lyases: maybe the posttranslational formed MIO-moiety does not only serve as electron sink but also as catalytic acid.

Studies on the phylogeny of ergothionase, TMH-lyase, aromatic amino acid lyase and the aspartase/fumarase superfamily propose that ergothionase has evolved prior to the aromatic amino acid lyases. The long evolutionary history of ergothionase underscores ergothioneine as ancient molecule. However, it is questioning that on the one hand an aromatic amino acid lyase represents the first step of the ubiquitous histidine degradation pathway, whereas on the other hand histidine builds the basis for ergothioneine biosynthesis. This finding might suggest the presence of an unknown alternative histidine degradation pathway.

In addition, we have not only studied the degradation but also the biosynthesis of ergothioneine. Thereby, we focused on the regulation of EgtD, the methyltransferase of ergothioneine biosynthesis, and showed that this enzyme is not subject of phosphorylation *in vitro*.

Table of Contents

Abbreviations

Abz	Aminobenzoic acid
AdoCbl	Adenosylcobalamin
ATP	Adenosine triphosphate
*Bp*ETL	Ergothioneine trimethylamine-lyase from *Burkholderia pseudomallei*
DMH	*N,N,*-α-Dimethylhistidine
DTT	Dithiothreitol
ESI-MS	Electrospray ionization mass spectroscopy
HAL	histidine ammonia-lyase
*Hd*Lyase	Trimethylhistidine trimethylamine-lyase from *Halomonas desiderata*
HEPES	4-(2-hydroxyethyl)-1-piperazineethanesulfonic acid
KIE	Substrate kinetic isotope effect
KSIE	Kinetic solvent isotope effect
LC-MS	Liquid chromatography coupled to mass spectroscopy
*Lt*Lyase	Trimethylhistidine trimethylamine-lyase from *Lihuaxuella thermophila*
*Me*Lyase	Ergothioneine sulfonic acid lyase from *Martelella endophytica*
MIO	4-methylideneimidazol-5-one
PAL	Phenylalanine ammonia-lyase
PDB	Protein data bank
PknD	Protein kinase D
PLP	Pyridoxal 5'-phophate
*Pp*HAL	Histidine ammonia-lyase from *Pseudomonas putida*
RMSD	Root-mean-square deviation
*Ro*Lyase	Trimethylhistidine trimethylamine-lyase from *Rhizobium oryzae*
SAH	*S*-Adenosyl homocysteine
SAM	*S*-Adenosyl methioneine
SDS	Sodium dodecyl sulfate
*Sm*EgtD	EgtD from *Mycobacterium smegmatis*
STPK	Serine/Threonine protein kinase
TAL	Tyrosine ammonia-lyase
*Tb*EgtD	EgtD from *Mycobacterium tuberculosis*
*Td*ETL	Ergothioneine trimethylamine-lyase from *Treponema denticola*
TMH	Trimethylhistidine
WT	Wild type

1 Introduction

More than 3 billion years ago, a single primordial cell embodied the origin for all organisms on earth.[1] Ever since, duplication and divergence of ancestral genes led to the evolution of novel enzymes. The variety of enzymes allowed organisms to adapt rapidly to changes in their environment. Accordingly, the enzymatic repertoire expanded all along and constituted the chemical basis of life. The progressive modification of enzymatic reactions led to a great diversity of functionality, structural folds and mechanisms. This diversity will be described in detail in the next section on the example of ammonia-lyase. The numerous solutions that Nature found to catalyze carbon-nitrogen bond cleavage underscore the fundamental role that these lyases play in biology.

1.1 Diversity of Ammonia-Lyases

Ammonia-lyases are functionally related enzymes that catalyze the reversible cleavage of carbon-nitrogen bonds.[2] The numerical classification scheme for enzymes categorizes ammonia-lyases as EC 4.3.1.X. While ammonia-lyases are functionally related proteins, many members of this enzyme class are structurally unrelated (Figure 1). Even structurally related lyases may not be mechanistically related, as will be highlighted throughout this thesis. Functionally related enzymes are expected to employ a common mechanism for catalysis, yet the deceptively simple deamination reaction catalyzed by the ammonia-lyases proceeds with an immense diversity of mechanisms.[3] The extensive mechanistic diversity observed for the relatively straightforward deamination reaction is remarkable. The following sections will provide an overview of this structurally and mechanistically diverse family.

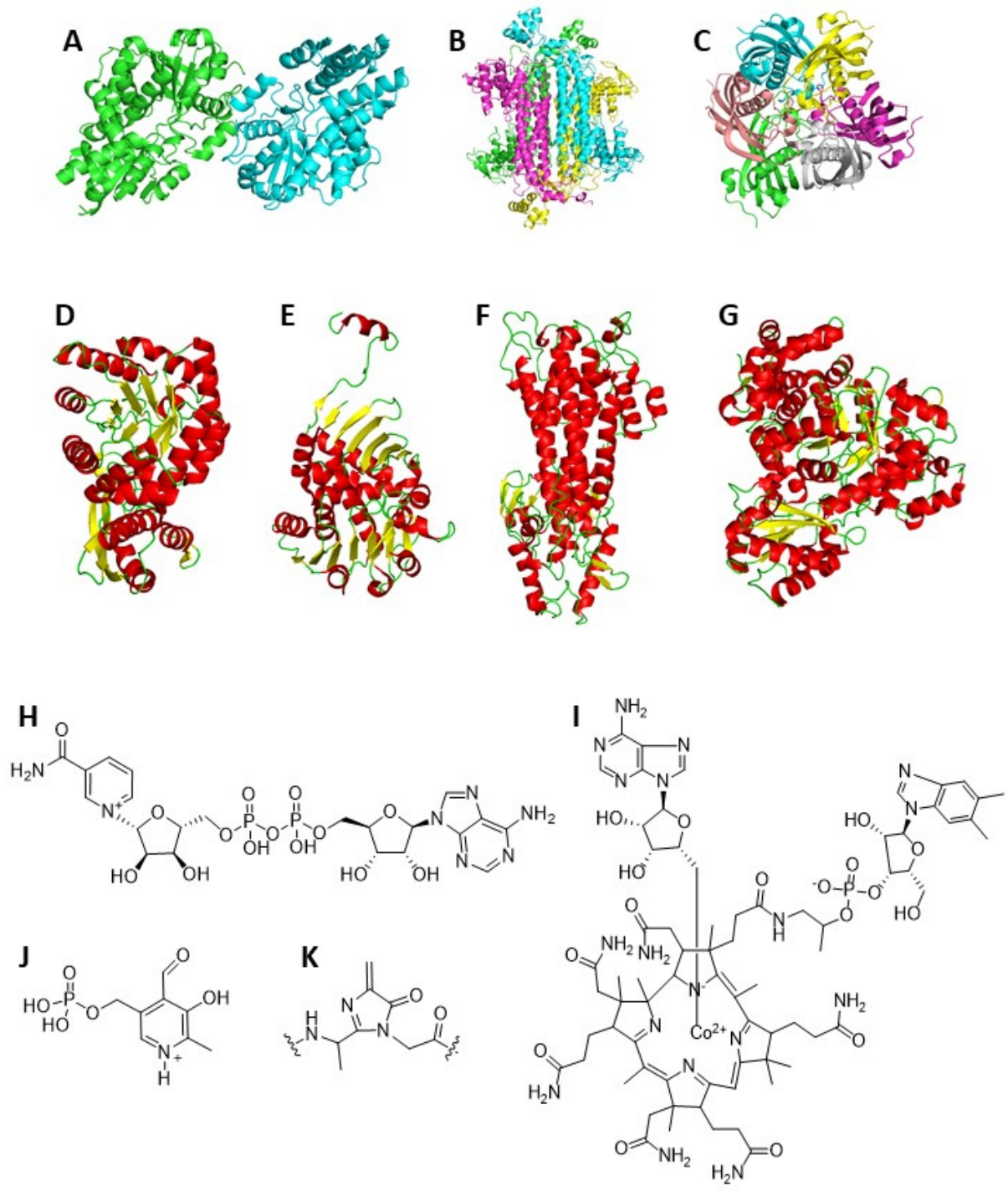

Figure 1. Diversity of quaternary structures (A – C), protein fold (D – G), and cofactors (H – K) of ammonia-lyases. A: dimer of diaminopropionate ammonia-lyase (PDB: 4D9K). B: tetramer of aspartase (PDB: 1JSW). C: hexamer of β-alanyl-CoA ammonia-lyase (PDB: 4MZQ). D: TIM-barrel fold of a subunit of methylaspartase (PDB: 1KKO). E: Rossmann fold of a subunit of ornithine cyclodeaminase (PDB: 1U7H). F: helix bundle of a subunit of histidine ammonia-lyase (PDB: 1B8F). G: functional subunit of ethanolamine ammonia-lyase (PDB: 3ABO). H: Cofactor NAD^+ of cyclodeaminase. I: adenosylcobalamine of ethanolamine ammonia-lyase. J: pyridoxal 5'-phophate of diaminopropionate ammonia-lyase. K: 4-methylideneimidazol-5-one of aromatic amino acid ammonia-lyase.

1.1.1 Aspartase/Fumarase Superfamily

The most common ammonia-lyases are part of the aspartase/fumarase superfamily. The aspartase/fumarase superfamily represents a class of C-N/ C-O lyases with a common reaction mechanism and a characteristic tertiary fold and quaternary structure.[4] The sequence identity within superfamily members is low (15%), however their members share three highly conserved regions in their amino acid sequence.[5] The best studied members of the superfamily besides aspartase (EC 4.3.1.1) and fumarase (EC 4.2.1.2) are argininosuccinate lyase with δ-crystallin (EC 4.3.2.1) and adenylosuccinat lyase (EC 4.3.2.2). In the following, we will focus on the highly specific enzymes aspartase and fumarase.

Aspartases catalyze the reversible deamination of L-aspartic acid to fumarate (Figure 2).[6] Considering the physiological function, aspartase plays an important role in microbial nitrogen metabolism. The amino acid degradation enzyme is involved in controlling the nitrogen flux of the organism.[7]

Fumarases catalyze the reversible dehydration of L-malate to form fumarate (Figure 2). The fumarase family can be classified into two types: the class-I and class-II fumarases.[8] Class-I fumarases are iron-dependent dimeric proteins, whereas class-II members are part of the aspartase/fumarase superfamily. Here, we will focus on class-II fumaraes. Fumarases are ubiquitous proteins that are conserved from prokaryotes to humans and play an important part in the tricarboxylic acid cycle.[9] The tricarboxylic acid cycle is the major energy-yielding metabolic pathway for all aerobic organisms. The ubiquity of this pathway and the importance of the protein fumarase within this pathway shows that fumarases might be the common ancestor of lyases and thus play a crucial role in evolution.

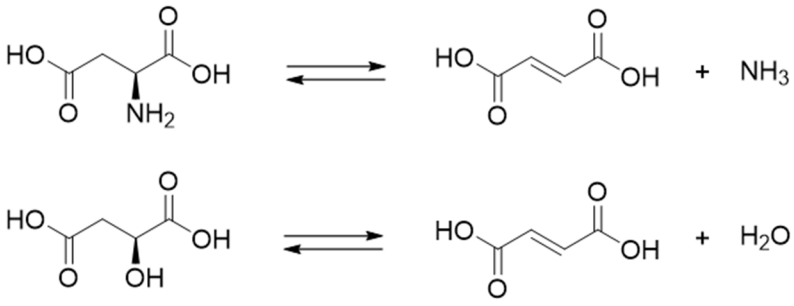

Figure 2. Reversible deamination of L-aspartic acid to fumarate catalyzed by aspartate ammonia-lyases (top) and reversible dehydration of L-malate to fumarate catalyzed by fumarase (below).

Both aspartase and fumarase catalyze the reversible *anti*-1,2-addition-elimination reaction in a common mechanism, which has been elucidated based on crystallographic and kinetic studies.[4] The proteins of the superfamily are homo-tetramers with each subunit consisting of mainly alpha-helical

domains (Figure 1).[10,11] Each protein possesses four identical active sites located at the interface of three subunits. Based on pH-rate profiles, an acid-base dependent $E1_{cb}$ mechanism was suggested (Figure 3).[12] A general base mediates the removal of the *pro-R* proton from the β-position of the substrate L-malate (in the case of fumarase) or L-aspartic acid (in the case of aspartase). Abstraction of the β-proton is facilitated by binding-induced distortion of the geometry of the substrate to resemble a sp^2 hybridization.[13] The catalytic base that performs this abstraction is located on a highly flexible loop that undergoes conformational changes upon substrate binding and catalysis.[14] It was suggested that an oxyanion species on a serine residue acts as a base. After proton abstraction, the resulting carbanion is stabilized as *aci*-carboxylate; the transition state analogue 2-amino-3-nitro-propionate is a potent inhibitor, which provided strong evidence for formation of the carbanion intermediate.[15] The substrate itself can function as electron-sink and a conserved lysine residue stabilizes the *aci*-carboxylate-like formation.[13] Subsequent ketonization of the carboxylate-intermediate implements cleavage of the C-O bond (in the case of fumarase) or the C-N bond (in the case of aspartase). In aspartase a significant isotope effect was observed with ^{15}N-substituted substrate, corroborating that cleavage of the C-N bond is the rate-determining step in this enzyme.[16] This cleavage of the C-N bond, or C-O bond in fumarases, can be facilitated by the presence of a catalytic acid that donates a proton to the leaving group. In aspartase, a histidine residue within the active site has been suspected to be the catalytic acid,[11] however this residue is not fully conserved in all aspartases.[17] Thus, it remains questionable whether the leaving group in aspartase is the ammonium ion or free ammonia.[18] In contrast, in fumarases the catalytic acid histidine, which forms a charge relay with a conserved glutamate residue, is essential to generate the H_2O leaving group.[4,19]

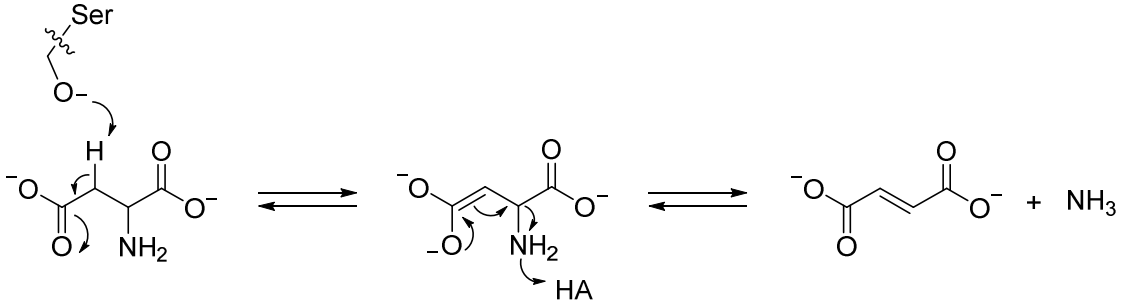

Figure 3. Proposed mechanism of aspartase. The requirement of the catalytic acid is not fully elucidated yet.

1.1.2 Methylaspartate Ammonia-Lyase

In contrast to the aspartase/fumarase superfamily, the methylaspartate ammonia-lyase requires a divalent cation for their activity. Methylaspartate ammonia-lyase (EC 4.3.1.2) catalyzes the reversible deamination of (2*S*,3*S*)-*threo*-3-methylaspartate to mesaconic acid (Figure 4). Methylaspartase activity

was first detected in 1959 in the anaerobic bacterium *Clostridium tetanomorphum*.[20] This enzyme is part of the mesaconate pathway for anaerobic glutamate degradation to yield acetyl-coenzyme A (acetyl-CoA).[21] Methylaspartate ammonia-lyase was also found to be important in haloarchaea.[22] Accordingly, a new biosynthetic pathway to oxidize acetyl-CoA to glyoxylate was proposed with methylaspartate ammonia-lyase appearing to be a key enzyme in this pathway.

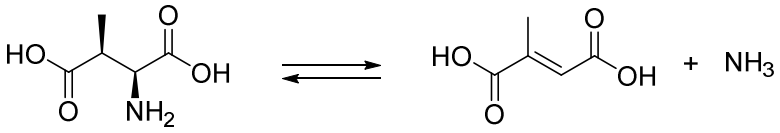

Figure 4. Reaction catalyzed by 3-methylaspartate ammonia-lyase (MAL). Reversible deamination of (2*S*,3*S*)-*threo*-3-methyylaspartate to mesaconic acid.

Methylaspartate ammonia-lyase was first purified and characterized in 1992 and was suggested to represent a new class of enzyme without any convincing homology to any other lyases known at this point.[23] The solved crystal structures and kinetic studies revealed that the structural and mechanistic features resembles the enolase superfamily.[24,25] Methylaspartate ammonia-lyase is a homo-dimeric protein with a characteristic TIM barrel fold and β-strands wrapping around the barrel (Figure 1). This is a significant structural difference to the aspartase/fumarase superfamily. Furthermore, Mg^{2+} and K^{+} cations are crucial for methylaspartase activity.[23]

The β-proton of the substrate is abstracted by a catalytic base (Figure 5). Considering the catalytic base, it is important to mention that methylaspartate ammonia-lyase is not diastereoselective; not only the *anti*-deamination, but also the *syn*-deamination is catalyzed.[26] Hence, there are two different residues acting as catalytic base.[27] A lysine residue acts as catalytic base for the major *anti*-elimination reaction, whereas a histidine residue acts as a base for the minor *syn*-elimination. If this histidine residue is mutated to alanine, the enzyme gets diastereoselective.[27] After proton abstraction, the resulting ene-diolate is stabilized by the divalent Mg^{2+} cation (Figure 5).[24,25] Mg^{2+} assisted binding of the *aci*-carboxylate intermediate causes a lower pK_a of the β-proton. Finally, the enolate intermediate collapses and ammonia is released to form the product mesaconate.

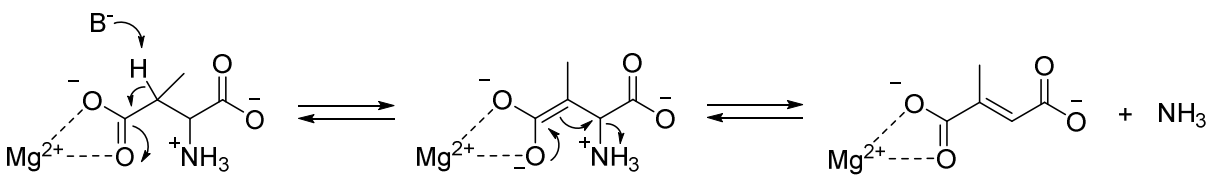

Figure 5. Proposed mechanism of methylaspartate ammonia-lyase.

1.1.3 Aminoacyl-CoA Ammonia-Lyase

Aminoacyl-CoA ammonia-lyase is not dependent on divalent cations. Instead, this enzyme requires the electron-withdrawing capacity of the thioester linkage of substrates that are conjugated to CoA.

The enzyme β-alanyl-CoA ammonia-lyase (EC 4.3.1.6) catalyzes the reversible deamination reaction of β-alanine-CoA to yield acrylyl-CoA and ammonia (Figure 6).[28] Degradation of β-alanine by activation of the CoA-thioester and subsequent deamination was found in the anaerobic bacterium *Clostridium propionicum*. There are two genes to express β-alanyl-CoA ammonia-lyase; one is constitutively expressed to obtain low basal activity, whereas the other is induced at high β-alanine concentrations.[29] The excessive protein production plays a secondary role in binding acrylyl-CoA, and thus avoids the toxicity of this strong nucleophilic compound.

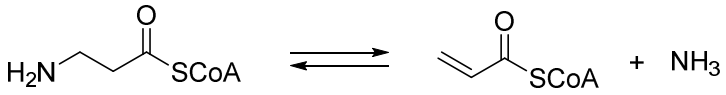

Figure 6. Reaction catalyzed by β-alanyl-CoA ammonia-lyase. Reversible deamination of β-alanine-CoA to acrylyl-CoA.

The protein β-alanyl-CoA ammonia-lyase consists of five stranded anti-parallel β-sheets and a long α-helix, a so-called "hot-dog fold".[30] The active site is located at the interface of two subunits. Three of these functional dimers are combined to give a homo-hexamer (Figure 1). Interestingly, the protein structure does not show similarities to other lyases that catalyze similar reactions, yet the protein entails high structural similarity to acyl-CoA thioesterase. The crystal structure of β-alanyl-CoA ammonia-lyase revealed a tyrosine residue as the likely proton acceptor of the α-methylene proton (Figure 7). Acidity of the proton is increased through the electron withdrawing of the thioester linkage. The resulting enolate is stabilized by the dipole of the α-helix that facilitates the initial proton abstraction. After the retro-Michael elimination the ammonia is protonated by a side-chain threonine residue. However, further experiments are required to provide further evidence for this proposed mechanism.[30]

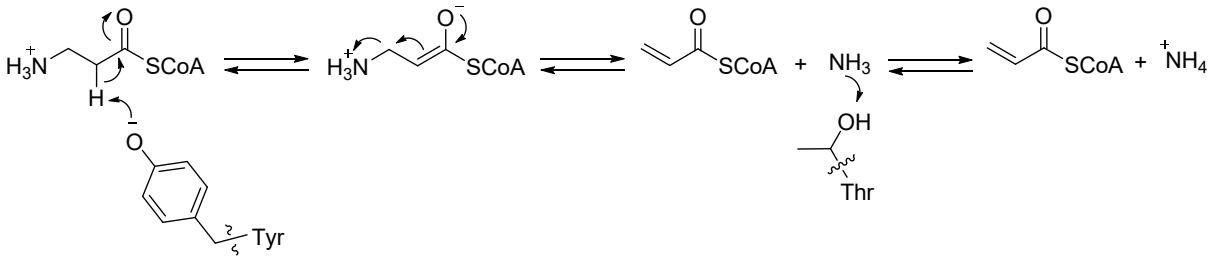

Figure 7. Proposed mechanism of β-alanyl-CoA ammonia-lyase.

The enzyme 3-aminobutyryl-CoA ammonia-lyase (EC 4.3.1.14), first identified in *Clostridium subterminale*, catalyzes the reversible deamination of 3-aminobutyryl-CoA to produce crotonyl-CoA and ammonia (Figure 8).[31] 3-Aminobutyryl-CoA ammonia-lyase is part of lysine fermentation to acetate, butyrate and ammonia in anaerobic bacteria. Based on the discovery of 3-aminobutyryl-CoA ammonia-lyase in *Brevibacterium,* it is postulated that this enzyme is similar to β-alanyl-CoA ammonia-lyase.[32] However, no mechanistic studies have been reported yet.

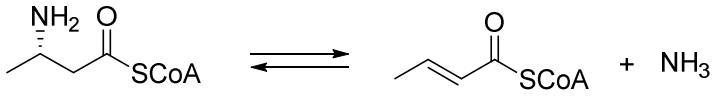

Figure 8. Reaction catalyzed by 3-aminobutyryl-CoA ammonia-lyase. Reversible deamination of 3-aminobutyryl-CoA to crotonyl-CoA.

1.1.4 Hydroxy Amino Acid Dehydratase/Deaminase

In contrast to the other presented lyases, the members of the hydroxy amino acid dehydratase/deaminase family are pyridoxal 5'-phophate (PLP) dependent enzymes.[5] One representative of the hydroxy amino acid dehydratase/deaminase family is the enzyme diaminopropionate ammonia-lyase (EC 4.3.1.15) which catalyzes the α,β-elimination reaction of both L- and D-diaminoproionate to form pyruvate and ammonia (Figure 9).[33] Other representative enzymes catalyzing the dehydratase/deaminase reaction through a similar PLP-dependent mechanism are D- (EC 4.3.1.18), and L-serine ammonia-lyase (EC 4.3.1.17), L-threonine ammonia-lyase (EC 4.3.1.19), D-glucosaminate ammonia-lyase (EC 4.3.1.9), *threo*-3-hydroxy-L-aspartate ammonia-lyase (EC 4.3.1.16), *erythro*-3-hydroxy-L-aspartate ammonia-lyase (EC 4.3.1.20), *threo*-3-hydroxy-D-aspartate ammonia-lyase (EC 4.3.1.27), carbamoyl-serine ammonia-lyase (EC 3.4.1.13).[2,5]

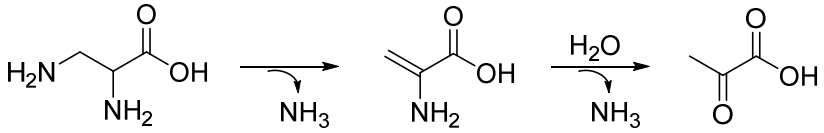

Figure 9. Reaction catalyzed by diaminopropionate ammonia-lyase. Diaminopropionate is degraded via aminoacrylate to give pyruvate.

Diaminopropionate ammonia-lyase is the first PLP dependent enzyme found to catalyze the elimination of an amino group at the β-position of the substrate.[33] Most substrates of the other representative enzymes of this PLP-dependent lyase family possess a hydroxyl-group at the β-

position.[5] Therefore, it is more convenient to name this family as dehydratase/deaminase, instead of lyase. The diaminopropionate degrading enzyme is prokaryotic and has not been reported to exist in eukaryotes.[34] Beside conversion of both the D- and L- isoform of diaminopropionate, the enzyme possesses a narrow substrate specificity.[34,35]

The crystal structure of diaminopropionate ammonia-lyase of *Escherichia coli* revealed a dimeric protein with one active site in each of the two protomers (Figure 1).[36] Each protomer consists of a large and a small domain with a β-sheet core surrounded by α-helices. PLP is bound at the interface between the large and the small domain through a lysine residue that anchors the PLP as a Schiff-base using its ε-amino group. Upon substrate binding, the neutral α-amino group of diaminopropionate forms the external aldimine with PLP while the lysine residue is released (Figure 10). For the proceeding step, two different residues are suggested as base for each enantiomer: the lysine residue acts as catalytic base for the L-isoform of the substrate, whereas an aspartate residue acts as catalytic base for the D-enantiomer. Abstraction of the α-proton of the substrate leads to the release of the β-amino group. Formation of the PLP-aminoacrylate intermediate is then followed by the approach of the lysine residue towards C4 of PLP, whereby aminoacrylate is released. Finally, aminoacrylate undergoes a spontaneous, non-enzymatic hydrolysis to form pyruvate and ammonia.

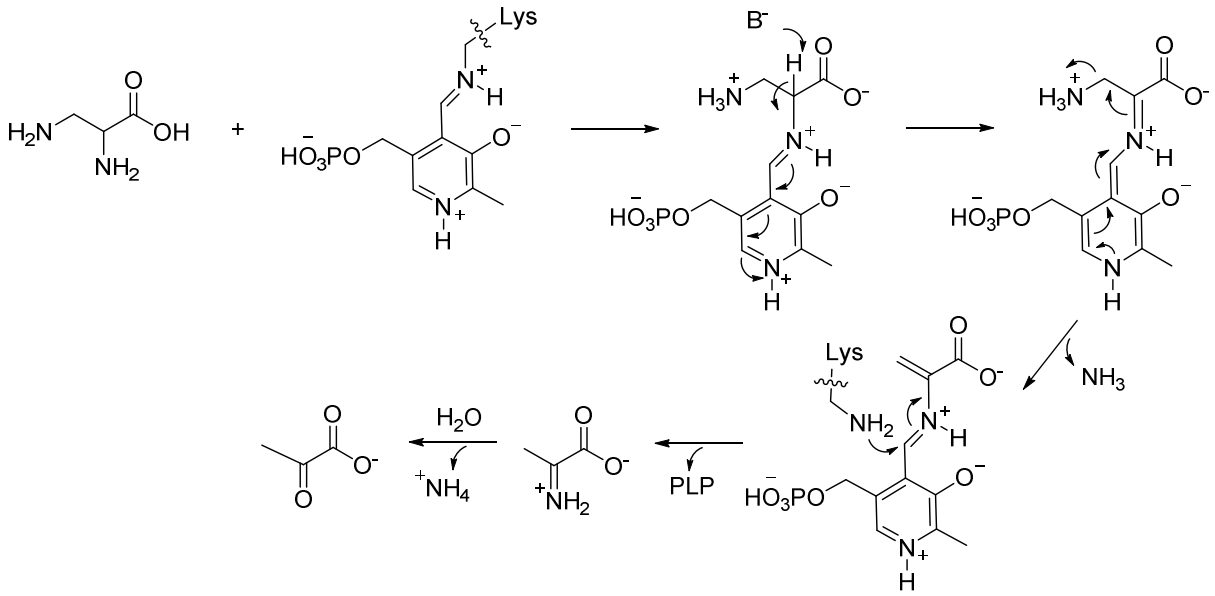

Figure 10. Proposed mechanism of diaminopropionate ammonia-lyase.

The crystal structure of diaminopropionate ammonia-lyase from *E. coli* revealed a disulfide bond close to the active site, which is suggested to be important for stabilizing a channel that regulates the entry to the active site.[36] However, the disulfide bond is absent in the crystal structure of *Salmonella*

typhimurium diaminopropionate ammonia-lyase.[37] In contrast, the structure of the lyase of *S. typhimurium* possesses a phosphate ion in the active site at a position corresponding to the aminoacrylate intermediate. Therefore, it is proposed that monovalent metal ions enhance the catalytic rate of *S. typhimurium* diaminopropionate ammonia-lyase by chelating the phosphate ion.

In prokaryotes, diaminopropionate interferes with enzymes involved in amino acid metabolism, causing growth inhibition.[38] Thus, degradation of diaminopropionate via diaminopropionate ammonia-lyase is highly important to prevent its toxicity.

1.1.5 Ethanolamine Ammonia-Lyase

The only ammonia-lyase that utilizes a hydrogen radical abstraction mechanism is responsible for the fermentation of ethanolamine.[39][40] The first enzyme of the ethanolamine degradative pathway of bacteria is ethanolamine ammonia-lyase (EC 4.3.1.7), which reversibly converts ethanolamine into acetaldehyde and ammonia (Figure 11). Catalysis involving hydrogen radical abstraction is unusual and completely unrelated to other ammonia-lyases mechanisms and requires the cofactor adenosylcobalamine (AdoCbl) (Figure 1). This naturally occurring organo-metallic compound contains a unique Co-C bond and represents a classical cofactor for enzymatic radical reactions.[41]

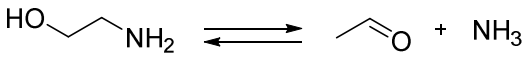

Figure 11. Reaction catalyzed by ethanolamine ammonia-lyase. Ethanolamine is converted to give acetaldehyde and ammonia.

The crystal structure of ethanolamine ammonia-lyase of *Escherichia coli* revealed that the enzyme is a hexamer and each of the six functional subunits comprises a α- and β-subunit and AdoCbl cofactor (Figure 1).[42] The α-subunit is folded into a TIM-barrel structure and the β-subunit partially covers the AdoCbl that is bound in the interface of both subunits. The tight interaction through hydrogen bonds and van der Waals contacts between enzyme and the cobalamin-binding site and the adenine ring-binding site causes tensile forces that lead to an enzyme-induced homolysis of the Co-C bond. This results in cob(II)alamin and a 5'-deoxyadenosyl radical (Figure 12). The 5'-deoxyadenosyl radical removes a hydrogen atom from the C2 position of the substrate and thus generates the initial substrate radical.[43] This is followed by migration of the amine from the C1 to the C2 position of the substrate. The resulting hemiaminal radical abstracts a hydrogen atom of the 5'-deoxyadenosyl radical. Finally, the hydrolytically unstable hemiaminal decomposes to form the products acetaldehyde and ammonia.

The products leave the active site of the enzyme through displacement by water molecules.[42] However, it is not known if the substrate binds as neutral or protonated form, which might also change during the reaction.

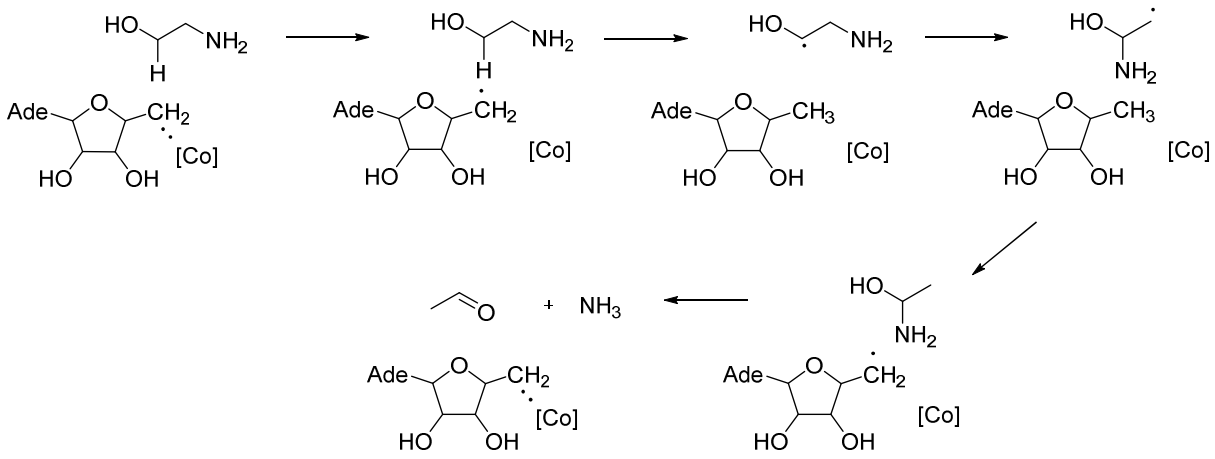

Figure 12. Proposed mechanism of ethanolamine ammonia-lyase.

The presented ethanolamine ammonia-lyase is the first enzyme of the degradative pathway of ethanolamine.[39] The acetaldehyde produced by the lyase is further used for acetyl-CoA formation, which is utilized in many metabolic processes.[44] The ethanolamine catabolism is used by a variety of bacteria in the intestine of mammals. Phosphatidylethanolamine is a phospholipid in the gut which is important for proper gut functioning. The bacterial breakdown of phosphatidylethanolamine might cause disease linked to disrupting gut functions.[44]

1.1.6 Amino Acid Cyclodeaminase

Amino acid cyclodeaminases are NAD^+ dependent, which is a unique feature among the family of lyases.[3] L-Ornithine cyclodeaminase (EC 4.3.1.12) is the first identified amino acid cyclodeaminase.[45] This enzyme produces L-proline and ammonia (Figure 13). Another cyclodeaminase, namely L-lysine cyclodeaminase (EC 4.3.1.28), forms L-pipecolic acid was only found in 1998 (Figure 13).[46] Both cyclodeaminases resemble oxidoreductases, however the overall reaction consists of both a reduction and oxidation. Thus, the whole process is redox neutral and the cofactor NAD^+ is recycled to its original oxidation state through the reaction cycle. Therefore, the classification as lyase, rather than oxidoreductase is appropriate.[5]

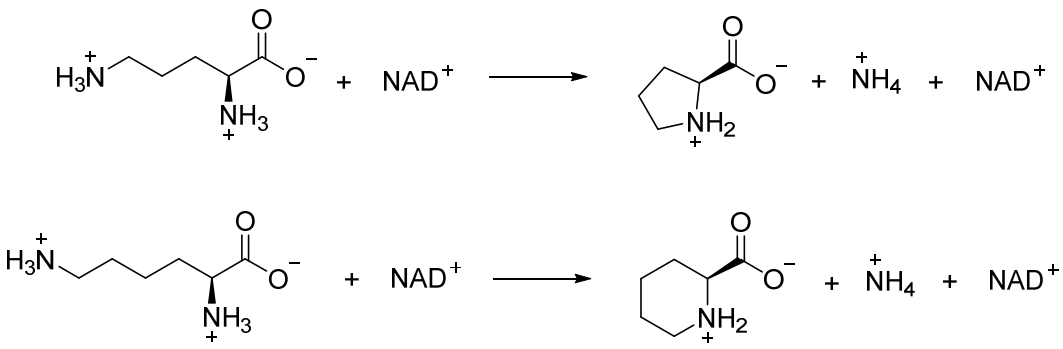

Figure 13. Reaction catalyzed by ornithine cyclodeaminase (top) and lysine cyclodeaminase (below).

The crystal structure of ornithine cyclodeaminase of *Pseudomonas putida* comprises a homodimeric fold of two functional subunits.[47] Each subunit possesses a cofactor binding domain and a substrate binding domain. The substrate binding site consists of a 14 stranded β-barrel after oligomerization. The cofactor binding domain is located in a Rossmann fold with six parallel β-strands and helices as crossover elements (Figure 1). Thus, two NAD^+ molecules are bound within the dimer.

The first investigation into the mechanism for ornithine cyclodeaminase proposed a deamination of the α-amino group of lysine prior to cyclization and finally reduction to form proline.[48] However, based on the crystal structure an alternative mechanism is now favored (Figure 14).[47] Goodman et *al*. proposed a hydride transfer from the C2 position of the substrate to NAD^+ supported by an active site aspartate residue. This dehydrogenation results in formation of an imine intermediate. Subsequently, the δ-amine gets deprotonated and attacks the C2 position, leading to the ring closure and formation of the α-amino proline intermediate. Finally, elimination of ammonia is followed by hydride transfer from NADH back to the electrophilic C2 position to form the product proline.

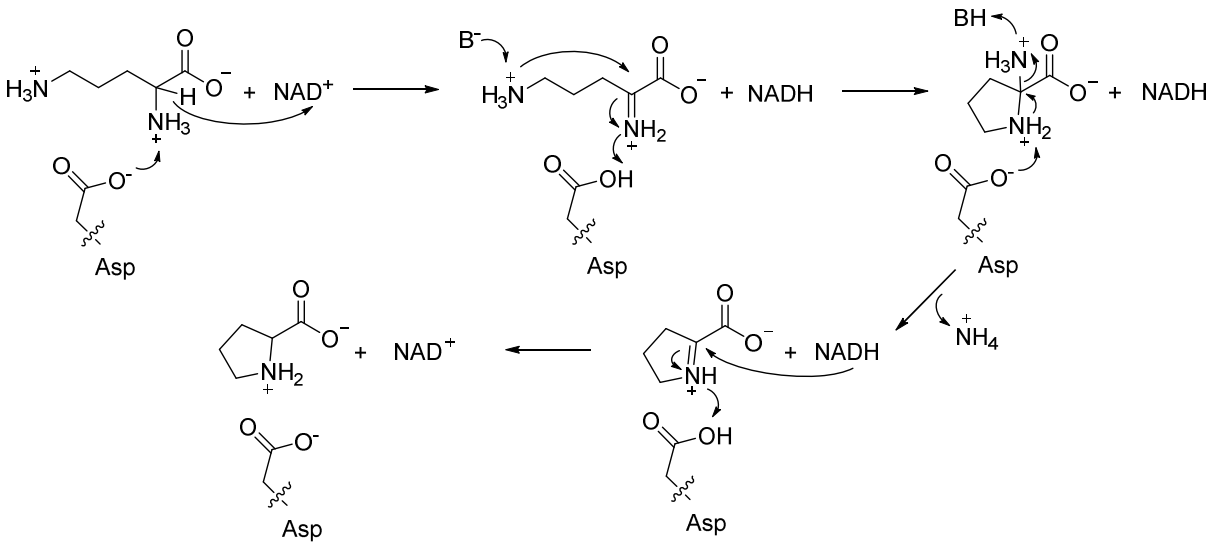

Figure 14. Proposed mechanism of ornithine cyclodeaminase.

Lysine cyclodeaminase shows strong sequence homology to ornithine cyclodeaminase.[49] *In vitro* characterization of lysine cyclodeaminase with isotopically labeled substrate showed the loss of the α-amine throughout the reaction. Based on the crystal structure of lysine cyclodeaminase of *Streptomyces pristinaespiralis* it is presumed that both cyclodeaminases act by a similar mechanism.[50]

1.1.7 Aromatic Amino Acid Ammonia-Lyase

Aromatic amino acid ammonia-lyases catalyze the reversible elimination of ammonia from the amino acids histidine (histidine ammonia-lyase, HAL, EC 4.3.1.3), tyrosine (tyrosine ammonia-lyase, TAL, EC 4.3.1.23) or phenylalanine (phenylalanine ammonia-lyase, PAL, EC 4.3.1.24) to form the corresponding α-β unsaturated acids (Figure 15).[51] So far, the existence of a tryptophan ammonia-lyase has not been confirmed.[52] The PAL-mediated reaction occurs mainly in plants and fungi, whereas in animals and most bacteria phenylalanine reacts via a PLP-dependent transaminase reaction to the corresponding 2-keto acid phenylpyruvate.[53] PAL activity serves a biosynthetic purpose as it represents the first step in the phenylpropanoid pathway. Thereby, the α-β unsaturated cinnamic acid is the precursor for lignin and flavonoid biosynthesis. Similar to PAL activity, TAL activity and the corresponding product *p*-coumaric acid is involved in the phenylpropanoid pathway. HAL activity gives urocanate, a component that protects the skin from UV radiation.[54] The involvement of HAL in the histidine degradation pathway will be described in detail in section 1.3.

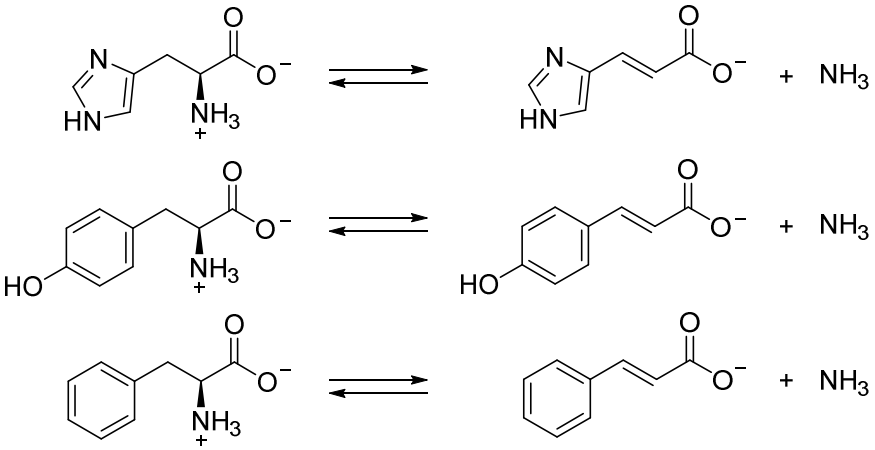

Figure 15. Reaction catalyzed by histidine ammonia-lyase, HAL (top), tyrosine ammonia-lyase, TAL (middle), phenylalanine ammonia-lyase, PAL (below).

The overall structure of HAL, PAL and TAL is a homo-tetramer composed of multiple parallel α-helices (Figure 1).[55–57] The enzymes possess four identical active sites, each built of residues from three different subunits.

In order to catalyze the elimination reaction, aromatic amino acid ammonia-lyases have to abstract the non-acidic proton at the β-position of the substrate (pK_a 40)[58], while the hydrogen at the α-amino group must remain untouched to maintain leaving-group abilities.[59] To manage this challenge, these enzymes possess a highly conserved structural feature. Early studies suggested the presence of an electrophilic dehydroalanine within the active site that acts as a Michael-acceptor.[60] However, the first crystal structure of HAL from *Pseudomonas putida* revealed the presence of the five-membered heterocycle 4-methylideneimidazol-5-one (MIO).[57] The MIO-moiety is formed posttranslational and autocatalytically by cyclization and double dehydration of the active site tripeptide Ala-Ser-Gly (Figure 16). In some cases, alanine is replaced by threonine, serine or cysteine residues.[59,61] The tripeptide is highly conserved among the class of aromatic amino acid ammonia-lyases and is essential for their activity.

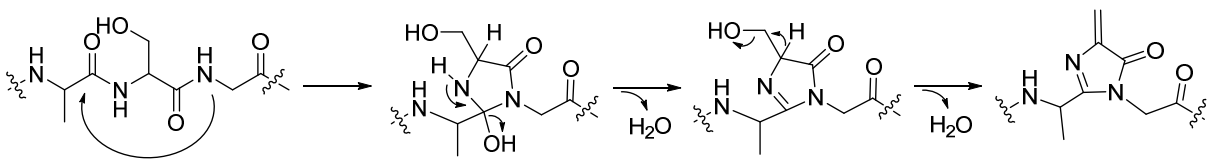

Figure 16. Formation of the 4-methylideneimidazol-5-one (MIO) moiety from the tripeptide Ala-Ser-Gly.

Two reaction mechanisms for these MIO-dependent enzymes have been suggested: a Friedel-Craft-type mechanism[62] and a MIO-adduct mechanism[63].

The Friedel-Craft type mechanism suggests addition of the aromatic side chain of the substrate to the electrophilic alkene of the MIO-group (Figure 17).[64] In this mechanistic proposal the main function of the MIO-group is acidification of the β-protons through electrophilic activation in their close vicinity.

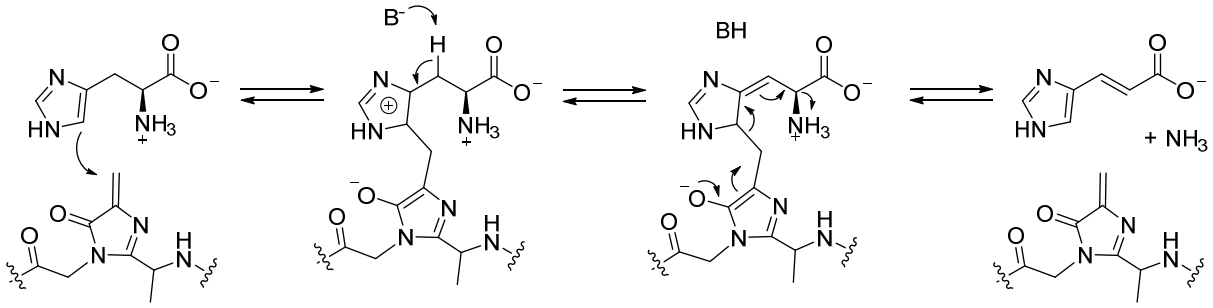

Figure 17. Proposed Friedel-Craft type mechanism of aromatic amino acid ammonia-lyase.

The MIO-adduct mechanism relies on the formation of a covalent adduct between the amino group of the substrate and the exocyclic alkene of the MIO-group (Figure 18).[51,63] It is proposed that the formation of a secondary ammonium ion increases its leaving-group abilities.[63,65] A highly conserved tyrosine residue, which is located on a flexible loop covering the active site, acts as essential enzymatic base and abstracts the β-proton of the substrate.[66]The resulting carbanion intermediate can be stabilized by the dipole of the α-helices that point with their positive end towards the active site.[55] Upon loss of the MIO-NH_2 leaving group, the product is released.

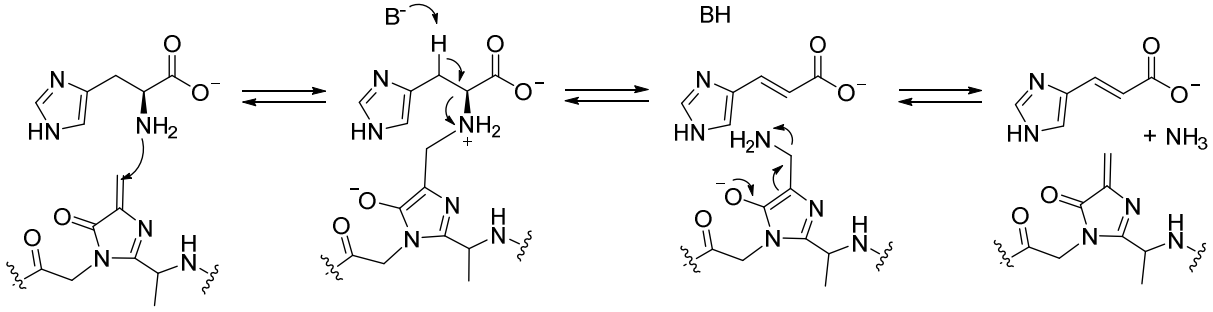

Figure 18. Proposed MIO-adduct mechanism of aromatic amino acid ammonia-lyase.

Nowadays, the MIO-adduct mechanism is generally preferred: The structure of a TAL variant with bound inhibitor 2-aminoindan-2-phosphonate showed a covalent bond between the amino group of

the ligand to the methylidene carbon of the MIO-moeity of the enzyme.[56] Additionally, docking studies of a PAL structure and theoretical studies with HAL further supports the MIO-adduct mechanism.[67][68] Detailed conseredations of the crystal structures of related aminomutases also favored this mechanistic pathway.[66,69] Molecular mechanistic calculations rouled out the Friedel-Craft type mechanism due to the high energy of the reaction intermediates.[70] However, the difficulty of deprotonating a benzylic methylene proton is not fully resolved by the MIO-adduct mechanism.[51]

1.2 Application in Biocatalysis of Ammonia-Lyases

The described mechanistic and structural diversity of ammonia-lyases provides opportunities for their use in a variety of different applications. Particularly, the formation of chiral amino acids from olefinic acids and ammonia is very difficult to accomplish non-enzymatically. Some ammonia-lyases are of high value for industrial application as will be outlined in the following.

Aspartase. The earliest success for industrial application of an ammonia-lyase was achieved by aspartase. The high specificity and activity of the enzyme was useful for the industrial preparation of L-aspartic acid.[71] The enantiopure compound is required for the synthesis of artificial dipeptide sweeteners and as a building block for pharmaceuticals.[72] Aspartase can further be used for enantioselective synthesis of labeled L-aspartic acid. However, due to the high specificity of aspartase and the complex flexibility of the loop covering the active site, the synthesis of substituted aspartic acid derivatives remains difficult.[73] Molecular engineering of aspartase is needed to shape the active site in order to accommodate different substrates.[74] On the contrary, the narrow substrate range of aspartase can be advantageous for multi-enzymatic cascades.[75] Aspartase can be added to reaction cascades with ammonia as byproduct. The enzyme utilizes ammonia to catalyze its reaction, and thus can shift the equilibria of the reaction cascade towards the product site.

Methylaspartate ammonia-lyase. In contrast to aspartase, methylaspartate ammonia-lyase does not undergo large conformational changes upon substrate binding resulting in a broad substrate tolerance.[76] That makes the enzyme in particular interesting as a biocatalyst for generating building blocks for chemical synthesis. The high activity of methylaspartate ammonia-lyase on non-natural substrates has long been established.[77] However, only the finding of a diastereoselective methylaspartase mutant paved the way for further investigations into the asymmetric synthesis of 3-substituted aspartic acid derivatives.[27] Redesigning of the active site of methylaspartase extended the range of accessible aspartic acid derivatives.[78] Two distinct single-point mutations exhibit a wide substrate scope for either electrophilic fumarate derivatives or nucleophilic non-native amines.

Aminoacyl-CoA ammonia-lyase. In theory, usage of aminoacyl-CoA ammonia-lyase might be useful for the production of small β-amino acids since the enzyme tolerates different substrate derivatives.[29] However, application for large scale production is unlikely due to the difficulty to access CoA derivatives as substrates.[5]

Diaminopropionate ammonia-lyase. The enzyme diaminopropionate ammonia-lyase is responsible for degradation of the toxic compound diaminopropionate.[33] The seeds of the drought resistant legume *Lathyrus sativus* contain 2,3-dioxalyl diaminopropionate, which leads to toxicity when large quantities are consumed.[79] Engineering transgenic plants that overexpress diaminopropionate ammonia-lyase might reduce the content of toxine in seeds. However, this engineering idea has not been realized so far and there is no other known application to date.

Ethanolamine ammonia-lyase. To date, no alternative substrates for this enzyme has been found. Additionally, the usage of the cofactor AdoCbl further complicates the usage of this enzyme; thus, possible applications remain limited.[5]

Amino acid cyclodeaminases. Both ornithine and lysine cyclodeaminase are highly enantioselective and efficient enzymes and therefore interesting as biocatalysts for the industrial production of L-proline and L-pipecolic acid.[47][50] An engineered strain of *E. coli* achieved an efficient fermentative overproduction of L-pipecolic acid from glucose.[80] In addition, a directed evolution approach opened ways to broaden the substrate specificity of lysine cyclodeaminase to catalyze cyclodeamination of alternative molecules.[81] The resulting derivatives of substituted pipecolic acid are interesting precursor molecules for the pharmaceutical industry. A great benefit for industrial applications is that NAD^+ is reconverted throughout the reaction. Therefore, there is no need to continually supply the cofactor during synthesis.

Aromatic amino acid ammonia-lyase. The reversibility of the deamination/amination reaction of aromatic amino acid ammonia-lyases enables the production of enantiopure L-amino acids from the inexpensive aryl acrylic acid substrates.[5] A high concentration of ammonia can shift the equilibrium of the reaction to favor amination. The first industrial application of PAL was patented 1976 for L-phenylalanine production. Beside direct production of the L-enantiomer, aromatic amino acid ammonia-lyase can also be used for enantiopure synthesis of the D-enantiomer.[82,83] After chemical racemic amination, the enzyme selectively deaminates the L-product, and thus only the D-product remains. Immobilization of arylalanine ammonia-lyase further improved enzyme stability and catalytic efficiency, which is advantageous for industrial biocatalysis application.[84] The broad substrate tolerance known today for PAL provides access to a sustainable synthesis of non-natural amino acid derivatives, even if amination with any other nitrogen nucleophiles remains unsuccessful. A PAL variant

was found with increased activity for *p*-bromo cinnamic acid, that enables a broad spectrum of further chemical reactions, which is of great interest for the chemical industry.[85] One example for an application of green chemistry is the chemoenzymatic cascade to produce *S*-2-indolinecarboxylic acid, a precursor of the antihypertensive indolapril.[86] Thereby, PAL-mediated amination of a cinnamic acid derivative is followed by cupper catalyzed cyclization, without the usage of an organic solvent. A completely different application of TAL and PAL is the introduction of the phenylpropanoid pathway into *Saccharomyces cerevisiae* for *in vivo* production of secondary metabolites.[87] Since 2017, pegylated PAL is a FDA-approved enzyme substitution therapy for the treatment of phenylketonuria, a genetic inborn disorder, leading to accumulation of phenylalanine.[88]

1.3 Histidine Degradation

The aromatic amino acid ammonia-lyase HAL presents the first step in the histidine degradation pathway. Degradation of histidine results in glutamate, ammonia and a one-carbon compound, either formamide or formate (Figure 19).[89] Genes for proteins participating in the histidine utilization pathway are encoded in the *hut* operon. The hut-system is a ubiquitous and highly conserved pathway.

The degradation of most amino acids starts with the conversion to the corresponding keto-acids catalyzed by a PLP-dependent transaminase. In contrast, the first step in histidine degradation is non-oxidative elimination of the α-amino group catalyzed by HAL. As outlined in section 1.1.7, HAL contains the posttranslational formed electrophilic MIO-moiety, which is crucial for activity. HAL is a highly conserved protein, with bacterial and mammalian representatives sharing >40% sequence identity, indicating that HAL is presumably the oldest MIO-containing lyase.[90] In the second step of the hut-pathway, the α-β unsaturated product urocanate is hydrated by the NAD^+ dependent urocanase (Figure 19).[91,92] In this reaction, NAD^+ serves as electrophile that gets attacked by the imidazole of the substrate. After addition of water to the covalent adduct, the product hydroxy-imidazolepropionate tautomerizes to generate imidazolonepropionate. Subsequently, the third step of the hut-pathway is ring cleavage by a hydrolase to form *S*-formiminoglutamate (Figure 19). Even if imidazolonepropionate is unstable, the enzymatic cleavage is essential in order to use histidine as carbon source.[93] Furthermore, it has been shown that hydrolase-deficiency leads to poisoning, indicating that regulation of the hut-pathway is essential.[94]

These first three steps of the histidine utilization pathway are similar for all genera, whereas the following removal of the formimino-group follows three different pathways (Figure 19).[89] One pathway (A) leads to formation of formamide and glutamate in a one-step-reaction, mainly occurring

in enteric bacteria in which formamide is excreted as the waste product. The other pathway (B), mainly occurring in *Pseudomonas*, possesses two enzymes. First, a zinc-dependent deiminase catalyzed reaction to yield formylglutamate and ammonia, followed by hydrolysis to formate and glutamate.[60] Thus, the second pathway gives a second molecule of ammonia from each molecule of histidine. In mammals (C), the formimino-group is transferred to tetrahydrofolate (FH_4).[53]

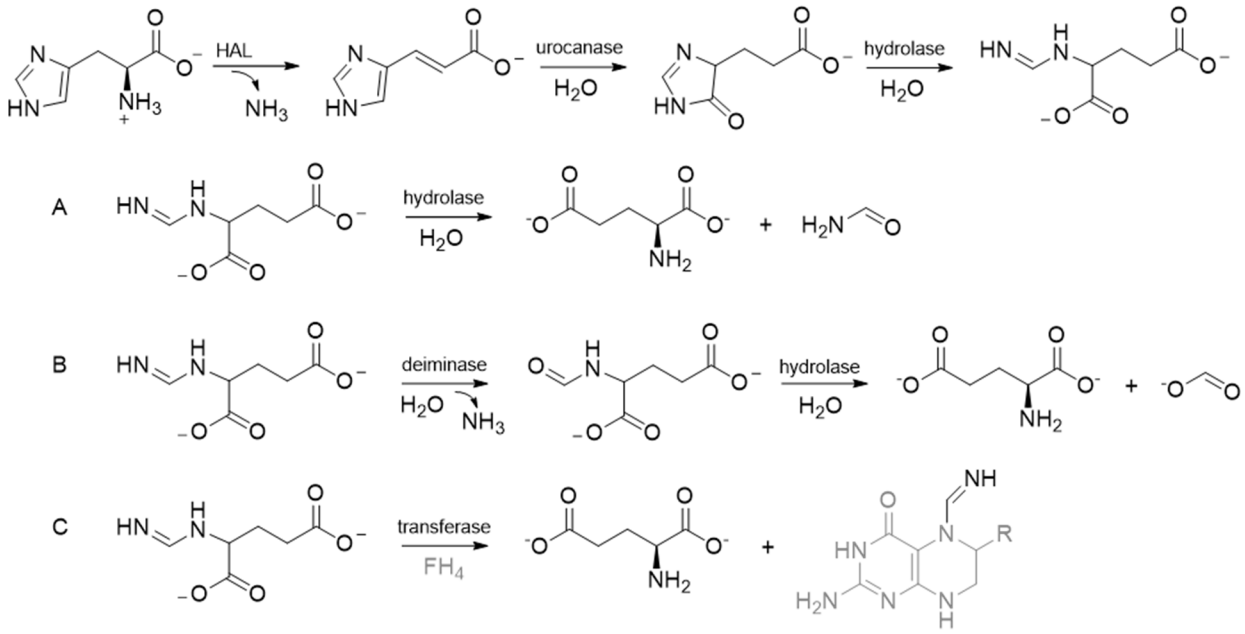

Figure 19. Histidine degradation pathway. The first three steps are universal. A occurs mainly in enteric bacteria, B occurs mainly in *Pseudomonas* and C occurs in mammals.

Due to the high energy cost of histidine synthesis, tight regulation of its degradation is essential.[89] Therefore, induction of the hut-system should be avoided if the available amount of histidine is needed for protein synthesis. The expression for the genes of the hut-operon is in most organisms induced by urocanate, the product of the HAL reaction.[95] Regulation of gene expression by the first pathway intermediate guarantees that the hut-system is only activated when enough histidine is available to lead to an accumulation of urocanate. As histidine can serve as a carbon and ammonia source, *hut* expression is repressed if a better carbon source such as glucose or an excess of ammonia is available.[96] In contrast, nitrogen limitation activates *hut* expression.[97]

The strong conservation of the involved enzymes, the genetic clustering of the hut-operon and its ubiquity among different organisms suggests that the presented histidine degradation pathway has a long evolutionary history.[89]

1.4 Ergothioneine

Ergothioneine is a trimethylated thiourea derivative of histidine (Figure 20). In 1909, the small molecular weight thiol was isolated from the ergot fungus.[98] At physiological conditions, the thione-thiol tautomere exists predominantly in its thione form, which helps to prevent autooxidation.[99]

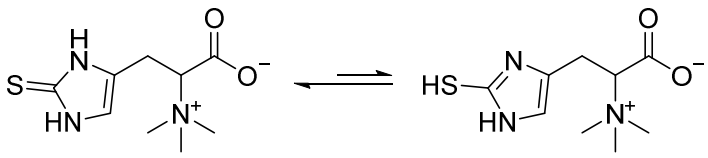

Figure 20. Tautomerization of ergothioneine.

The redox potential of ergothioneine, -60 mV, is comparable high.[100] Other small molecular weight thiols such as glutathione or mycothiole possess redox potentials of -200 to -320 mV (SHE).[101] It has been shown that ergothioneine is an effective scavenger for reactive oxidative species *in vitro*.[102,103] There are numerous *in vitro* studies about the excellent antioxidant properties of ergothioneine, however solid *in vivo* studies are rare.[104] Strictly anaerobic organisms are able to biosynthesize ergothioneine, indicating that the function of ergothioneine is likely not limited to antioxidative properties.[105] This finding was further indispensable as it shows that emergence of ergothioneine might predate the rise of atmospheric oxygen 2.4 billion years ago. The coupling of ergothioneine to mycothiol has been reported to play an important role in the biosynthesis of the antibiotic lincomycin.[106] Furthermore, several bacterial species have been found to live on ergothioneine as their sole source of nitrogen.[107] These bacterial species are able to degrade ergothioneine to thiourocanic acid and trimethylamine. The enzyme ergothionase that catalyzes the degradation reaction will be the focus of this thesis.

A wide range of living organisms like microorganisms, fungi, plants, animals and even the human body contain levels of ergothioneine.[108] However, only certain bacteria and fungi are able to biosynthesize ergothioneine.[109,110] For humans, dietary goods like mushrooms or beans are the major ergothioneine source.[111] A specific transporter (OCTN-1) is responsible for ergothioneine uptake in the cells.[112] The presence of the specific ergothioneine transporter implies that ergothioneine must have a useful function in mammals. Animals with OCTN-1 knockout are more susceptible for oxidative stress,[113] furthermore, the *octn-1* gene is associated with rheumatoid arthritis,[114] and Crohns disease.[115] Ergothioneine is stated to be a potential treatment for diseases like neurodegenerative disease, cardiovascular disease, diabetes or cancer.[116] In the case of tissue injury, it has been hypothesized that supplementation with ergothioneine might be beneficial.[108] Furthermore, it has been suggested

that ergothioneine can even be considered as a vitamin.[117] However, health benefits of the consumption of large amounts of ergothioneine are questionable, as will become apparent throughout this thesis.

We can conclude that the exact physiological role of ergothioneine is not completely understood yet. However, the ubiquity of ergothioneine among all kingdoms of life suggests an important function. Investigation of the degradation of ergothioneine and investigation on the regulatory mechanism of ergothioneine biosynthesis can contribute to gain a deeper understanding of this unique compound.

1.4.1 Biosynthesis of Ergothioneine

The biosynthesis of ergothioneine has been subject to research for over half a century. In 1956, Genghof *et al*. showed the synthesis of ergothioneine in fungi for the first time.[110] Later, ergothioneine biosynthesis was shown in cell-free extracts from *Neurospora crassa*.[118–120] In 2010, the discovery of a five-gene cluster in *mycobacteria*, called *egtABCDE*, paved the way for the biochemical understanding of ergothioneine biosynthesis.[121] The first step in the biosynthesis of ergothioneine is trimethylation of the α-amino group of histidine (Figure 21). All three SAM-dependent methylation reactions are catalyzed by one enzyme, namely EgtD. EgtA is a ligase responsible for adenosine triphosphate (ATP)-dependent dipeptide formation of cysteine and glutamate to produce γ-glutamyl cysteine. Subsequently, TMH and γ-glutamyl cysteine are substrates for the iron-dependent sulfoxide synthase EgtB. The glutamyl moiety is cleaved off by EgtC and finally the pyridoxal-phosphate dependent β-lyase EgtE forms the product ergothioneine. Identification of the biosynthetic gene cluster in *Mycobacterium smegmatis* provides the basis for the discovery of alternative biosynthetic pathways of this unique compound.

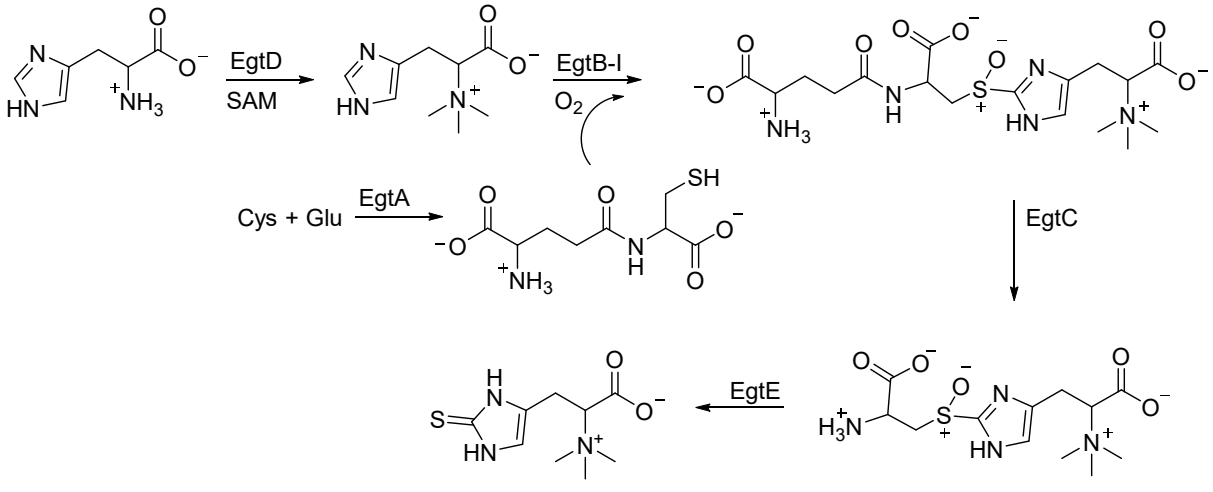

Figure 21. Ergothioneine biosynthetic pathway in mycobacteria.

This five-gene pathway appears to be limited to the phylum of actinobacteria.[122] However, it was shown that other bacteria like *Burkholderia spp*. or *Chloracidobacterium thermophilum* are also able to synthesize ergothioneine.[123,124] The main difference is that EgtB does not utilize γ-glutamyl cysteine as shown before. Instead, EgtB uses cysteine as sulfur donor for the oxygen dependent C-S bond formation at the C2-position of TMH (Figure 22). Therefore, EgtA and EgtC are not required here, shortening ergothioneine synthesis to a three step process in these organisms.

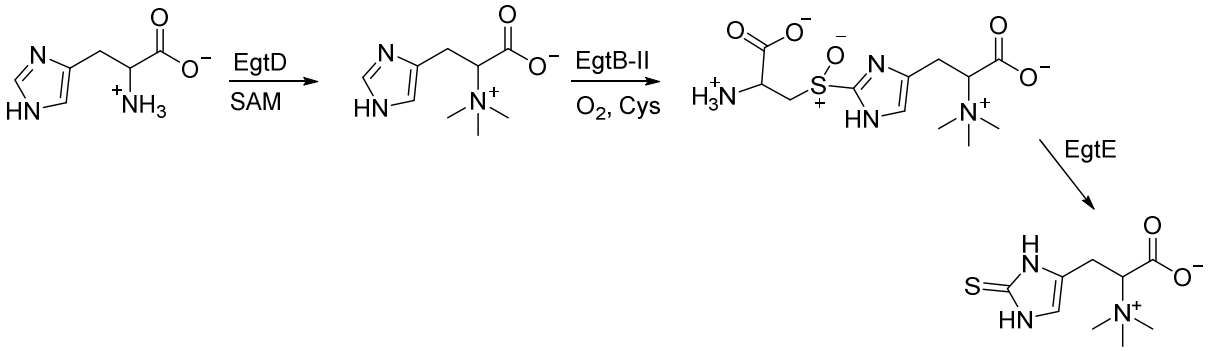

Figure 22. Ergothioneine biosynthetic pathway in bacteria like *Burkholderia spp.* or *Chloracidobacterium thermophilum*.

Fungal ergothioneine biosynthesis also utilises cysteine as the sulfur donor.[125] The fungus *Neurospora crassa* possesses a fusion of EgtD-like and EgtB-like enzyme, called Egt-1, that combines trimethylation of histidine and subsequent C-S bond formation with cysteine (Figure 23). The second enzyme of the biosynthetic pathway, Egt-2, is a PLP-dependent C-S lyase catalyzing the final step of ergothioneine biosynthesis. A similar two-step pathway has also been reported for the fission yeast *Schizosaccharomyces pombe.*[126]

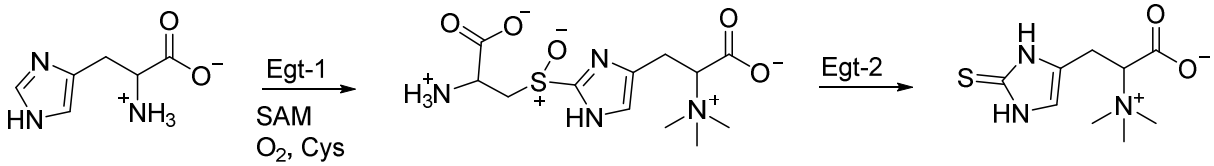

Figure 23. Ergothioneine biosynthetic pathway in fungi.

In addition to these oxygen-dependent biosynthetic pathways, anaerobic ergothioneine biosynthesis has recently been found (Figure 24).[105] The anaerobic green sulfur bacterium *Chlorobium limicola* encodes for an EgtD-like SAM-dependent methyltransferase, EanA, which produces TMH from histidine. EanA is co-encoded with EanB, a rhodanese-like sulfur transferase. EanB contains an active

site cysteine in the persulfide state that acts as a nucleophile and attacks the C2-position of the imidazolium of TMH for anaerobic C-S bond formation.[127]

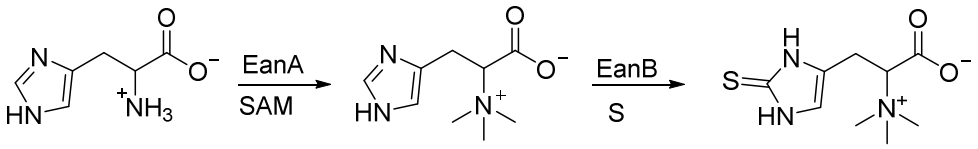

Figure 24. Anaerobic ergothioneine biosynthetic pathway.

Thorough structural and biochemical characterization of the enzymes involved in the three different routes for ergothioneine biosynthesis suggests that ergothioneine biosynthesis may have evolved several times independently throughout history.[128] The ubiquity of these enzymes underscores the physiological importance of this thiol-containing compound in Nature.[129]

1.4.2 Degradation of Ergothioneine

As described above, the molecular and biochemical description of ergothioneine biosynthesis led to substantial achievements. In contrast, little is known about ergothioneine degradation. The existence of the enzyme ergothionase has been reported to be responsible for cleavage of the trimethylamine group of ergothioneine, resulting in the unsaturated thiourocanic acid (Figure 25). In 1957, disappearance of ergothioneine and emergence of thiourocanic acid was first shown in *Alcaligenes faecalis*.[130] In the early 1960's, ergothionase activity was demonstrated in cell-free experiments.[107,131] Identification of the gene coding for ergothionase allowed a first characterization of the recombinant produced and purified enzyme.[132] In this thesis, we describe extensive kinetic studies and the first structural characterization of an ergothionase, which provide a substantial insight into the enzymatic mechanism.[133]

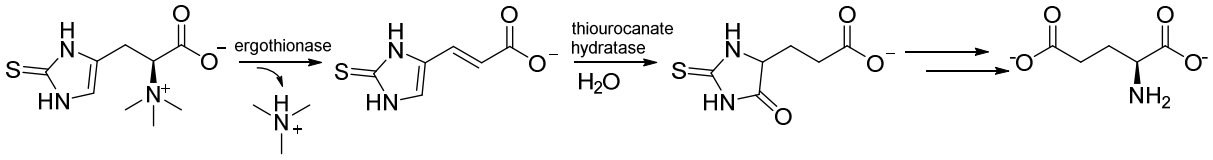

Figure 25. Proposed catabolism of ergothioneine.

In the next step of the ergothioneine degradation pathway, the enzyme thiourocanate hydratase transforms thiourocanic acid to 3-(5-oxo-2-thioxoimidazolidin-4-yl) propionic acid (Figure 25).[134] The

similarity of these first two steps in ergothioneine degradation to the histidine utilization pathway is striking, suggesting that the product 3-(5-oxo-2-thioxoimidazolidin-4-yl) propionic acid is also further metabolized to glutamic acid.[134]

2 Aim of this Thesis

Ergothioneine is ubiquitous amongst Nature and appears to be an important molecule. The consumption of ergothioneine is generally regarded as safe, however, the molecular mechanism of action of this low-molecular weight thiol is not fully elucidated. One approach to understand its role in biology is to explore the biochemistry of its degradation. The goal of this thesis is to elucidate the mechanism of the ergothioneine degradation enzyme ergothionase. Identification of catalytic residues will then allow classification of ergothionase producing organisms. Furthermore, a previously unknown TMH-lyase will be characterized. The suggested mechanism of this lyase will shed new light on the mechanism of the well-known MIO-dependent aromatic amino acid lyases. Finally, the comparison of ergothionase and TMH-lyase to MIO-dependent lyases and the aspartase/fumarase superfamily will provide the basis for the ancestral reconstruction of these lyases.

3 The Mechanism of Ergothionase

Ergothionase (EC 4.3.1.) is a lyase responsible for the degradation of ergothioneine to thiourocanic acid and trimethylamine.[107] The enzyme cleaves both the β-C-H and the α-C-N bonds of the substrate resulting in the formation of the α-β unsaturated product thiourocanic acid and the leaving group trimethylamine (Figure 26).

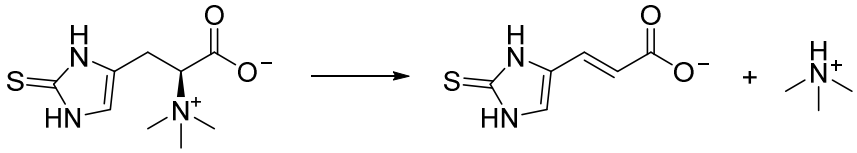

Figure 26. Reaction catalyzed by ergothionase. Ergothioneine is degraded to thiourocanic acid and trimethylamine.

The enzymatic activity of ergothionase was first described in 1957, when Yanasugondha *et al.* found out that the organism *Alcaligenes faecalis* was able to uptake ergothioneine as a source of carbon and energy.[130] They cultured fourteen different strains of bacteria in the presence of ergothioneine. At various time points they tested the amount of ergothioneine and thiourocanic acid. In the presence of the gram-negative soil bacteria *Alcaligenes faecalis* they were able to follow disappearance of ergothioneine and at the same time accumulation of thiourocanic acid. Four years later Kelly *et al.* were able to show degradation of ergothioneine by cell-free enzyme preparations of *A. faecalis*.[131] In 1962, Wolff showed ergothionase activity in a cell-free extract of *Escherichia coli* W.[107] Furthermore, he developed a spectrophotometric assay to follow the formation of thiourocanic acid at 311 nm.

Muramatsu *et al.* presented the first detailed characterization of ergothionase in 2013.[132] They identified the gene encoding ergothionase by Edman degradation. With the sequence of ergothionase at hand, they were able to work with the purified enzyme of *Burkholderia* sp. HME13 yielded by recombinant protein production in *Escherichia coli*. One interesting finding was that ergothionase is not able to produce ergothioneine from a high concentration of thiourocanic acid (2.5 mM) and a four-fold excess of trimethylamine. After a 12 h incubation, they could not detect any ergothioneine suggesting that the degradation reaction is irreversible. Muramatsu *et al.* also demonstrated that ergothionase from *Burkholderia* sp. HME13 loses its activity above 70 °C. This high stability could be advantageous when using ergothionase for the quantification of ergothioneine in blood or food samples as proposed by the authors.

Ergothionase presents a novel enzyme type that shows relation to the aspartase/fumarase superfamily and to the aromatic amino acid ammonia-lyases. Whereas, the catalytic important MIO-moiety of the

aromatic amino acid ammonia-lyases is not present in ergothionase. Furthermore, ergothionase is the first known enzyme that catalyzes the Hofmann elimination. As there is little known about ergothionase up to date, the aim of this chapter is to reveal the distinct mechanism of this enzyme.

3.1 Selection of a Specific Enzyme for Kinetic and Structural Characterization

Research on bacterial enzymes in the postgenomic era has the advantage that for any enzyme type there are a wide variety of homologs, which can be chosen for detailed characterization. Criteria for the selection of a specific protein for further analysis may include (I) the accessibility by recombinant production in *E. coli*, (II) the stability *in vitro* and (III) the activity and the propensity to crystalize. To identify an optimal candidate, we chose five sequences for further analysis, representing all putative ergothionase homologs.

Ergothionase from *Thermotalae metallivorans* was not accessible by recombinant production in *E. coli.* In contrast, ergothionase from *Streptococcus thermophilus* was producible in yields up to 10 mg/L of culture, however the protein was not stable *in vitro*. Production of the ergothionase candidate from *Synergistes jonesii* had good yields (5 mg/L of culture) and the enzyme was stable, however activity on ergothioneine was low (<0.007 s^{-1}).

Only the ergothioneine trimethylamine lyases from *Treponema denticola* (*Td*ETL) and *Burkholderia pseudomallei* (*Bp*ETL) allowed further studies. *B. pseudomallei* belongs to the phylum of β-proteobacteria and occurs mainly in subtropical and tropical regions. It is a pathogen bacterium causing the disease melioidosis.[135] Interestingly, *B. pseudomallei* contains the genes encoding for EgtD and EgtB, proteins involved in ergothioneine biosynthesis.[123] This shows that the bacteria is also able to produce ergothioneine. A closer look into the sequence of *Bp*ETL revealed an N-terminal leader sequence (`MQRFLTRSAIALALFAAVPAFA`). The leader sequence contains 22, mainly hydrophobic, amino acids. The function of this leader sequence is to direct the way of the protein towards a channel in the plasma membrane. Hence, *Bp*ETL is an extracellular protein. After successful translocation of the protein, the signal peptide is cleaved and digested by proteases.[136] In summary, *B. pseudomallei* is able to both produce and degrade ergothioneine. However, due to the leader sequence of ergothionase, we assume that the degradation of ergothioneine occurs extracellularly, whereas ergothioneine production occurs intracellularly. Thus, *B. pseudomallei* strictly separates the production and degradation of ergothioneine.

The gram-negative spirochete *T. denticola* is a pathogenic bacteria associated with parodontitis.[137] In contrast to *B. pseudomallei*, *T. denticola* degrades ergothioneine intracellular, but does not contain the genes for ergothioneine biosynthesis.

Sequence alignments of *Bp*ETL and *Td*ETL revealed 50% sequence similarity. Comparison of the catalytic parameters between *Bp*ETL and *Td*ETL revealed that at their corresponding pH-optima ergothioneine turnover of *Td*ETL is around 25-times faster than ergothioneine turnover of *Bp*ETL (Table 1). Furthermore, the K_M of *Bp*ETL increases around 5-times in comparison to *Td*ETL. Due to the loss in catalytic efficiency of *Bp*ETL compared to *Td*ETL, we decided to run further kinetic experiments with *Td*ETL.

Table 1. Observed kinetic parameters at the pH-optima of *Td*ETL (pH 7.5) and *Bp*ETL (pH 6).

	k_{cat} [s^{-1}]	K_M [µM]	k_{cat}/K_M [$M^{-1}s^{-1}$]
***Td*ETL**	64 ± 3	45 ± 4	1.4×10^6
***Bp*ETL**	2.4 ± 0.1	240 ± 15	1.0×10^4

3.2 Ergothionase Activity: Acid-Base Catalysis

Acid-base catalysis is an important chemical process in biology. The concerted action of perfectly positioned functional groups acting as base and acid enables enzymes to catalyze even difficult elimination or addition reactions. In this regard, ergothionase is a remarkable enzyme because it is the first known enzyme that catalyzes the Hofmann elimination. In 1957, Yanasugondha *et al.* recognized a pH-dependence on the reactivity of ergothionase; the disappearance of ergothioneine was fast between pH 8 – 9 but negligible at pH 6.[130] However, they did not work with pure enzymes but on whole cell lysates, and therefore their observed pH-dependence is influenced by many variables. Nevertheless, Wolff also found ergothionase from *E. coli* showed maximum activity between pH 8.5 – 9.[107] Muramatsu *et al.* also reported that the maximum activity of ergothionase from *B. pseudomallei* HME13 was at pH 8.[132] Given the observation that activity of this enzyme has a narrow pH optimum at around neutral pH, the possibility raised that this enzyme requires base and acid for catalysis. To eluciate the role of the acid- and base-catalyzed steps, we initiated a more detailed mechanistic and structural investigation of *Td*ETL.

3.2.1 Activity of Ergothionase in Dependence of pH

Based on the work of Wolff, we developed a spectrophotometric assay to follow ergothionase activity.[107] Strong absorbance of the unsaturated thiourocanic acid at 311 nm provided a convenient method to follow the enzymatic reaction ($\varepsilon_{311,\ \text{thiourocanic acid}}$ = 22500 $M^{-1}cm^{-1}$). The wavelength of 311 nm is specific for the product and no other contents of the assay showed absorbance at this specific wavelength. Thus, we could monitor product formation in a continuous reaction. With the knowledge of the extinction coefficient of the product and the concentration of used enzyme, we could calculate the reaction rate. The catalytic parameters presented in this thesis were determined using this assay.

First, we examined the pH dependence of *Td*ETL. For this purpose, we determined the Michaelis-Menten parameters at a pH ranging from pH 5.5 up to pH 9.5. Both, k_{cat} and k_{cat}/K_M showed a bell-shaped pH-dependence (Figure 27). To determine the pK_a values of these critical proton transfer equilibria, the point of inflection was calculated by fitting the obtained k_{cat} and k_{cat}/K_M parameters to the following equation: $y = k_{HA}/ (1+10^{(pKa1-pH)} + 10^{(pH-pKa2)})$.[138] The calculated p$K_a$1 and p$K_a$2 represent the p$K_a$ values of the corresponding acid and base, respectively.

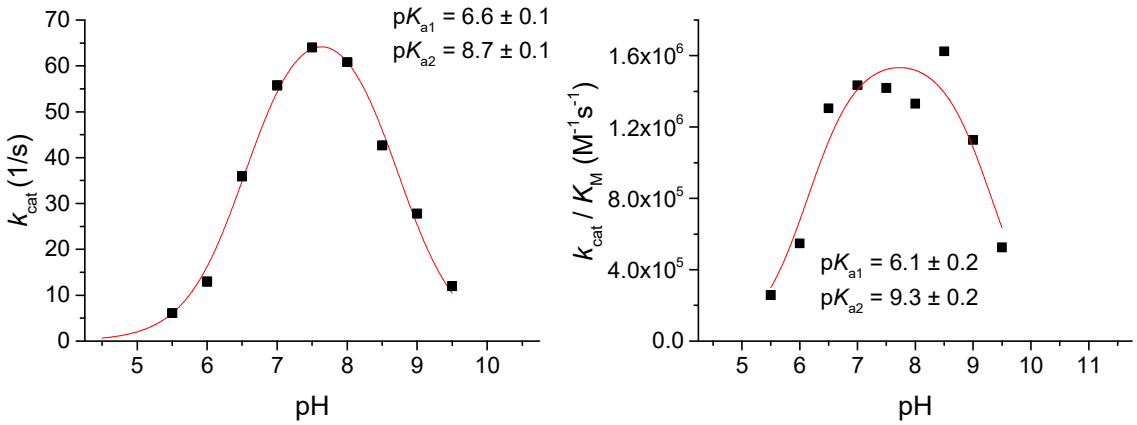

Figure 27. pH-Dependent k_{cat} and k_{cat}/K_M values of *Td*ETL WT. pH dependent kinetic parameters were fitted to $y = k_{HA}/ (1+10^{(pKa1-pH)} + 10^{(pH-pKa2)})$.

For *Td*ETL, the obtained pK_a values for k_{cat} were pK_a1 = 6.6 ± 0.1 and pK_a2 = 8.7 ± 0.1. In case of k_{cat}/K_M the obtained pK_a values were pK_a1 = 6.1 ± 0.2 or pK_a2 = 9.3 ± 0.2. In general, pH activity profiles for enzymatic reactions can give insights about the protonation state of either the substrate or the amino acid side chain of the protein. In our case, the substrate ergothioneine has a quite acidic pK_a of 1.3 due to the carboxylic acid, and the imidazole-H has a pK_a value of 10.8.[139] As the identified pK_a values for the catalyzed reaction are in between pH 6 – 9, we can assume that the pK_a values obtained from the calculation above are not related to the substrate but rather emerge from the protein. Hence, the

observed pH-dependent activity is set by pK_a values of key ionizable groups within the active site of *Td*ETL. This data suggests that certain protonation states of specific protein residues are important to provide the protons or charges needed in the catalytic mechanism of *Td*ETL.

One side chain residue of *Td*ETL has a kinetic pK_a = 6.6 ± 0.1. At pH levels below this pK_a, the residue is protonated and the activity of the enzyme drops. We therefore propose that this residue functions as a catalytic base for the degradation reaction. At pH levels above pK_a2 = 8.7 ± 0.1, the enzyme activity decreases again due to the deprotonation of another important residue. This active site group might be the catalytic acid.

The observed pH-dependence suggests that *Td*ETL catalysis follows an acid-base dependent mechanism (Figure 28). The base is responsible for the abstraction of the β-proton of the substrate. The nature of the acid-catalyzed step is less obvious. Further structural, mutational and kinetic studies will contribute to reveal the function of the acid catalysis in ergothionase and elucidate which residues act as the general acid and base. In the case of related MIO-dependent aromatic amino acid ammonia-lyases, the need of an acid has never been investigated. For the enzyme fumarase a catalytic acid is essential to generate the leaving group H_2O.[19] Whereas for aspartase the need of an acid has not been definitively elucidated and it remains questioning if the leaving group is free ammonia or the ammonium ion.[18]

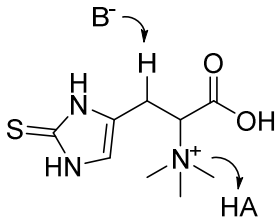

Figure 28. General proposed acid base dependent mechanism for the degradation of ergothioneine.

3.2.2 Crystal Structure

*Td*ETL was crystallized and the structure was solved by Florian Leisinger. The crystal structures were solved in the apo-form (PDB: 6S7J, resolution 2.2 Å), covalently bound to the product thiourocanic acid and in complex with the substrate analogue desmethyl-ergothioneine sulfonic acid (PDB: 6S7Q, resolution 2.7 Å).[133] The obtained structures are the first known crystal structures of ergothionase. The structure is part of the protein domain family lyase_aromatic pfam00221. A high similarity (RMSD 1.58 Å) to the structure of histidine ammonia-lyase from *Pseudomonas putida* (*Pp*HAL, pdb: 1B8F)[57]

was assessed. The overall structure of *Td*ETL composes a basic α-helical homo-tetrameric structure (Figure 29). The α-helices are arranged in parallel.

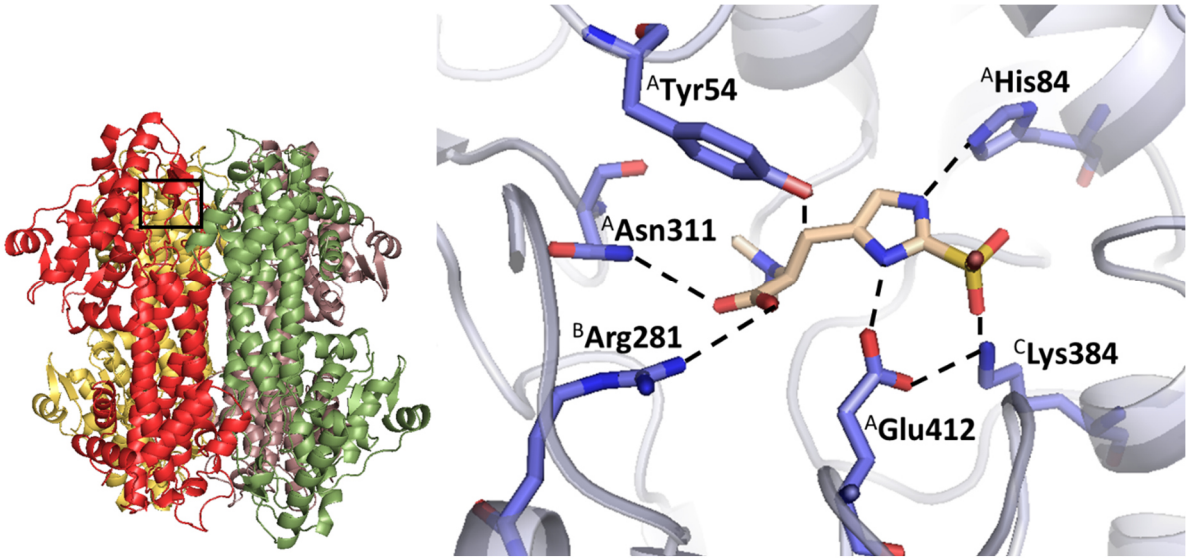

Figure 29. Crystal structure of the homo-tetramer of *Td*ETL (pdb: 6S7Q) (left). The black box indicates the active site of subunit A that is shown in detail on the right. The ligand desmethyl ergothioneine sulfonic acid is depicted in wheat.

The four active sites of the tetramer are located at the interfaces between the monomers. Each active site contains residues from three different subunits. The imidazole moiety of desmethyl ergothioneine sulfonic acid hydrogen bonds to His84 and Glu412 (Figure 29). Glu412 is coordinated to Lys384 that hydrogen bonds the sulfonic acid moiety of the ligand. The carboxylate of desmethyl-ergothioneine sulfonic acid approaches Asn311 and Arg281. The active site is covered by a loop that is positioned in a closed conformation in all structures. The native and the liganded structure do not show conformational changes upon substrate binding (Figure 30). A more detailed description of the crystal structure will be given in context with the kinetic data.

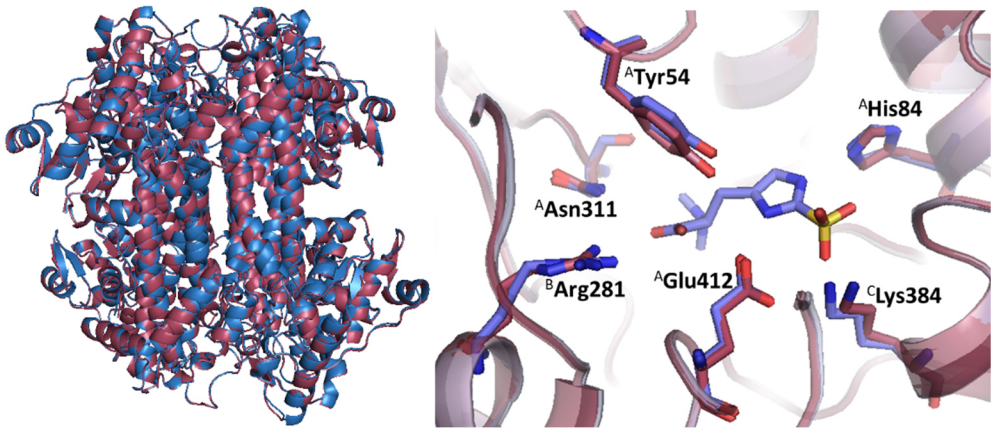

Figure 30. Superimposed structure of *Td*ETL in the apo form (raspberry, PDB: 6S7J) and in complex with desmethyl ergothioneine sulfonic acid (blue, PDB: 6S7Q). No conformational changes are observed upon substrate binding.

3.2.3 Identification of Important Catalytic Residues: Activity of Mutants

The observed pH-dependent activity profile reveals that ergothionase follows an acid-base dependent mechanism (section 3.2.1). One side chain residue of the protein functions as a general base to abstract the β-proton of the substrate, whereas another residue is responsible for leaving group protonation and therefore functions as a general acid.

The closely related MIO-dependent lyases all contain a highly conserved tyrosine residue. In 2004, Ritter and Schulz found that their variant Y110F of phenylalanine ammonia-lyase of *Petroselinum crispum* (*Pc*PAL) loses activity. However, they initially hypothesized that Tyr110 was not very important for catalysis, but suggested that the variant causes competitive inhibition with the substrate phenylalanine.[140] Later, the tyrosine residue was found to be the general base.[56,66,141] The function of this conserved tyrosine residue is the abstraction of the β-proton of the substrate. The sequence alignment suggests that the equivalent tyrosine residue is conserved in ergothionases (Figure 31). Therefore, we surmised that Tyr54 could be the catalytic base of *Td*ETL.

```
                  54          143          384          412
TdETL      ...KPVYGLNR...SIG-EGDIT...GTIQKTFTM...GTI--EDHAS...
BpETL      ...QQIYGLTV...SIG-EADIT...GAMEKPPTA...GGI--EDIAT...
PpHAL      ...RTAYGINT...SVGASGDLA...MIAQVTAAA...ANQ--EDHVS...
RsTAL      ...RHVYGLTT...TVGASGDLT...MGAQVTATA...-NAANQDVVS...
PcPAL      ...TDSYGVTT...TITASGDLV...KGAEIAMAS...AEQHNQDVNS...
```

Figure 31. Abbreviated sequence alignment of the ergothionases *Td*ETL and *Bp*ETL and the aromatic amino acid lyases *Pseudomonas putida* histidine ammonia-lyase (*Pp*HAL), *Rhodobacter sphaeroides* tyrosine ammonia-lyase (*Rs*TAL) and *Petroselinum crispum* phenylalanine ammonia-lyase (*Pc*PAL). The catalytic important residues for ergothionase activity are highlighted in turquoise, the conserved amino acids forming the MIO-moiety are highlighted in pink. Counting is based on *Td*ETL.

Analysis of the structure of *Td*ETL in complex with desmethyl-ergothioneine sulfonic acid showed that Tyr54 is located above the β-methylene group, well-positioned for abstraction of the pro-*S* proton of the substrate (Figure 29). In addition, the crystal structure of *Td*ETL co-crystallized with thiourocanic acid showed that the β-carbon of the product was covalently attached to Tyr54 (Figure 32). These findings gave strong indication that Tyr54 might be the catalytic base of *Td*ETL.

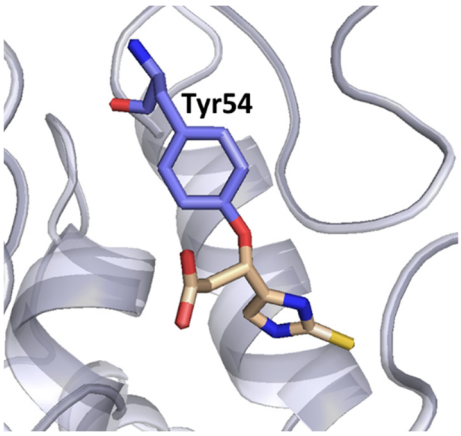

Figure 32. Crystal structure of *Td*ETL in complex with thiourocanic acid. The catalytic base Tyr54 is shown in blue, the covalently bound product thiourocanic acid is shown in wheat.

In order to test our hypothesis, we mutated Tyr54 to Phe. Michaelis-Menten kinetics from the Y54F variant were determined at the previously observed pH-optima for *Td*ETL (pH 7.5). This mutation caused a dramatic reduction in activity, the k_{cat} dropped over 3000-times in comparison to the wild type enzyme (Table 2). The equivalent variant in *Pp*HAL caused a 10^4 reduction in activity.[142] We therefore propose that Tyr54, in its phenolate ionization state, functions as a general base catalyst.

Table 2. Observed kinetic parameters at pH 7.5 of *Td*ETL WT and variants using ergothioneine as substrate.

	k_{cat} [s^{-1}]	K_M [μM]	k_{cat}/K_M [$M^{-1}s^{-1}$]
***Td*ETL WT**	64 ± 3	45 ± 4	1.4 x 10^6
***Td*ETL Y54F**	0.02 ± 0.01	31 ± 5	6.5 x 10^2
***Td*ETL K64M**	0.11 ± 0.01	1.0 ± 0.1	1.1 x 10^5
***Td*ETL E412Q**	0.05 ± 0.01	210 ± 20	2.4 x 10^2
***Td*ETL K384M**	0.02 ± 0.01	46 ± 4	5.0 x 10^2

The pH-dependent activity profile showed that, besides the catalytic base, a catalytic acid is also needed for catalysis. A closer look into the crystal structure of *Td*ETL revealed that Glu412 and Lys384

were positioned as potential catalytic acids (Figure 29). Glu412 hydrogen bonds with an imidazole N-H group of the substrate (2.7 Å distance). The structural conservation of Glu412 in *Pp*HAL underscores the importance of this residue for imidazole N-H binding (Figure 33). In contrast, Tyr- or Phe-lyases do not contain a conserved glutamate at the analogous position.

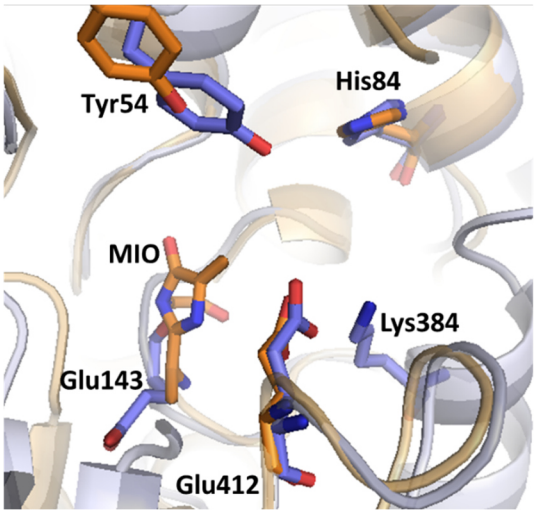

Figure 33. Superimposed structure of *Td*ETL (blue, PDB:6S7J) and *Pp*HAL (orange, PDB:1B8F). Tyr54, His84 and Glu412 (counting based on *Td*ETL) are structurally highly conserved, whereas Glu143 in *Td*ETL is located on the position of MIO in *Pp*HAL.

Lys384 belongs to the third subunit of *Td*ETL; in the homo-tetramer, this residue points in hydrogen bonding distance (3 Å) towards the sulfur group of the substrate (Figure 29).

To further study the function of Glu412 and Lys384, both residues were mutated to E412Q and K384M, respectively. The K384M variant causes a decrease in k_{cat} by 3000-times (Table 2). Based on the strong decrease in activity of that variant and based on the crystal structure, we suggest that the cationic lysine residue has a complementary charge on the sulfur group of the substrate. In order to bind to the active site, the substrate ergothioneine must attain a zwitterionic state with an anionic sulfur head-group and a cationic imidazolium (Figure 34). The variant K384M lacks a positive charge and may therefore no longer bind the zwitterionic state of the substrate. This charge separation appears to be crucial for catalysis and will be discussed in detail in the context of substrate activation in section 3.3. The decrease in k_{cat} by over 1000-times in the E412Q variant can be explained as Glu412 hydrogen bonds with N-H of the imidazolium of the substrate, and upon catalysis, Glu412 transfers a proton from Lys384 to the leaving group trimethyl amine (Table 2).

The dramatic effects on k_{cat} and catalytic efficiency of the presented variants Y54F, K384M and E412Q demonstrate that these three residues are absolutely essential for catalysis.

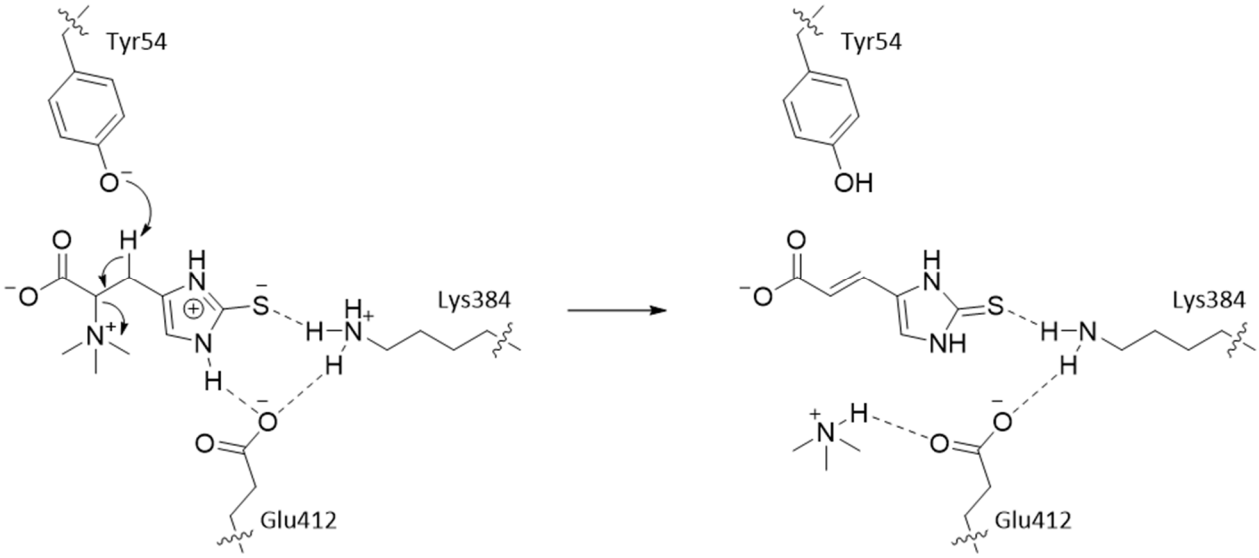

Figure 34. Mechanistic proposal of ergothioneine degradation within the active site of *Td*ETL.

3.2.4 Function of Lys64

Our previous investigation into the pH-dependent activity profile of *Td*ETL WT revealed a bell-shaped pH-dependence. The observed pK_a values are set by key ionizable groups within the active site of *Td*ETL. The acidic limb of the activity profile reflects the deprotonation of the catalytic base Tyr54 (pK_a1_{WT} = 6.6 ± 0.1) (Figure 27). A tyrosine residue without any interaction has a pK_a of 10. Thus, the obtained pK_a value is lower than expected. Therefore, the anionic form of Tyr54 might be stabilized by a neighboring residue. Lys64 is a possible residue for stabilization; this residue is located on a flexible loop covering the active site in neighborhood to the catalytic base Tyr54. The obtained crystal structure of *Td*ETL co-crystallized with desmethyl-ergothioneine presents Lys64 in a conformation, rotated away from Tyr54 (8.7 Å distance between Tyr54 and Lys64) (Figure 35). However, another data-set with low ligand occupancy revealed a flexible Lys64 in close contact to Tyr54.[133]

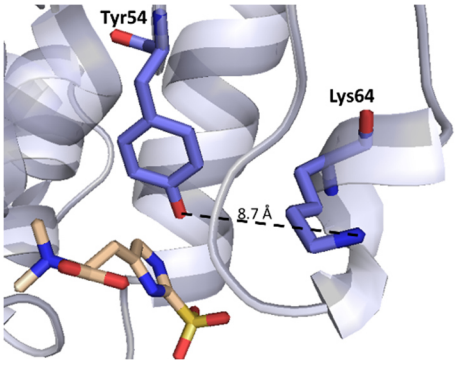

Figure 35. Crystal structure of *Td*ETL in complex with desmethyl-ergothioneine sulfonic acid (pdb: 6S7Q). The catalytic base Tyr54 and Lys64 are colored in blue. Here, Lys64 is rotated away; thus, the distance between phenolate of Tyr54 and the ε-amino group of Lys64 is only 8.7 Å. However, Lys64 can also be rotated, and thus allow coordination to Tyr54.

In order to investigate into the influence of Lys64, we designed the K64M variant. At pH 7.5, the K64M variant causes a minor decrease in activity in comparison to Y54F, E412Q or K384M (Table 2). The hydrogen bond interaction with Lys64 could account for the depressed pK_a of Tyr54 (Figure 36). To test this idea, we recorded a pH-dependent activity profile for the K64M variant.

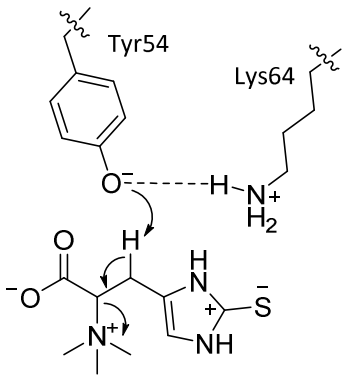

Figure 36. Interaction between Lys64 and the catalytic base Tyr54 within the active site of *Td*ETL.

In a similar experiment as run for the wild type enzyme, we obtained a bell-shaped pH-dependence for the mutant (Figure 37). However, the single point-mutation was found to cause a shift in the pH-optimum of *Td*ETL. In contrast to the wild type, the pK_a1 of K64M was increased by 1.6 pH units (pK_a1_{WT} = 6.6 ± 0.1 vs. pK_a1_{K64M} = 8.2 ± 0.2). This effect is consistent with the postulated activating role of Lys64.

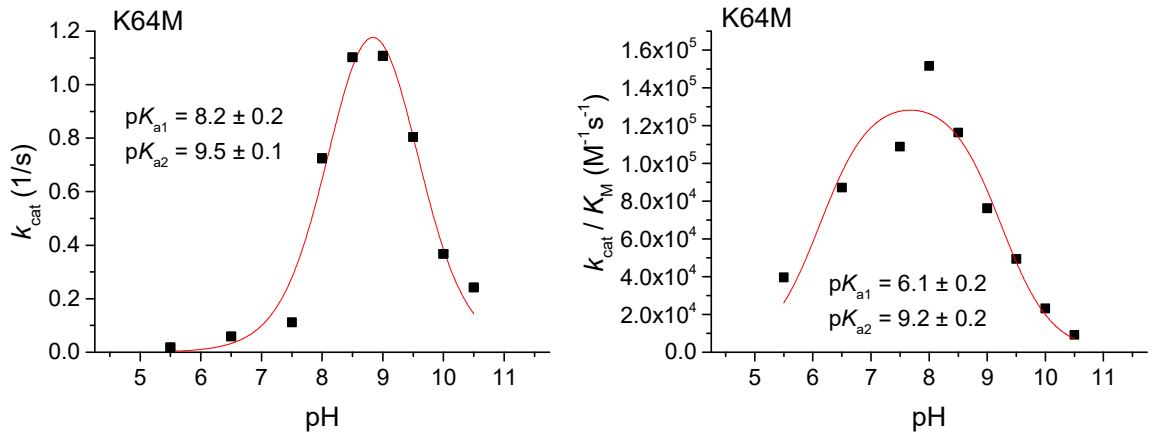

Figure 37. pH-Dependent k_{cat} and k_{cat}/K_M values of *Td*ETL K64M. Obtained kinetic parameters were fitted to y = k_{HA}/ (1+$10^{(pKa1-pH)}$ + $10^{(pH-pKa2)}$).

Interestingly, in the pH-dependent activity profile of K64M, not only pK_a1 was is shifted, but also pK_a2 was elevated by 0.8 pH units (pK_a2_{WT} = 8.7 ± 0.1 vs. pK_a2_{K64M} = 9.5 ± 0.1). As pointed out earlier, pK_a1

reflects the catalytic base, whereas pK_a2 reflects the catalytic acid of the reaction. Thus, it first seems surprising that the K64M variant influences the pK_a2 value as well. However, we have to consider that the total activity of K64M had dropped. Therefore, the inflection point representing pK_a2 dropped as well. This results in a shift of the observed pK_a2 of K64M in comparison to the wild type. Nevertheless, this shift does not present any direct influence of K64M on pK_a2. Anyway, the elevation of pK_a1 is obviously higher (ΔpK_a1 = 1.6 pH-units; ΔpK_a2 = 0.8 pH-units).

3.3 Substrate Activation

Ground-state destabilization of a substrate, along with transition-state stabilization, is a major component in enzyme catalysis.[143] Ground-state destabilization is important for lowering the activation energy barrier, while converting substrate molecules to products. An example of ground-state destabilization through substrate polarization can be seen in the enzyme uracil DNA deglycosylase, which polarizes its substrate in order to catalyze the C-N bond cleavage reaction (Figure 38).[144] The substrate uracil is polarized by active site residues to the higher energy structure, similar to the enolate form when it is bound in the enzyme. This polarized substrate closely resembles the transition state structure, and thus facilitates bond-cleavage. Das *et al.* outlined the importance of tautomeric strain in raising the energy of substrates in enzymes.[144]

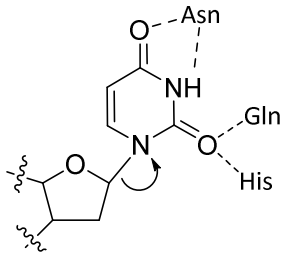

Figure 38. Scheme of the active site of uracil DNA deglycosylase. The substrate gets polarized in order to facilitate C-N bond cleavage.[144]

However, it is important to note that ground-state destabilization accelerates catalysis only under the condition that the energy needed to distort the reacting part of the substrate is compensated either by (I) strong attractive interactions with other parts of the substrate and the enzyme, or (II) by stabilization of the entire protein fold upon ligand binding. If this condition is not fulfilled, the destabilizing interactions simply decreases the concentration of the enzyme:substrate complex, which in turn reduces the overall reaction rate. Ergothionase fulfills this condition: substrate binding seems

to be irreversible (as will be described in section 3.4.1), meaning that the binding of the substrate at a concentration higher than K_M gets exergonic.

One major challenge for the enzyme ergothionase is the abstraction of the non-acidic β-proton of ergothioneine. The β-proton of an amino-acid has a pK_a of 40.[58] In order to allow the abstraction of the β-proton, the ground-state of ergothioneine must be destabilized, leading to an increase in acidity at the β-position.

We propose that ergothionase binds the substrate ergothioneine in its polarized form (Figure 39). The resonance structure of ergothioneine places the positive charge in vicinity of the β-proton; the electron withdrawal facilitates C-H bond cleavage.

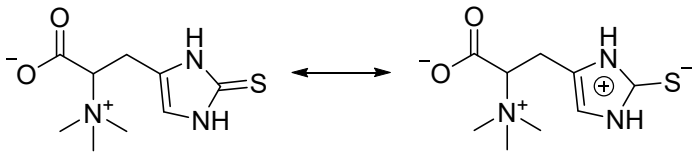

Figure 39. Resonance structure of ergothioneine.

We suggest that the stabilization of the imidazolium thiolate form of the substrate might be important in the catalysis of ergothionase. The crystal structure of *Td*ETL with desmethyl-ergothioneine sulfonic acid gives closer insights how the protein stabilizes the substrate. However, we have to consider that the obtained crystal structure shows desmethyl-ergothioneine sulfonic acid and not the substrate ergothioneine itself. Nevertheless, we analyzed the catalytic behavior of desmethyl-ergothioneine and ergothioneine sulfonic acid (section 0 and 3.3.4), and thus we can assume that desmethyl-ergothioneine sulfonic acid is a good model for ergothioneine. Both N-H protons of the imidazole moiety of the ligand can be stabilized by the active site residues Glu412 (2.7 Å distance) and His84 (3.0 Å distance) (Figure 40). His84 itself forms a hydrogen bonded triad with Ser83 and Asn79; this allows His84 to be a hydrogen bond donor towards the substrate. The π-electrons of the carbon-sulfur bond of the substrate can be polarized to the sulfur residue. The resulting thiolate is stabilized by Lys384 (2.7 Å distance). Hence, a cationic charge, stabilized by Glu412 and His84, remains on the imidazole moiety (Figure 41). This cationic charge causes an increase in acidity of the β-methylene group, which accelerates base-assisted C-H cleavage. Thus, the zwitterionic state of the substrate, leading to the cationic charge on the imidazole moiety, is indispensable for catalysis. In agreement with our earlier observation that C-H cleavage is a key step in catalysis, we understand that the described zwitterionic form of ergothioneine is crucial for ergothionase activity.

In the following subchapter, the hypothesis that ergothionase binds the substrate in a polarized form will be tested by investigations on substrate specificity of the wild type and the K384M variant in particular.

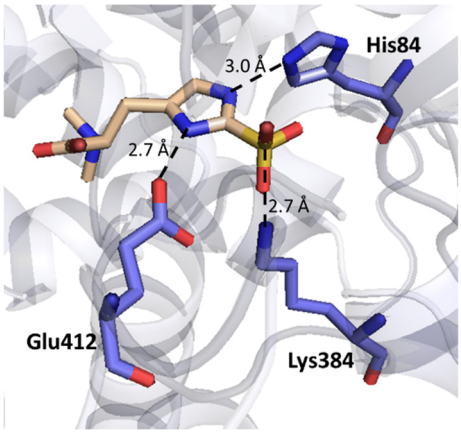

Figure 40. Crystal structure of *Td*ETL in complex with desmethyl-ergothioneine sulfonic acid (colored in wheat). The N-H protons of the imidazole moiety of desmethyl-ergothioneine sulfonic acid is coordinated to His84 and Glu412 (colored in blue). The sulfur moiety of desmethyl-ergothioneine sulfonic acid is coordinated to Lys384 (colored in blue).

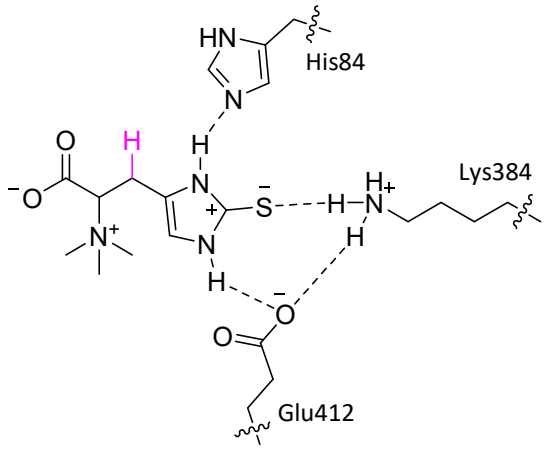

Figure 41. Ergothioneine binding within the active site of *Td*ETL. His84, Lys384 and Glu412 stabilize the zwitterionic state of the substrate. Thus, acidity of the β-methylene proton is increased (represented in pink).

3.3.1 Substrate Specificity

Kinetic investigations using substrate-related compounds and not only the main substrate, can help to gain a better understanding of enzyme mechanisms and is giving an important interpretive merit, especially regarding substrate activation. While ergothioneine appears to be the main substrate for ergothionase, we decided to investigate turnover of other histidine derivatives.

N,N,N-α-trimethylhistidine (TMH) was tested as substrate for *Td*ETL. TMH was transformed to urocanic acid with a rate of 0.04 s^{-1} (Table 3). Besides TMH, *S*-methyl ergothioneine was also found to be a poor substrate (rate = 0.001 s^{-1}). While both compounds seem structurally similar to ergothioneine, the activity of *Td*ETL was still found to be strongly reduced (1600-fold in the case of TMH and 64000-fold in the case of *S*-methyl ergothioneine).

Table 3. Observed activity of *Td*ETL WT on different substrates in HEPES buffer at pH 7.5 using 2 mM substrate.

	Ergothioneine	**TMH**	***S*-Methyl ergothioneine**
***Td*ETL WT [s^{-1}]**	64 ± 3	0.04 ± 0.01	0.001

The structural difference between ergothioneine and TMH is the absence of sulfur in TMH. During catalysis, the thiolate of ergothioneine is required for hydrogen bonding interaction to Lys384 (Figure 41). This hydrogen bonding interaction stabilizes the charge separation of the substrate. As described earlier, this cationic imidazolium is important to increase the acidity of the methylene group. However, the compound TMH cannot be stabilized in the charge separated form due to the missing sulfur. The crucial zwitterionic state for activity cannot be attained and TMH does neither hydrogen bond to Lys384, nor to Glu412 (Figure 42). Therefore, β-methylene acidity of the substrate is not increased, leading to a loss in activity for TMH.

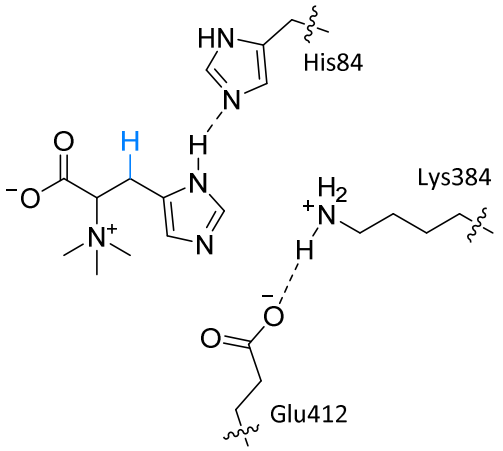

Figure 42. TMH binding within the active site of *Td*ETL. The enzyme does not stabilize a cationic charge on the imidazole moiety; thus, acidity of the β-methylene proton is not increased (represented in blue).

S-Methyl ergothioneine was also not accepted as a substrate by *Td*ETL (rate = 0.001 s^{-1}). The structural difference of *S*-methyl ergothioneine to ergothioneine is the addition of a methyl group on the sulfur

residue (Figure 43). The presence of this methyl group appears to have a strong effect on activity. Since ergothioneine sulfonic acid is an accepted substrate for ergothionase (as described below), it is unlikely that simple steric hindrance of the additional methyl group in *S*-methyl ergothioneine is the reason for the loss in activity. The activity loss can be explained as the crucial charge-separation of the thiolate and imidazolium is not possible for *S*-methyl ergothioneine. Thus, *S*-methyl ergothioneine binds with a neutral imidazole moiety and acidity of the β-methylene group is not increased.

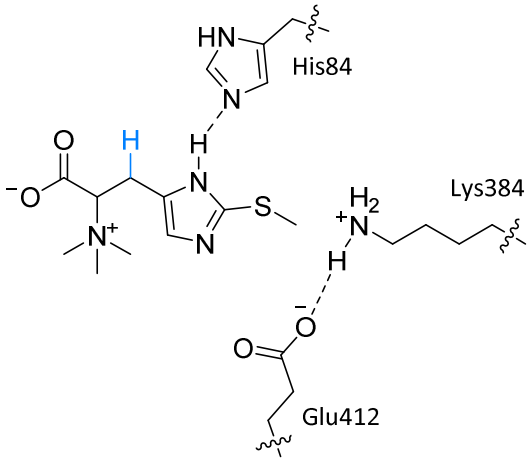

Figure 43. *S*-Methyl ergothioneine binding within the active site of *Td*ETL. The enzyme does not stabilize a cationic charge on the imidazole moiety; thus, acidity of the β-methylene proton is not increased (represented in blue).

We showed that the active site residue Lys384 is highly important for stabilizing the thiolate of the substrate ergothioneine. The compounds TMH and *S*-methyl ergothioneine do not hydrogen bond with Lys384, which explain their reduced reactivity. Therefore, it would be interesting to investigate the substrate specificity of the K384M variant.

3.3.2 Substrate Specificity of the K384M Variant

Lys384 is an important residue within the active site of *Td*ETL. As described earlier, we propose that Lys384 hydrogen bonds with the thiolate form of ergothioneine, and thus is responsible for stabilizing the crucial zwitterionic state of the substrate. To test this hypothesis, we constructed the K384M variant.

The K384M variant degrades ergothioneine around 3000-times slower than the wild type enzyme (Table 4). Furthermore, the variant shows only negligible turnover on ergothioneine sulfonic acid. Nevertheless, in contrast to the wild type, the activity of K384M for both TMH and *S*-methyl

ergothioneine increases five-times and 90-times, respectively. Thus, the single mutation not only decreased the activity of ergothionase but also impacts substrate specificity.

Table 4. Observed activity of *Td*ETL WT and *Td*ETL K384M on different substrates in HEPES buffer at pH 7.5 using 2 mM substrate.

	Ergothioneine	**Ergothioneine sulfonic acid**	**TMH**	***S*-Methyl ergothioneine**
***Td*ETL WT [s^{-1}]**	64 ± 3	17 ± 1	0.04 ± 0.01	0.001
***Td*ETL K384M [s^{-1}]**	0.02 ± 0.001	0.005 ± 0.002	0.2 ± 0.01	0.09 ± 0.001

This effect is likely caused by the change in the active site environment. The K384M variant leads to the loss of a positively charged residue within the active site of the protein. In the case of *S*-methyl ergothioneine, the neutral *S*-methyl head-group does not interfere with the neutral methionine. The protonated imidazolium moiety of *S*-methyl ergothioneine can still be stabilized by Glu412, and thus *S*-methyl ergothioneine can bind in a cationic form (Figure 44). As we have mentioned earlier, the cationic imidazolium is crucial for activity, while increasing acidity of the β-methylene group.

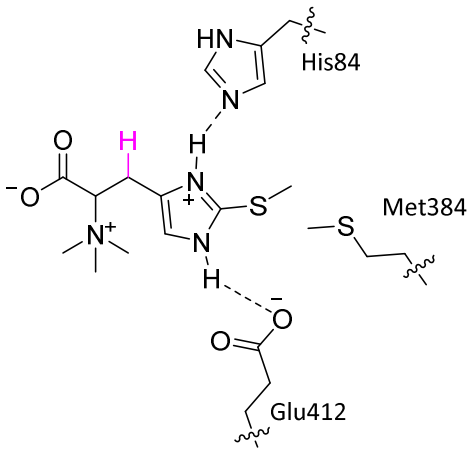

Figure 44. *S*-Methyl ergothioneine binding within the active site of the variant *Td*ETL K384M. The enzyme is able to stabilize the crucial cationic imidazolium moiety; thus, acidity of the β-methylene proton is increased (represented in pink).

The increase in activity of the K384M variant over the wild type for TMH can be explained in a similar fashion as for *S*-methyl ergothioneine (Figure 45). Due to the absence of a cationic residue within the active site of the variant, TMH can bind in the cationic imidazolium form stabilized by Glu412.

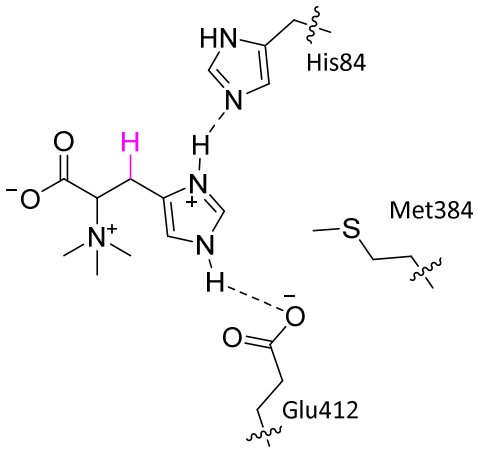

Figure 45. TMH binding within the active site of the variant *Td*ETL K384M. The enzyme is able to stabilize the crucial cationic imidazolium moiety; thus, acidity of the β-methylene proton is increased (represented in pink).

The observed activity of the K384M variant supports the hypothesis of the crucial charge separation of the substrate during catalysis of *Td*ETL.

3.3.3 Ergothioneine Sulfonic Acid as Substrate

Ergothioneine sulfonic acid was first identified as a stable oxidation product of ergothioneine.[145] Servillo *et al.* confirmed the formation of both ergothioneine sulfonic acid and TMH after reaction of ergothioneine with the superoxide anion in cell-free experiments. Two years later, ergothioneine sulfonic acid was found to emerge during ergothioneine oxidation in the presence of high-glucose oxidative stress in endothelial cells.[146] However, the fate of the stable compound ergothioneine sulfonic acid was stated to be unknown so far.[99] Interestingly, *Td*ETL also accepts ergothioneine sulfonic acid in considerable efficiency with a k_{cat} of 17 ± 1 s^{-1} and a catalytic efficiency (k_{cat}/K_M) of 1.1 x 10^5 $M^{-1}s^{-1}$ (Table 5). It appears that the large anionic head group of ergothioneine sulfonic acid fits into the active site and does not disturb the protein. Furthermore, the compound is able to obtain a zwitterionic state comparable to ergothioneine (Figure 46). Thus, the overall neutral complex is a good substrate for *Td*ETL. The crystal structure reveals that the anionic head group can interact with Lys384. The remaining cationic imidazolium moiety can interact with Glu412. As stated earlier, this positive charge is crucial for catalysis as it increases acidity of the β-methylene proton.

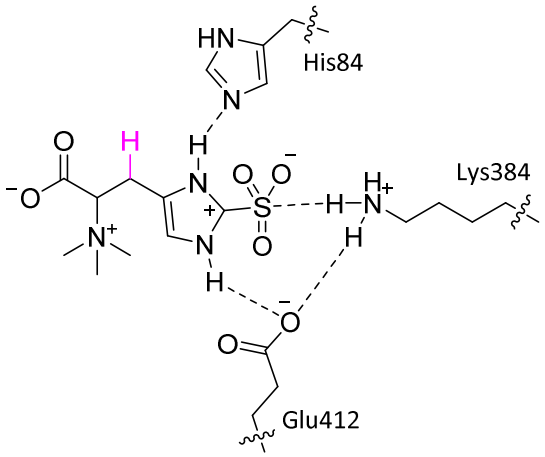

Figure 46. Ergothioneine sulfonic acid binding within the active site of *Td*ETL. His84, Lys384 and Glu412 stabilize the zwitterionic state of the substrate. Thus, acidity of the β-methylene proton is increased (represented in pink).

The activities of the variants Y54F, E412Q and K384M, using ergothioneine sulfonic acid as substrate were as drastically decreased as observed for ergothioneine (Table 5).

Table 5. Observed kinetic parameters at pH 7.5 of *Td*ETL WT and variants using ergothioneine sulfonic acid as substrate.

	k_{cat} [s^{-1}]	K_M [µM]	k_{cat}/K_M [$M^{-1}s^{-1}$]
***Td*ETL WT**	17 ± 1	150 ± 20	1.1 x1 0^5
***Td*ETL Y54F**	0.003 ± 0.002	150 ± 30	1.7 x 10^1
***Td*ETL E412Q**	0.002 ± 0.001	4 ± 1	4.6 x 10^2
***Td*ETL K384M**	0.005 ± 0.002	1900 ± 200	0.3 x 10^1

Due to the absence of the catalytic base, the k_{cat} value, using ergothioneine sulfonic acid as the substrate, decreases over 5000-times for the Y54F mutant in comparison to the wild type. In agreement with our observation for ergothioneine, the variants E412Q and K384M lose activity over three orders of magnitude for ergothioneine sulfonic acid. The increased catalytic efficiency of E412Q (k_{cat}/K_M = 4.6 x 10^2 $M^{-1}s^{-1}$) in contrast to the other variants, can be explained by the omitted repulsion of the anionic head group and Glu412. Lys384 and Glu412 are both important for activity: Lys384 acts as proton donor; Glu412 helps stabilizing the cationic imidazolium and is responsible for proton transfer to the leaving group trimethylamine. Based on these findings, we proposed that ergothioneine sulfonic acid reacts in a similar mechanism as ergothioneine.

3.3.4 Impact of Desmethyl-Ergothioneine

The crystal structure obtained with desmethyl-ergothioneine sulfonic acid showed that the desmethylated substrate derivative can bind to the active site of *Td*ETL. Therefore, we investigated if desmethyl-ergothioneine sulfonic acid and desmethyl-ergothioneine are also substrates.

The observed activity of the desmethylated substrate derivatives was in both cases reduced by over three orders of magnitude in comparison to ergothioneine and ergothioneine sulfonic acid (Table 6).

Table 6. Observed activity of *Td*ETL WT on different substrates in HEPES buffer at pH 7.5 using 2 mM substrate.

	Ergothioneine	Desmethyl-ergothioneine	Ergothioneine sulfonic acid	Desmethyl-ergothioneine sulfonic acid
***Td*ETL WT [s^{-1}]**	64 ± 3	0.012	17 ± 1	0.0022

The much lower reactivity of desmethylated compounds can be rationalized as follows: The elimination of ergothioneine or ergothioneine sulfonic acid produces neutral trimethylamine with a pK_a only slightly above the physiological pH (pK_a 9- 10). In contrast to ergothioneine and ergothioneine sulfonic acid, the desmethylated compounds likely bind to the active site with a neutral amino group because the corresponding pocket is largely apolar and provides no counter charge to stabilize the dimethylamino function in protonated form. Elimination of this leaving group would produce an anionic dimethylamine that is characterized by a much higher pK_a. Clearly, dimethylamine is a poor leaving group.

The observation that the desmethylated compounds are poor substrates highlights a second part of the substrate activation strategy of *Td*ETL: binding of the trimethylammonium moiety in an apolar pocket destabilizes the leaving group.

Additionally, we investigated in the inhibitory influence of desmethyl-ergothioneine. Given its low reactivity, desmethyl-ergothioneine acts essentially as a substrate competitive inhibitor. Michaelis-Menten kinetics of *Td*ETL inhibition by desmethyl-ergothioneine were run by measuring the apparent $K_{M,ergothioneine}$ in the presence of different concentrations (250, 500, 1000, 1500, 2000 µM) of desmethyl-ergothioneine. The k_{cat} remained unchanged upon addition of the inhibitor whereas the K_M value increased (Figure 68). From these data set, K_i was calculated using the equation $K_i = \frac{K_M * [I]}{K_{M(app.)} - K_M}$.[147] The value of K_i for desmethyl-ergothioneine (250 ± 30 µM) should be taken with care because substrate binding of *Td*ETL might be irreversible, as will be discussed in section 3.4.1. Therefore, it is

possible that binding of desmethyl-ergothioneine might also be partially irreversible. Hence, the physical meaning of K_i is obscure.

3.3.5 Analysis of the Substrate and Solvent Isotope Effect of k_{cat}

In general, three different mechanisms for elimination reactions can be distinguished, namely E1, $E1_{cb}$ and E2 (Figure 47). E1-elimination is a unimolecular reaction, whereby the reaction velocity depends only on the concentration of the substrate. The formation of the carbocation through cleavage of the leaving group is the rate-determining step. In the case of $E1_{cb}$-elimination, a carbanion is formed prior to cleavage of the leaving group, which is stabilized by conjugation prior to leaving group departure. E2-elimination is a bimolecular reaction, dependent on the concentration of both substrate and base. Thereby, C-H abstraction and cleavage of the leaving group occurs in one concerted step. Furthermore, E2-elimination demands an antiperiplanar arrangement (180°) of the cleaved leaving group and the C-H bond because it aligns the orbitals responsible for forming the π-bond. In organic chemistry, E1, $E1_{cb}$ and E2 mechanisms are distinguished by the different kinetic behavior. In the case of ergothionase the reaction certainly behaves as unimolecular reaction. Whereas the presented nomenclature distinguishes the sequence of the elementary steps, meaning that in an E1 reaction the trimethylamine leaves the substrate first under formation of a carbocation; in an $E1_{cb}$ elimination the C-H cleavage occurs first, whereas an E2 elimination describes a concerted reaction.

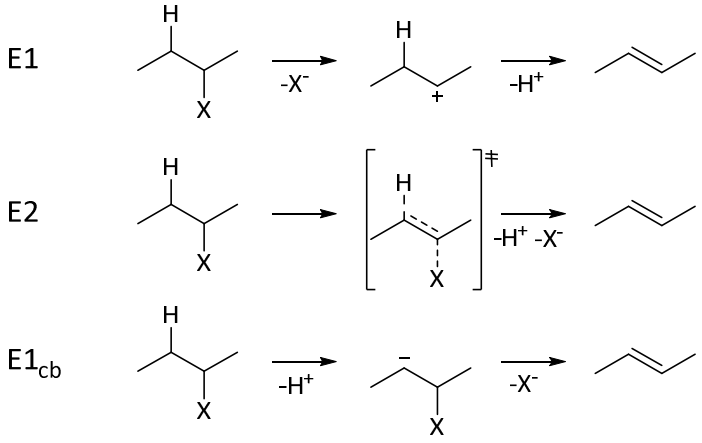

Figure 47. Scheme of the different types of elimination reaction.

In order to identify the rate-limiting step of ergothionase, we determined the substrate kinetic isotope effect (KIE) for *Td*ETL activity. Isotope substituted substrates require more energy to reach the transition state for C-D bond cleavage. If this bond cleavage is involved in the rate-limiting step, the deuterium-labelled ergothioneine will react at a slower rate, presented by a KIE > 1. In order to

produce deuterated ergothioneine, the ergothioneine biosynthetic enzyme EanB and the starting material TMH (D_5, 98%; $^{15}N_3$, 98%) were used (Figure 48).[105]

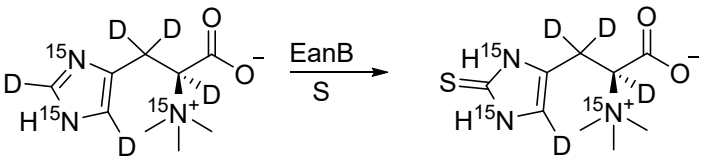

Figure 48. Enzyme-based production of deuterated ergothioneine from deuterated TMH (D_5, 98%; $^{15}N_3$, 98%).

We determined the KIE by following turnover of *Td*ETL using ergothioneine or deuterated ergothioneine as the substrate. The ratio k_H/k_D indicated a KIE = 1.8 ± 0.2, suggesting that the cleavage of the β-C-H bond of the substrate is the rate-limiting step.

The kinetic solvent isotope effect (KSIE) examines the effect of solvent deuterium substitution on reaction velocity. However, KSIE are often difficult to interpret. Unlike specific deuteration of the substrate, deuteration of the solvent is not a specific perturbation. The exchange of water with deuterium oxide changes the viscosity of the solvent and the pK_a values of functional groups. This in turn can affect conformational preferences of the protein, its flexibility and the protonation equilibria in the active site. The following discussion of these effects should be viewed as a tentative explanation of the observed effects. In this discussion, effects that are smaller than 1.4-fold are not considered significant because of the associated experimental error and viscosity effects. Isotope effects larger than 1.4 indicate that proton transfer is taking place during the transition state of a rate-limiting step. In the absence of proton inventory experiments, we cannot exclude the possibility that the observed isotope effects are caused by multiple coupled proton transfers.

For the elimination reaction of *Td*ETL, we determined a KSIE = 1.7 ± 0.1. This comparatively large effect is consistent with the idea that proton transfer occurs during a rate-limiting step. Given the above indications that *Td*ETL activity depends on acid catalysis, it is possible that the observed isotope effect is related to proton transfer from the enzyme to eliminated trimethylamine. Mechanistically, this proton transfer could occur either coupled with or subsequent to C-H cleavage. If both protons are moving during the same transition state, one would expect that substrate and solvent isotope effects would cumulate by multiplication.

To test this idea, we measured both the KSIE using deuterated ergothioneine as substrate and the KIE in D_2O (Table 7). In both cases, no distinct effect was observable (KIE_{D2O} = 1.3 ± 0.2; $KSIE_{deut.\text{-}ergothioneine}$ = 1.0 ± 0.2). This result is clearly not concomitant with the expectation that the combination of

deuterated substrate with deuterated solvent should produce a larger effect – if the two proton transfer events would be coupled. In contrast, our observations suggest that the two events are not coupled. Both energy barriers are independent and equal rate-limiting steps. The diminished effects observed in the combined substrate and solvent deuteration experiments suggest that the two deuterium-sensitive steps occur sequentially.

Table 7. Observed substrate kinetic isotope effects (KIE) and kinetic solvent isotope effect (KSIE) at pH 7.5 of *Td*ETL WT.

	KIE (k_{cat})	**KSIE (k_{cat})**
H_2O	1.8 ± 0.2	---
D_2O	1.3 ± 0.2	---
Ergothioneine	---	1.7 ± 0.1
Deut.-Ergothioneine	---	1.0 ± 0.2

The nature of the step, which is slowed down by deuteration of the substrate, can be clearly attributed to C-H cleavage by Tyr54. The identity of the step that is sensitive to solvent deuteration is less clear. Based on the mechanistic proposal depicted in Figure 34 we can identify two possibilities:

I) Solvent deuteration changes the proton distribution between the substrate and residues Glu412, Lys384 and His84. This distribution could reduce the positive charge on the mercaptoimidazole ring, which in turn would reduce the acidity of the scissile β-proton of the substrate. However, this effect would make C-H cleavage slower and result in a multiplicative substrate/solvent kinetic isotope effect. This is not what we observed.

II) Alternatively, it is possible that protonation of the expelled trimethylamine by the Glu412-Lys384 dyad is partially rate-limiting and therefore slows the overall reaction in D_2O. This proton transfer could occur either coupled to C-H abstraction or afterwards. The observed coupled isotope effects would support the latter option. Indeed, inspection of the crystal structure showed that the position of Glu412 relative to the dimethylamino group of desmethyl ergothioneine sulfonic acid is not amenable to direct proton transfer because the side chain of Glu412 is not positioned in the same axis as the Cα-N bond of the substrate. Therefore, protonation of the leaving group has to occur after C-N cleavage and realignment of trimethylamine to point its lone pair towards Glu412. The structure does not reveal any other acidic residue that could protonate trimethylamine instead. Based on this analysis, we propose that the solvent-sensitive step is the protonation of trimethylamine by the Glu412-Lys384 dyad.

Additionally, we investigated in the the KSIE of the variants Y54F, E412Q and K384M in order to examine if active site residues are involved in proton transfer (Table 8). As previously rationalized, the interpretation of the KSIE is only a tentative explanation.

Table 8. Observed kinetic solvent isotope effect (KSIE) on k_{cat} at pH 7.5 of *Td*ETL WT and variants.

	KSIE (k_{cat})
***Td*ETL WT**	1.7 ± 0.1
***Td*ETL Y54F**	1.3 ± 0.1
***Td*ETL E412Q**	1.0 ± 0.1
***Td*ETL K384M**	1.5 ± 0.1

For all variants, we observed a reduced KSIE in contrast to the wild type enzyme. The variant E412Q reduced the effect to unity, which might indicate that Glu412 is most intimately involved in the proton transfer step that is reflected by the solvent isotope effect. Possibly, in the E412Q variant the leaving group trimethylamine is no longer protonated, hence, the KSIE vanishes completely. The variant K384M has a KSIE of 1.5 ± 0.1. We propose that Lys384 stabilizes the thiolate of the zwitterionic state of the substrate and that Lys384 is the proton donor for the catalytic acid dyad with Glu412, therefore the variant K384M has a reduced KSIE in comparison to the wild type. For the Y54F variant we do not observe a significant KSIE ($KSIE_{Y54F}$ = 1.3 ± 0.1). Due to the absence of the catalytic base, which causes slow β-C-H cleavage of the substrate, we barely see reactivity of that variant. Because the rate-limiting C-H cleavage step is decreased drastically in Y54F, the second step of the mechanism, namely the protonation of the leaving group is hard to analyze.

3.4 Irreversible Substrate Binding Mechanism

The crystal structure of *Td*ETL revealed that the active site is occluded by a loop region that contains the catalytic base Tyr54. Closely-related MIO-dependent ammonia-lyases possess an equivalent loop region. The crystal structure of *Pc*PAL (PDB: 1W27) showed that the tyrosine residue is located in great distance of the active site (~17 Å) (Figure 49).[140] This observation was a first indication for a high flexibility of the tyrosine containing loop-region.[148] Indeed, numerous homologous lyases have been crystallized with the active site loop in disordered conformations (PDB: 1Y2M, 1T6J, 2NYN, 2NYF).[55,56,149,150] Based on the first ordered PAL structure (PDB: 3CZO), it can be suggested that conformational switches of the loop region are responsible for controlling access to the active site and that the stability of the closed loop-conformation might influence catalytic efficiency.[67] Site-directed mutagenesis on a structurally-related aminomutase showed that the introduction of a glycine residue

in the active site loop allowed greater loop flexibility, which caused an increase in lyase over mutase activity (PDB: 4V2R).[151] In the following subchapter, we will focus on the substrate binding mechanism of *Td*ETL and investigate the role of the active site loop.

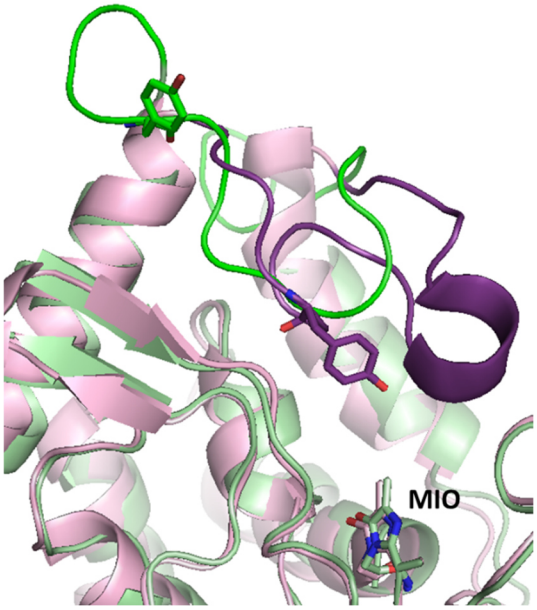

Figure 49. Superimposed structure of PAL with open loop conformation from *Petroselinum crispum* (green, PDB: 1W27) and PAL with closed loop conformation from *Anabaena variabilis* (violet, PDB: 3CZO). The catalytic base tyrosine located on the loop and the MIO-moiety in the active site are depicted in stick presentation.

3.4.1 Substrate Isotope Effect Reveals Partial Irreversible Substrate Binding

As discussed earlier, *Td*ETL displays a substrate isotope effect of KIE (k_{cat}) = 1.8 ± 0.2 (section 0). We deduced that the cleavage of the C-H bond of the substrate is the rate-limiting step of catalysis. In the case of the deuterated substrate, the β-C-D bond requires more activation energy for cleavage and therefore, the turnover in saturated substrate conditions for the deuterated substrate is reduced in comparison to the non-deuterated substrate. However, we could only observe a KIE on k_{cat}. There was no distinct KIE when the substrate concentration was not saturated: KIE (k_{cat}/K_M) = 1.2 ± 0.1 (Table 9). These findings revealed that C-H cleavage is only rate-limiting if the protein is saturated with substrate, whereas at low substrate concentrations, the formation of the enzyme:substrate complex is dominating. These results implicate that formation of the enzyme:substrate complex is partially irreversible, meaning that the forward reaction is more likely than the decay of the enzyme:substrate complex. Therefore, we did not observe a KIE on k_{cat}/K_M. If the formation of the enzyme:substrate complex becomes the rate-limiting step, we have to focus on the definition of the K_M value for *Td*ETL. Usually, the K_M value is defined as a constant describing the substrate affinity of the enzyme:[147]

$$K_M = \frac{k-1+k2}{k1}$$

$$E + S \underset{k_{-1}}{\overset{k_1}{\rightleftharpoons}} [ES] \xrightarrow{k_2} [EP] \rightleftharpoons E + P$$

In the case of *Td*ETL, the forward reaction of the enzyme:substrate complex is more likely than substrate unbinding. This is represented by $k_2 > k_{-1}$. Thus, substrate binding becomes an almost irreversible step. Therefore, K_M can be redefined to $K_M = \frac{k2}{k1}$.

In addition, we also determined the KIE of the Y54F variant. The k_{cat} of Y54F is reduced three orders of magnitude in comparison to the wild type (section 3.2.3). However, we observed that substrate unbinding is slower than C-H cleavage, similar as shown for the wild type enzyme (KIE (k_{cat}) = 2.0 ± 0.2 KIE (k_{cat}/K_M) = 1.2 ± 0.1) (Table 9).

Table 9. Observed substrate kinetic isotope effects (KIE) of *Td*ETL WT and *Td*ETL Y54F at pH 7.5 using ergothioneine as substrate.

	KIE (k_{cat})	**KIE (k_{cat}/K_M)**
***Td*ETL WT**	1.8 ± 0.2	1.2 ± 0.1
***Td*ETL Y54F**	2.0 ± 0.2	1.2 ± 0.1

The presented irreversible substrate binding might result from a closed conformation of the active site loop domain. Therefore, we aimed at rendering substrate binding reversible by introducing several mutations that may impact loop conformation. These results are described in the following section.

3.4.2 Destabilization of the Closed Loop Formation

The loop region that covers the active site of *Td*ETL, consisting of residues 50-69, contains three conserved glycine residues (Gly55, Gly59, Gly61) (Figure 50).

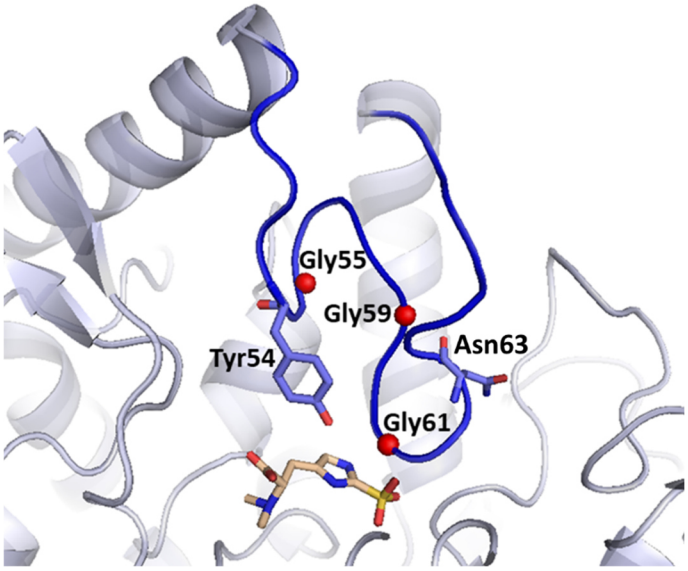

Figure 50. Crystal structure of *Td*ETL in complex with desmethyl-ergothioneine sulfonic acid (colored in wheat) (PDB: 6S7Q). The loop, consisting of residues 50–69 covering the active site, is colored in dark blue. The catalytic base Tyr54 and Asn63 are depicted in stick representation. Cα of the three glycine residues, Gly55, Gly59 and Gly61, are shown as red spheres.

These glycine residues are also conserved in MIO-dependent ammonia-lyases (Figure 51). Louie *et al.* suggested that conservation of the three glycine residues might facilitate the mobility of the active site loop in PAL.[56]

```
                  54        63
TdETL       ...GKPVYGLNRGVGWNKDKEFD...
BpETL       ...GQQIYGLTVGVGLNKDREMV...
PpHAL       ...DRTAYGINTGFGLLASTRIA...
RsTAL       ...ARHVYGLTTGFGPLANRLIS...
PcPAL       ...GTDSYGVTTGFGATSHRRTK...
```

Figure 51. Sequence alignment of the lid-loop of ergothionases *Td*ETL and *Bp*ETL and the aromatic amino acid lyases *Pseudomonas putida* histidine ammonia-lyase (*Pp*HAL), *Rhodobacter sphaeroides* tyrosine ammonia-lyase (*Rs*TAL) and *Petroselinum crispum* phenylalanine ammonia-lyase (*Pc*PAL). The conserved residues are highlighted in turquoise. Asn63 is only conserved in ergothionases (highlighted in violet). Counting based on *Td*ETL.

Since glycine has no side chain, this residue can adopt conformations that are not permissible for other amino acids. Thus, glycine residues often play the role of a hinge in non-canonical secondary protein

structures.[152] In order to determine if conformational changes of the active site loop are essential for substrate binding in *Td*ETL, we aimed to destabilize the closed loop formation by mutation of the glycine residues.

Since Gly55 is directly adjacent to the catalytic base Tyr54, we did not further investigate in this residue. Kinetic investigations of the G61A variant revealed a 500-times decrease in k_{cat} and catalytic efficiency compared to the wild type (Table 10). The crystal structure suggests that Gly61 makes van der Waals contacts with the substrate, which explains the decrease in activity.

Table 10. Observed kinetic parameters at pH 7.5 of *Td*ETL WT and variants using ergothioneine as substrate.

	k_{cat} [s^{-1}]	K_M [µM]	k_{cat}/K_M [$M^{-1}s^{-1}$]
***Td*ETL WT**	64 ± 3	45 ± 4	1.4 x 10^6
***Td*ETL G59V**	< 0.001	---	---
***Td*ETL G59A**	0.44 ± 0.01	34 ± 2	1.3 x 10^4
***Td*ETL G61A**	0.11 ± 0.01	27 ± 4	4.0 x 10^3

Gly59 is located on the active site lid-loop and might work as a hinge for loop-flexibility. The idea was that the introduction of a sterically more hindered valine residue at this position might cause a drastic decrease in loop flexibility. Indeed, the variant G59V did not show measurable activity ($k_{cat,G59V}$ < 0.001 s^{-1}). Inspection of the crystal structure suggests that in the closed conformation the propyl side chain of Val59 would clash with residues Asn63 and Lys66. Therefore, we constructed the variant G59A. Alanine is still less flexibility than glycine, though it is less sterically hindered than valine. Kinetic investigation of G59A showed a 150-fold decrease in k_{cat} and catalytic efficiency in comparison to the wild type (Table 10). The KIE both on k_{cat} and catalytic efficiency of that variant (KIE (k_{cat}) = 2.1 ± 0.1, KIE (k_{cat}/K_M) = 1.6 ± 0.2) showed that for G59A the decay of the enzyme:substrate complex is fast relative to the forward reaction. A possible explanation for the reduced k_{cat} might be that the variant induces a distortion of the closed enzyme:substrate complex. However, as shown above, even the slow Y54F variant do not render substrate binding reversible. It appears more likely that the G59A variant destabilizes the closed loop conformation which allows reversible substrate binding, represented by the KIE on catalytic efficiency of G59A.

3.4.3 Impact of the N63C Variant

In order to further investigate destabilization of the closed form of the active site loop, we constructed the variant N63C. Asn63 is part of the loop, however this residue is about 9 Å distance apart from the

active site (Figure 50). Asn63 forms a hydrogen bond to the side chain of Arg367 from chain C. Additionally Asn63 is connected to the backbone carbonyls of Arg367 and Ile377 from chain C *via* a crystallographic water (Figure 52). Arg367 interacts with Asp65 and Trp62, these two residues are located on the active site loop. Among ergothionase Asn63 is conserved, however not in MIO-dependent ammonia-lyases (Figure 51).

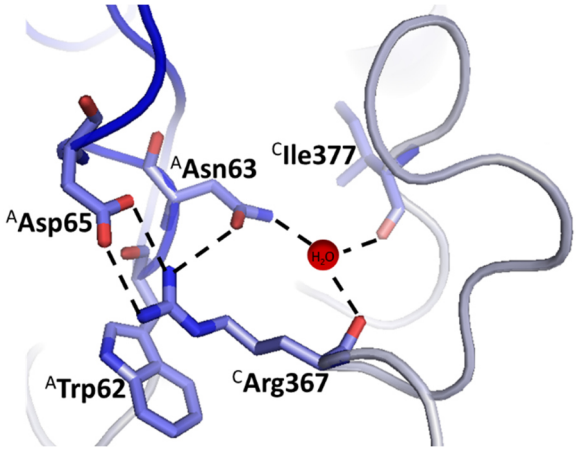

Figure 52. Close up view on the interactions of Asn63 and Arg367 in the crystal structure of *Td*ETL (PDB: 6S7Q). The active site loop is colored in dark blue. Asn63, Asp65 and Trp62 are part of the loop. Figure 50 gives an overview of the position of Asn63 within the loop.

Michaelis-Menten kinetics of N63C showed that k_{cat} is reduced 350-fold in comparison to the wild type (Table 11). The dramatic effect of that variant seems surprising because Asn63 is not part of the active site of *Td*ETL. Whereas, the great impact on catalysis of the N63C variant suggests that Asn63 might play a crucial role in stabilizing the closed conformation of the active site loop.

Table 11. Observed kinetic parameters of *Td*ETL WT and *Td*ETL N63C at pH 7.5 and pH 9 using ergothioneine as substrate.

		k_{cat} [s^{-1}]	K_M [µM]	k_{cat}/K_M [$M^{-1}s^{-1}$]
pH 7.5	**WT**	64 ± 3	45 ± 4	1.4 x 10^6
	N63C	0.18 ± 0.01	16 ± 3	1.2 x 10^4
pH 9	**WT**	28 ± 2	25 ± 5	1.1 x 10^6
	N63C	1.4 ± 0.1	25 ± 3	5.4 x 10^4

In order to investigate this proposition, we determined the substrate KIE of the N63C variant. The observed KIE on both k_{cat} (KIE = 2.4 ± 0.1) and on k_{cat}/K_M (KIE = 2.8 ± 0.1) at pH 7.5 shows that substrate binding is reversible and only C-H cleavage is rate-limiting (Table 12).

Table 12. Observed substrate kinetic isotope effects (KIE) of *Td*ETL N63C at pH 7.5 and pH 9 using ergothioneine as substrate.

		KIE (k_{cat})	KIE (k_{cat}/K_M)
N63C	**pH 7.5**	2.4 ± 0.1	2.8 ± 0.1
N63C	**pH 9**	1.8 ± 0.1	1.3 ± 0.1

A possible explanation is that the N63C variant destabilizes the closed loop conformation. As previously mentioned, Asn63 hydrogen bonds to Arg367. This hydrogen bond might stabilize the closed conformation of the active site loop. Since the thiol side chain of cysteine of N63C is a weak hydrogen bond acceptor, the stability of the closed loop conformation is reduced in the variant. Collectively, these results suggest that the N63C variant might allow reversible substrate binding through an open conformation of the active site loop.

Additionally, the substrate KIE of the N63C variant at pH 9 was only significant on k_{cat} (KIE = 1.8 ± 0.1) but not on k_{cat}/K_M (KIE = 1.3 ± 0.1) (Table 12). This finding can be rationalized because at pH 9, the introduced cysteine is mostly present in its thiolate form which forms a salt bridge to Arg367. This salt bridge stabilizes a closed loop conformation, similar as observed for the wild type enzyme (Figure 53). The influence on activity of the N63C variant at pH 9 also resembles more to the wild type and reduced k_{cat} only 20-fold in contrast to the 350-fold activity reduction observed at pH 7.5 (Table 11).

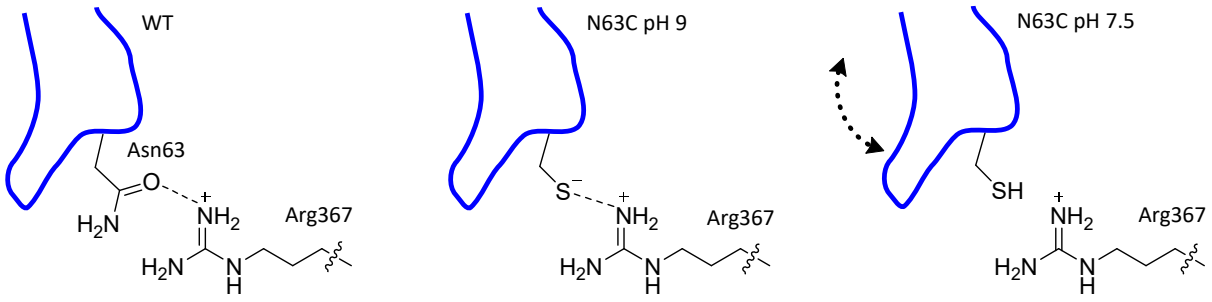

Figure 53. Interaction between Asn63 and Arg367 in the wild type enzyme (left) and the influence of the variant N63C on the interaction with Arg367 at pH 9 (middle) and pH 7.5 (right). The schematic active site loop is depicted in blue.

We further investigated the solvent KSIE of N63C at pH 7.5 (KSIE (k_{cat}) = 1.1 ± 0.1; KSIE (k_{cat}/K_M) = 1.4 ± 0.1). As outlined in section 0, the KSIE in *Td*ETL reflects protonation of the leaving group

trimethylamine, however interpretation of solvent isotope effects needed to be handled with care. The solvent KIE of the N63C variant could be off-set due to the isotope effect on the pK_a of the thiol because D_2O might lower the pK_a of the thiol.

In conclusion, the G59A variant and the N63C variant at pH 7.5 enabled reversible substrate binding due to destabilization of the closed loop-conformation. However, we have to consider that these results were based on kinetic data and molecular dynamics simulations may be necessary to predict the behavior of the loop domain in detail. Furthermore, a crystal structure of the N63C variant would be interesting for studying the orientation and possible interactions of the cysteine residue.

3.5 Occurrence of Ergothionase

Based on the presented characterization of *Td*ETL, we identified four residues, which are crucial for the degradation of ergothioneine and ergothioneine sulfonic acid (Tyr54, Lys64, Lys384, Glu412). We ran a UniProt database search and found around 300 homologue proteins with strict conservation of these four residues. These proteins are encoded by proteobacteria (185), firmicutes (77), synergistetes (19), and miscellaneous species from other phyla (Table 16). This group includes many species of gastrointestinal bacteria, such as *Blautia spp*., *Campylobacter spp*., *Clostridium spp*., *Escherichia spp*., *Paenibacillus spp*., and *Peptoniphilus spp*. The occurrence of ergothionase in the gastrointestinal system shows that ergothioneine degradation in the gut is widely distributed. This finding is in particular interesting because ergothioneine is recognized as an important micronutrient for humans that protects against inflammatory, cardiovascular or infective disease, cancer and neurodegeneration.[116] Whereas, ergothionase-mediated degradation of ergothioneine leads to the emergence of trimethylamine and the corresponding oxidative degradation product trimethylamine N-oxide. These degradative products are associated with atherosclerosis and severe cardiovascular diseases.[153–155] Our finding of ergothioneine degradation in the gut microbiome therefore questions the medical benefit of ergothioneine uptake.

3.6 Identification of a New Ergothioneine Sulfonic Acid Lyase

Beside the described ergothionase, we also worked on a related lyase from *Martelella endophytica* (*Me*Lyase). *Me*Lyase and *Td*ETL share over 45% sequence similarity and the catalytic important residues Tyr54, Lys384 and Glu412 (counting based on *Td*ETL) are conserved. Therefore, we suggest that both enzymes run the elimination reaction through a similar mechanism.

However, investigation on substrate specificity showed only barely turnover of ergothioneine (Table 13). The main substrate of *Me*Lyase is ergothioneine sulfonic acid (k_{cat} = 12 s^{-1}, k_{cat}/K_M = 3.2 x 10^4 $M^{-1}s^{-1}$) (Figure 54). The second best found substrate was *S*-methyl ergothioneine. All other tested compounds show negligible slow turnover by *Me*Lyase (Table 13).

Table 13. Observed activity of *Me*Lyase on different substrates in HEPES buffer at pH 7.5 using 2 mM substrate.

	Ergothioneine	TMH	Ergothioneine sulfonic acid	Desmethyl-ergothioneine	DMH	Desmethyl-ergothioneine sulfonic acid	*S*-Methyl ergothioneine
***Me*Lyase [1/s]**	4.7 x 10^{-5} ± 8 x 10^{-6}	2.4 x 10^{-5} ± 8 x 10^{-6}	12 ± 1	6.9 x 10^{-5} ± 9 x 10^{-6}	4.3 x 10^{-5} ± 5 x 10^{-6}	7.0 x 10^{-4} ± 3 x 10^{-5}	5.0 x 10^{-3} ± 1 x 10^{-4}

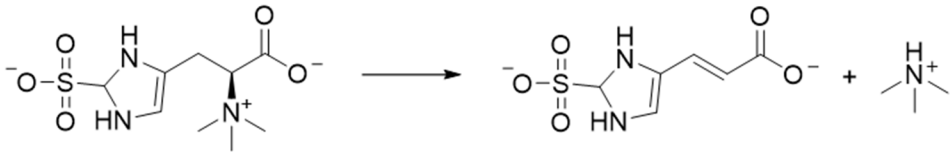

Figure 54. Catalyzed reaction of ergothioneine sulfonic acid lyase.

A sequence alignment of *Me*Lyase and ergothionases revealed that His84 (*Td*ETL counting) is not present in *Me*Lyase (Figure 55). Instead, *Me*Lyase has an arginine on this position (Arg87, *Me*Lyase counting). Histidine ammonia-lyases have a conserved histidine residue, which is suggested to be involved in zinc-dependent binding and orienting of the imidazole moiety of the substrate.[142] Mutation of this histidine to leucine in *Pp*HAL caused a complete loss in activity. In tyrosine ammonia-lyases a His-Leu dyad at the equivalent position is important for substrate specificity.[56] The mutation of histidine to phenylalanine in *Rs*TAL shifted TAL activity towards PAL activity.

```
                54          84          384         412
TdETL      ...KPVYGLNR...LLNSHCLGV...GTIQKTFTM...GTIEDHAS...
BpETL      ...QQIYGLTV...LIHAHSGSV...GAMEKPPTA...GGIEDIAT...
MeLyase    ...KPVYGLTT...VPQARAVGV...ATVQKTVSA...DGVEDHAS...
```

Figure 55. Abbreviated sequence alignment of the ergothionases *Td*ETL and *Bp*ETL and ergothioneine sulfonic acid lyase of *Martelella endophytica* (*Me*Lyase). The catalytic important residues for ergothionase activity are highlighted in turquoise, the conserved Arg residue for class-3 lyase activity is highlighted in orange. Counting based on *Td*ETL.

For *Td*ETL, His84 works as a hydrogen bond donor to Nτ of the imidazole moiety of the substrate (Figure 40). Hence, His84 participates in the stabilization of the crucial zwitterionic charge separation within the substrate during catalysis. Due to the cationic Arg87 in *Me*Lyase, ergothioneine cannot bind in the

cationic imidazolium state. Since the zwitterionic side chain of ergothioneine is crucial for catalysis, *Me*Lyase is barely active on ergothioneine. Whereas, the anionic head group of ergothioneine sulfonic acid can bind to Arg87, and thus allows turnover.

A UniProt database search suggested around 170 homologue lyases that possess a conserved arginine residue, in addition to the important catalytic residues, Tyr54, Lys384, Glu412 (counting based on *Td*ETL). Interestingly around 75% of these lyases belong to a family of rhizobia bacteria (Table 17). Rhizobia are aerobic, diazotrophic gram-negative bacteria that live symbiotically in roots nodules of plants, where they are responsible for N_2 fixation.[156]

In contrast, ergothionase mainly occurred in gut bacteria as outlined above (section 3.5). The different environment of the bacteria producing ergothionase or ergothioneine sulfonic acid lyases underlines that both lyases occur in a different type of bacteria. Ergothioneine sulfonic acid is an important metabolite of ergothioneine that emerges upon non-enzymatic oxidation of ergothioneine. We suggest that bacteria diverged to use ergothioneine sulfonic acid because of its availability in an oxidative environment.

3.7 Conclusion

This chapter outlined the key principles in the mechanism of ergothionase. Ergothionase catalyzes the first degradation step of ergothioneine, namely the elimination of the trimethylamine group, resulting in the formation of unsaturated thiourocanic acid. In the first part of this chapter, we outlined the acid-base dependent mechanism: the enzyme possesses a conserved tyrosine residue as base to abstract the β-proton of the substrate and a conserved glutamate and lysine residue to protonate the leaving group trimethylamine. In the second part of this chapter, we examined the substrate activation strategy of *Td*ETL. The enzyme stabilizes the polarized form of ergothioneine as thiolate and imidazolium. The cationic imidazolium in vicinity to the β-position increases the acidity of the β-proton of the substrate which facilitates β-C-H-bond cleavage. Additionally, *Td*ETL activates the leaving group through desolvation by binding the trimethylammonium group in an apolar pocket. The third part of the chapter focused on the loop, covering the active site of the enzyme. The absence of a KIE on k_{cat}/K_M suggests partially irreversible substrate binding. Replacement of a glycine residue within the loop by a more rigid alanine residue renders substrate binding reversible due to destabilization of the closed loop conformation. Furthermore, replacement of an asparagine with a cysteine residue within the loop enabled pH-dependent opening and closing of the active site loop. The finding that ergothionase is mainly produced by gut bacteria suggests that bacterial ergothioneine degradation should be considered while determining the availability and distribution of dietary ergothioneine in human tissues. Additionally, we identified a related new lyase that is responsible for ergothioneine sulfonic acid degradation.

3.8 Experimental

Recombinant Protein Production and Purification. The synthetic genes of *tdetI* wild type and variants were purchased from BioCat GmbH encoded on a pET28 plasmid. The gene of *bpetI* was already recloned without its leader sequence in a pET28 plasmid equipped with C-terminal His-tag in a previous work in our lab.

For gene expression, the plasmids were transformed into $CaCl_2$ competent *E.coli* BL21(DE3). In case of *bpetI*, the plasmid was transformed into $CaCl_2$ competent *E.coli* BL21(DE3) coexpressing molecular chaperones. Cells were grown at 37 °C in LB-medium supplemented with kanamycin (50 µg/mL), chloramphenicol (34 µg/mL) and in case of *bpetI* additionally ampicillin (100 µg/mL). As soon as optical density reached OD_{600} 0.6, isopropyl-β-D-thiogalactopyranosid (0.1 mM) was added. The cultures were incubated for either 4 h at 37 °C or 16 h at 18 °C. Cells were harvested by centrifugation (20 min, 15000 x g) and the pellet was stored at -20 °C.

Frozen cell-pellet was lysed by sonication (Sonifier 250, Branson) in lysis buffer (300 mM NaCl, 50 mM Na_2HPO_4 pH 8). Cell debris was removed by centrifugation (1 h, 80000 x g). The soluble protein was purified by Ni^{2+} NTA affinity chromatography (Qiagen). Proteins were washed using increasing concentrations of imidazole (10 mM, 20 mM) in lysis buffer, afterwards purified protein was eluted by lysis buffer supplemented with 250 mM imidazole. The protein was dialyzed into Tris-HCl (50 mM, pH 8) and NaCl (50 mM). Protein concentration was determined by UV at 280 nm (Nanodrop2000, Thermo Scientific) using the calculated extinction coefficient.[157] Protein homogeneity was assessed by SDS-PAGE.

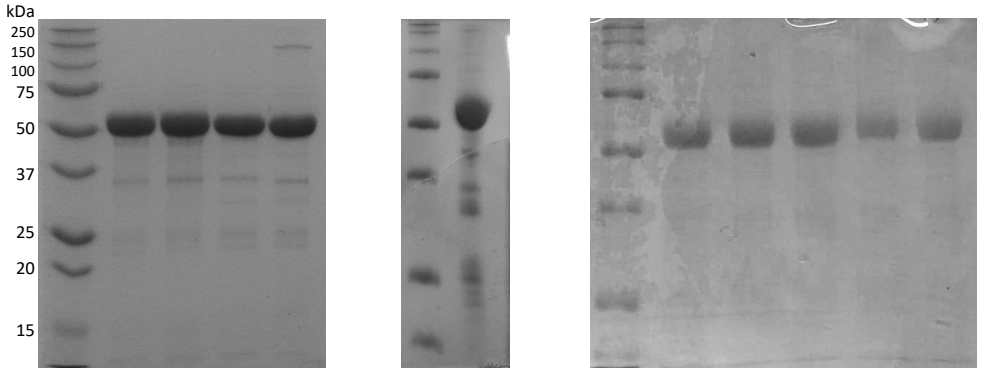

Figure 56. SDS-PAGE of the purified proteins *Td*ETL WT, Y54F, K64M, E412Q (left gel, lane 2-5), K384M (middle gel, lane 2), *Td*ETL WT, G59A, G59V, G61A, N63C (right gel, lane 2 – 6). Lane 1 in all gels shows the protein standard (Precision Plus Protein Standard, Bio-Rad).

>*Treponema denticola* ETL wild type (Accession number: WP_010693216)

MGSSHHHHHHSSGLVPRGSHMDALILTGKPLSLEDVYSVAYNNRQVKISDDAEERVKKARQILFDMAAEGKPVYG
LNRGVGWNKDKEFDEDFFATYNRNLLNSHCLGVKPYHPDEQVRAILLLRLNKALTGHTGISAELLHHYRDFLNYG
IHPRIPMRSSIGEGDITTLSHIGLAFIGEEDVSFNGEIMNSKKAMEKAGLKPAKLGPKDGLSIVSCNAQGEAMTA
IVLKEIEDLVYMSNLIFCLSLEGLNGVVQSLREDVNAVRGIKGQIKAAEMCREFLKGSFLYDPDPERALQDPLSF
RCAHSVNGTMYDAMDYVREQLLTTMNTTDDNPCIIIDEHSSFVSANFEITSLAIGVEMLATALSHLSKTSCYRMI
KLADPSFTKLNRFLTPQDVKTIAFGTIQKTFTMLDTQNRGLANPSSMDFYSLAGTIEDHASNLPLACYKIFQMLD
NIRYIIGIEAMHAAQAIDLRGNKKLGEGTKKAYSLIREVLPFYNEDRNISRDIETMYEFIKSKKLLNI

In order to confirm the sequence of *Td*ETL WT, the protein was digested using 0.8 mg/mL *Td*ETL WT was incubated with 0.08 mg/mL Chymotrypsin in Tris-HCl (50 mM, pH 8) for 16 h. The digested fragments were analysed by UPLC-HR-ESI-MS (Bruker, maXis II ESI-TOF).

Table 14. Chymotryptic fragments of *Td*ETL WT.

Fragment	Expected mass [m/z]	Observed mass [m/z]
NNRQVKISDDAEERVKKARQIL	2610.4434	2610.4673
REDVNAVRGIKGQIKAAEM	2085.1233	2085.1432
NTTDDNPCIIIDEHSSF	1920.8280	1920.8413
GVKPYHPDEQVRAIL	1721.9333	1721.9868
NEDRNISRDIETM	1592.7333	1592.7028
GSSHHHHHHSSGL	1416.6264	1416.612
AGTIEDHASNLPL	1337.6695	1337.6463
RSSIGEGDITTL	1248.6430	1248.6201
SIVSCNAQGEAM	1209.5238	1209.5173
TPQDVKTIAF	1119.6044	1119.6113
RCAHSVNGTM	1075.4771	1075.4811
TGHTGISAEL	985.4949	985.4771
GIHPRIPM	920.5134	920.5142
DPDPERAL	912.4421	912.4428
IGEEDVSF	895.4043	895.3879
IREVLPF	873.5192	873.5035
GEGTKKAY	853.4414	853.4546
HAAQAIDL	838.4417	838.4263
AAEGKPVY	834.4356	834.4198
DTQNRGL	803.4006	803.392
GTIQKTF	794.4407	794.4312
VPRGSHM	783.3930	783.373
NKDKEF	780.3886	780.3749
IIGIEAM	746.4117	746.3974
KEIEDL	746.3930	746.3974
IKSKKL	716.5029	716.5086
NGVVQSL	716.3937	716.3959

RGNKKL	715.4573	715.4628
NRGVGW	688.3525	688.3573
SKTSCY	688.2970	688.3031
DNIRY	680.3362	680.3368
NSKKAM	678.3603	678.3639
VREQL	644.3726	644.3678
AIGVEM	619.3119	619.2999
ANPSSM	606.2552	606.2601
GPKDGL	586.3195	586.3116
NSHCL	573.2449	573.2353
NGEIM	563.2494	563.2379
EITSL	562.3082	562.2969
KPAKL	556.3817	556.3706
CREF	554.2391	554.2474
VSANF	537.2667	537.2561
ADPSF	536.2351	536.2312
SHIGL	526.2983	526.2877
EDVY	525.2191	525.2288
DEDF	525.1827	525.1904
EKAGL	517.2980	517.2957
TAIVL	516.3391	516.3286
NRNL	516.2889	516.2878
TGKPL	515.3187	515.3148

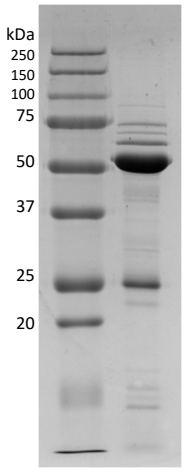

Figure 57. SDS-PAGE analysis of the purified protein *B.pseudomallei* ETL (lane 2). Lane 1 shows the protein standard (Precision Plus Protein Standard, Bio-Rad).

> *Burkholderia pseudomallei* ETL wild type (Accession number WP_004535976.1)
GDVTLDGRSVTPESIARIADGEAVSIAPAARQRVAAAHEVLLKAAAAGQQIYGLTVGVGLNKDREMVDAHGKLSQ
EVIDASTRFNIGLIHAHSGSVGPDMSVRVARAAMAARLNAMLDGGAGVQPAIVDAYAQFLNRGVTPAMPADGSIG

EADITILSHVGLAMLGEGDVYYQGRKLAAADALKLAGI**A**TIYPYGKDALAILSSNAYSAGMAALALTDMARLARV
SKLVFALGLQGLNGNVSPFREDTLALRPFPAALRAGAALRTLLAGSSLWNKDPDRPLQDPLSFRSGVYLLGEEDR
TYDEARALLQVQLNSSDDNPGVAVSVAPKSNRAQDAAGYVDGGGAVLPSANFEPLPWVLAFEQLGLALGHNALAS
AQRIVKLNDSHLSGLSRFLGTEETVHAFGAMEKPPTALAMTIKTLATPVSLDYLPVAGGIEDIATNAPEVVQRVQ
KQIDASYTLLGLELVEAAQAIDLRRRRQSSFTLAPATQPLYRALRAKVAFLERDRPLTPDFRAADTLLRAYRDLE
HHHHHH

The mass of the purified protein *Bp*ETL was determined on a Bruker maXis II ESI-TOF coupled to Shimadzu Nexera-X2 equipped with a Phenomex C4 column (Jupiter, 300A, 50 x 2 mm, 5 Microns).

MW_{obs} = 56236 Da

MW_{exp} (*Bp*ETL WT) = 56206 Da

MW_{exp} (*Bp*ETL A189T) = 56236 Da

The observed mass difference to the initial expected mass of *Bp*ETL WT was 30 Da. Renewed sequencing of *bpetI* revealed the mutation A189T. Considering the mutation the observed mass is correct. As Ala189 is not conserved in ergothionases we assume the mutation does not affect activity.

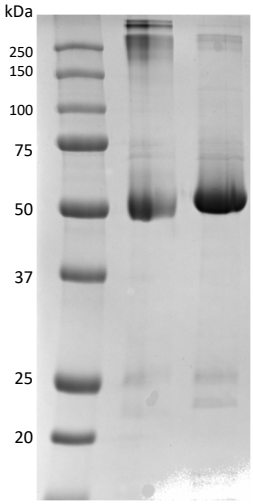

Figure 58. SDS-PAGE analysis of the purified protein *S.jonesii* ETL (lane 2 and lane 3). Lane 1 shows the protein standard (Precision Plus Protein Standard, Bio-Rad).

> *Synergistes jonesii* ETL wildtype (Accession number WP_037974058.1)
GSSHHHHHHSSGLVPRGSHMKVILTGNDLTVDKVWDIAVKGAEVEISPEADATLEASRKLVYELVDADVPVYGFN
TGVGWNKDHKIAKEFFEEFNRKLIYCHTFGVGAEASEAEVRAVMAVRLNCLLLGYTGVQPAVARRYAELLNAGVH

PVVPEKGSVGEADLTQLAHIGLAMIGEGEVNYKGRRMSSAEAHKLAGLEPVVLGPKDGLAVVSSSSFSAGEAALV
FKELAELADMGDIISSLSLEGLNGNTSPLEAEVMAARGLAGQAKCAENMRGYLEGSDIYEAYPGKPVQDPLCFRG
AAYVNGSLRDALEYAEKYLFIQMNSTDDNPCLLLKEKRIISNSNFETTTLATAMEMLAIVLSHVSRMSCYRMLRL
ANPELTHLSRFLSHDGGESHCFGTIQKCFASLDTEIRHLSNPCSVDYLSLSGSIEDHANNTPLVVQHLRQIVQDL
QYIYGIELIHACQAIELRKRQGGFTLGRGTAAAYDAFRRALPLYTNDRPLAPDVKKAYEFVKSAALVESVKR

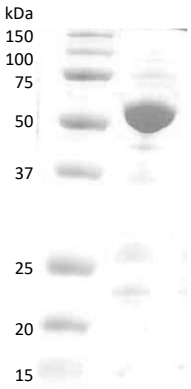

Figure 59. SDS-PAGE analysis of the purified protein *Me*Lyase (lane 2). Lane 1 shows the protein standard (Precision Plus Protein Standard, Bio-Rad).

>*Me*Lyase (Accession number WP_045679505.1)
MGSSHHHHHHSSGLVPRGSHMVVSSHLVFGQSAVSHADIIAVARHGARVSLAPELLQALADCRSLIDRAIAEDKP
VYGLTTGLGAGVDTRLDVADLVAFQNRVPQARAVGVGAALPAETVRALMAARLAGFTSASSGASPSVAEALAAAL
NAHFHPVVPALGSIGTADLSPLSAMVRGLMGHGEVALDGDIMEAAEALSKAGLEPLKLGPRDGHALVVGNSLSIG
RACLALDDLGRLLDWSFASLALSFEAFRASVTVLDQRALARRPAFGQQEAGERLSALLAGSSLLKEGAARRLQDP
LSYRCAPQIWGALVHAFEEAAVATEIELAGAGDNPIVLADEGELIHNGNFDTTAFALSWERLGLAIAQCASATAW
RTMKIMSPGISELPRFLTAHGGSRTGFATVQKTVSALEAEIRHLAHPVAFAPIPVADGVEDHASMAPSVIAKTEA
MIERFRYLVAIELVATAQAAELRGVESELGAGTAVAYEKVRGQVPPLTEDRAMGPDFQKLSEFIRLNDAGR

Reagents. Ergothioneine, desmethyl-ergothioneine, *S*-methyl ergothioneine and trimethylhistidine were synthesized by David Lim.

Ergothioneine sulfonic acid and desmethyl-ergothioneine sulfonic acid were obtained from Tetrahedron (http://www.tetrahedron.fr).

Deuterated N-α-trimethylhistidine (D_5, 98%; $^{15}N_3$, 98%; ReseaChem GmbH) was converted to deuterated ergothioneine by using the enzyme EanB.(Burn et al., 2017) For this purpose, 5 mM TMH was incubated in the presence of Na_2S (100 mM) and EanB (20 µM) for 50 h in phosphatebuffer

(100 mM, pH 8) and NaCl (100 mM). Both TMH and deuterated TMH were used as substrate and treated equally. Finally, EanB was denaturated by heat-shock and precipitated protein as well as precipitated sulfur was removed by centrifugation. The purity and concentration of both ergothioneine and deuterated ergothioneine was examined by ion-exchange chromatography (Figure 60). MS: *m/z* calc. for $C_9H_{16}N_3O_2S$ $[M]^+$ 230.10, found 230.15. *m/z* calc. for $C_9H_{12}D_4{}^{15}N_3O_2S$ $[M]^+$ 237.12, found 237.15.

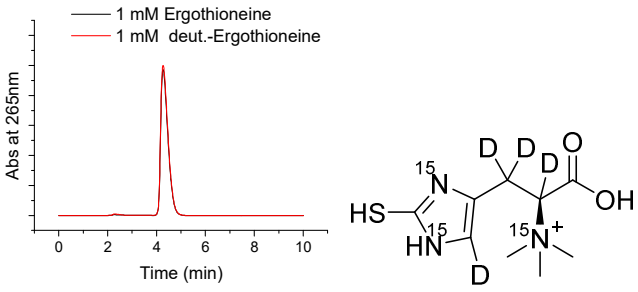

Figure 60. Ion-Exchange HPLC Chromatogram of 1 mM deuterated and 1 mM non-deuterated ergothioneine recorded at 265 nm.

Product Identification. The products formed during the elimination reaction were analyzed by ESI-MS (Bruker Esquire3000plus).

Thiourocanic acid: $[M+H]^+_{calc.}$ = 171.01, $[M+H]^+_{obs.}$ = 171.02

Sulfono urocanic acid: $[M+H]^+_{calc.}$ = 219.00, $[M+H]^+_{obs.}$ = 219.10

S-methyl urocanic acid: $[M+H]^+_{calc.}$ = 185.03, $[M+H]^+_{obs.}$ = 185.10

Urocanic acid: $[M+H]^+_{calc.}$ = 139.04, $[M+H]^+_{obs.}$ =139.05

pH-Dependence of *Td*ETL WT

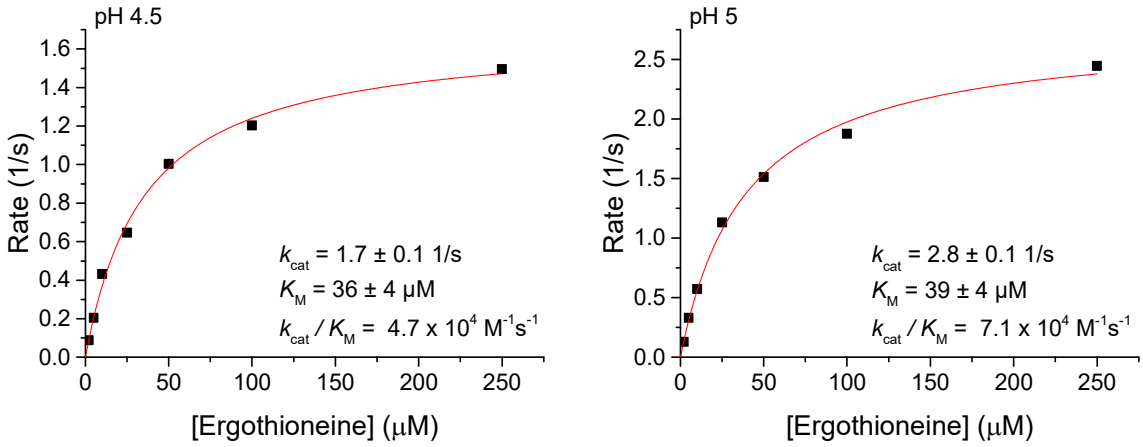

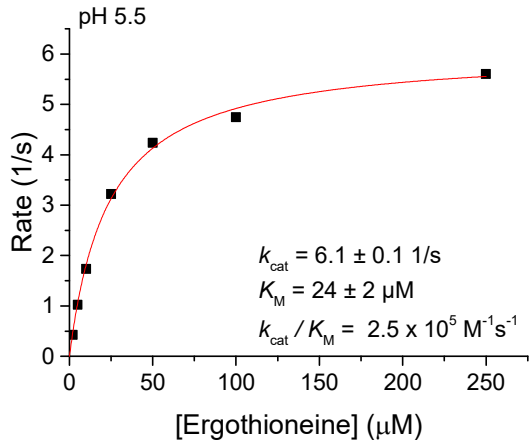

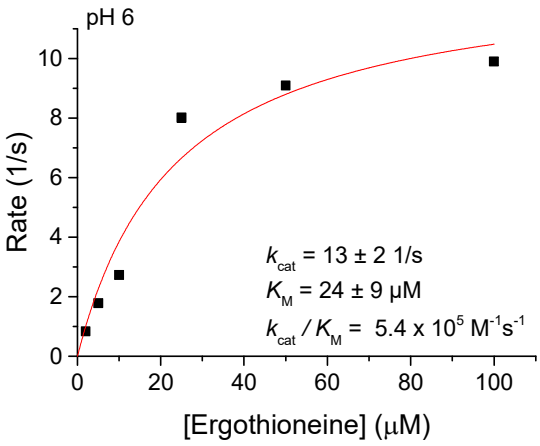

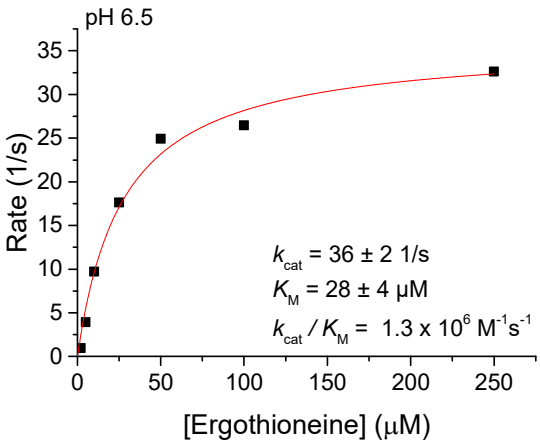

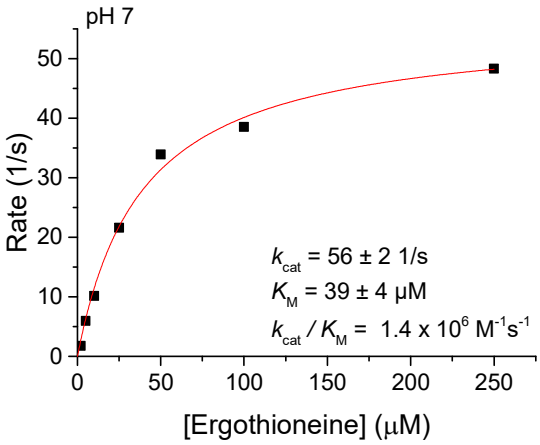

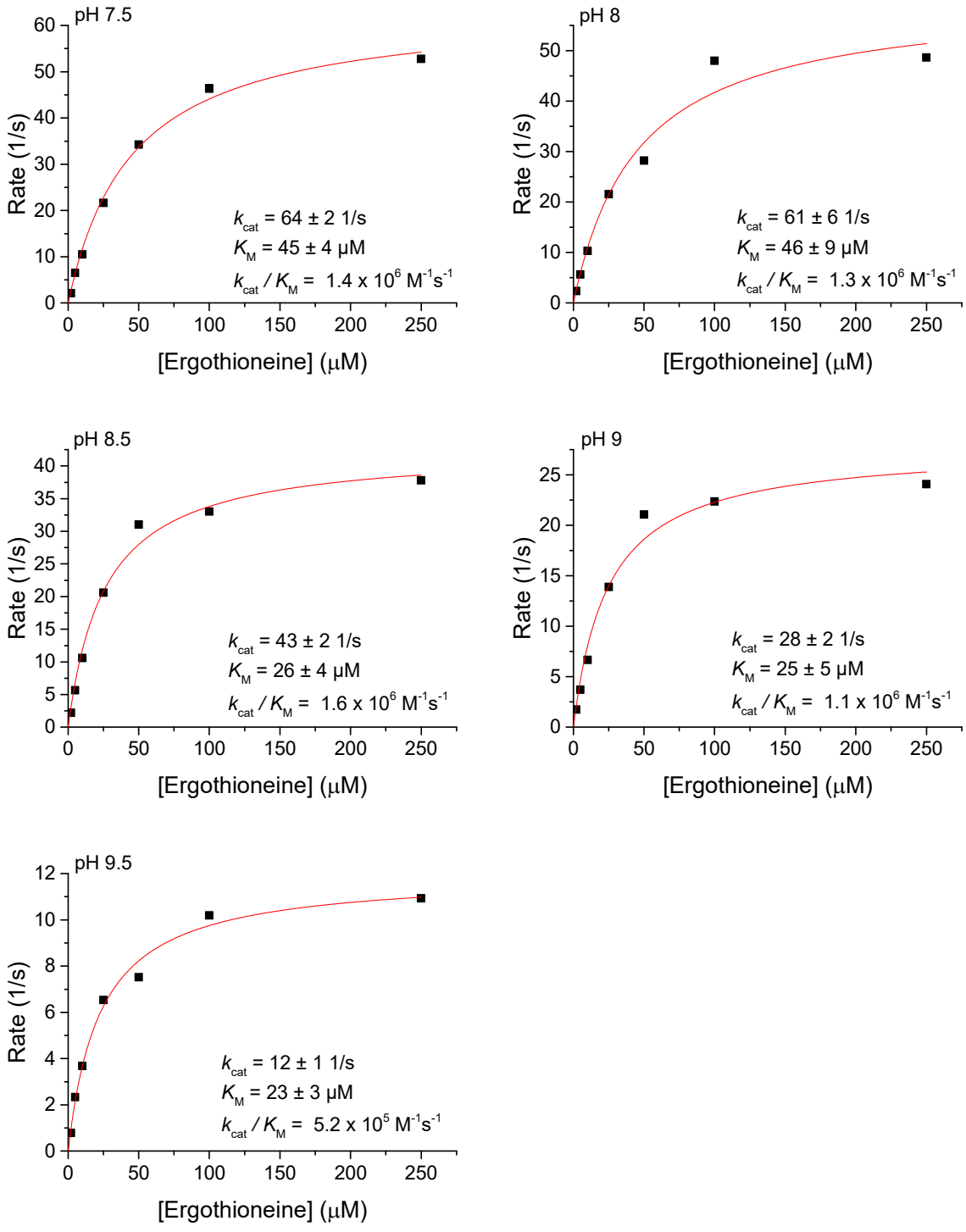

Figure 61. Michaelis-Menten Kinetics of *Td*ETL WT at pH 4.5 – pH 9.5. A buffer solution containing 40 mM acetic acid, 40 mM boric acid and 40 mM phosphoric acid (BR-buffer) was adjusted with NaOH to the desired pH. Ergothioneine substrate concentration was in between 2 µM and 250 µM. Enzyme concentration was in between 0.01 µM and 0.2 µM. Formation of the product thiourocanic acid at 23 °C was monitored using the spectrophotometer (Variant Cary 300 UV-Vis spectrophotometer). $\varepsilon_{311\,nm}$ (thiourocanic acid) = 22500 $M^{-1}cm^{-1}$.

pH-Dependence of *Bp*ETL

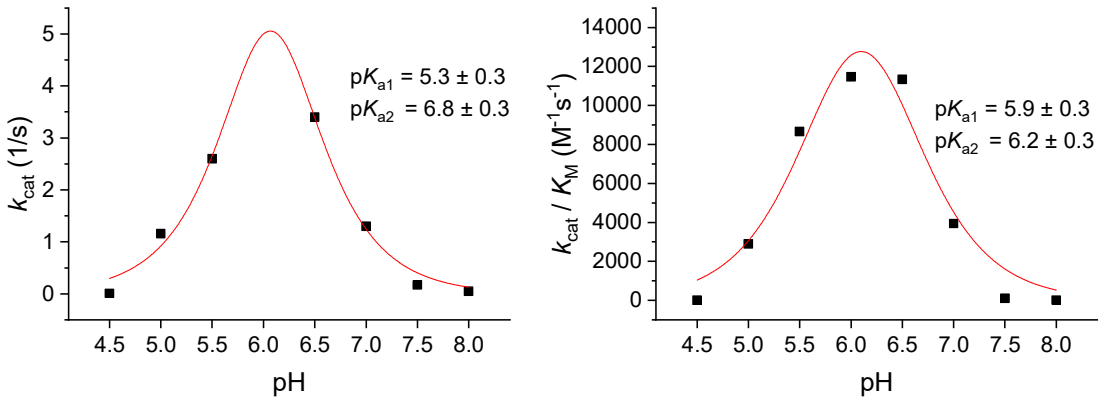

Figure 62. pH-Dependent k_{cat} and k_{cat}/K_M values of *Bp*ETL WT. pH dependent kinetic parameters were fitted to y = k_{HA}/ $(1+10^{(pKa1-pH)} + 10^{(pH-pKa2)})$.

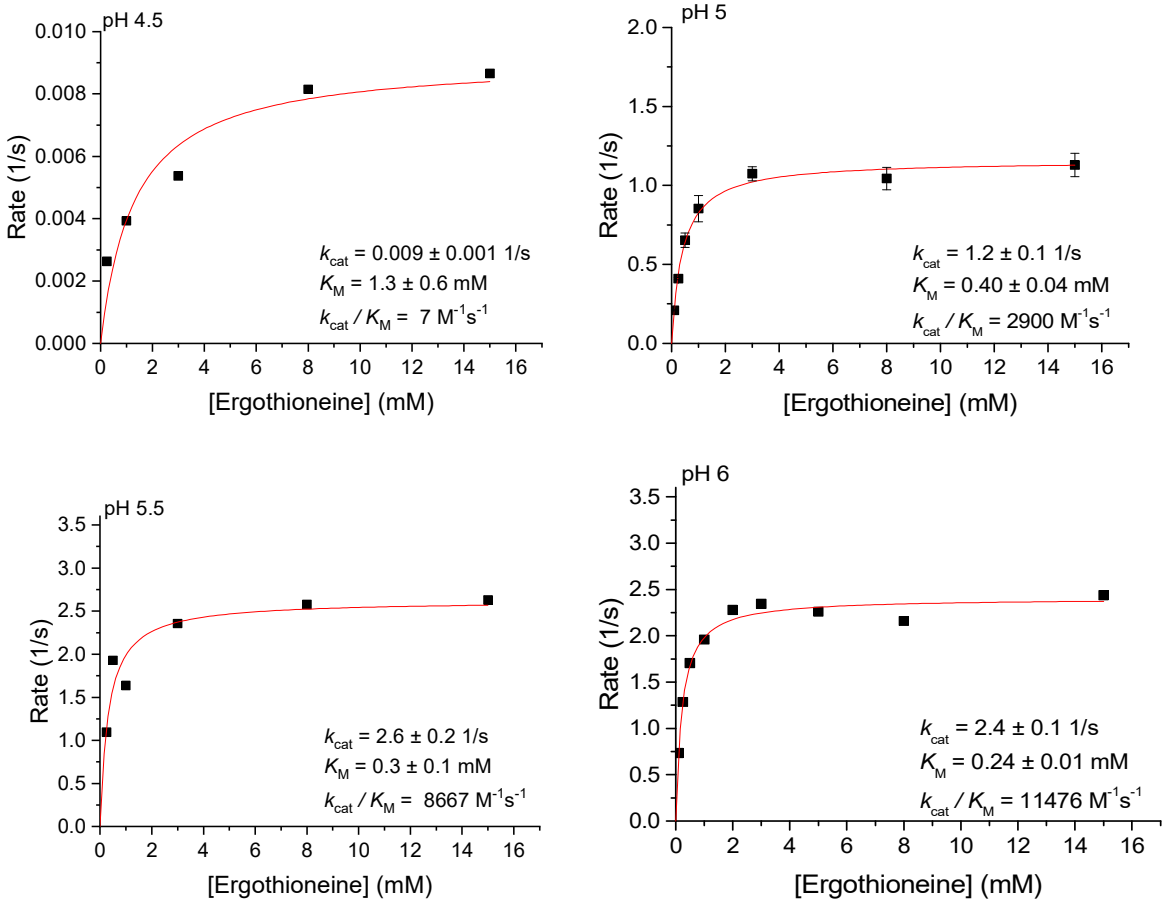

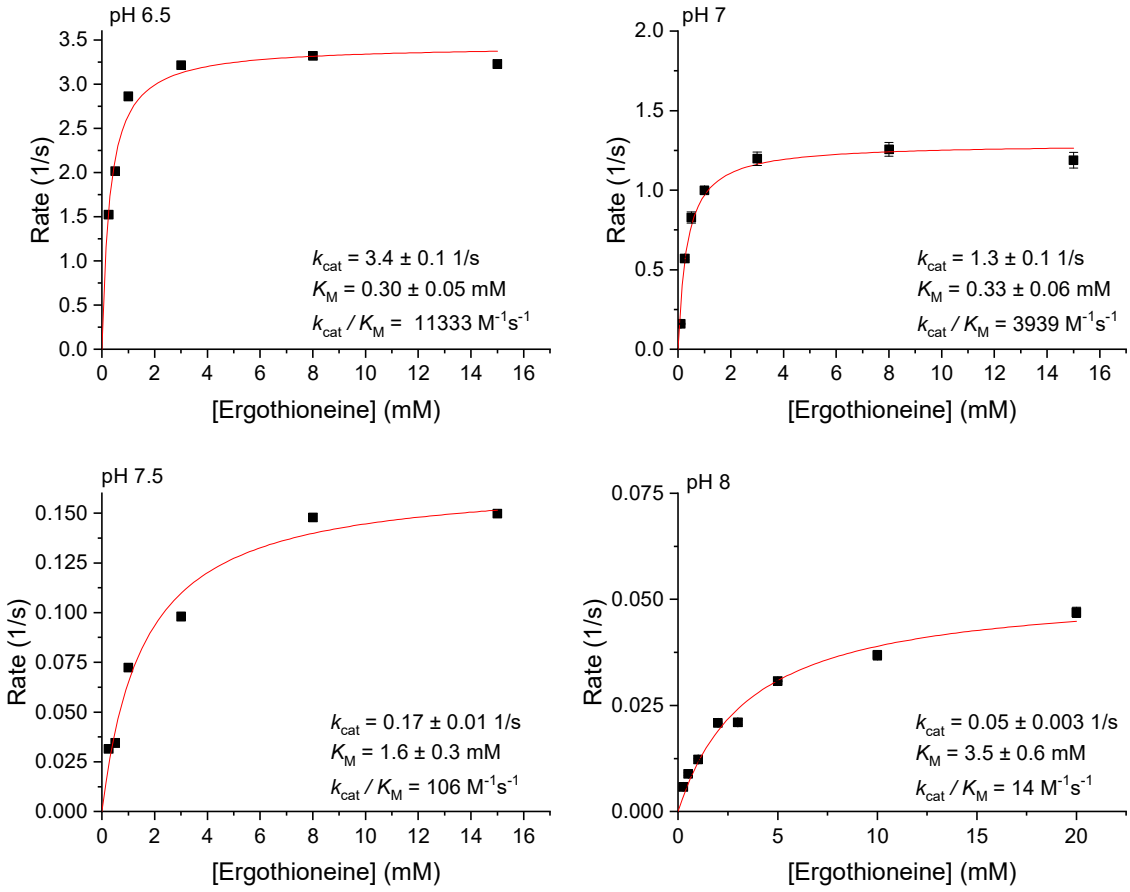

Figure 63. Michaelis-Menten Kinetics of *Bp*ETL WT at pH 4.5 – pH 8. A buffer solution containing 40 mM acetic acid, 40 mM boric acid and 40 mM phosphoric acid (BR-buffer) was adjusted with NaOH to the desired pH. Ergothioneine substrate concentration was in between 0.1 mM and 20 mM. Enzyme concentration was in between 0. 1 µM and 1 µM. Formation of the product thiourocanic acid at 23 °C was monitored using the spectrophotometer (Variant Cary 300 UV-Vis spectrophotometer). $\varepsilon_{311\ nm}$ (thiourocanic acid) = 22500 $M^{-1}cm^{-1}$.

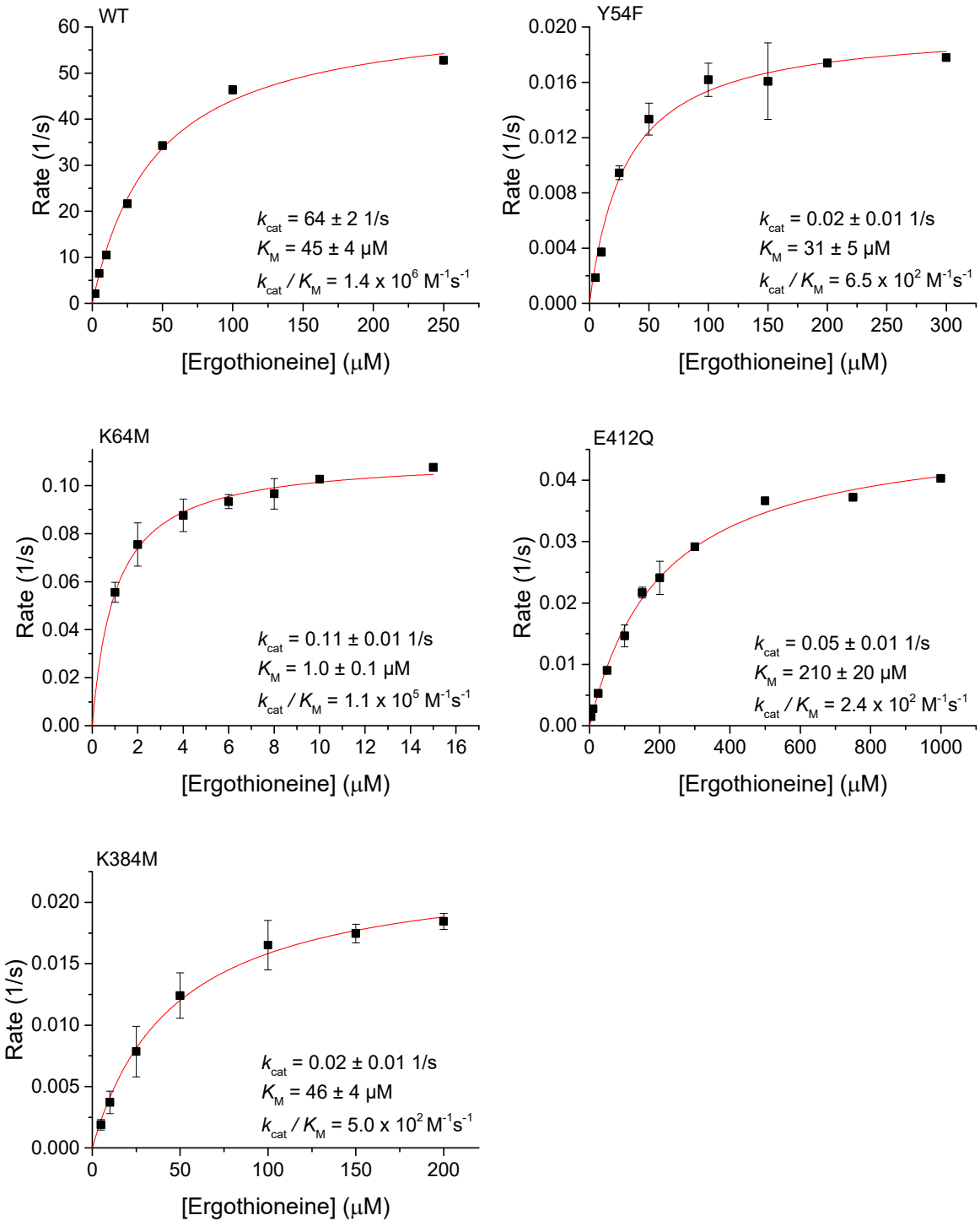

Figure 64. Michaelis-Menten Kinetics of *Td*ETL WT, Y54F, K64M, E412Q, K384M at pH 7.5. Ergothioneine substrate concentration was in between 1 μM and 1000 μM. Enzyme concentration was 2 μM for Y54F, E412Q and K384M and 0.2 μM for K64M. Formation of the product thiourocanic acid at 23 °C was monitored using the spectrophotometer (Variant Cary 300 UV-Vis spectrophotometer). ε_{311nm} (thiourocanic acid) = 22500 $M^{-1}cm^{-1}$.

pH-Dependence of *Td*ETL K64M

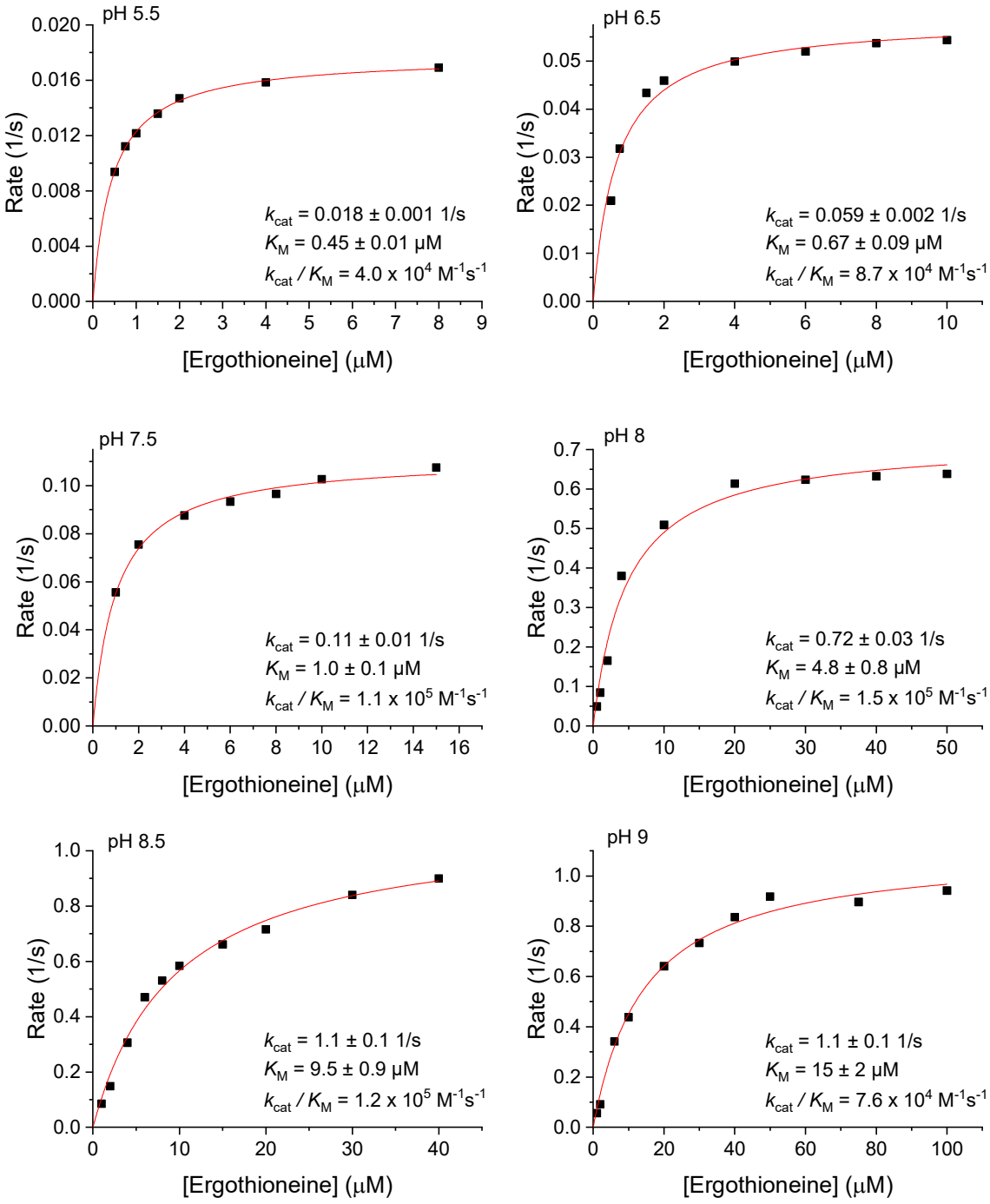

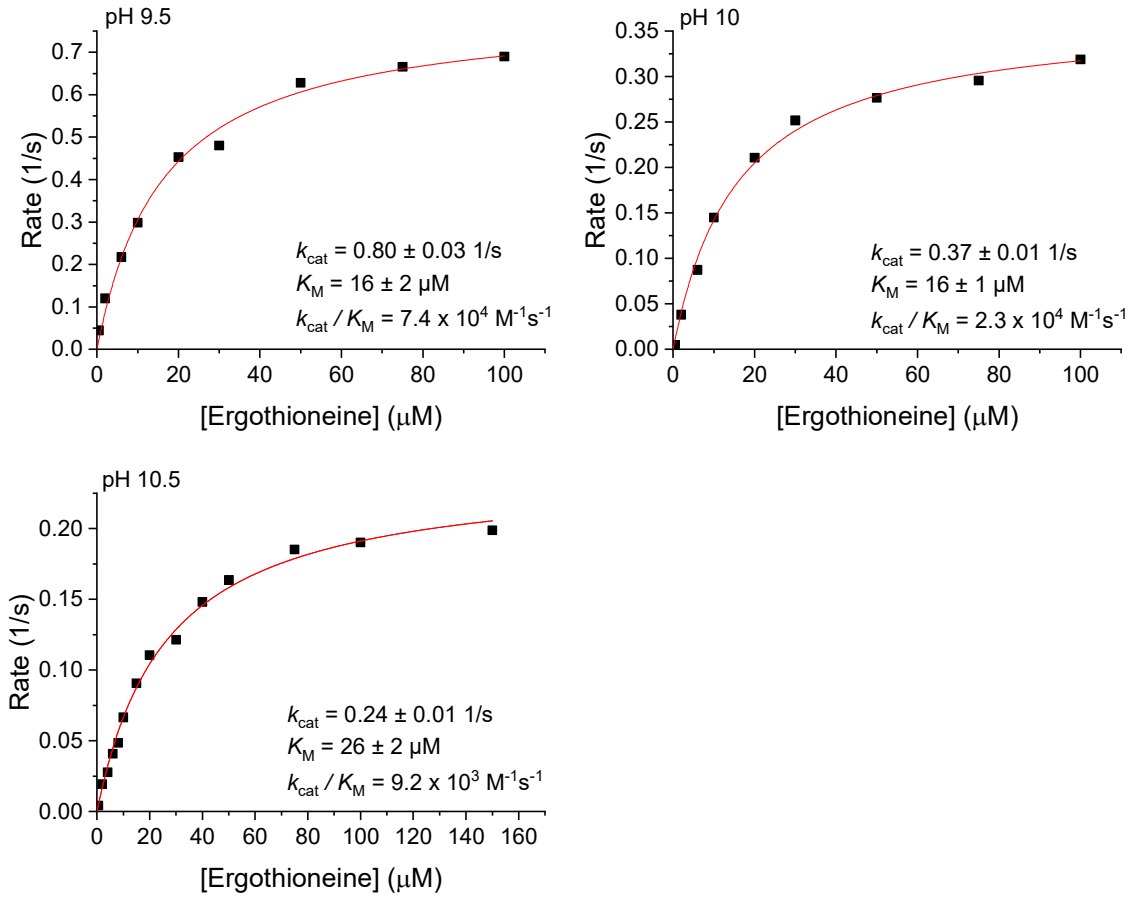

Figure 65. Michaelis-Menten Kinetics of *Td*ETL K64M at pH 5.5 – pH 10.5. A buffer solution containing 40 mM acetic acid, 40 mM boric acid and 40 mM phosphoric acid (BR-buffer) was adjusted with NaOH to the desired pH. Ergothioneine substrate concentration was in between 0.5 µM and 160 µM. Enzyme concentration was in between 0.2 µM and 0.5 µM. Formation of the product thiourocanic acid at 23 °C was monitored using the spectrophotometer (Variant Cary 300 UV-Vis spectrophotometer). $\varepsilon_{311\ nm}$ (thiourocanic acid) = 22500 M^{-1}cm^{-1}.

Substrate specificity. Substrate specificity was monitored in HEPES buffer at pH 7.5 using 2 mM of substrate by measuring the rate of product formation at 23 °C in a 1 cm quartz cuvette using a Variant Cary 300 UV-Vis spectrophotometer. If the activity was too low to determine Michaelis-Menten kinetics, enzyme concentration of 5 µM was used to follow turnover. ε_{311}.(thiourocanic acid) = 22500 M^{-1}cm^{-1}; ε_{295}.(urocanic acid, pH 7.5) = 38565 M^{-1}cm^{-1}, ε_{295}.(sulfono thiourocanic acid) = 15890 M^{-1}cm^{-1}; ε_{295}.(*S*-methyl thiourocanic acid) = 12170 M^{-1}cm^{-1}.

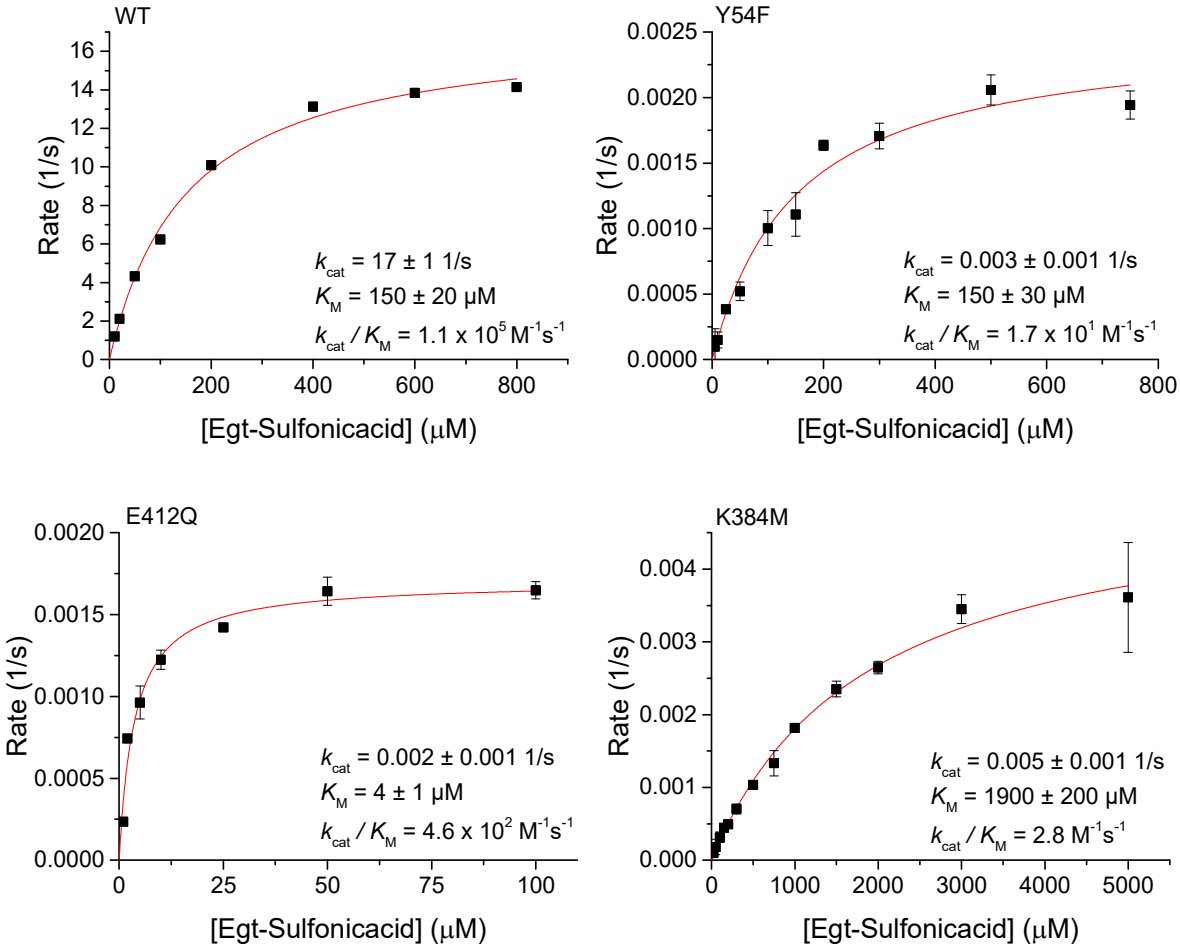

Figure 66. Michaelis-Menten Kinetics of *Td*ETL WT (upper left), Y54F (upper right), E412Q (lower left), K384M (lower right). Ergothioneine sulfonic acid substrate concentration was in between 1 μM and 5000 μM. Enzyme concentration was 0.02 μM for WT and 4 μM for Y54F, E412Q and K384M. Formation of the product was monitored using the spectrophotometer (Variant Cary 300 UV-Vis spectrophotometer). ε_{295nm} (sulfono thiourocanic acid) = 15890 $M^{-1}cm^{-1}$.

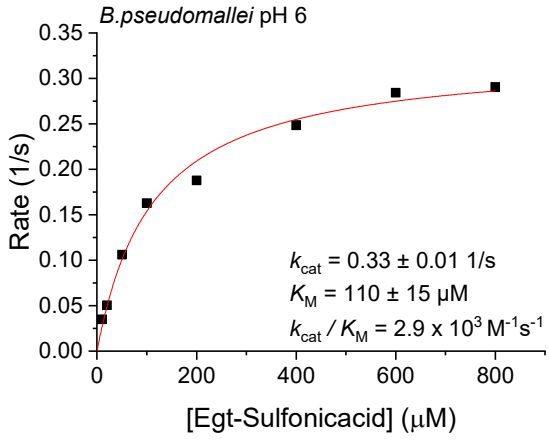

Figure 67. Michaelis-Menten Kinetics of *Bp*ETL WT. Ergothioneine sulfonic acid substrate concentration was in between 20 μM and 800 μM. Enzyme concentration was 1 μM. Formation of the product was monitored using the spectrophotometer (Variant Cary 300 UV-Vis spectrophotometer). ε_{295nm} (sulfono thiourocanic acid) = 15890 $M^{-1}cm^{-1}$.

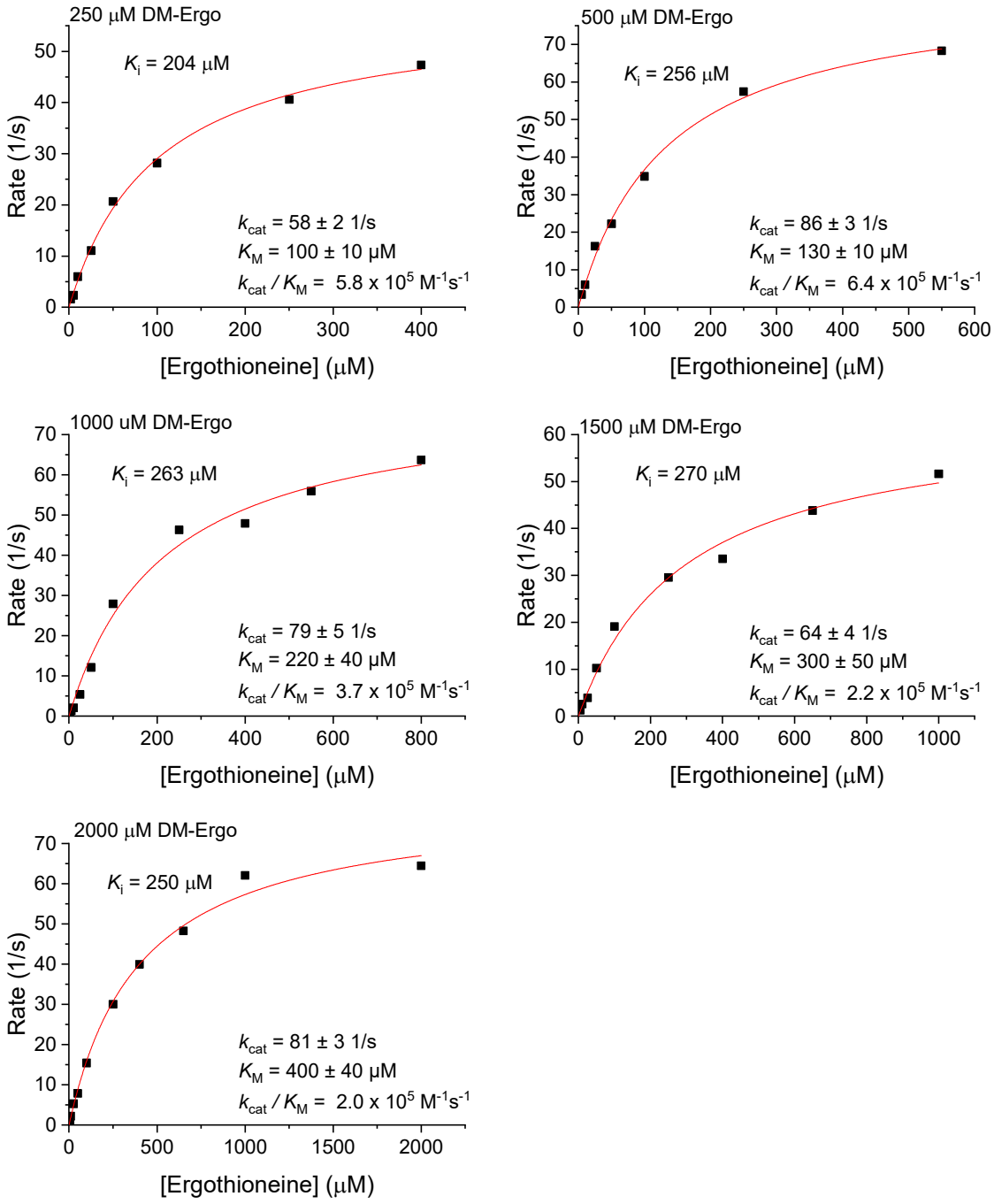

Figure 68. Michaelis-Menten Kinetics of *Td*ETL WT in HEPES buffer at pH 7.5 using ergothioneine as substrate in the presence of 250 - 2000 µM desmethyl ergothioneine. Formation of the product was monitored using the spectrophotometer (Variant Cary 300 UV-Vis spectrophotometer). ε_{311}.(thiourocanic acid) = 22500 M^{-1}cm^{-1}. Desmethyl-ergothioneine inhibits *Td*ETL in a competitive model with ergothioneine. Obtained kinetic data were fit to $\boldsymbol{K_i = \frac{K_M * [I]}{K_{M(app.)} - K_M}}$. K_i (desmethyl ergothioneine) = 249 ± 23 µM.

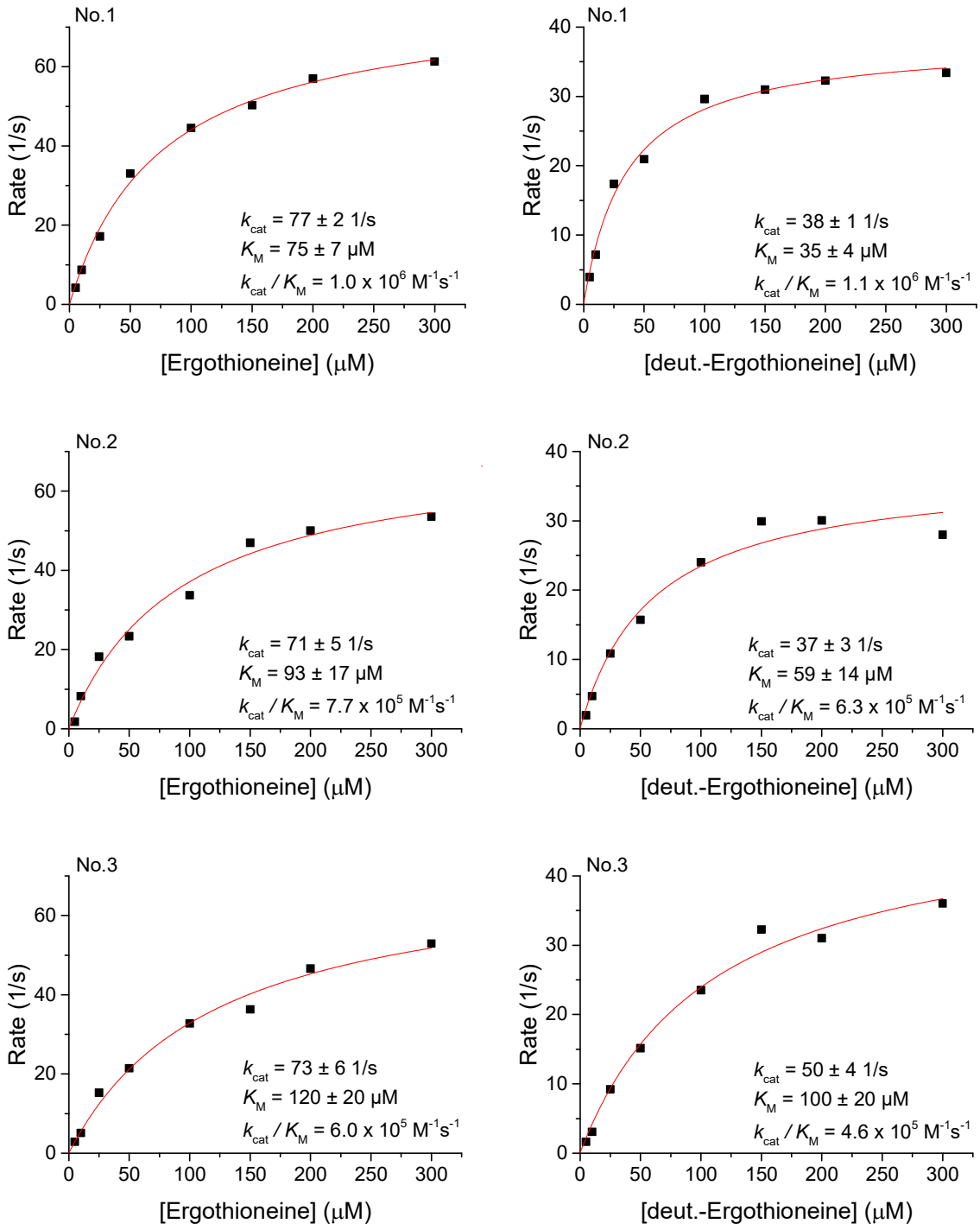

Figure 69. Michaelis-Menten Kinetics of *Td*ETL WT in HEPES buffer at pH 7.5 using ergothioneine (left figures) or deuterated ergothioneine (right figures) as substrate. Deuterated histidine (D_5, 98%; $^{15}N_3$, 98%; ReseaChem GmbH) was converted to deuterated N-α-trimethyl histidine according to the published protocol.[158] Deuterated N-α-trimethyl histidine was converted to deuterated ergothioneine using the enzyme EanB.[105] Substrate concentration was in between 5 μM and 300 μM. Enzyme concentration was 0.01 μM. Formation of the product was monitored using the spectrophotometer (Variant Cary 300 UV-Vis spectrophotometer). ε_{311}.(thiourocanic acid, pH 7.5) = 22500 M^{-1}cm^{-1}.

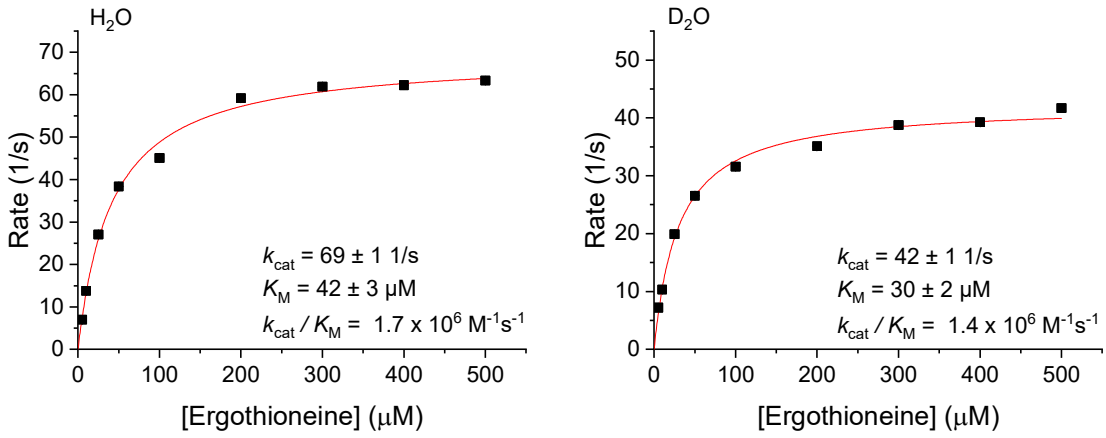

Figure 70. Michaelis-Menten Kinetics of *Td*ETL WT at pH 7.5 using HEPES buffer in H_2O (left graph) or D_2O (right graph). The pH of the buffer was adjusted to 7.5 for the reaction in H_2O and to 7.10 for the reaction in D_2O. Both buffers were lyophilized and dissolved in H_2O or D_2O, respectively. Ergothioneine substrate concentration was in between 5 µM and 500 µM. Enzyme concentration was 0.01 µM. Formation of the product thiourocanic acid at 23 °C was monitored using the spectrophotometer (Variant Cary 300 UV-Vis spectrophotometer). ε_{311}.(thiourocanic acid) = 22500 $M^{-1}cm^{-1}$. KSIE (k_{cat}) = 1.7 ± 0.1; KSIE (k_{cat}/K_M) = 1.2 ± 0.1.

Kinetic solvent isotope effect using deuterated ergothioneine as substrate. To determine the kinetic solvent isotope effect of *Td*ETL WT using deuterated ergothioneine as substrate turnover at pH 7.5 in HEPES buffer in H_2O or D_2O was followed. The pH of the buffer was adjusted to 7.5 for the reaction in H_2O and to 7.10 for the reaction in D_2O. Both buffers were lyophilized and dissolved in H_2O or D_2O, respectively. 200 µM ergothioneine or deuterated ergothioneine were used as substrate. Deuterated histidine (D_5, 98%; $^{15}N_3$, 98%; ReseaChem GmbH) was converted to deuterated TMH according to the published protocol.[158] Deuterated TMH was converted to deuterated ergothioneine using the enzyme EanB.[105] The reaction rates were determined by following product formation at 23 °C using the spectrophotometer (Variant Cary 300 UV-Vis spectrophotometer). ε_{311}.(thiourocanic acid) = 22500 $M^{-1}cm^{-1}$. The ratio $\frac{rate\ in\ H_2O}{rate\ in\ D_2O}$ presents the kinetic solvent isotope effect. KSIE = 1.0 ± 0.2.

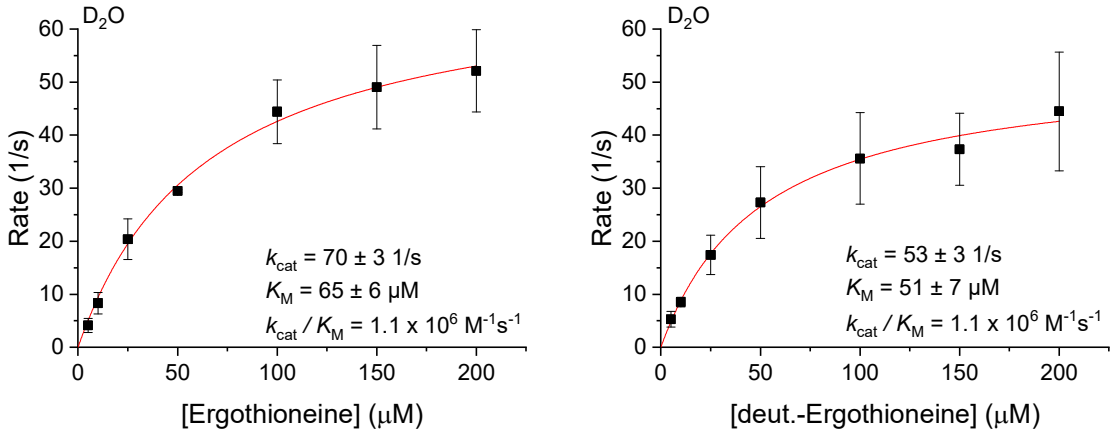

Figure 71. Substrate isotope effect of *Td*ETL WT at pH 7.5 in HEPES buffer in D_2O using ergothioneine or deuterated ergothioneine as substrate. Deuterated histidine (D_5, 98%; $^{15}N_3$, 98%; ReseaChem GmbH) was converted to deuterated N-α-trimethyl histidine according to the published protocol.[158] Deuterated N-α-trimethyl histidine was converted to deuterated ergothioneine using the enzyme EanB.[105] The pH of the buffer was adjusted to 7.10, lyophilized and dissolved in D_2O (final pD 7.5). Formation of the product was monitored using the spectrophotometer (Variant Cary 300 UV-Vis spectrophotometer). ε_{311}.(thiourocanic acid) = 22500 $M^{-1}cm^{-1}$. KIE (k_{cat}) = 1.3 ± 0.2; KIE (k_{cat}/K_M) = 1.0 ± 0.3.

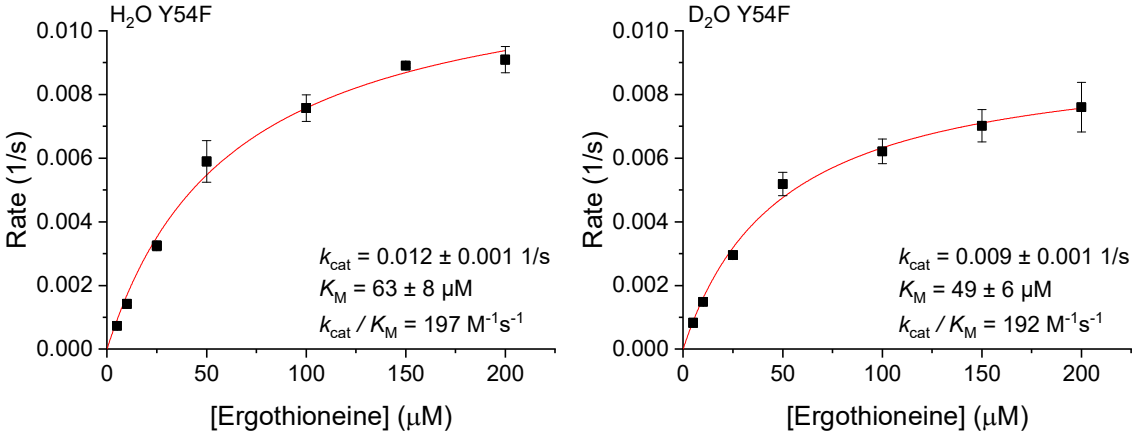

Figure 72. Michaelis-Menten Kinetics of *Td*ETL Y54F at pH 7.5 using HEPES buffer in H_2O (left graph) or D_2O (right graph). The pH of the buffer was adjusted to 7.5 for the reaction in H_2O and to 7.10 for the reaction in D_2O. Both buffers were lyophilized and dissolved in H_2O or D_2O, respectively. Ergothioneine substrate concentration was in between 5 µM and 200 µM. Enzyme concentration was 2 µM. Formation of the product thiourocanic acid at 23 °C was monitored using the spectrophotometer (Variant Cary 300 UV-Vis spectrophotometer). ε_{311}.(thiourocanic acid) = 22500 $M^{-1}cm^{-1}$. KSIE (k_{cat}) = 1.3 ± 0.1; KSIE (k_{cat}/K_M) = 1.0 ± 0.1.

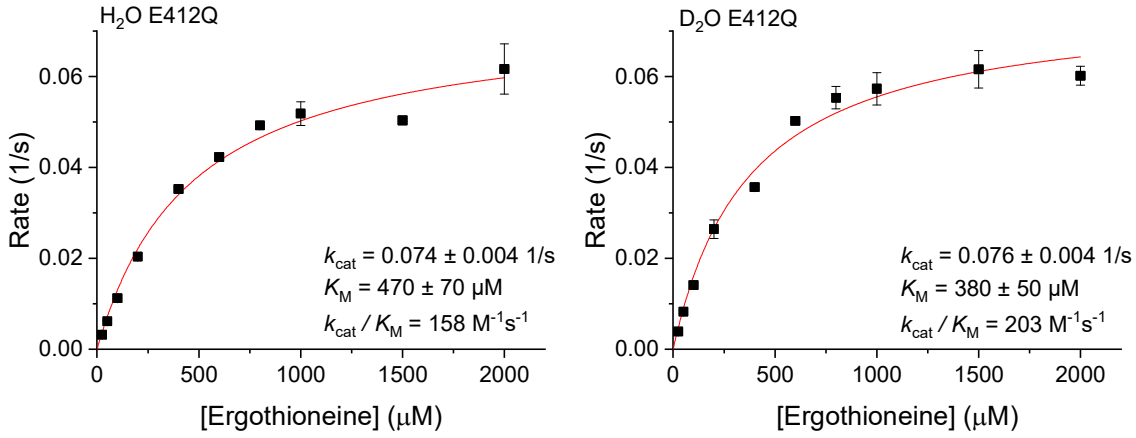

Figure 73. Michaelis-Menten Kinetics of *Td*ETL E412Q at pH 7.5 using HEPES buffer in H_2O (left graph) or D_2O (right graph). The pH of the buffer was adjusted to 7.5 for the reaction in H_2O and to 7.10 for the reaction in D_2O. Both buffers were lyophilized and dissolved in H_2O or D_2O, respectively. Ergothioneine substrate concentration was in between 50 µM and 2000 µM. Enzyme concentration was 2 µM. Formation of the product thiourocanic acid at 23 °C was monitored using the spectrophotometer (Variant Cary 300 UV-Vis spectrophotometer). ε_{311}.(thiourocanic acid) = 22500 $M^{-1}cm^{-1}$. KSIE (k_{cat}) = 1.0 ± 0.1; KSIE (k_{cat}/K_M) = 0.8 ± 0.1.

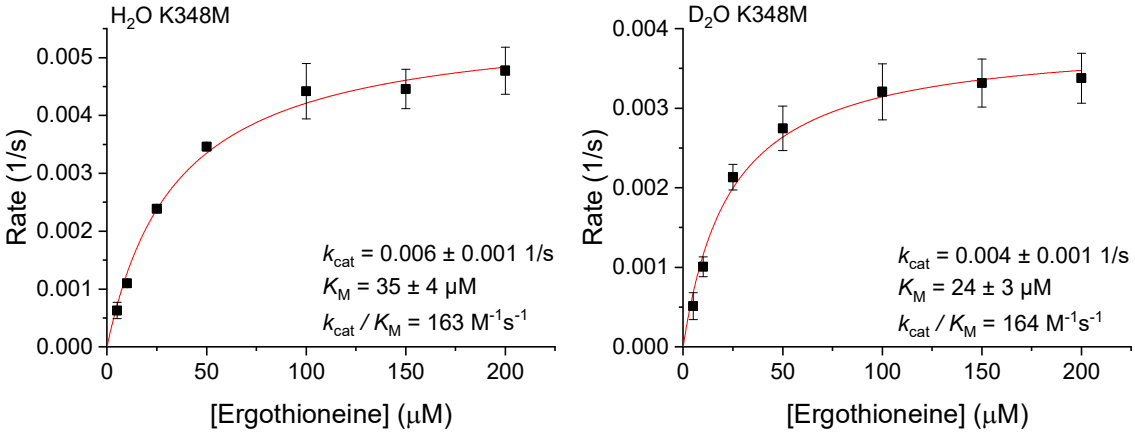

Figure 74. Michaelis-Menten Kinetics of *Td*ETL K384M at pH 7.5 using HEPES buffer in H_2O (left graph) or D_2O (right graph). The pH of the buffer was adjusted to 7.5 for the reaction in H_2O and to 7.10 for the reaction in D_2O. Both buffers were lyophilized and dissolved in H_2O or D_2O, respectively. Ergothioneine substrate concentration was in between 5 µM and 200 µM. Enzyme concentration was 2 µM. Formation of the product thiourocanic acid at 23 °C was monitored using the spectrophotometer (Variant Cary 300 UV-Vis spectrophotometer). ε_{311}.(thiourocanic acid) = 22500 $M^{-1}cm^{-1}$. KSIE (k_{cat}) = 1.5 ± 0.1; KSIE (k_{cat}/K_M) = 1.0 ± 0.1.

Table 15. Summary of the observed KSIE effects of *Td*ETL WT and variants in HEPES buffer at pH 7.5 using ergothioneine as substrate.

	KSIE (k_{cat})	KSIE (k_{cat}/K_M)
***Td*ETL WT**	1.7 ± 0.1	1.2 ± 0.1
***Td*ETL Y54F**	1.3 ± 0.1	1.0 ± 0.1
***Td*ETL E412Q**	1.0 ± 0.1	0.8 ± 0.1
***Td*ETL K384M**	1.5 ± 0.1	1.0 ± 0.1

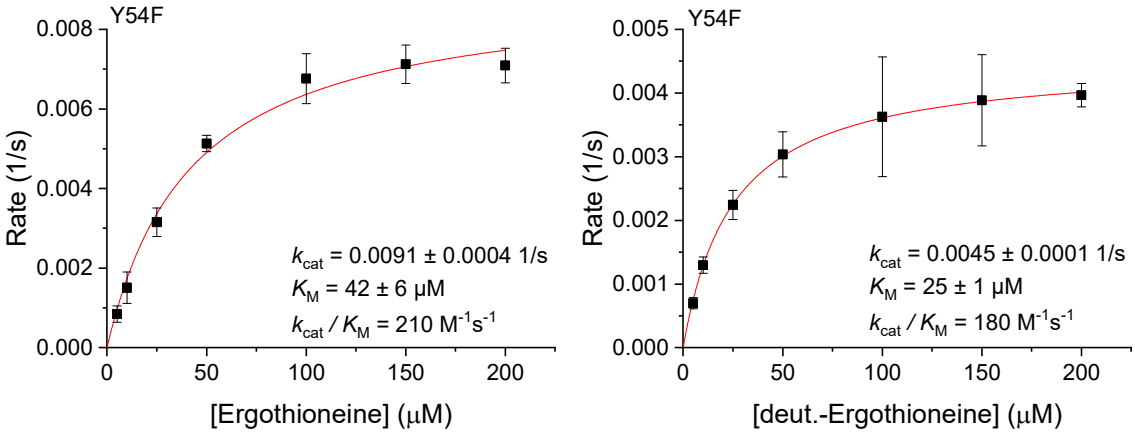

Figure 75. Michaelis-Menten Kinetics of *Td*ETL Y54F in HEPES buffer at pH 7.5 using ergothioneine (left figures) or deuterated ergothioneine (right figures) as substrate. Deuterated histidine (D_5, 98%; $^{15}N_3$, 98%; ReseaChem GmbH) was converted to deuterated N-α-trimethyl histidine according to the published protocol.[158] Deuterated N-α-trimethyl histidine was converted to deuterated ergothioneine using the enzyme EanB.[105] Substrate concentration was in between 5 µM and 200 µM. Enzyme concentration was 2 µM. Formation of the product thiourocanic acid at 23 °C was monitored using the spectrophotometer (Variant Cary 300 UV-Vis spectrophotometer). ε_{311}.(thiourocanic acid, pH 7.5) = 22500 $M^{-1}cm^{-1}$. KIE (k_{cat}) = 2.0 ± 0.2; KIE (k_{cat}/K_M) = 1.2 ± 0.1.

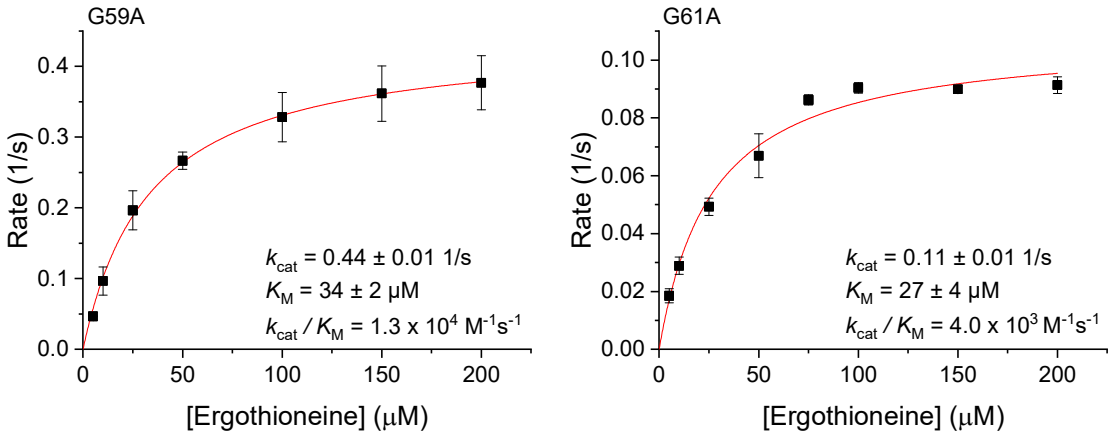

Figure 76. Michaelis-Menten Kinetics of *Td*ETL G59A and G61A at pH 7.5. Ergothioneine substrate concentration was in between 5 µM and 200 µM. Enzyme concentration was 0.1 µM for G59A and 1 µM for G61A. Formation of the product thiourocanic acid at 23 °C was monitored using the spectrophotometer (Variant Cary 300 UV-Vis spectrophotometer). ε_{311nm} (thiourocanic acid) = 22500 $M^{-1}cm^{-1}$.

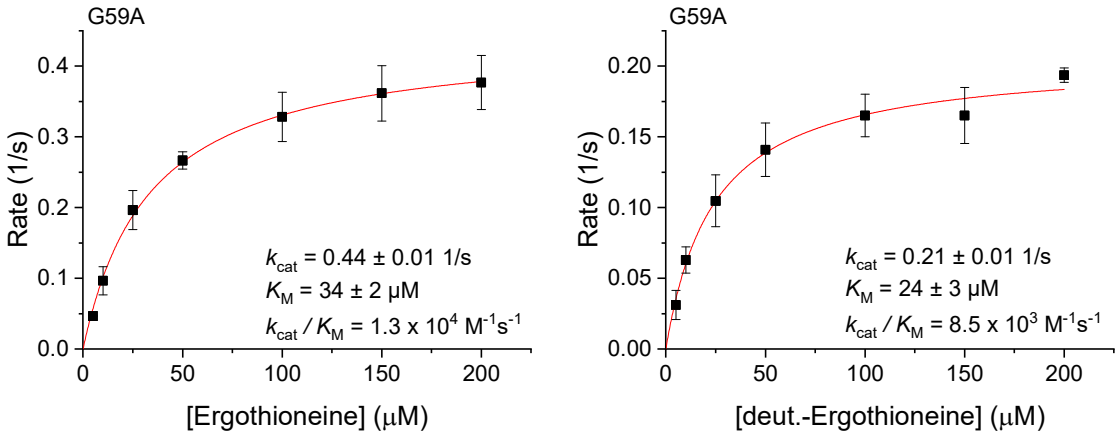

Figure 77. Michaelis-Menten Kinetics of *Td*ETL G59A in HEPES buffer at pH 7.5 using ergothioneine (left figures) or deuterated ergothioneine (right figures) as substrate. Deuterated histidine (D_5, 98%; $^{15}N_3$, 98%; ReseaChem GmbH) was converted to deuterated N-α-trimethyl histidine according to the published protocol.[158] Deuterated N-α-trimethyl histidine was converted to deuterated ergothioneine using the enzyme EanB.[105] Substrate concentration was in between 5 µM and 200 µM. Enzyme concentration was 0.1 µM. Formation of the product thiourocanic acid at 23 °C was monitored using the spectrophotometer (Variant Cary 300 UV-Vis spectrophotometer). ε_{311}.(thiourocanic acid, pH 7.5) = 22500 $M^{-1}cm^{-1}$. KIE (k_{cat}) = 2.1 ± 0.1; KIE (k_{cat}/K_M) = 1.6 ± 0.2.

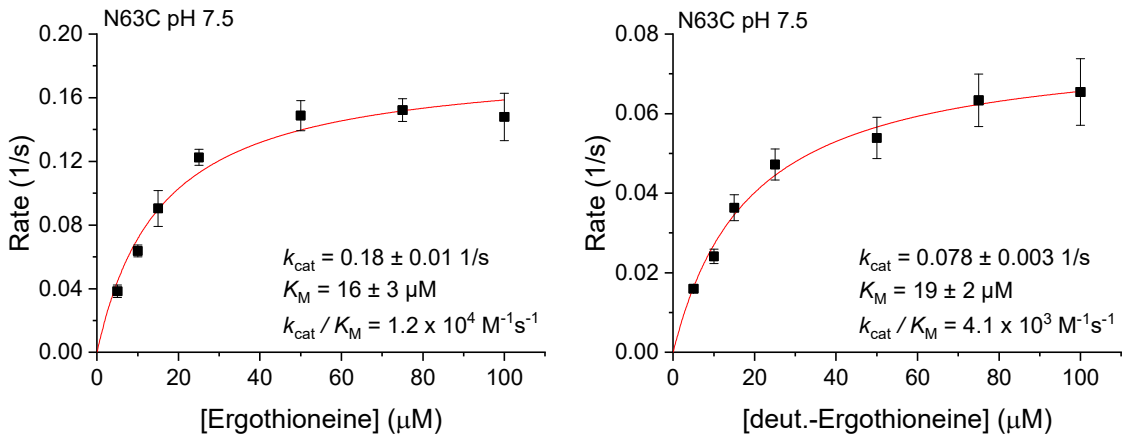

Figure 78. Michaelis-Menten Kinetics of *Td*ETL N63C in HEPES buffer at pH 7.5 using ergothioneine (left figures) or deuterated ergothioneine (right figures) as substrate. Deuterated histidine (D_5, 98%; $^{15}N_3$, 98%; ReseaChem GmbH) was converted to deuterated N-α-trimethyl histidine according to the published protocol.[158] Deuterated N-α-trimethyl histidine was converted to deuterated ergothioneine using the enzyme EanB.[105] Substrate concentration was in between 5 µM and 100 µM. Enzyme concentration was 0.1 µM. Formation of the product thiourocanic acid at 23 °C was monitored using the spectrophotometer (Variant Cary 300 UV-Vis spectrophotometer). ε_{311}.(thiourocanic acid, pH 7.5) = 22500 M^{-1}cm^{-1}. KIE (k_{cat}) = 2.4 ± 0.1; KIE (k_{cat}/K_M) = 2.8 ± 0.1.

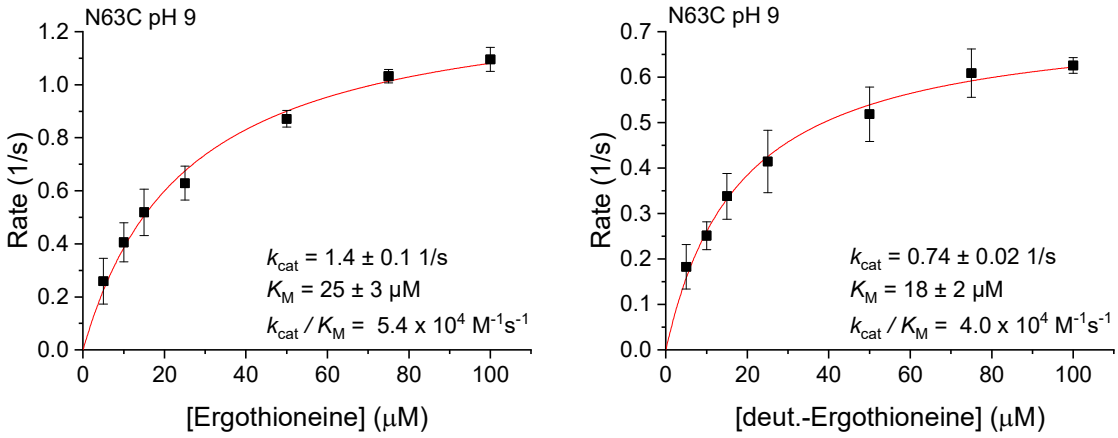

Figure 79. Michaelis-Menten Kinetics of *Td*ETL N63C in BR-buffer (described above) at pH 9 using ergothioneine (left figures) or deuterated ergothioneine (right figures) as substrate. Deuterated histidine (D_5, 98%; $^{15}N_3$, 98%; ReseaChem GmbH) was converted to deuterated N-α-trimethyl histidine according to the published protocol.[158] Deuterated N-α-trimethyl histidine was converted to deuterated ergothioneine using the enzyme EanB.[105] Substrate concentration was in between 5 µM and 100 µM. Enzyme concentration was 0.1 µM. Formation of the product thiourocanic acid at 23 °C was monitored using the spectrophotometer (Variant Cary 300 UV-Vis spectrophotometer). ε_{311}.(thiourocanic acid, pH 7.5) = 22500 M^{-1}cm^{-1}. KIE (k_{cat}) = 1.8 ± 0.1; KIE (k_{cat}/K_M) = 1.3 ± 0.1.

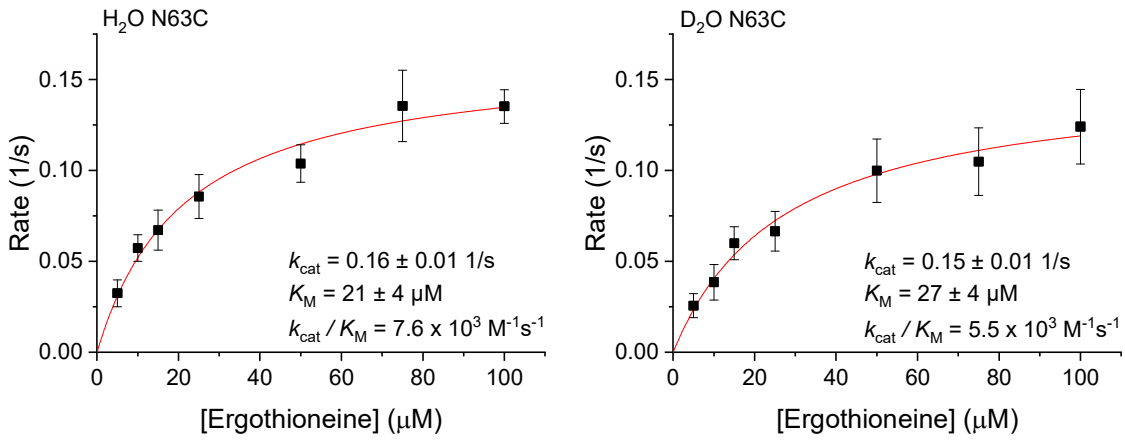

Figure 80. Michaelis-Menten Kinetics of *Td*ETL N63C at pH 7.5 using HEPES buffer in H_2O (left graph) or D_2O (right graph). The pH of the buffer was adjusted to 7.5 for the reaction in H_2O and to 7.10 for the reaction in D_2O. Both buffers were lyophilized and dissolved in H_2O or D_2O, respectively. Ergothioneine substrate concentration was in between 5 µM and 100 µM. Enzyme concentration was 0.1 µM. Formation of the product thiourocanic acid at 23 °C was monitored using the spectrophotometer (Variant Cary 300 UV-Vis spectrophotometer). ε_{311}.(thiourocanic acid) = 22500 $M^{-1}cm^{-1}$. KSIE (k_{cat}) = 1.1 ± 0.1; KSIE (k_{cat}/K_M) = 1.4 ± 0.1.

Table 16. Phylum, organism and accession number of putative ergothionase homologs. Homologs were found by creating a Sequence Similarity Network based on the UniProt database using *Td*ETL sequence as an input sequence.[159] Conservation of the catalytic important residues Tyr54, Lys64, Lys384 and Glu412 was used as a requirement for putative ergothionases.

Phylum	**Organism**	**Accession Number**
Acidobacteria	*Acidobacteria bacterium.*	A0A2V9QRG7
Bacteroidetes	*Microscilla marina ATCC 23134.*	A1ZWV6
candidate division NC10	*candidate division NC10 bacterium RIFCSPLOWO2_02_FULL_66_22.*	A0A1F4PYG1
candidate division NC10	*candidate division NC10 bacterium RIFCSPLOWO2_12_FULL_66_18.*	A0A1F4QK64
Chlamydiae	*Chlamydia trachomatis.*	A0A0E9GAP9
Chlamydiae	*Chlamydia trachomatis.*	A0A0E9EV04
Cyanobacteria	*Leptolyngbya sp. PCC 7375.*	K9F598
Cyanobacteria	*Leptolyngbya sp. PCC 7376.*	K9Q1N5
Firmicutes	*Acidaminobacter hydrogenoformans DSM 2784.*	A0A1G5S0B1
Firmicutes	*Anaeromicrobium sediminis.*	A0A267MKA2
Firmicutes	*Anaerosphaera aminiphila DSM 21120.*	A0A1M5RMG5

Firmicutes	*Anaerovirgula multivorans.*	A0A239I834
Firmicutes	*Bacillus sp. FJAT-26390.*	A0A1B8W885
Firmicutes	*Bacillus sp. FJAT-26390.*	A0A1B8WBJ0
Firmicutes	*Bacillus sp. FJAT-27264.*	A0A1B8WEI8
Firmicutes	*Bacillus sp. FJAT-27264.*	A0A1B8WEW0
Firmicutes	*Blautia producta.*	A0A2S4GLB0
Firmicutes	*Blautia producta.*	A0A2S4GMW9
Firmicutes	*Blautia sp. YL58.*	A0A1C7I7W8
Firmicutes	*Blautia sp. YL58.*	A0A1C7ICE6
Firmicutes	*Candidatus Carbobacillus altaicus.*	A0A2R6Y2G9
Firmicutes	*Clostridia bacterium BRH_c25.*	A0A101WNZ4
Firmicutes	*Clostridium aceticum.*	A0A0D8I7S1
Firmicutes	*Clostridium ljungdahlii.*	A0A162J9E2
Firmicutes	*Clostridium sp. 7_3_54FAA.*	G5FFL7
Firmicutes	*Clostridium sp. 7_3_54FAA.*	G5FEN4
Firmicutes	*Clostridium sp. HMb25.*	A0A2N0KBS0
Firmicutes	*Clostridium sp. HMP27.*	A0A099RQF7
Firmicutes	*Clostridium symbiosum*	A0A174CFW7
Firmicutes	*Clostridium symbiosum*	A0A174H5D0
Firmicutes	*Clostridium symbiosum ATCC 14940.*	U2DAB6
Firmicutes	*Clostridium symbiosum ATCC 14940.*	U2BTG2
Firmicutes	*Clostridium symbiosum WAL-14163.*	E7GKQ7
Firmicutes	*Clostridium symbiosum WAL-14163.*	E7GIG0
Firmicutes	*Clostridium termitidis CT1112.*	S0FKX7
Firmicutes	*Clostridium ultunense Esp.*	A0A1M4PLN0
Firmicutes	*Cohnella kolymensis.*	A0A0C2UIY0
Firmicutes	*Dethiosulfatibacter aminovorans DSM 17477.*	A0A1M6AAG9
Firmicutes	*Dethiosulfatibacter aminovorans DSM 17477.*	A0A1M6G2C4
Firmicutes	*Enterococcus malodoratus ATCC 43197.*	R2QJZ3
Firmicutes	*Enterococcus malodoratus.*	A0A2X1LPU2
Firmicutes	*Eubacterium yurii subsp. margaretiae ATCC 43715.*	E0QHA3
Firmicutes	*Firmicutes bacterium ASF500.*	V2XW62
Firmicutes	*Firmicutes bacterium ASF500.*	V2YC09

Firmicutes	*Firmicutes bacterium CAG:129_59_24.*	A0A1Q6QC58
Firmicutes	*Firmicutes bacterium CAG:129_59_24.*	A0A1Q6QCM7
Firmicutes	*Geosporobacter ferrireducens.*	A0A1D8GCM4
Firmicutes	*Geosporobacter subterraneus DSM 17957.*	A0A1M6I960
Firmicutes	*Maledivibacter halophilus.*	A0A1T5KZP2
Firmicutes	*Maledivibacter halophilus.*	A0A1T5M9E4
Firmicutes	*Natronincola ferrireducens.*	A0A1G9HD03
Firmicutes	*Paenibacillus borealis.*	A0A089MKG9
Firmicutes	*Paenibacillus durus*	A0A089HJ17
Firmicutes	*Paenibacillus durus ATCC 35681.*	A0A0F7CGW2
Firmicutes	*Paenibacillus ferrarius.*	A0A1V4HLC4
Firmicutes	*Paenibacillus naphthalenovorans.*	A0A0U2WFR1
Firmicutes	*Paenibacillus riograndensis SBR5.*	A0A0E4HBC3
Firmicutes	*Paenibacillus sabinae T27.*	X4ZXH0
Firmicutes	*Paenibacillus sophorae.*	A0A1H8VQP4
Firmicutes	*Paenibacillus sp. 276b.*	A0A1H4BIT9
Firmicutes	*Paenibacillus sp. A59.*	A0A0M9BLP7
Firmicutes	*Paenibacillus sp. FSL A5-0031.*	A0A1R1A1N6
Firmicutes	*Paenibacillus sp. JCM 10914.*	V9GAF1
Firmicutes	*Paenibacillus sp. LK1.*	A0A2G7M2N4
Firmicutes	*Paenibacillus sp. OV191.*	A0A2V4W4F3
Firmicutes	*Paenibacillus sp. Root444D2.*	A0A0Q7JBM1
Firmicutes	*Paenibacillus sp. Soil724D2.*	A0A0Q9K4T2
Firmicutes	*Peptoanaerobacter stomatis*	J5UPN6
Firmicutes	*Peptoanaerobacter stomatis*	V9HLH1
Firmicutes	*Peptoanaerobacter stomatis*	G9XE22
Firmicutes	*Peptoniphilus asaccharolyticus DSM 20463.*	A0A1W1V430
Firmicutes	*Peptoniphilus grossensis.*	A0A1U7M2E5
Firmicutes	*Peptoniphilus indolicus ATCC 29427.*	G4D1P9
Firmicutes	*Peptoniphilus sp. oral taxon 386 str. F0131.*	D7N6A3
Firmicutes	*Peptostreptococcaceae bacterium AS15.*	G9WXX7
Firmicutes	*Peptostreptococcaceae bacterium AS15.*	J4K8R1
Firmicutes	*Seinonella peptonophila.*	A0A1M5AZW6
Firmicutes	*Sporolactobacillus laevolacticus DSM 442.*	V6IXX0

Firmicutes	*Sporomusa malonica.*	A0A1W2C325
Firmicutes	*Sporomusa sphaeroides DSM 2875.*	A0A1U7MIZ9
Firmicutes	*Thermotalea metallivorans.*	A0A140L7C4
Firmicutes	*Tindallia californiensis.*	A0A1H3MI16
Firmicutes	*uncultured Clostridium sp.*	A0A1C5ZVS6
Firmicutes	*uncultured Clostridium sp.*	A0A1C6DS28
Firmicutes	*uncultured Sporomusa sp.*	A0A212LUU0
Fusobacteria	*Fusobacterium naviforme.*	A0A2P8EQ63
Fusobacteria	*Fusobacterium nucleatum subsp. animalis 11_3_2.*	F7L375
Fusobacteria	*Fusobacterium nucleatum subsp. animalis 11_3_2.*	F7L438
Proteobacteria	*Achromobacter insolitus.*	A0A167CPW9
Proteobacteria	*Achromobacter insuavis AXX-A.*	F7SYB1
Proteobacteria	*Achromobacter insuavis AXX-A.*	F7SXG1
Proteobacteria	*Achromobacter insuavis AXX-A.*	A0A1R1JQB7
Proteobacteria	*Achromobacter marplatensis.*	A0A225NCR7
Proteobacteria	*Achromobacter piechaudii HLE.*	J4PBZ7
Proteobacteria	*Achromobacter pulmonis.*	A0A2N8KQ02
Proteobacteria	*Achromobacter sp.*	A0A0M7EBE7
Proteobacteria	*Achromobacter sp.*	A0A0M7K465
Proteobacteria	*Achromobacter sp.*	A0A0M7MF41
Proteobacteria	*Achromobacter xylosoxidans (strain A8)*	E3HLA6
Proteobacteria	*Achromobacter xylosoxidans (strain A8)*	E3HNF8
Proteobacteria	*Agrobacterium fabrum.*	A0A2W5FBK6
Proteobacteria	*Agrobacterium genomosp. 13 str. CFBP 6927.*	A0A1S7R922
Proteobacteria	*Agrobacterium genomosp. 13 str. CFBP 6927.*	A0A1S7RBP2
Proteobacteria	*Agrobacterium genomosp. 3 str. CFBP 6623.*	A0A1S7RRC6
Proteobacteria	*Agrobacterium genomosp. 5 str. CFBP 6626.*	A0A1S7RTM1
Proteobacteria	*Agrobacterium genomosp. 7 str. NCPPB 1641.*	A0A1S7U7I5
Proteobacteria	*Agrobacterium radiobacter DSM 30147.*	W1KKH8
Proteobacteria	*Agrobacterium sp. LY4.*	A0A0X7A063
Proteobacteria	*Agrobacterium sp. SUL3.*	A0A0L6K5Q8
Proteobacteria	*Agrobacterium tumefaciens F2.*	F7UDC5

Proteobacteria	*Albidiferax sp. OV413.*	A0A1H0SZU2
Proteobacteria	*Alcaligenes xylosoxydans xylosoxydans*	A0A0X8P1Z2
Proteobacteria	*Alcaligenes xylosoxydans xylosoxydans*	A0A109XXI6
Proteobacteria	*Alcaligenes xylosoxydans xylosoxydans*	A0A2T5CSE9
Proteobacteria	*Alcaligenes xylosoxydans xylosoxydans (Achromobacter xylosoxidans)*	A0A0M7FW64
Proteobacteria	*Alcaligenes xylosoxydans xylosoxydans (Achromobacter xylosoxidans)*	A0A0D6INA3
Proteobacteria	*Arcobacter canalis.*	A0A2G1CWD0
Proteobacteria	*Arcobacter halophilus.*	A0A2N1J1J7
Proteobacteria	*Arcobacter marinus.*	A0A1T5CRN4
Proteobacteria	*Arcobacter marinus.*	A0A2G1DA93
Proteobacteria	*Bordetella genomosp. 2.*	A0A261VFK0
Proteobacteria	*Bordetella genomosp. 6.*	A0A261VXL6
Proteobacteria	*Bordetella trematum.*	A0A157K554
Proteobacteria	*Bordetella trematum.*	A0A2X1CQS6
Proteobacteria	*Budvicia aquatica.*	A0A2C6DUF4
Proteobacteria	*Burkholderia cepacia*	A0A0J5XFB7
Proteobacteria	*Burkholderia cepacia JBK9.*	A0A118RZD7
Proteobacteria	*Burkholderia lata*	A0A1D7ZNJ2
Proteobacteria	*Burkholderia lata (strain 383)*	A0A105L8S8
Proteobacteria	*Burkholderia lata (strain ATCC 17760)*	Q390I8
Proteobacteria	*Burkholderia lata (strain DSM 23089)*	A0A102EIG2
Proteobacteria	*Burkholderia lata (strain LMG 22485)*	A0A2A4CJ37
Proteobacteria	*Burkholderia lata (strain NCIMB9086)*	A0A0U4D2I0
Proteobacteria	*Burkholderia lata (strain R18194)*	A0A2A9L6A5
Proteobacteria	*Burkholderia pseudomallei*	A0A095GPC0
Proteobacteria	*Burkholderia pseudomallei (strain 1026b)*	A0A0H3HQ18
Proteobacteria	*Burkholderia pseudomallei (strain 1106a)*	A3NVD9
Proteobacteria	*Burkholderia pseudomallei (strain 1710b)*	Q3JS71
Proteobacteria	*Burkholderia pseudomallei (strain K96243)*	Q63UD0
Proteobacteria	*Burkholderia pseudomallei 1710a.*	A0A0E1W8R9
Proteobacteria	*Burkholderia pseudomallei 406e.*	A8EDJ4
Proteobacteria	*Burkholderia pseudomallei 576.*	A0A0E1TYJ5

Proteobacteria	*Burkholderia pseudomallei MSHR2543.*	A0A0F6GBL2
Proteobacteria	*Burkholderia pseudomallei MSHR346.*	C4KLN0
Proteobacteria	*Burkholderia pseudomallei MSHR4000.*	A0A0F6LB82
Proteobacteria	*Burkholderia pseudomallei Pakistan 9.*	A0A0E1UJX7
Proteobacteria	*Burkholderia pseudomallei S13.*	B1HJ69
Proteobacteria	*Burkholderia puraquae.*	A0A084DNS9
Proteobacteria	*Burkholderia pyrrocinia*	A0A104NMV4
Proteobacteria	*Burkholderia sp. D7.*	A0A2C9BBG5
Proteobacteria	*Burkholderia sp. D7.*	A0A2C9BN69
Proteobacteria	*Burkholderia sp. HME13.*	A0A1X1PNB3
Proteobacteria	*Burkholderia sp. IDO3.*	A0A118HTM9
Proteobacteria	*Burkholderia sp. JKS000303.*	K4PZA7
Proteobacteria	*Burkholderia sp. KK1.*	A0A1B4PM34
Proteobacteria	*Burkholderia sp. MSh2.*	A0A069B857
Proteobacteria	*Burkholderia sp. PAMC 28687.*	A0A242N6D4
Proteobacteria	*Burkholderia sp. RF2-non_BP3.*	A0A1P9XUU5
Proteobacteria	*Burkholderia stabilis.*	A0A106PKF7
Proteobacteria	*Burkholderia ubonensis.*	A0A103P858
Proteobacteria	*Burkholderiales bacterium 1_1_47.*	D9Y3S2
Proteobacteria	*Burkholderiales bacterium YL45.*	A0A1C7HL58
Proteobacteria	*Caballeronia mineralivorans PML1*	A0A0J1G0Q2
Proteobacteria	*Caballeronia sordidicola.*	A0A242M5G6
Proteobacteria	*Campylobacter blaseri.*	A0A2P8QZX2
Proteobacteria	*Campylobacter fetus subsp. fetus (strain 82-40)*	A0RMB1
Proteobacteria	*Campylobacter fetus subsp. fetus.*	A0A0S4RNI9
Proteobacteria	*Campylobacter fetus subsp. testudinum.*	A0A2S5J965
Proteobacteria	*Campylobacter fetus subsp. venerealis 293.*	A0A2S0JAW0
Proteobacteria	*Campylobacter fetus subsp. venerealis cfvi03.*	W0D8I6
Proteobacteria	*Campylobacter geochelonis.*	A0A128EBH4
Proteobacteria	*Campylobacter hyointestinalis subsp. hyointestinalis LMG 9260.*	A0A172SPB5
Proteobacteria	*Campylobacter hyointestinalis subsp. hyointestinalis.*	A0A2X4P4V8
Proteobacteria	*Campylobacter mucosalis.*	A0A071L8M5

Proteobacteria	*Campylobacter pinnipediorum subsp. caledonicus.*	A0A1S6U835
Proteobacteria	*Campylobacter pinnipediorum subsp. pinnipediorum.*	A0A1T2XPU7
Proteobacteria	*Campylobacter rectus RM3267.*	B9CZV2
Proteobacteria	*Campylobacter sp. FOBRC14.*	J4KTT0
Proteobacteria	*Campylobacter subantarcticus LMG 24374.*	A0A0A8H9C0
Proteobacteria	*Citrobacter freundii.*	A0A2T3RNW5
Proteobacteria	*Citrobacter sp. 92.*	A0A2S4QF24
Proteobacteria	*Citrobacter sp. 92.*	A0A212HFV8
Proteobacteria	*Citrobacter sp. MGH106.*	A0A0J1PA51
Proteobacteria	*Comamonas testosteroni*	A0A096FCF7
Proteobacteria	*Comamonas testosteroni*	A0A096FDM7
Proteobacteria	*Comamonas testosteroni*	A0A1Y1JB67
Proteobacteria	*Desulfovibrio bizertensis DSM 18034.*	A0A1T4VRQ5
Proteobacteria	*Ensifer sojae CCBAU 05684.*	A0A249PKJ0
Proteobacteria	*Enterobacteriaceae bacterium 9_2_54FAA.*	E5YH86
Proteobacteria	*Enterobacteriaceae bacterium bta3-1.*	A0A0C5WBM2
Proteobacteria	*Escherichia albertii B156.*	A0A1X3JQ66
Proteobacteria	*Escherichia albertii KF1.*	W0AR86
Proteobacteria	*Escherichia albertii.*	A0A2S6P482
Proteobacteria	*Escherichia coli*	A0A210G163
Proteobacteria	*Escherichia coli*	A0A2B7LL73
Proteobacteria	*Escherichia coli*	A0A0A1A7N5
Proteobacteria	*Escherichia coli*	A0A1D7PXJ9
Proteobacteria	*Escherichia coli*	A0A1X0PKJ9
Proteobacteria	*Escherichia coli O7:K1 (strain IAI39 / ExPEC)*	A0A0H3MF89
Proteobacteria	*Escherichia coli O7:K1 str. CE10.*	A0A0E0V382
Proteobacteria	*Escherichia coli.*	A0A1M2J2H7
Proteobacteria	*Escherichia coli.*	A0A0K4JRR6
Proteobacteria	*Escherichia coli.*	A0A2U2VEY5
Proteobacteria	*Escherichia coli.*	A0A2W6P050
Proteobacteria	*Escherichia sp. KTE159.*	S1MFV0
Proteobacteria	*Escherichia sp. KTE52.*	S1CQE4

Proteobacteria	*Escherichia sp. MOD1-EC5451.*	A0A2T3BIE5
Proteobacteria	*Ferrimonas balearica (strain DSM 9799 / CCM 4581 / PAT)*	E1SV38
Proteobacteria	*Ferrimonas sediminum.*	A0A1G8JY84
Proteobacteria	*Gammaproteobacteria bacterium.*	A0A2G6ELY6
Proteobacteria	*Gammaproteobacteria bacterium.*	A0A2G6LDZ9
Proteobacteria	*Hafnia alvei ATCC 51873.*	G9Y7H0
Proteobacteria	*Hafnia alvei.*	A0A1C6Z7N0
Proteobacteria	*Hafnia paralvei.*	A0A2A2MDV2
Proteobacteria	*Helicobacter sp. 11S03491-1.*	A0A268TFD6
Proteobacteria	*Klebsiella oxytoca.*	A0A168VFH5
Proteobacteria	*Legionella clemsonensis.*	A0A222P3S0
Proteobacteria	*Legionella gratiana.*	A0A0W0UF88
Proteobacteria	*Legionella maceachernii.*	A0A0W0WDX4
Proteobacteria	*Leminorella grimontii ATCC 33999 = DSM 5078.*	A0A085HFJ0
Proteobacteria	*Leminorella richardii.*	A0A2X4Y3V6
Proteobacteria	*Morganella morganii*	A0A2S1BA97
Proteobacteria	*Morganella psychrotolerans.*	A0A1B8H210
Proteobacteria	*Paraburkholderia sp. SOS3.*	A0A126YU72
Proteobacteria	*Paraburkholderia sp. SOS3.*	A0A1L6HTZ5
Proteobacteria	*Paracoccus denitrificans (strain Pd 1222)*	A1B7U5
Proteobacteria	*Paracoccus saliphilus.*	A0A1N7NBZ3
Proteobacteria	*Parasutterella excrementihominis CAG:233.*	R5DY36
Proteobacteria	*Parasutterella excrementihominis CAG:233.*	R5E7S4
Proteobacteria	*Parasutterella excrementihominis YIT 11859.*	F3QJ16
Proteobacteria	*Parasutterella excrementihominis YIT 11859.*	F3QK73
Proteobacteria	*Polaromonas sp. (strain JS666 / ATCC BAA-500)*	Q120I2
Proteobacteria	*Polaromonas sp. OV174.*	A0A1I1LXE8
Proteobacteria	*Polaromonas sp. YR568.*	A0A1I7KJA3
Proteobacteria	*Proteobacteria bacterium CAG:139.*	R6A805
Proteobacteria	*Proteobacteria bacterium CAG:139.*	R6A045
Proteobacteria	*Providencia stuartii.*	A0A1S1HS62
Proteobacteria	*Pseudomonas gingeri NCPPB 3146 = LMG 5327.*	A0A2K1FFU2
Proteobacteria	*Pseudorhodoferax sp. Leaf274.*	A0A0S9MTX7

Proteobacteria	*Ralstonia sp. MD27.*	A0A0J9E039
Proteobacteria	*Raoultella terrigena*	A0A1V2BU72
Proteobacteria	*Rhizobium radiobacter*	A0A024J059
Proteobacteria	*Rhizobium sp. Root651.*	A0A0Q8FD29
Proteobacteria	*Rhodoferax sp. YR267.*	A0A2U0YVW7
Proteobacteria	*Serratia grimesii.*	A0A2H1LEX0
Proteobacteria	*Serratia proteamaculans.*	A0A1W5DIY9
Proteobacteria	*Serratia quinivorans.*	A0A2X2GG94
Proteobacteria	*Serratia sp. LCN16.*	A0A0X2NZE9
Proteobacteria	*Shewanella algae.*	A0A2T3H024
Proteobacteria	*Shewanella benthica KT99.*	A9DB79
Proteobacteria	*Shewanella bicestrii.*	A0A220UNI3
Proteobacteria	*Shewanella chilikensis.*	A0A1S2TY49
Proteobacteria	*Shewanella decolorationis S12.*	V1DE01
Proteobacteria	*Shewanella halifaxensis (strain HAW-EB4)*	B0TSP0
Proteobacteria	*Shewanella loihica (strain ATCC BAA-1088 / PV-4)*	A3QF98
Proteobacteria	*Shewanella oneidensis (strain MR-1)*	Q8ECS5
Proteobacteria	*Shewanella oneidensis.*	A0A2W5DPW1
Proteobacteria	*Shewanella pealeana (strain ATCC 700345 / ANG-SQ1)*	A8H7Z6
Proteobacteria	*Shewanella putrefaciens (strain ATCC BAA-453)*	A0A2V4W9E6
Proteobacteria	*Shewanella putrefaciens (strain CN-32)*	A4Y869
Proteobacteria	*Shewanella sediminis (strain HAW-EB3)*	A8FQ33
Proteobacteria	*Shewanella sp. (strain ANA-3)*	A0KVA5
Proteobacteria	*Shewanella sp. cp20.*	A0A0C3LN95
Proteobacteria	*Shewanella sp. FDAARGOS_354.*	A0A1Z4A7I0
Proteobacteria	*Sinorhizobium meliloti (strain BL225C)*	A0A0E0ULX2
Proteobacteria	*Sinorhizobium meliloti (strain SM11)*	F7XCM2
Proteobacteria	*Stigmatella aurantiaca (strain DW4/3-1)*	Q098W6
Proteobacteria	*Stigmatella erecta.*	A0A1I0DHZ1
Proteobacteria	*Sutterella sp. KLE1602.*	A0A139JRY8
Proteobacteria	*Sutterella wadsworthensis 2_1_59BFAA.*	K1JY86
Proteobacteria	*Tatlockia micdadei*	A0A098GF27

Proteobacteria	*Turicimonas muris.*	A0A227KGA2
Proteobacteria	*Turicimonas muris.*	A0A227KSA1
Spirochaetes	*Treponema denticola SP33.*	M2BPW8
Spirochaetes	*Treponema phagedenis F0421.*	E7NQ07
Spirochaetes	*Treponema phagedenis.*	A0A0B7GW92
Synergistetes	*Acetomicrobium mobile (strain ATCC BAA-54 / DSM 13181 / JCM 12221 /NGA)*	I4BXM9
Synergistetes	*Aminomonas paucivorans DSM 12260.*	E3CYY6
Synergistetes	*Cloacibacillus evryensis DSM 19522.*	A0A010YTQ8
Synergistetes	*Cloacibacillus porcorum.*	A0A1B2I5L2
Synergistetes	*Cloacibacillus sp. An23.*	A0A1Y4GEV9
Synergistetes	*Cloacibacillus sp. An23.*	A0A1Y4GFU5
Synergistetes	*Dethiosulfovibrio peptidovorans.*	A0A2G6M1E6
Synergistetes	*Dethiosulfovibrio salsuginis.*	A0A1X7IZU0
Synergistetes	*Synergistales bacterium 53_16.*	A0A117LMB5
Synergistetes	*Synergistales bacterium 54_9.*	A0A101IRU6
Synergistetes	*Synergistes jonesii.*	A0A073J785
Synergistetes	*Synergistes sp. 3_1_syn1.*	G9PVB9
Synergistetes	*Synergistes sp. 3_1_syn1.*	G9PXA9
Synergistetes	*Synergistetes bacterium HGW-Synergistetes-1.*	A0A2N1QT95
Synergistetes	*Thermanaerovibrio acidaminovorans (strain ATCC 49978 / DSM 6589 /Su883)*	D1B828
Synergistetes	*Thermanaerovibrio velox DSM 12556.*	H0UQM1

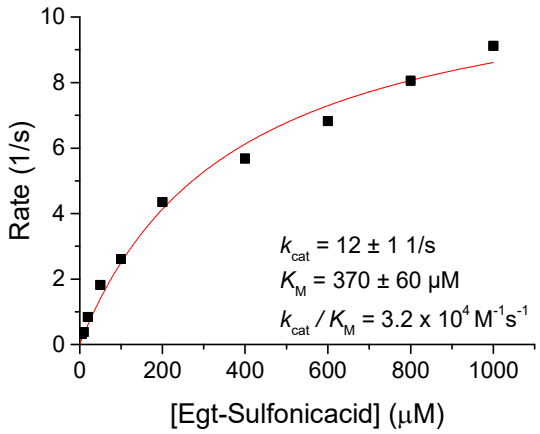

Figure 81. Michaelis-Menten Kinetics of *Me*lyase. Substrate concentration of ergothioneine sulfonic acid was in between 5 μM and 1000 μM. Enzyme concentration was 0.1 μM. Formation of the product was monitored using the spectrophotometer (Variant Cary 300 UV-Vis spectrophotometer). $\varepsilon_{295\ nm}$ (sulfono urocanic acid) = 15890 $M^{-1}cm^{-1}$.

Table 17. Phylum, Organism and Accession Number of putative ergothioneine sulfonic acid lyase homologs. Homologs were found by creating a Sequence Similarity Network based on the UniProt database using *Td*ETL (accession number: WP_010693216) and *Me*lyase sequence as an input sequence.[159] Conservation of the catalytic important residues Tyr57, Arg87 Lys387 and Glu415 (counting based on *Me*lyase) was used as a requirement for putative ergothioneine sulfonic acid lyase.

Phylum	**Organism**	**Accession Number**
Actinobacteria	*Actinobacteria bacterium OK074.*	A0A0N0MKZ3
Actinobacteria	*Prauserella muralis.*	A0A2V4AQF0
Actinobacteria	*Streptomyces antibioticus.*	A0A101QGJ9
Actinobacteria	*Streptomyces sp. A217.*	A0A2P8Q1V8
Actinobacteria	*Streptomyces turgidiscabies Car8.*	L7F0I9
Proteobacteria	*Acetobacter malorum.*	A0A149R7L7
Proteobacteria	*Agrobacterium radiobacter (strain K84 / ATCC BAA-868)*	B9JID5
Proteobacteria	*Agrobacterium rhizogenes NBRC 13257.*	A0A061MWB1
Proteobacteria	*Agrobacterium rhizogenes.*	A0A071IL44
Proteobacteria	*alpha proteobacterium BAL199.*	A8TQH4
Proteobacteria	*Azospirillum lipoferum.*	A0A1X7QBK3
Proteobacteria	*Azospirillum sp. (strain B510)*	D3NYZ8
Proteobacteria	*Azospirillum sp. TSH64.*	A0A2U1XFA2

Proteobacteria	*Bosea lathyri.*	A0A1H6C5T1
Proteobacteria	*Bosea lupini.*	A0A1H7TC09
Proteobacteria	*Bosea sp. 1131.*	A0A2S4LY50
Proteobacteria	*Bosea sp. 32-68-6.*	A0A258D5E3
Proteobacteria	*Bosea sp. AAP35.*	A0A0N1BC31
Proteobacteria	*Bosea sp. BIWAKO-01.*	A0A1E1V193
Proteobacteria	*Bosea sp. LC85.*	A0A085EW28
Proteobacteria	*Bosea sp. OK403.*	A0A1I3LXI4
Proteobacteria	*Bosea sp. PAMC 26642.*	A0A126NXS9
Proteobacteria	*Bosea sp. RAC05.*	A0A1B3NKD2
Proteobacteria	*Bosea sp. Root483D1.*	A0A0Q9IUG3
Proteobacteria	*Bosea vaviloviae.*	A0A0N0MC47
Proteobacteria	*Bosea vaviloviae.*	A0A1D7TZ70
Proteobacteria	*Brenneria sp. CFCC 11842.*	A0A2U1UCU2
Proteobacteria	*Chelativorans sp. (strain BNC1)*	Q11E25
Proteobacteria	*Citrobacter koseri*	A0A078LHJ6
Proteobacteria	*Citrobacter koseri*	A0A2X2VDX3
Proteobacteria	*Citrobacter koseri (strain ATCC BAA-895 / CDC 4225-83 / SGSC4696)*	A8AKL9
Proteobacteria	*Enterobacter sp. 10-1.*	A0A267RII3
Proteobacteria	*Inquilinus limosus.*	A0A211ZTK6
Proteobacteria	*Labrys okinawensis.*	A0A2S9Q4B1
Proteobacteria	*Martelella endophytica.*	A0A0D5LLV5
Proteobacteria	*Martelella mediterranea DSM 17316.*	A0A1U9Z848
Proteobacteria	*Mesorhizobium amorphae CCNWGS0123.*	G6YBD2
Proteobacteria	*Mesorhizobium amorphae.*	A0A2W4ZPB6
Proteobacteria	*Mesorhizobium australicum (strain HAMBI 3006 / LMG 24608 / WSM2073)*	L0KNI4
Proteobacteria	*Mesorhizobium delmotii*	A0A2P9AXX8
Proteobacteria	*Mesorhizobium helmanticense.*	A0A2T4IQA8
Proteobacteria	*Mesorhizobium huakuii 7653R.*	A0A068D833
Proteobacteria	*Mesorhizobium japonicum (strain LMG 29417 / CECT 9101 / MAFF 303099)*	Q98JY1
Proteobacteria	*Mesorhizobium kowhaii.*	A0A2W7C9J0

Proteobacteria	*Mesorhizobium mediterraneum.*	A0A271L823
Proteobacteria	*Mesorhizobium opportunistum (strain LMG 24607 / HAMBI 3007 / WSM2075)*	F7YDI3
Proteobacteria	*Mesorhizobium plurifarium.*	A0A090DPU8
Proteobacteria	*Mesorhizobium plurifarium.*	A0A090EV99
Proteobacteria	*Mesorhizobium plurifarium.*	A0A090G9B6
Proteobacteria	*Mesorhizobium plurifarium.*	A0A0K2VPB5
Proteobacteria	*Mesorhizobium soli.*	A0A2P7RPK5
Proteobacteria	*Mesorhizobium sp. 65-26.*	A0A1Q4AJQ3
Proteobacteria	*Mesorhizobium sp. AA22.*	A0A1A5TAR8
Proteobacteria	*Mesorhizobium sp. BSA136.*	A0A2A6FB12
Proteobacteria	*Mesorhizobium sp. L103C105A0.*	X6KNW9
Proteobacteria	*Mesorhizobium sp. L103C119B0.*	X6K8U6
Proteobacteria	*Mesorhizobium sp. L103C120A0.*	V7HKF1
Proteobacteria	*Mesorhizobium sp. L103C131B0.*	X6JI92
Proteobacteria	*Mesorhizobium sp. L103C565B0.*	X6J8N5
Proteobacteria	*Mesorhizobium sp. L2C054A000.*	X6IJV0
Proteobacteria	*Mesorhizobium sp. L2C066B000.*	X6IBI6
Proteobacteria	*Mesorhizobium sp. L2C067A000.*	X6HK44
Proteobacteria	*Mesorhizobium sp. L2C084A000.*	X6GLB7
Proteobacteria	*Mesorhizobium sp. L2C085B000.*	X6G5H3
Proteobacteria	*Mesorhizobium sp. L2C089B000.*	V7H7S3
Proteobacteria	*Mesorhizobium sp. LCM 4576.*	A0A1S1SGE3
Proteobacteria	*Mesorhizobium sp. LNHC209A00.*	X6FGQ1
Proteobacteria	*Mesorhizobium sp. LNHC220B00.*	X6E869
Proteobacteria	*Mesorhizobium sp. LNHC221B00.*	X6DIU1
Proteobacteria	*Mesorhizobium sp. LNHC229A00.*	X6F5F1
Proteobacteria	*Mesorhizobium sp. LNHC232B00.*	X6CG07
Proteobacteria	*Mesorhizobium sp. LNJC372A00.*	X6C9N2
Proteobacteria	*Mesorhizobium sp. LNJC386A00.*	X6AY22
Proteobacteria	*Mesorhizobium sp. LNJC391B00.*	A0A0E2P1G0
Proteobacteria	*Mesorhizobium sp. LNJC394B00.*	V7G761
Proteobacteria	*Mesorhizobium sp. LNJC395A00.*	X5ZPA2
Proteobacteria	*Mesorhizobium sp. LNJC399B00.*	X5YP03

Proteobacteria	*Mesorhizobium sp. LNJC405B00.*	X5Y750
Proteobacteria	*Mesorhizobium sp. LSHC412B00.*	X5XFZ5
Proteobacteria	*Mesorhizobium sp. LSHC414A00.*	A0A0E2NC56
Proteobacteria	*Mesorhizobium sp. LSHC422A00.*	X5VM34
Proteobacteria	*Mesorhizobium sp. LSHC426A00.*	X5UD94
Proteobacteria	*Mesorhizobium sp. LSJC264A00.*	V7F6E4
Proteobacteria	*Mesorhizobium sp. LSJC265A00.*	X5S1I0
Proteobacteria	*Mesorhizobium sp. LSJC269B00.*	X5QPQ9
Proteobacteria	*Mesorhizobium sp. LSJC277A00.*	X5PGA8
Proteobacteria	*Mesorhizobium sp. LSJC285A00.*	X5QS57
Proteobacteria	*Mesorhizobium sp. NFR06.*	A0A1I5G908
Proteobacteria	*Mesorhizobium sp. ORS 3324.*	A0A090F2E9
Proteobacteria	*Mesorhizobium sp. ORS 3359.*	A0A090GRZ5
Proteobacteria	*Mesorhizobium sp. Root172.*	A0A0Q8KGY0
Proteobacteria	*Mesorhizobium sp. SEMIA 3007.*	A0A1E2T2G2
Proteobacteria	*Mesorhizobium sp. SOD10.*	A0A090EHA6
Proteobacteria	*Mesorhizobium sp. STM 4661.*	M5FF31
Proteobacteria	*Mesorhizobium sp. WSM3859.*	A0A2A3E142
Proteobacteria	*Mesorhizobium sp. WSM3860.*	A0A2A3D7I2
Proteobacteria	*Mesorhizobium sp. WSM3864.*	A0A2A3CSR2
Proteobacteria	*Mesorhizobium sp. WSM3866.*	A0A2A3B5V7
Proteobacteria	*Mesorhizobium sp. WSM3873.*	A0A1A5S1U6
Proteobacteria	*Mesorhizobium sp. WSM3876.*	A0A2A3C641
Proteobacteria	*Mesorhizobium sp. WSM4308.*	A0A2A3BTW1
Proteobacteria	*Mesorhizobium sp. WSM4313.*	A0A2A3AMD6
Proteobacteria	*Mesorhizobium sp. YR577.*	A0A1I7EFU9
Proteobacteria	*Mesorhizobium temperatum.*	A0A271LPB7
Proteobacteria	*Mesorhizobium wenxiniae.*	A0A271KGC9
Proteobacteria	*Paracoccus aminophilus JCM 7686.*	S5XUM9
Proteobacteria	*Phyllobacterium brassicacearum.*	A0A2P7BEM8
Proteobacteria	*Phyllobacterium endophyticum.*	A0A2P7ANN3
Proteobacteria	*Phyllobacterium myrsinacearum.*	A0A2S9JQA3
Proteobacteria	*Phyllobacterium sophorae.*	A0A2P7B9V6
Proteobacteria	*Phyllobacterium sp. OV277.*	A0A1H0UID8

Proteobacteria	*Phyllobacterium sp. YR531.*	J3CFV9
Proteobacteria	*Phyllobacterium zundukense.*	A0A2N9VTN8
Proteobacteria	*Prosthecomicrobium hirschii.*	A0A0N8GFR1
Proteobacteria	*Proteobacteria bacterium ST_bin15.*	A0A1W9KGW6
Proteobacteria	*Pseudooceanicola sp.*	A0A2E2PAE0
Proteobacteria	*Rhizobiales bacterium GAS113.*	A0A1H1EVZ7
Proteobacteria	*Rhizobiales bacterium GAS188.*	A0A1H4VTU5
Proteobacteria	*Rhizobiales bacterium GAS191.*	A0A1H4SBE6
Proteobacteria	*Rhizobiales bacterium.*	A0A2W4T2N0
Proteobacteria	*Rhizobium acidisoli.*	A0A0N1DQ59
Proteobacteria	*Rhizobium etli 8C-3.*	A0A1L5PHN5
Proteobacteria	*Rhizobium freirei PRF 81.*	N6V2P0
Proteobacteria	*Rhizobium hainanense.*	A0A1C3VFC0
Proteobacteria	*Rhizobium laguerreae.*	A0A1S9GZG6
Proteobacteria	*Rhizobium leguminosarum bv. trifolii WSM1689.*	W0IM90
Proteobacteria	*Rhizobium leguminosarum bv. trifolii WSM2012.*	J0VG82
Proteobacteria	*Rhizobium leguminosarum bv. trifolii WSM2297.*	J0CHG4
Proteobacteria	*Rhizobium leguminosarum bv. trifolii WSM597.*	I9XBR0
Proteobacteria	*Rhizobium leguminosarum bv. trifolii.*	A0A1B8R9C6
Proteobacteria	*Rhizobium leguminosarum bv. viciae (strain 3841)*	Q1M368
Proteobacteria	*Rhizobium leguminosarum bv. viciae (strain WSM1455)*	J0US37
Proteobacteria	*Rhizobium leguminosarum bv. viciae.*	A0A1Q8HLJ8
Proteobacteria	*Rhizobium leguminosarum bv. viciae.*	A0A222U4U6
Proteobacteria	*Rhizobium leguminosarum bv. viciae.*	A0A2L1CPB6
Proteobacteria	*Rhizobium leguminosarum.*	A0A1B1CI88
Proteobacteria	*Rhizobium leguminosarum.*	A0A2K9ZE12
Proteobacteria	*Rhizobium loessense.*	A0A1G4QVR2
Proteobacteria	*Rhizobium loti*	A0A117N3J6
Proteobacteria	*Rhizobium loti*	A0A1A5HRE7
Proteobacteria	*Rhizobium loti*	A0A1A5QH25
Proteobacteria	*Rhizobium loti*	A0A1A5R4W2
Proteobacteria	*Rhizobium loti*	A0A1B4YGQ6
Proteobacteria	*Rhizobium lusitanum.*	A0A1C3XE19

Proteobacteria	*Rhizobium miluonense.*	A0A1C3VF14
Proteobacteria	*Rhizobium multihospitium.*	A0A1C3TVG9
Proteobacteria	*Rhizobium sp. 11515TR.*	A0A248WAG4
Proteobacteria	*Rhizobium sp. 60-20.*	A0A1M3Q932
Proteobacteria	*Rhizobium sp. AC27/96.*	A0A1B9S3G1
Proteobacteria	*Rhizobium sp. AP16.*	J2CWP4
Proteobacteria	*Rhizobium sp. CF142.*	J1TC54
Proteobacteria	*Rhizobium sp. H4.*	A0A2A6R4T7
Proteobacteria	*Rhizobium sp. L43.*	A0A2A6HSS8
Proteobacteria	*Rhizobium sp. L9.*	A0A2A6KSI3
Proteobacteria	*Rhizobium sp. NFR03.*	A0A1H9WZC8
Proteobacteria	*Rhizobium sp. NFR07.*	A0A1I0VUJ4
Proteobacteria	*Rhizobium sp. NXC14.*	A0A1W6Q3K8
Proteobacteria	*Rhizobium sp. NXC24.*	A0A2L0W7N1
Proteobacteria	*Rhizobium sp. P44RR-XXIV.*	A0A1V3G1K7
Proteobacteria	*Rhizobium sp. SEMIA4064.*	A0A2T3GTY4
Proteobacteria	*Rhizobium sp. WYCCWR10014.*	A0A198YF95
Proteobacteria	*Rhizobium sp. YK2.*	A0A1E4Y2S8
Proteobacteria	*Rhizobium tropici CIAT 899.*	L0LXF7
Proteobacteria	*Rhizobium tubonense.*	A0A2W4C6N3
Proteobacteria	*Rhizobium tumorigenes.*	A0A2W4DHA7
Proteobacteria	*Rhodobacteraceae bacterium.*	A0A2E0RFB9
Proteobacteria	*Rhodospirillaceae bacterium.*	A0A2E2CUY2
Proteobacteria	*Rhodospirillaceae bacterium.*	A0A2E2DYB2
Proteobacteria	*Rhodospirillales bacterium.*	A0A2D9I5I5
Proteobacteria	*Roseovarius mucosus.*	A0A1V0RMQ0
Proteobacteria	*Roseovarius sp. TM1035.*	A6E627
Proteobacteria	*Salmonella sp. HMSC13B08.*	A0A1F2K7Y7

4 TMH-Lyase

The enzyme ergothionase, characterized in the previous chapter, is in particular interesting because it shares an overall high similarity with the aromatic amino acid lyases, although ergothionase does not form their catalytic important MIO-moiety. Beside ergothionase, we found another lyase that also did not possess the active site residues that build the basis for MIO-formation. Instead, the new lyase has a conserved tyrosine residue at the equivalent position (Figure 82).

```
                147
LtLyase     ...SVGY---LS...
TdETL       ...SIG-EGDIT...
PpHAL       ...SVGASGDLA...
```

Figure 82. Abbreviated sequence alignment of the new class of lyase from *Lihuaxuella thermophila* (*LtLyase*), ergothionases *Td*ETL and histidine ammonia-lyase from *Pseudomonas putida* (*Pp*HAL). The amino acids forming the MIO-moiety in *Pp*HAL are highlighted in pink, Tyr147 of the new lyase is highlighted in green.

The overall high similarity of the new lyase to ergothionase and aromatic amino acid lyases indicates the close relation of these three lyases. However, the absence of the MIO-moiety and the conservation of the tyrosine residue in the active site suggests profound differences in the mechanism. The new lyase is not simply a homologue of ergothionase with a slightly different substrate specificity profile. The comparison of sequences, structures and catalytic behavior demonstrate that the two enzymes use different catalytic strategies and may have evolved through independent events.

In the following chapter, we will identify the substrate of the new lyase, we will outline important catalytic residues and we will present a possible mechanism. Our results also shed light on the mechanism by which the MIO-moiety catalyzes the elimination reaction in aromatic amino acid ammonia-lyases. Based on the structural and mechanistic knowledge of this new class of lyase, ergothionase and histidine ammonia-lyase in the context with the aspartase/fumarase superfamily, we will also discuss the evolutionary history of these enzymes.

4.1 Identification of a TMH-Lyase

In order to identify the new lyase, we produced three homologue lyases deriving from *Lihuaxuella thermophila* (*LtLyase*), *Halomonas desiderata* (*Hd*Lyase) and *Rhizobium oryzae* (*Ro*Lyase) recombinantly in *E. coli*. All proteins were soluble and produced in yields up to 10 mg/L of culture. We demonstrated the activity of *Ro*Lyase and *Hd*Lyase (Figure 107, Figure 108). However, for our detailed

kinetic investigations, we continued with *Lt*Lyase. The crystal structure of *Hd*Lyase was solved. *Lt*Lyase and *Hd*Lyase share 53% sequence similarity.

The sequence of the new lyase revealed a profound difference in the active site compared to ergothionase and histidine lyase (Figure 82). Indeed, the slow turnover of ergothioneine (2.1×10^{-5} s^{-1}) corroborated that the new lyase is no ergothionase. Therefore, our first goal was to identify the substrate of the new lyase. Investigation into the substrate specificity (described in detail in section 4.3.1) revealed that the new class of lyase is responsible for the 1,2-elimination of TMH to yield *trans*-urocanic acid and trimethylamine (Figure 83).

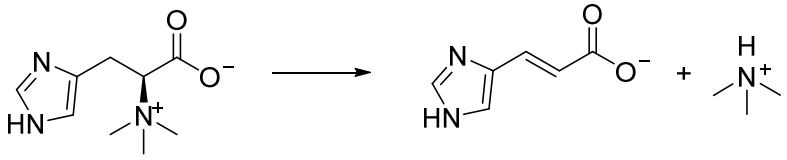

Figure 83. Reaction catalyzed by TMH-lyase. TMH is degraded to *trans*-urocanic acid and trimethylamine.

The k_{cat} of *Lt*Lyase for TMH turnover to urocanic acid at pH 9 was $k_{cat} = 7.2 \pm 0.2$ s^{-1} (Table 18). The K_M of *Lt*Lyase for its main substrate TMH seemed to be high ($K_{M,TMH} = 900 \pm 80$ µM) in regard to the low K_M of *Td*ETL for ergothioneine ($K_{M,ergothioneine} = 45 \pm 4$ µM). However, the reported K_M ($K_{M,His} = 3900$ µM) of the histidine ammonia-lyase from *Pseudomonas putida* (*Pp*HAL) is even higher than the K_M we observed for *Lt*Lyase.[142]

Table 18. Kinetic parameters at the corresponding pH-optima of *Lt*Lyase (pH 9, TMH as substrate), *Td*ETL (pH 7.5, ergothioneine as substrate), *Pp*HAL (pH 9.3, histidine as substrate).[142]

	k_{cat} [s^{-1}]	K_M [µM]	k_{cat}/K_M [$M^{-1}s^{-1}$]
***Lt*Lyase**	7.2 ± 0.2	900 ± 80	7.9×10^3
***Td*ETL**	64 ± 3	45 ± 4	1.4×10^6
***Pp*HAL[142]**	86 ± 6	3900 ± 900	2.2×10^4

The high K_M of *Pp*HAL might be advantageous to avoid histidine degradation at low histidine concentrations; the affinity of histidyl-tRNA-synthetase for histidine should exceed the affinity for histidine degradation in order to circumvent histidine wastage and to ensure proper protein synthesis.[89] The comparatively low K_M of ergothionase can be a sign for an extremely optimized enzyme that has adapted to the low concentration of ergothioneine in the environment.

Furthermore, we showed that the reaction product urocanic acid is a competitive inhibitor of *Lt*Lyase ($K_{i,\ urocanic\ acid}$ = 74 ± 13 µM) (data shown in the experimental section, Figure 111). Product inhibition might be essential to avoid accumulation of urocanic acid and to keep a homeostasis with TMH availability. Thus, product inhibition helps to regulate the activity of the lyase.

4.2 Crystal Structure

The TMH-lyase *Hd*Lyase was crystallized and the structure was solved by Florian Leisinger. The structure was co-crystallized with the product of the reaction, urocanic acid. Similar to ergothionase and MIO-dependent lyases, TMH-lyase is a homo-tetramer with a chain fold mainly consisting of α-helices (Figure 84). The structure is part of the protein domain family lyase_aromatic pfam00221. The backbones of *Hd*Lyase and *Td*ETL superimpose with an RMSD of 2.73 Å while sharing 31.5% sequence identity. The four identical active sites of *Hd*Lyase are lined by residues from three different subunits.

Similar as shown for *Td*ETL, the carboxylate side chain of the ligand approaches the side chains of Asn313 (3.3 Å) and Arg283 (3.3 Å) in *Hd*Lyase (Figure 84). The imidazole moiety of urocanic acid hydrogen bonds to His88 (Nτ, 2.8 Å) and Glu416 (Nπ, 2.8 Å). Glu416 in turn hydrogen bonds with Tyr388 (2.5 Å) and approaches Tyr147 (2.8 Å) which is a main difference in the active site architecture of *Hd*Lyase in contrast to *Td*ETL.

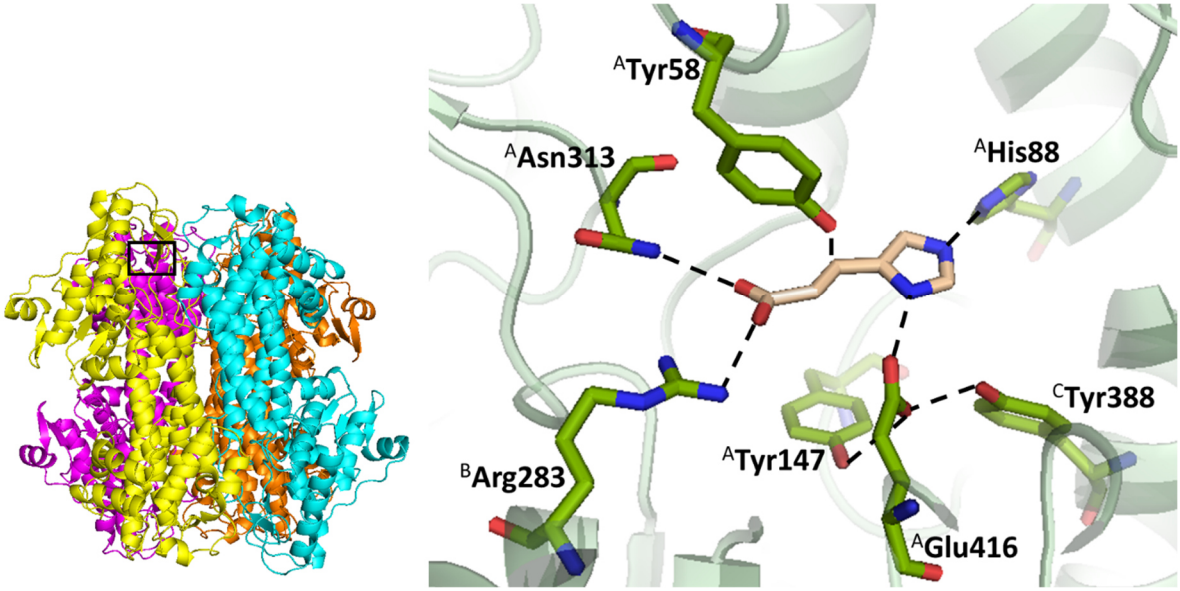

Figure 84. Crystal structure of the homo-tetramer of *Hd*Lyase (left). The black box indicates the active site of subunit A that is shown in detail on the right. The ligand urocanic acid is depicted in wheat.

In contrast to *Lt*Lyase and *Td*ETL, *Pp*HAL requires zinc for substrate binding and optimal activity.[160] It is suggested that in *Pp*HAL, Zn^{2+} coordinates the imidazole ring of the substrate to the equivalents of His88 and Met384 during catalysis.[68] The crystal structure of *Hd*Lyase with urocanic acid in the active site and our studies on zinc-dependent activity of *Lt*Lyase (Table 23) gave evidence that TMH-lyases are not zinc-dependent.

The crystal structure provides key information for the identification of important catalytic residues to understand the mechanism of TMH-lyase and provides the basis for insights into the phylogenetic origin. With the crystal structure of *Hd*Lyase at hand, we investigated the catalytic behavior of TMH-lyase, which allowed us to outline parallels and differences of this enzyme and ergothionase.

4.3 Kinetic Investigations of the Wild Type

4.3.1 Substrate Specificity

In order to closely analyze the reactivity of TMH-lyase and to understand the mechanism, we investigated the substrate specificity of *Lt*Lyase. Studies on substrate specificity can give insights into the distinctive feature of an enzymatic reaction. Following product formation by *Lt*Lyase using different compounds, we found that TMH turnover to give urocanic acid and trimethylamine is the favored reaction of *Lt*Lyase (1.7 ± 0.1 s^{-1} at pH 7.5). *Lt*Lyase-mediated turnover of DMH was 100-fold lower than turnover of the trimethylated variant (Table 19). However, the activity reduction of the desmethylated substrate derivative is clearly less dramatic than observed in ergothionase (5300-fold). Additionally, *Lt*Lyase shows turnover on *S*-methyl ergothioneine, whereas *Lt*Lyase was barely active on ergothioneine and ergothioneine sulfonic acid (Table 19).

Table 19. Observed activity of *Lt*Lyase on different substrates in HEPES buffer at pH 7.5 using 2 mM substrate.

	TMH	DMH	*S*-Methyl ergothioneine	Ergothioneine	Desmethyl-ergothioneine	Ergothioneine sulfonic acid	Desmethyl-ergothioneine sulfonic acid
***Lt*Lyase[s^{-1}]**	1.7 ± 0.1 x 10^{0}	1.6 ± 0.1 x 10^{-2}	7.0 ± 0.1 x 10^{-2}	2.1 ± 0.1 x 10^{-5}	4.0 ± 0.1 x 10^{-4}	8.5 ± 0.1 x 10^{-5}	1.2± 0.1 x 10^{-3}

In a way, TMH-lyase is characterized by a substrate specificity profile that is complementary to that of ergothionase. In contrast to ergothioneine and ergothioneine sulfonic acid, TMH and *S*-methyl ergothioneine were efficient substrates.

Both TMH and *S*-methyl ergothioneine possess similar chemical properties, since both compounds can stabilize a cationic charge on their imidazole moiety (Figure 85).

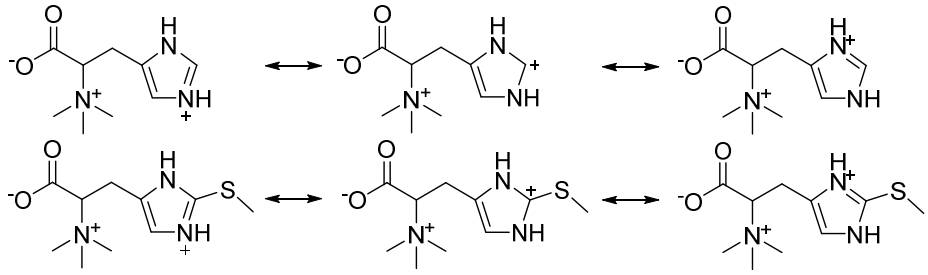

Figure 85. Resonance structures of cationic TMH and S-methyl ergothioneine.

The imidazolium appears to be crucial for the activity of the lyase while increasing acidity of the β-proton of the substrate. Abstraction of the β-proton is a key step in *Lt*Lyase activity, similar to that shown for ergothionase and histidine ammonia-lyase.[161] The acidity of the β-proton in ergothionase is increased by the electron-withdrawing capacity of the imidazolium in the zwitterionic form of ergothioneine that binds in the active site. In *Td*ETL, Lys384 is important for stabilizing the polarized form of the substrate. In the previous chapter, we showed that the mutant K384M possesses decreased activity towards ergothioneine and increased activity towards TMH. Indeed, comparison of the active sites of *Td*ETL and *Lt*Lyase shows that the structural equivalent of Lys384 is Tyr388 in TMH-lyases, which explains the differences in substrate specificity of both enzymes (Figure 86).

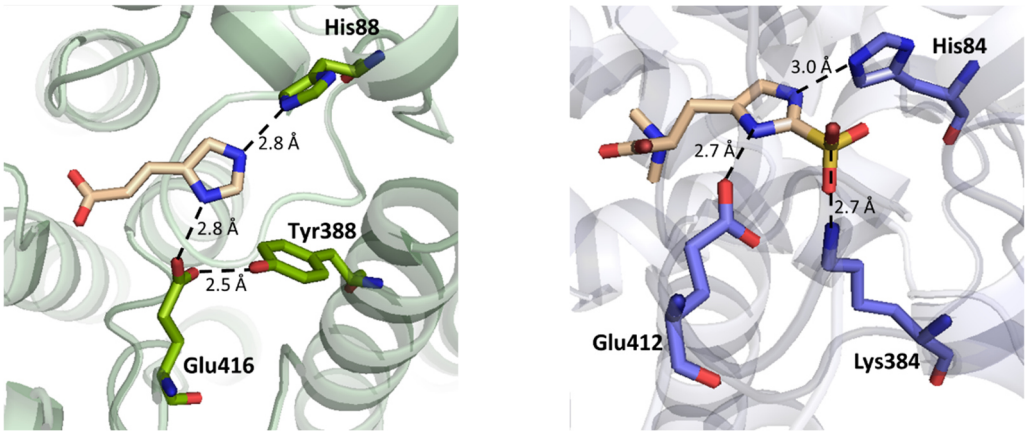

Figure 86. Crystal structure of *Hd*Lyase in complex with urocanic acid (left) and *Td*ETL in complex with desmethyl-ergothioneine sulfonic acid (right, PDB: 6S7Q). The imidazole moiety of the ligands in both proteins are coordinated to equivalent His and Glu residues, whereas Tyr388 in *Hd*Lyase is located on the position of Lys384 in *Td*ETL.

4.3.2 pH-Dependence

The substrate specificity was assessed at pH 7.5. To gain a deeper understanding in the reactivity of *Lt*Lyase, we investigated the pH-dependence of the 1,2-elimination reaction. Studies on the pH-dependence of an enzymatic reaction can give insights into the protonation states of the substrate or the catalytic residues of the enzyme that are required for activity. In the case of *Lt*Lyase, we analyzed pH-dependent Michaelis-Menten kinetics using TMH and DMH as substrates. The k_{cat} for TMH-turnover increased with increasing pH (Figure 87). In contrast to ergothionase, the pH-dependence of k_{cat} was not bell-shaped which is a major difference of both enzymes. Maximal catalytic efficiency was observed at pH 9 and decreased at higher pH values. The pH-dependent measurements of *Lt*Lyase with DMH also showed a similar pattern (data shown in the experimental section, Figure 114).

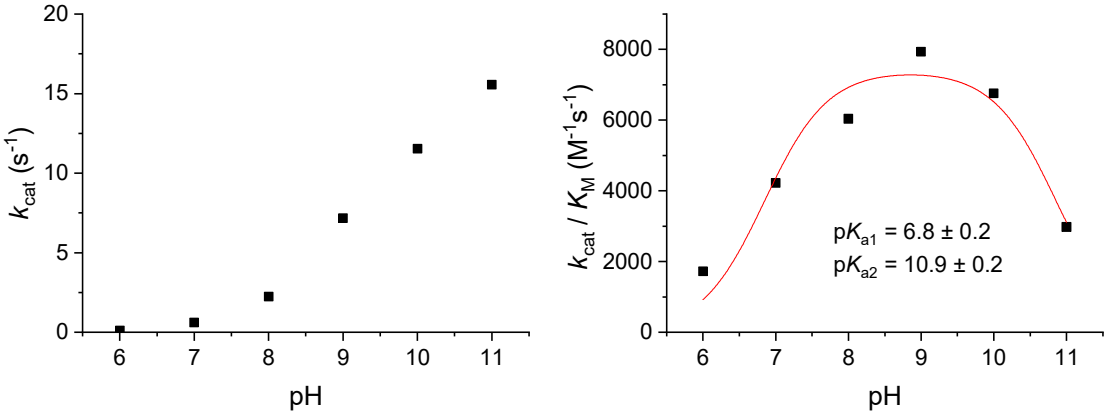

Figure 87. Summary of the observed pH-dependent kinetic parameters of *Lt*Lyase WT using TMH as substrate. Obtained k_{cat}/K_M values were fitted to y = k_{HA}/ (1+$10^{(pKa1-pH)}$ + $10^{(pH-pKa2)}$) (right figure).

The reduced catalytic efficiency at high pH suggests that the formation of the enzyme:substrate complex requires a proton. Indeed, the crystal structure suggests a hydrogen bonding network between His88, Glu416, Tyr147, Tyr388 and the substrate (Figure 84). At higher pH, less protons are available and formation of the enzyme:substrate complex is reduced, presented by a decrease in catalytic efficiency at higher pH. However, once the substrate is bound to the enzyme, catalysis occurs. Therefore, we do not see a reduced k_{cat} at higher pH.

4.3.3 Substrate and Solvent Isotope Effects

In order to determine the substrate isotope effect (KIE) of *Lt*Lyase, we measured Michaelis-Menten kinetics using deuterated TMH as substrate and calculated the ratio of catalytic parameters observed with the non-deuterated substrate. We observed a substrate isotope effect on k_{cat} of *Lt*Lyase (KIE (k_{cat})

= 2.2 ± 0.2), indicating that the cleavage of the β-C-H bond of the substrate is the rate-limiting step of the reaction. Similar as observed for *Td*ETL, the KIE on k_{cat}/K_M was negligible (KIE (k_{cat}/K_M) = 1.4 ± 0.2), suggesting that substrate binding is partially irreversible (section 3.4.1).

We also investigated in the solvent isotope effect (KSIE) of *Lt*Lyase, however solvent isotope effects are difficult to interpret because exchange of the solvent causes multiple changes in the reaction system and not only a specific variation like the substrate isotope effect. The observation of a KSIE on k_{cat} (KSIE (k_{cat}) = 2.3 ± 0.2) and on catalytic efficiency (KSIE (k_{cat}/K_M) = 1.8 ± 0.1) indicates that proton transfer occurs during a rate-limiting step. We suggest that protonation of the leaving group trimethylamine is reflected by the KSIE which might indicate an E2 elimination. Additionally, we measured a KIE in D_2O (KIE_{D2O} = 1.6 ± 0.1) and a KSIE with deuterated substrate ($KSIE_{deut.-TMH}$ = 1.5 ± 0.2), both double deuterated effects were reduced (Table 20).

Table 20. Observed substrate kinetic isotope effects (KIE) and kinetic solvent isotope effect (KSIE) at pH 7.5 of *Lt*Lyase.

	KIE (k_{cat})	**KSIE (k_{cat})**
H_2O	2.2 ± 0.2	---
D_2O	1.6 ± 0.1	---
Ergothioneine	---	2.3 ± 0.2
Deut.-Ergothioneine	---	1.5 ± 0.2

In the case of *Td*ETL, the KIE and KSIE of the double deuterated experiments vanish, suggesting a sequential order acid-base catalysis for *Td*ETL. For *Lt*Lyase, the reduced double deuterated effects also suggest a sequential order acid-base catalysis for *Lt*Lyase-mediated TMH-degradation, in which a base is responsible for the abstraction of the β-proton of the substrate and an acid is responsible for protonation of the leaving group.

4.4 Important Catalytic Residues of TMH-Lyase Compared to Ergothionase and Histidine Ammonia-Lyase

Studies of the crystal structure of proteins and site-directed mutagenesis are valuable tools in order to identify the important catalytic residues of an enzyme. In the case of TMH-lyase, it is also helpful to compare the active site to the related previously described *Td*ETL and the well-known enzyme *Pp*HAL.

All the three lyases *Lt*Lyase, *Td*ETL and *Pp*HAL catalyze a 1,2-elimination of the amine or trimethylamine group of histidine or a histidine derivative. In *Td*ETL and *Pp*HAL, this elimination is initiated by a

conserved active site tyrosine (Tyr54 in *Td*ETL) that cleaves the β–C-H bond of the substrate.[68,142] The equivalent residue in *Lt*Lyase is Tyr58. Mutation of this residue to phenylalanine caused a 10^5-times decrease in k_{cat}, which shows that this tyrosine residue is indeed crucial for activity (Table 21).

Table 21. Observed kinetic parameters at pH 9 of *Lt*Lyase WT and variants using TMH as substrate.

	k_{cat} [s^{-1}]	K_M [μM]	k_{cat}/K_M [$M^{-1}s^{-1}$]
***Lt*Lyase WT**	7.2 ± 0.2	900 ± 80	7.9×10^{3}
***Lt*Lyase Y58F**	$6.6 \times 10^{-5} \pm 7 \times 10^{-6}$	700 ± 200	9.0×10^{-2}
***Lt*Lyase Y147F**	$9.3 \times 10^{-2} \pm 1 \times 10^{-3}$	700 ± 100	1.4×10^{2}
***Lt*Lyase E416Q**	$3.4 \times 10^{-3} \pm 3 \times 10^{-4}$	1600 ± 300	2.1×10^{0}

The crystal structure of *Hd*Lyase with urocanic acid shows proximity between the oxygen atom of Tyr58 and the β-position of the product (2.7 Å) which gave evidence that Tyr58 is the catalytic base (Figure 88). Considering the catalytic base, we found high similarities among the three classes of lyases, whereas other catalytic residues have distinct differences as will be outlined in the following.

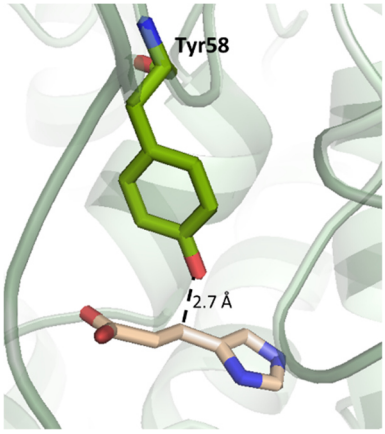

Figure 88. Crystal structure of *Hd*Lyase in complex with urocanic acid (colored in wheat). Tyr58 is positioned as catalytic base (colored in green).

In the active site of *Lt*Lyase, a tyrosine residue (Tyr147) is located at the equivalent position of the MIO-moiety in *Pp*HAL (Figure 89). The ergothionase *Td*ETL has a glutamate residue (Glu143) at that position; however, this glutamate points away from the active site and we suggest that this residue is not involved in catalysis. The phenol of Tyr147 in *Lt*Lyase is located in hydrogen bonding distance to the carboxylate of Glu416 (2.8 Å) (Figure 84, Figure 90).

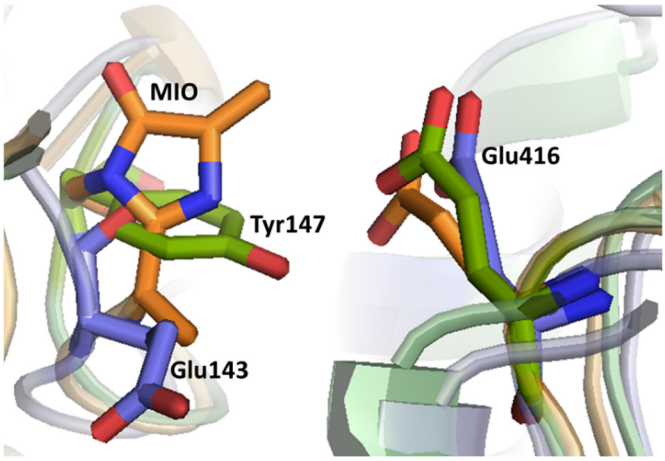

Figure 89. Superimposed structure of *Hd*Lyase (green), *Td*ETL (blue, PDB: 6S7Q) and *Pp*HAL (orange, PDB: 1B8F). Glu416 (counting based on *Hd*Lyase) is structurally highly conserved, whereas Tyr147 (*Hd*Lyase) is located on the position of MIO in *Pp*HAL and Glu143 in *Td*ETL.

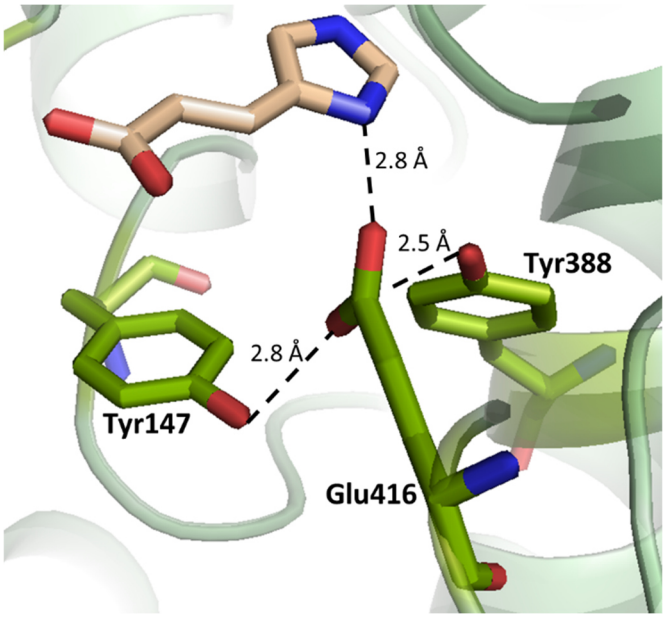

Figure 90. Crystal structure of *Hd*Lyase in complex with urocanic acid (colored in wheat). Glu416 hydrogen bonds with Nπ of urocanic acid and Tyr388 and Tyr147.

The variant Y147F caused an 80-fold reduction in k_{cat} (Table 21). We further investigated the pH-dependence of Y147F (Figure 91). Similar to the wild type, k_{cat} was found to increase with pH, whereas catalytic efficiency decreased at a higher pH.

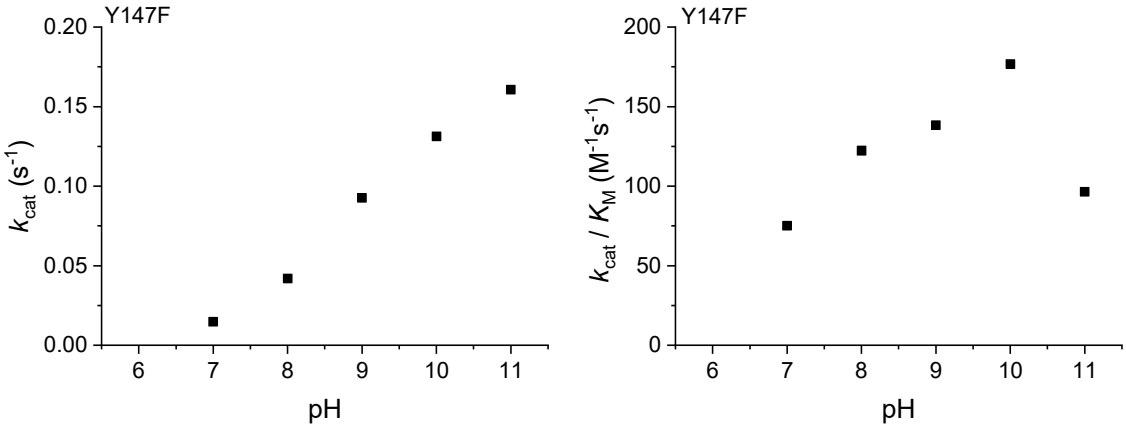

Figure 91. Summary of the observed pH-dependent kinetic parameters of *Lt*Lyase Y147F using TMH as substrate. Details are shown in the experimental section (Figure 118).

One possible function of Tyr147 would be that this residue is involved in protonation of the leaving group trimethylamine (Figure 93). Usually, the pK_a of a tyrosine residue is around 10; however, the hydrogen bonding network of Tyr147 with Glu416 influences the pK_a which might allow protonation of the trimethylamine group which has a pK_a of 9-10.

Due to the hydrogen bonding distance between Tyr147 and Glu416 (2.8 Å), we propose that Glu416 assists in stabilizing the acid proton as a hydrogen bond acceptor (Figure 90, Figure 93). The crystal structure also revealed hydrogen bonding distance (2.8 Å) between Glu416 and Nπ of the substrate.

The variant E416Q reduced k_{cat} and catalytic efficiency by over three orders of magnitude (Table 21). The pH-dependence of that variant showed an increase in k_{cat} with increase in pH similar as observed for the wild type enzyme and variant Y147F (Figure 92).

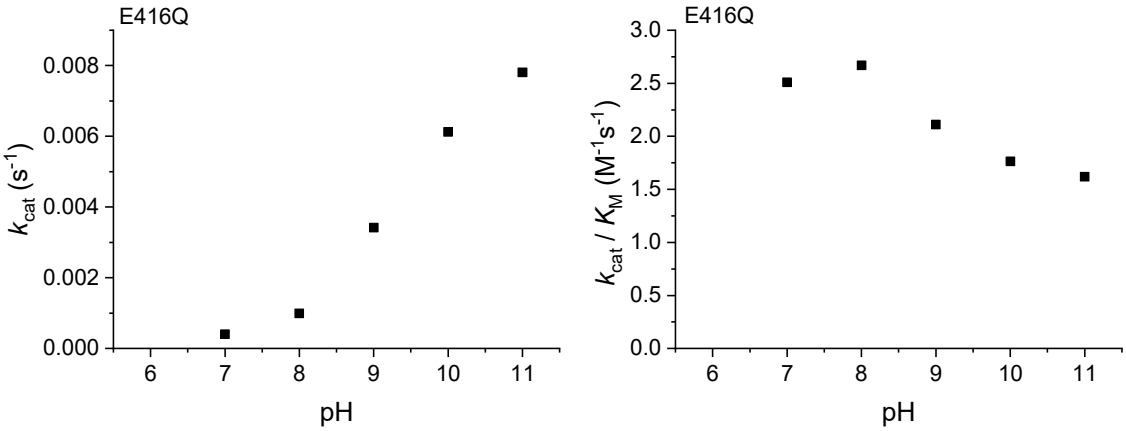

Figure 92. Summary of the observed pH-dependent kinetic parameters of *Lt*Lyase E416Q. Details are shown in the experimental section (Figure 119).

Glutamine substitution of the equivalent glutamate in *Td*ETL (Glu412) caused a similar decrease in k_{cat} and catalytic efficiency. In *Td*ETL, Glu412 is important for binding the N-H group of the substrate and for transferring the proton from Lys384 to the leaving group trimethylamine. The equivalent variant E414Q in *Pp*HAL also caused a similar reduction in k_{cat} and catalytic efficiency.[142] Computational investigations of the *Pp*HAL reaction showed hydrogen bonding distance between Glu414 and Nπ of the substrate,[68] similar as we found for *Td*ETL and *Lt*Lyase. Whereas in *Pp*HAL, the hydrogen bonding network of the glutamate residue is not known to be required for proton transfer or catalytic acid stabilization. During formation of the MIO-moiety, the hydrogen bonding network of Glu414 in *Pp*HAL facilitates hydroxyl elimination.[162]

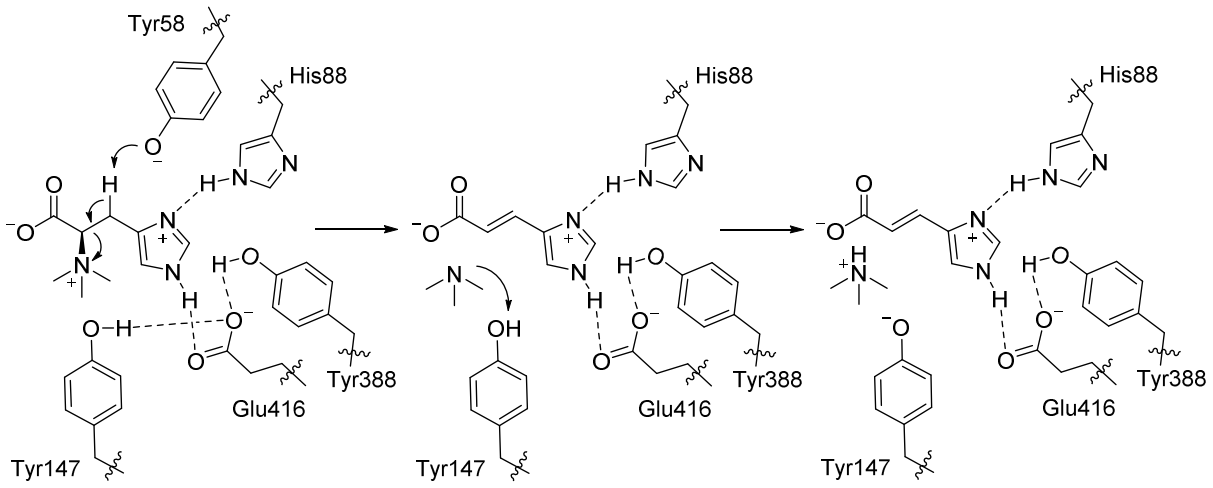

Figure 93. Mechanistic proposal of TMH degradation within the active site of TMH-lyase.

4.4.1 Implications on the Mechanism of MIO-dependent Enzymes

In aromatic amino acid lyases, such as *Pp*HAL, the MIO-moiety is formed posttranslational from the tripeptide Ala142-Ser143-Gly144.[57] Proper formation of the MIO-moiety is crucial for catalysis of *Pp*HAL.[142] Sequence alignment of *Lt*Lyase and *Pp*HAL revealed a deletion of three amino acids and the conservation of Tyr147 in *Lt*Lyase at the position of the Ala-Ser-Gly tripeptide in *Pp*HAL (Figure 82). Structural alignment of *Pp*HAL (PDB: 1B8F) and *Hd*Lyase indicates that the MIO-moiety in *Pp*HAL is exactly at the position of Tyr147 in *Hd*Lyase (Figure 94). As shown above, we suggest that Tyr147 protonates the leaving group trimethylamine (Figure 93).

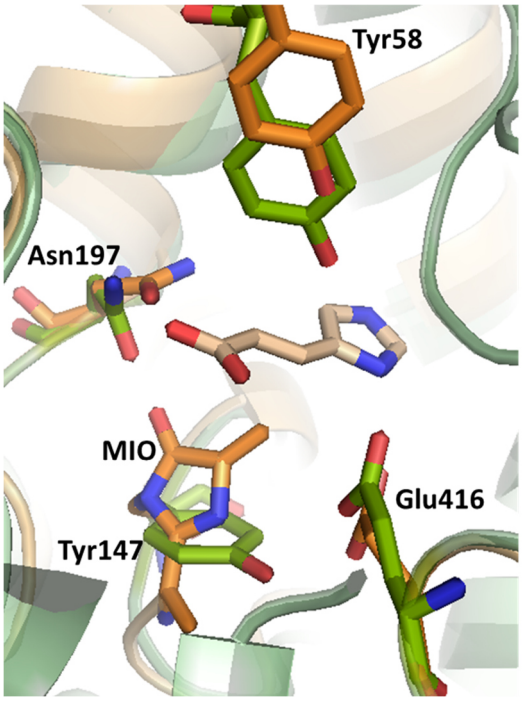

Figure 94. Superimposed structure of *Hd*Lyase (green) and *Pp*HAL (orange, PDB:1B8F). The ligand urocanic acid of the *Hd*Lyase structure is colored in wheat. Counting based on *Hd*Lyase.

The contribution of Tyr147 to catalysis in *Lt*Lyase highlights an interesting analogy to MIO-dependent enzymes. The phenol ring of Tyr147 might support the 1,2-elimination in a similar way as the enol/enolate function of the MIO-moiety in aromatic amino acid lyases. So far, the literature suggests that the α-amino group of the substrate is activated as leaving group upon covalently attachment to the MIO-moiety.[56,67,149,163] However, it is not precisely clear whether monoalkylation would activate a primary amine as a leaving group. In most accounts on the mechanism of MIO-dependent enzymes, the cofactor is drawn in the deprotonated enolate form. The dominant protonation state of this moiety has not yet been established.

Based on our finding of tyrosine as catalytic acid in TMH-lyases, we suggest that the MIO-moiety might also have a similar function. The MIO-oxygen might be proton-activated leading to an enol intermediate (Figure 95). The enol might then be responsible for leaving group protonation, similar as we have proposed for the catalytic acid tyrosine in TMH-lyase. The hydrogen transfer to MIO might be an overseen important additional function of that catalytically-relevant moiety.

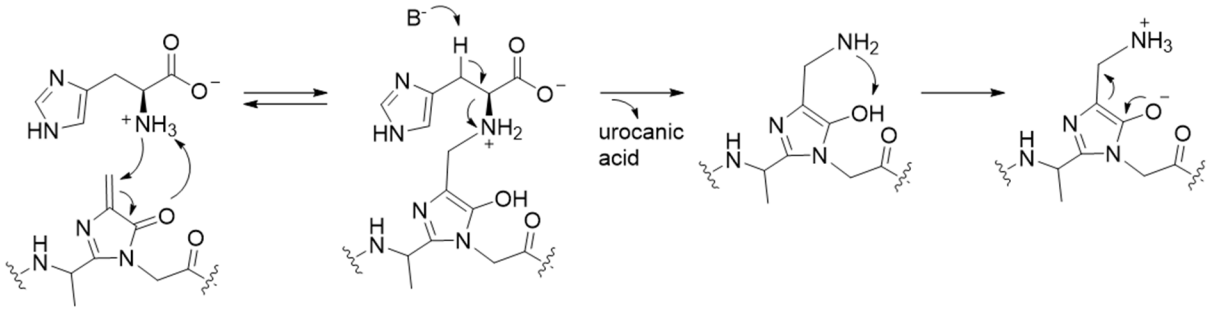

Figure 95. Proposed mechanism of the MIO-dependent deamination of histidine under formation of an enol intermediate.

We found that in *Pp*HAL (PDB: 1B8F), Asn195 points towards the oxygen of MIO (Figure 94). Maybe this Asn195 is important to aid stabilization of the MIO-enol form during catalysis. This hypothesis might explain the reported drastic reduction in activity of the N195A variant.[142] TMH-lyases have either a serine or asparagine residue at that position. In the structure of *Hd*Lyase, the oxygen of Tyr147 does not point in the same direction as the oxygen of MIO which might explain why the corresponding Asn195 is not fully conserved in TMH-lyases.

From an evolutionary point of view, we would propose that TMH-lyases first used a common active site tyrosine residue as a catalytic acid to protonate the leaving group trimethylamine. Later emergence of the MIO-moiety in histidine ammonia-lyases mimics both a catalytic acid and a higher substituted amino group to catalyze the reaction in an overall similar fashion as TMH-lyases. Thus, we suggest that MIO-dependent lyases might have evolved from TMH-lyases.

4.5 Important Residues for MIO-Formation in Histidine Ammonia-Lyase

Considering MIO-formation in *Pp*HAL, it was postulated that, beside the crucial tripeptide Als142-Ser143-Gly144, also Asp145, Asn195, Tyr280 and Phe329 serve important functions (Figure 96).[68,142,162,164]

```
                142       195     280      329
PpHAL      ...SVGASGDL...LLNG...DPYS...GGNFH...
TdETL      ...SIG-EGDI...IVSC...DPLS...SANFE...
LtLyase    ...SVGY---L...LISG...DALS...GCNCD...
HdLyase    ...SVGY---L...LVNG...DALS...QANPH...
```

Figure 96. Sequence alignment of *Pp*HAL, *Td*ETL, *Lt*Lyase and *Hd*Lyase. The residues important for MIO-formation are highlighted in purple. The Cys-motif in *Lt*Lyase is highlighted in yellow. Counting based on *Pp*HAL.

In *Pp*HAL, Asp145 is the bordering residue in MIO-formation and is strongly fixed in a hydrogen bonding network.[162] The crystal structure of *Pp*HAL_D145A (PDB: 1GK3) gave evidence that MIO formation is defective in the absence of Asp145. Even if ergothionase does not form the MIO-moiety, the corresponding Asp145 is conserved in *Td*ETL. Whereas, *Lt*Lyase has a deletion of three residues at that position.

It is proposed that Asn195 in *Pp*HAL activates N-Gly144 as nucleophile for MIO-formation.[164] A possible explanation for the observed lack in activity of the N195A variant[142] might be its inability to form MIO,[164] however evidence for this hypothesis is lacking. *Td*ETL has a conserved serine at that position, whereas TMH-lyases have a serine or an asparagine residue. The fact that TMH-lyases have variations at that position show that this residue might not be crucial for their activity.

Tyr280 serves as an acid-base catalyst during MIO-formation and is, together with Glu414, responsible for the exocyclic dehydration step.[164] *Lt*Lyase and *Td*ETL both have a conserved leucine at that position.

Another important residue for MIO-formation in *Pp*HAL is Phe329. The variant F329A is still able to form MIO (PDB: 1EB4), whereas F329G failed to form MIO (PDB: 1GK2).[162] Therefore, C-β of Phe329 is proposed to be an important counteracting anchor point for the MIO-forming cyclization step. Even if variant F329A possesses the MIO-moiety, the activity of this variant remained low (0.04% activity of the wild type).[165] For *Td*ETL, we showed that the equivalent Phe327 packs the aromatic plane against the N-α-methyl groups of the substrate.[133]

*Lt*Lyase does not have a conserved aromatic residue. Instead, a cysteine residue (Cys331) is located at that position (Figure 96). There is also a second cysteine (Cys329) in close proximity, separated by an asparagine residue. These cysteine residues are not conserved throughout TMH-lyases; the crystallized *Hd*Lyase has an Ala329-Asn330-Pro331 motif at the same position. The structure revealed that this tripeptide is located on a loop-region in the protein close to the active site. In order to determine the function of the two cysteine residues in *Lt*Lyase, we constructed a double-mutant C329G_C331P. This variant leads to a more than two times increase in k_{cat} (Table 22).

Table 22. Observed kinetic parameters at pH 9 of *Lt*Lyase WT and C329G_C331P using TMH as substrate

	k_{cat} [s^{-1}]	K_M [µM]	k_{cat}/K_M [$M^{-1}s^{-1}$]
***Lt*Lyase WT**	7.2 ± 0.2	900 ± 80	7.9×10^3
***Lt*Lyase C329G_C331P**	17 ± 1	1400 ± 200	1.2×10^4

We suggest that the two cysteine residues might have a regulatory function as the Cys-Asn-Cys motif forms disulfide bonds in high probability. Since other representatives of TMH-lyase class do not have the Cys-Asn-Cys motif, we suggest that the disulfide bond is not advantageous for turnover. In the variant C329G_C331P disulfide bond formation is no longer possible what might explain the increase in activity.

We attempted to build a MIO-moiety in ergothionase by site-directed mutagenesis that introduced the described important residues into *Td*ETL (described in detail in the experimental section, Figure 123). However, we were not able to insert a MIO-moiety, most likely because such major changes in the active site of a protein leads to the problem of proper folding.

4.6 Phylogenetic Development

In the previous section, we showed distinct differences between the related lyases ergothionase, TMH-lyase and HAL. However, the overall functional and structural similarity of these three lyases suggest a common ancestor. In order to evaluate which lyase evolved first and constituted the basis for their development, we compared these lyases to aspartase. Aspartase catalyzes the elimination of the amino group of aspartate to yield fumarate (section 1.1.1). Aspartase belongs to the aspartase/fumarase superfamily that participate in the citric acid cycle. The affiliation of fumarase in the ubiquitous citric acid cycle gives evidence that the enzymes of the aspartase/fumarase superfamily represent the ancestor for the development of ergothionase, TMH-lyase and HAL.

The overall structure of aspartase, ergothionase, TMH-lyase and HAL are largerly conserved: all proteins are basically α-helical homo-tetramers.[13,133] The active site of these proteins is separated from the protein surface and contains residues from three different subunits. In contrast to the structural similarities, the mechanism of these proteins shows distinct differences. For aspartase, the carboxylate groups of the substrate stabilize the carbanion intermediate throughout the $E1_{cb}$ mechanism.[13] The need of an acid-catalyst that protonates the leaving group is not fully elucidated yet.[18] For HAL, the α-amino group of the substrate forms a covalent bond with the electrophilic carbon of the MIO-moiety, which is suggested to activate the amino group as leaving group.[63,65] Leaving group activation is also important for catalysis of ergothionase. In ergothionase, the leaving group abilities are increased through forcing the quaternary ammonium group in a nonpolar pocket. Additionally, the substrate ergothioneine is bound in a polarized form which increases acidity of the β-proton; substrate assistance was also shown for aspartase via the electron sink of the carboxylate groups. Accordingly, ergothionase in a way combines the mechanism of substrate-assistance of aspartase and leaving-group

activation of MIO-dependent HAL. This finding could be interpreted as a hint that ergothionase presents the phylogenetic transition of ancestral aspartase and MIO-dependent enzymes.

In order to further evaluate the phylogenetic development, we looked at the overall sequence similarity of aspartase to the three lyases (ergothionase, TMH-lyases, HAL). Because the degree of sequence identity sometimes reflects more the evolutionary distance between the species than differences in the protein,[148] we compared the aspartase sequence of the same organism to the corresponding lyase. Comparison of *Lt*Lyase to *Lt*Aspartase (WP_089965319) gave 16.0% sequence similarity, *Pp*HAL to *Pp*Aspartase (WP_029380744) showed 19.6% similarity, while the sequence of *Td*ETL and *Td*Aspartase (WP_002679739) shared 31.0% similarity. This finding shows that ergothionase is overall more similar to the ancestor aspartase which suggests that ergothionase might be older than TMH-lyase and HAL.

To further reconstruct the evolutionary history of these enzymes, we built a phylogenetic tree. A phylogenetic tree represents hypotheses about the evolutionary relationships among a group of enzymes.[166] We built an unrooted phylogenetic tree based on the protein sequences of ergothionase, TMH-lyase, MIO-dependent HAL and aspartase (Figure 97). To construct the phylogenetic tree, we selected the specific ergothionase and TMH-lyase characterized throughout this work (*Td*ETL, *Bp*ETL, *Sj*ETL, *Lt*Lyase, *Hd*Lyase, *Ro*Lyase). Furthermore, we selected the MIO-dependent *Pp*HAL because of the known crystal structure (PDB: 1B8F). Additionally, we added the MIO-dependent HAL deriving from the same organisms as ergothionase and TMH-lyase (*T. denticola* and *L. thermophila*). We proceeded similar while selecting the sequences of aspartase: known crystal structure of *Bacillus sp.* aspartase (PDB: 3R6V) and aspartase of *T. denticola* and *L. thermophila*. In the resulting phylogenetic tree, the branch of ergothionases (blue) is the closest to the branch of aspartase (grey), whereas the MIO-dependent HAL (orange) are located on the opposite branch of aspartases (Figure 97). This pattern of branching in the phylogenetic tree suggests that ergothionases have evolved from aspartases; later TMH-lyases (green) diverged and the MIO-dependent lyases are a comparative new class of enzymes. Thus, the emergence of MIO probably constituted a new innovation. In contrast, the deletion of three amino acids in the active site of TMH-lyase might show that MIO got lost over time, which would claim that the MIO-dependent HAL is older than TMH-lyase.

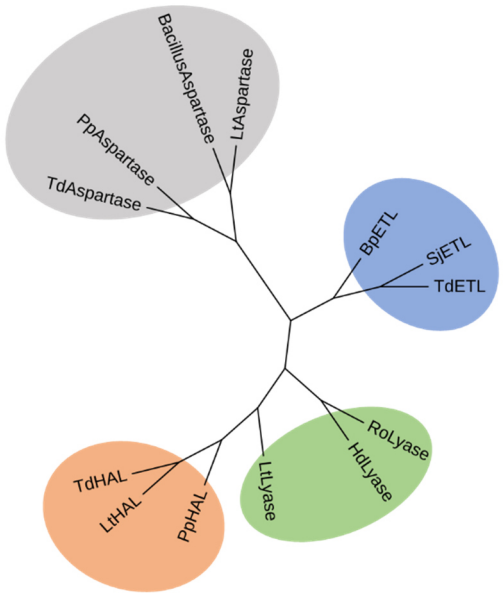

Figure 97. Phylogenetic tree of aspartases (highlighted in grey; from *T. denticola*, *P. putida*, *Bacillus sp.*, *L. thermophila*), ergothionases (highlighted in blue; from *B. pseudomallei*, *S. jonesii*, *T. denticola*), TMH-lyases (highlighted in green; from *R. oryzae*, *H. desiderata*, *L. thermophila*), MIO-dependent HAL (highlighted in orange, from *P. putida*, *L. thermophila*, *T. denticola*).

Additionally, we dissected the active site architecture of *Bacillus sp.* (PDB: 3R6V). Similar to *Td*ETL, *Hd*Lyase and *Pp*HAL, the active site of aspartase is covered by a highly flexible conserved loop.[13] This loop is important for substrate binding and catalysis. A serine residue, located on the loop, works as catalytic base in aspartase. In the case of ergothionase, TMH-lyase, and HAL, a tyrosine residue which is also located on the loop region is the catalytic base. Aspartase possesses a lysine residue that is important for stabilization of the carboxylate of the substrate.[13] Recently, it has been suggested that the equivalent lysine residue in *E. coli* fumarase is important for lowering the pK_a of the catalytic base.[14] Oxyanion stabilization of the catalytic base by a lysine residue (Lys64, *Td*ETL counting) is also a conserved feature of ergothionase as described in section 3.2.4. Neither HAL or TMH-lyase have a lysine residue with a similar function. The functional conservation of the lysine residue only throughout ergothionases and the aspartase/fumarase superfamily can be interpreted as a hint for a closer relation between these two enzymes.

Based on these findings, we suggest that ergothionase has probably evolved prior TMH-lyase and HAL. This finding seems surprising since HAL presents the first step of the universally conserved histidine degradation pathway hut. If ergothioneine degradation is older than the hut-system, this would pre-date ergothioneine emergence prior to histidine. However, histidine is needed for ergothioneine biosynthesis. One explanation would be that the hut-system known today was not the origin of

histidine degradation but rather the improved replacement for an alternative histidine degradation pathway. Perhaps, HAL is not native to the histidine degradation pathway but is recruited from another family of lyases and has adapted to allow histidine degradation. It was found that the *hut*-operon in *Pseudomonas* is accompanied by a gene *hutH1* which is similar to the gene coding for HAL.[167] However, the protein encoded in *hutH1* does not form the MIO-moiety but resembles a TMH-lyase. The function of *hutH1* within the hut-system is not clarified yet.[89] The finding of a second lyase encoded within the same operon might indicate that HAL has not always been part of the *hut*-operon.

4.7 Influence of Fluorine-Containing Substrates on Lyase Activity

An interesting and major difference between *Lt*Lyase and *Td*ETL is their reactivity with the fluorine-incorporated substrate derivatives fluor-TMH (F-TMH) or fluor-ergothioneine (F-ergothioneine). F-ergothioneine was an accepted substrate for *Td*ETL ($k_{cat}/K_{M,\ F\text{-}ergothioneine}$ = 5.5 x 10^5 M^{-1} s^{-1}); the catalytic efficiency is within the same range as observed when ergothioneine is used as a substrate ($k_{cat}/K_{M,\ ergothioneine}$ = 1.4 x 10^6 M^{-1} s^{-1}). Apparently, the replacement of one hydrogen atom with fluorine in the substrate does not interfere with *Td*ETL activity (Figure 124).

In contrast, turnover of F-TMH by *Lt*Lyase was barely detectable (<0.001 s^{-1}). In order to investigate if *Lt*Lyase was not able to bind F-TMH or whether it simply failed to turnover F-TMH, we examined whether F-TMH could inhibit *Lt*Lyase catalyzed turnover of TMH. First, we assessed the inhibitory activity under the assumption that F-TMH is a reversibly competitive inhibitor. Therefore, Michaelis-Menten kinetics of *Lt*Lyase inhibition by F-TMH were run by measuring the apparent $K_{M,TMH}$ in the presence of different concentrations (0.3 µM; 0.4 µM; 0.5 µM) of F-TMH (Figure 98). From these data, K_i was calculated using the equation $K_i = \frac{K_M * [I]}{K_{M(app.)} - K_M}$.[147] The very low value of K_i ($K_{i,\ F\text{-}TMH}$ = 0.09 µM) raised suspicions whether inhibition by F-TMH is reversible.

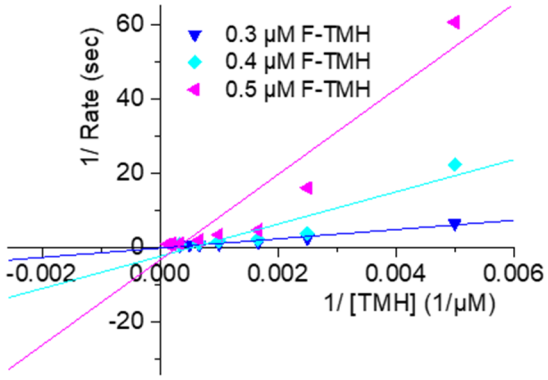

Figure 98. Lineweaver-Burk plot of the data used to examine *Lt*Lyase inhibition by F-THM. Turnover of TMH was followed in the presence of 0.3 µM (blue); 0.4 µM (turquoise); 0.5 µM (pink) F-THM.

In order to determine if inhibition of *Lt*Lyase by F-TMH is reversible, we investigated a time-dependent inhibition of *Lt*Lyase by pre-incubation of the enzyme (0.2 µM) with F-TMH (0.3 µM). After pre-incubation, TMH (1 mM) was added to start the reaction (Figure 99). Only for the first data point (t = 0 min) the reaction was started by the addition of *Lt*Lyase to examine the turnover of TMH in the presence of F-TMH (1.10 ± 0.07 s^{-1}). Incubation of *Lt*Lyase (0.2 µM) with F-TMH (0.3 µM) for 1 min reduced the catalytic activity to less than 2% (1.6 x 10^{-2} ± 1 x 10^{-3} s^{-1}). Most interestingly, the activity did not recover, even if the enzyme was pre-incubated up to 45 min (or indeed four hours, as found in

a single unconfirmed experiment). Incubation of the enzyme in the absence of F-TMH, did not reduce activity to the same extent (Figure 99, black squares). From these observations we learned that F-TMH inhibits *Lt*Lyase in a fast and almost stoichiometric reaction that leads to long lasting (if not irreversible) inhibition.

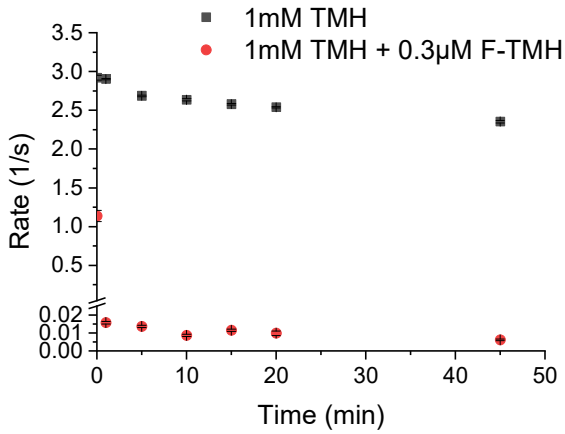

Figure 99. Observed activity of *Lt*Lyase WT (0.2 µM) on TMH (1 mM) at pH 7.5 after incubation (0, 1, 5, 10, 15, 20, 45 min) in the absence (black) and presence of 0.3 µM F-TMH (red). The error bars present the standard deviation of the three independent measurements. F-TMH caused 98.6% reduction of activity within the first minute.

The inhibitory behavior of F-TMH is characteristic for covalent inhibition. One possibility is that F-TMH could transfer its fluoromethyl group to a nucleophilic active site residue (Figure 100). In order to identify possible alkylation sites, we examined F-TMH treated and trypsin digested *Lt*Lyase by high-resolution ESI-MS; however, we only found the masses of unmodified peptides. This negative result does not necessarily rule out the possibility that active site residues are fluoromethylated because this modification may not be stable under the conditions used for tryptic digest and ESI-measurements.

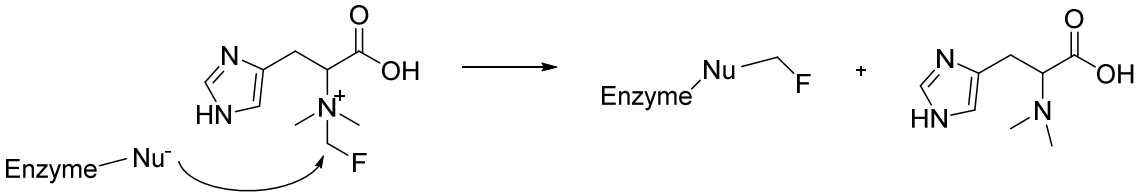

Figure 100. Reaction scheme of a possible enzyme modification by F-TMH.

As a second approach to identify a possible alkylation site, we surmised that if the enzyme is inhibited by alkylation of a specific active site residue, then the residual activity of the corresponding mutant lacking this residue should be resistant to inhibition. In this regard, Tyr147 is a particularly promising

candidate. This residue could make direct contact to the fluoromethyl group if F-TMH bound to the active site in a similar orientation as urocanic acid (Figure 84). The phenol function of this residue would provide a viable nucleophile. Incidentally, this idea would also explain why *Td*ETL is not inhibited: ergothionases do not contain a structurally equivalent tyrosine residue.

Contrary to our expectation, we found that the variant Y147F was also inhibited by F-TMH, although the observed activity reduction of Y147F was 10-fold instead of 100-fold for the wild type enzyme. Within the first minute, *Lt*Lyase Y147F (0.5 µM) lost 90.5% activity in the presence of F-TMH (0.3 µM) (t=0 min: 0.018 ± 0.006 s^{-1}; t=1 min: 0.0017 ± 0.0002 s^{-1}) (Figure 101, red dots). One explanation for the reduced inhibition of Y147F in contrast to the wild type might be the reduced ratio between enzyme and F-TMH. Nevertheless, the observed activity reduction of the variant Y147F shows that Tyr147 is at least not the only modified residue. Other possible modification targets might be Tyr388, Ser197, Cys68 or Cys412. Further mutational studies on these residues might help to identify another target of modification.

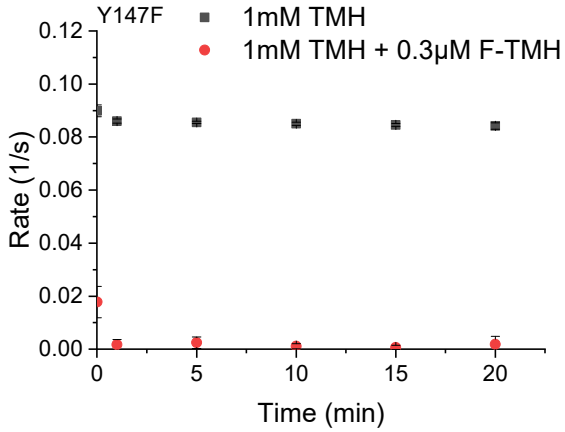

Figure 101. Observed activity of *Lt*Lyase_Y147F (0.5 µM) on TMH (1 mM) at pH 7.5 after incubation (0, 1, 5, 10, 15, 20 min) in the absence (black) and presence of 0.3 µM F-TMH (red). The error bars present the standard deviation of the three independent measurements. F-TMH caused 90.5% reduction of activity within the first minute.

In order to detect any possible fluorine transfer from F-TMH to *Lt*Lyase, we recorded ^{19}F-NMR spectra of F-TMH (1 mM) and of F-TMH (1 mM) in the presence of *Lt*Lyase (100 µM) (Figure 102). F-TMH shows a signal at -194.5 ppm. However, the sample that included F-TMH and *Lt*Lyase did not show a new ^{19}F-signal deriving from a fluoromethyl-modification on the enzyme. The new signal at -123.7 ppm in the sample of F-TMH and *Lt*Lyase derived from inorganic fluoride, the chemical shift was identical to the NaF control (spectra shown in the experimental section, Figure 127). The absence of a signal from a fluoromethyl-modification on the enzyme does not rule out the presence of such a modification. It

might be possible that we cannot detect transferred flourine on the large tetrameric enzyme (224 kDa) by NMR. However, the inorganic fluoride signal (-123.7 ppm) derived only in the presence of *Lt*Lyase. A possible explanation for the emergence of fluoride is that *Lt*Lyase, independent from any modification, at a very slow rate (<0.001 s^{-1}) degrades F-TMH to urocanic acid and fluor-trimethylamine. The leaving group, fluoro-trimethylamine, might then decompose to fluoride, dimethylamine and formaldehyde.

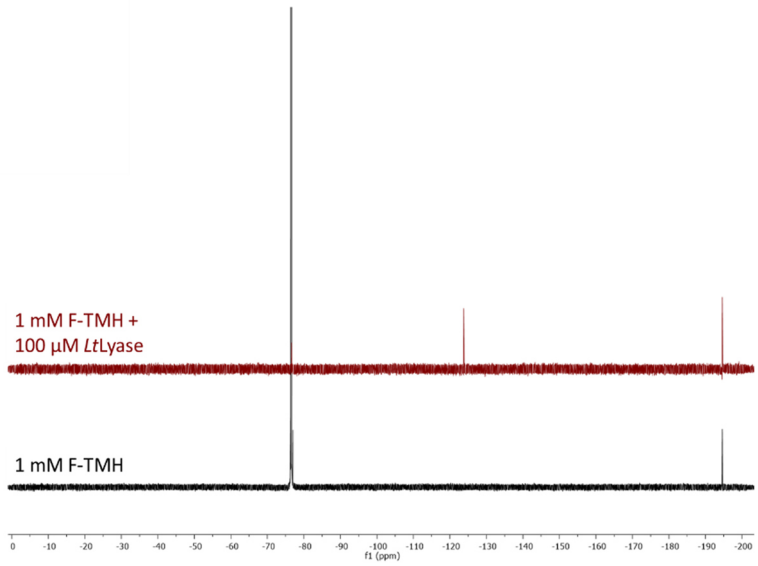

Figure 102. ^{19}F-NMR of F-TMH (1 mM, black) and F-TMH (1 mM) in the presence of *Lt*Lyase (100 µM, red). The signal at -76.55 ppm shows the reference trifluoracetic acid. The signal at -194.5 ppm shows F-TMH. The signal at -123.7 ppm in the reaction derives from inorganic F^-.

The difference in reactivity of *Lt*Lyase and *Td*ETL against the fluorine-incorporated substrates is an interesting finding that underlines the differences in the active site architecture or reaction mechanism of these two related enzymes. However, at this point in time, the exact mechanism of the irreversible inhibition of *Lt*Lyase still remains unclear. Since the mercaptoimidazole side chain of ergothioneine and the imidazole side chain of TMH are electronically isolated from the leaving group, we do not think that differences in the intrinsic reactivity could explain the different rates of enzyme-catalyzed turnover. It is more likely that the observed differences are related to the different catalytic strategies of the two enzymes. A test of this hypothesis might be to examine the rate of F-TMH degradation by *Td*ETL or by *Td*ETL_{K384M}, which has appreciable activity for TMH. We would expect that at least *Td*ETL_{K384M} could degrade F-TMH at a rate maximally 10-fold slower than that measured for TMH.

4.8 Conclusion

In this chapter, we characterized a new enzyme that is responsible for TMH degradation. With assistance of the crystal structure of a TMH-lyase and based on site-directed mutageneses, we proposed an acid-base dependent mechanism. Similar to the previously presented ergothionase and the well-known HAL, a tyrosine residue acts as catalytic base and abstracts the β-proton of the substrate. Whereas a catalytic acid tyrosine residue is unique to TMH-lyase. This tyrosine residue is located on the equivalent position to the catalytic important MIO-moiety in HAL. Based on the overall relation of TMH-lyase and HAL, we suggest that the MIO-moiety in HAL might not only function as electron sink but also as the catalytic acid.

Furthermore, analysis of the phylogeny of ergothionase, TMH-lyase and HAL in relation to the ancestral aspartase/fumarase superfamily suggests ergothionase as the oldest representative among TMH-lyase and HAL. If ergothionase is older than the MIO-dependent HAL, the presence of an alternative and currently unknown histidine degradation pathway seems likely.

TMH-lyase was strongly inhibited by the compound F-TMH. The fast and long-lasting inhibitory behavior of F-TMH suggests a covalent modification on the enzyme. In contrast, ergothionase demonstrated turnover on F-ergothioneine. The different reactivity towards the fluorine-incorporated substrate derivatives underscores the distinct catalytic strategies of both enzymes.

4.9 Experimental

Protein Production. The synthetic genes of *ltlyase* wild type and variants, *hdlyase, rolyase* and *tdetl* variants were purchased from BioCat GmbH encoded on a pET28 plasmid. Proteins were produced as described in section 3.8. Protein concentration was determined by UV at 280 nm (Nanodrop2000, Thermo Scientific) using the calculated extinction coefficient.[157] Protein homogeneity was assessed by SDS-PAGE (Figure 103, Figure 104, Figure 105).

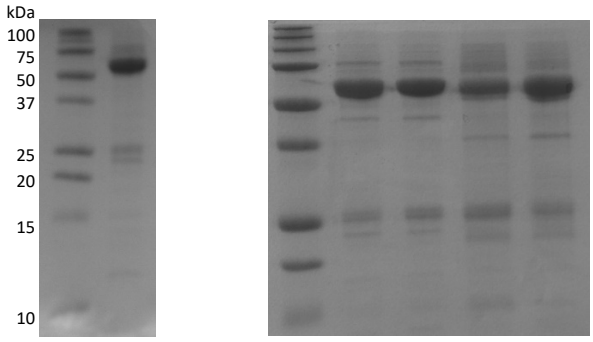

Figure 103. SDS-PAGE analysis of the purified protein *Lt*Lyase wild type (left gel, lane 2), E416Q (right gel, lane 2), C329G_C331P (right gel, lane 3), Y58F (right gel, lane 4), Y147F (right gel, lane 5). Lane 1 in both gels shows the protein standard (Precision Plus Protein Standard, Bio-Rad).

> *Lihuaxuella thermophila Lt*Lyase wildtype(Accession number SEM98045.1)

MGSSHHHHHHSSGLVPRGSHMRAKDIKKVTLGDPISMEEFVAIARFRAEVEFSDGYRQRVHRSRELVEKWMEEGK
VMYGVNTGFGALCTEWISLEETAQLQRNILLSHATSVGEPLSEEEVRATILMVLQNLGQGYSGVRLETLEMYRQF
LNLGLTPFAPREGSVGYLSPEAHMALVLMGEGMAFVDGELLPAKEALQRVGLKPITLTAKEGLALISGTTSPTGI
GALALYDMLKSALAADVIGTMTLEVLKGTTRAFDDRLMSVRPHPEQIHTAANIRKMLSDSMIAEKHVDDRLQDAL
SLRGIPQLHGAAKKSLYDALKTIEIEINSCTDNPILWPDEEGGGAISGCNCDSSYVGIELDSACIASTAIAKMSE
RRNNRLINGRLSGYPSFLIRKAGLNSGLMIPQYTQAGLLNDMKILSHPATVDNIPTCADQEDYVAMGYNAAKKAR
EVAVKLEYVLAIELLSIYCAHQFVESDLLPGSASRAVLDRISRTVPKMEEDLYLYPHLERLREMIHSGEIIECVE
DTIGKLL

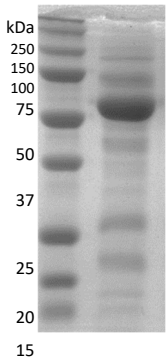

Figure 104. SDS-PAGE analysis of the purified protein *H.desiderata* Lyase (lane 2). Lane 1 shows the protein standard (Precision Plus Protein Standard, Bio-Rad).

> *Halomonas desiderata Hd*Lyase wildtype (Accession number WP_035578100.1)

GSSHHHHHHSSGLVPRGSHMSELSRYVEIGNTPPAWLEVVRVARDGYPMSLSPSAWEKVRCAREAVEKIAASSVP
HYGINTGLGALCDVVLKQDELQRLSHHTLMSHACGVGSPLRTEQVRAIMCSAVINYSHGYSGISPAVVEGLIRLL
NEQIIPVVPSRGSVGYLTHMAHIGLALIGHGDVEFRGQRMPAKQALEAIGMVPVTLGPKDGLSLVNGTPAMTGLA
CLALDDAARLSAWADIIGAMSFEALGGQLNAFMAEVTALKCHPGVQQTGDNLRRLLADSAHLARHKGQRLQDALS
LRSMPQVHGACRDQLDHAAKQVEKELNSATDNPLVIPVEDGYQVVSQANPHGASVAMACDLLAIAACEWSSISER
RAYRLVTPQANQLPPFLTTESGVKSGMMIAHYSAASLVADNKRLAQPAVTDNFITSGLQEDHLSFGESAALKLDK
SLDNAFYVLAIEYLLASQALDLIGSDEFAKGTSLAWKSLREVLPAYQEEHALHLDIEAAYQRLKETQVIDKLLSI
APNLLPSRQPSD

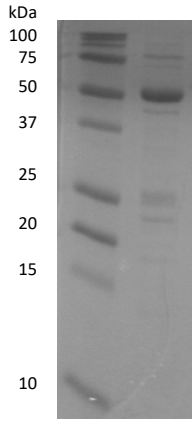

Figure 105. SDS-PAGE analysis of the purified protein *R.oryzae* Lyase (lane 2). Lane 1 shows the protein standard (Precision Plus Protein Standard, Bio-Rad).

> *Rhizobium oryzae Ro*Lyase wildtype (Accession number OLP61617.1)

MGHHHHHHAENLYFQGSGTIVLDQQLLTWADIAAVADGAVLRLAESAWARLARAASIVESLVETGVRAYGITTGV
GALSDTVVDRASQAALSRNILFSHACGVGPLLPREAVRAIIAAQIANFAHGYSGVRPVIVETLLALLEKDMIPEV
PAGGSAGYLTHNAHTALVLIGAGWVRCGDRRLTGREALAEIGREPLVLGAKEGLSLVNGTACSTGLAALALSHAL

RFLNWADAVSALTLEAAGAQMAAFDPDILALRPSEGIETVGRTLRARLAGSGLIAASLGRRTQDALSLRAIPHAH
GAARDLFDQVAATVDRELASVTDNPAVSGSPEAPIVSSQAHAVAPGLALAADGLAIALAQISAMSERRLDRLVNP
LVSGLPPFLASDAGSRSGFMIAQYTAAALANDSRRLAAPASTDGGVTSGLQEDFLAHPTAAALKLHTILDNAAQI
LAIEYLAAAQAHEFLTDVAPRAPGTQALYACLRRHIGPYADDRPLSDDMVAARALIRDQDAPA

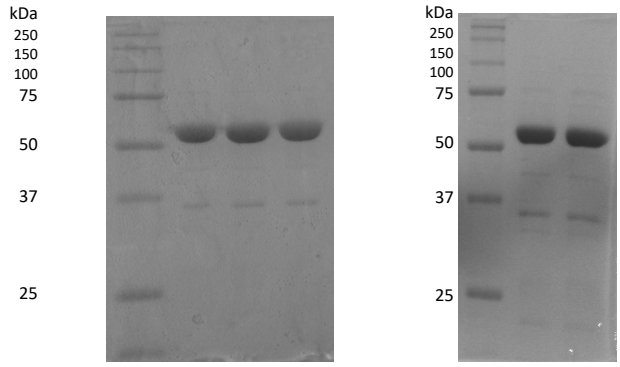

Figure 106. SDS-PAGE analysis of the purified protein *Td*ETL variant 1 - 3 (left gel, lane 2 - 4), *Td*ETL variant 4 -5 (right gel, lane 2 - 3). Lane 1 in both gels shows the protein standard (Precision Plus Protein Standard, Bio-Rad).

*Td*ETL variant-1 x144S
*Td*ETL variant-2 E143T x144S
*Td*ETL variant-3 E143A x144S
*Td*ETL variant-4 E143A_x144S_S195N
*Td*ETL variant-5 E143A_x144S_S195N_L278Y

Reagents. The same reagents as described in section 3.8 were used. *Ortho*-hydroxy-benzyl-histidine was synthesized by David Lim. F-TMH was synthesized by Carsten Bauer. F-ergothioneine was enzyme based produced using F-TMH as starting material following the protocol described in the reagents section in 3.8.

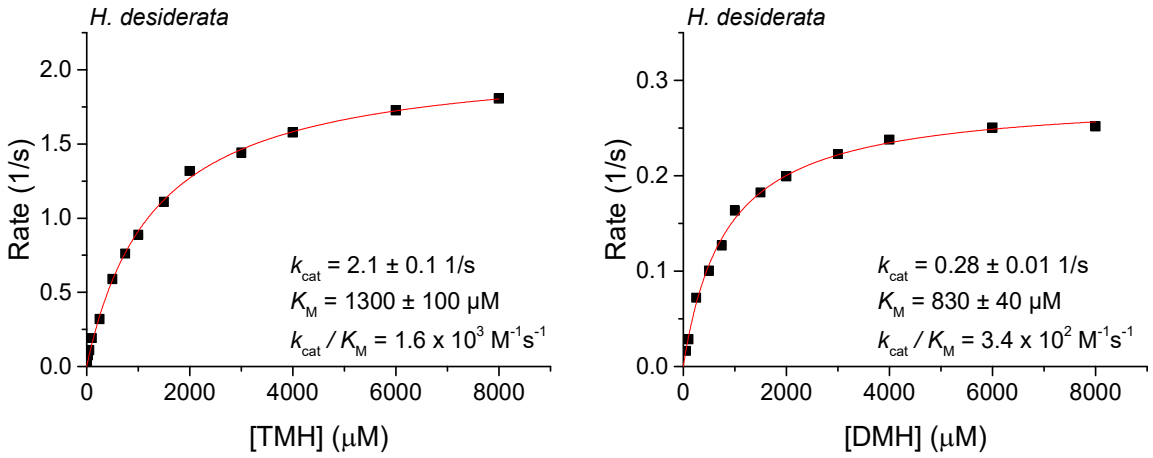

Figure 107. Michaelis-Menten Kinetics of *Hd*Lyase in HEPES buffer at pH 7.5 using TMH (left figure) or DMH (right figure) as substrate. Substrate concentration was in between 100 µM and 8000 µM. Enzyme concentration was in between 0.5 µM and 1 µM. Formation of the product urocanic acid at 23 °C was monitored using the spectrophotometer (Variant Cary 300 UV-Vis spectrophotometer). ε_{295}.(urocanic acid, pH 7.5) = 38565 M^{-1}cm^{-1}.

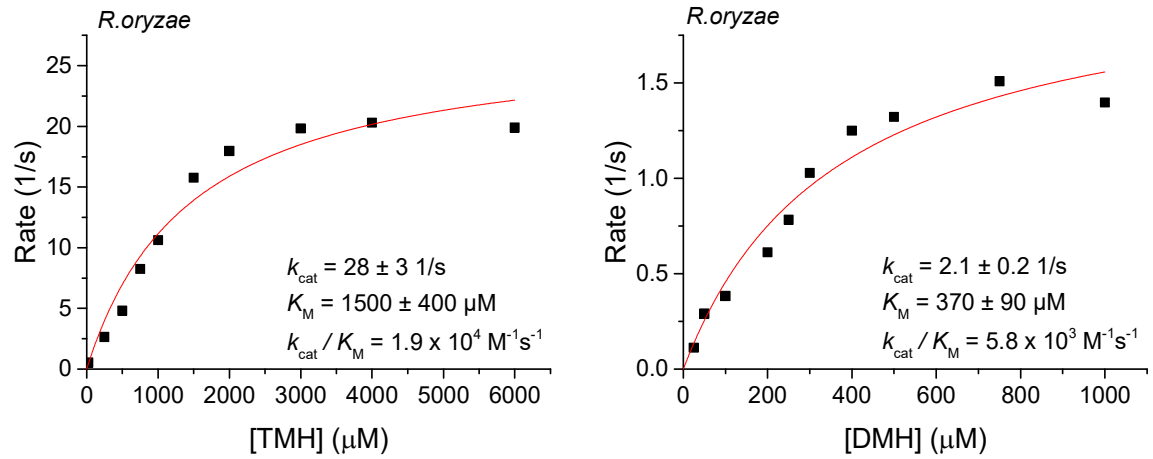

Figure 108. Michaelis-Menten Kinetics of *R. oryzae* Lyase in HEPES buffer at pH 7.5 using TMH (left figure) or DMH (right figure) as substrate. Substrate concentration was in between 25 µM and 6000 µM. Enzyme concentration was in between 0.02 µM and 0.5 µM. Formation of the product urocanic acid at 23 °C was monitored using the spectrophotometer (Variant Cary 300 UV-Vis spectrophotometer). ε_{295}.(urocanic acid, pH 7.5) = 38565 M^{-1}cm^{-1}.

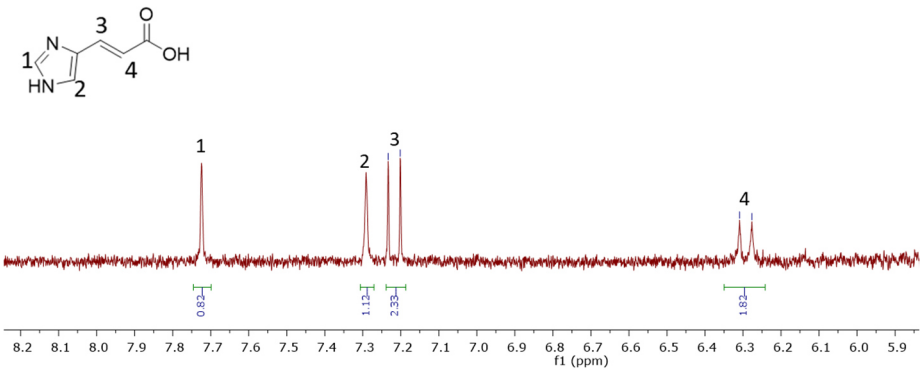

Figure 109. ^{1}H-NMR of *trans*-urocanic acid. 1 mM TMH was incubated for 16 h with 0.2 µM *Lt*Lyase in phosphate buffer at pH 7.5. The spectra was recorded on a Bruker Ascend™ 500 (500 MHz) spectrometer. The coupling constants of J(3) = 15 Hz and J(4) = 15 Hz gave evidence for the *trans*-product.

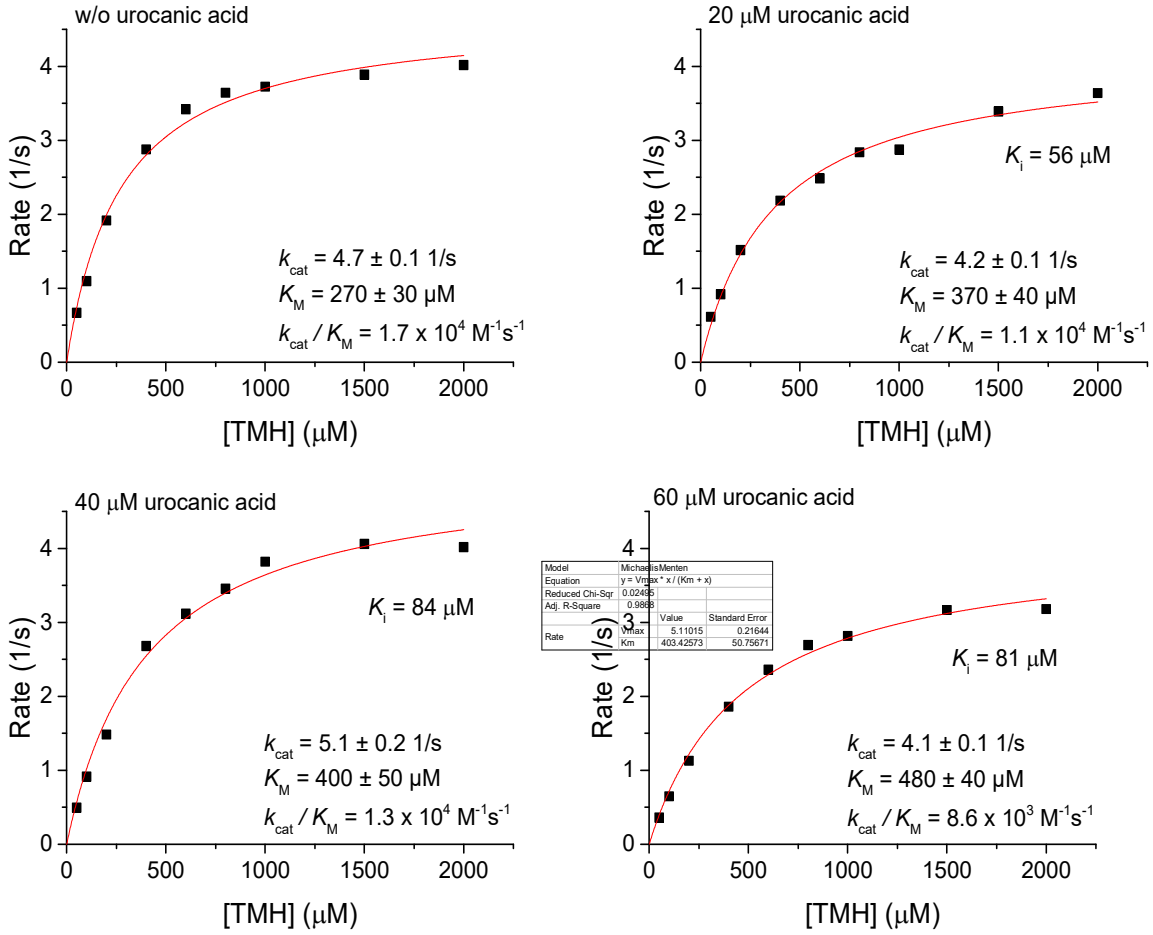

Figure 110. Michaelis-Menten Kinetics of *Lt*Lyase WT in HEPES buffer at pH 7.5 using TMH as substrate in the presence of 0, 20, 40, 60 µM additional urocanic acid. Product formation at 23 °C was monitored using the spectrophotometer (Variant Cary 300 UV-Vis spectrophotometer). ε_{295}.(urocanic acid, pH 7.5) = 38565 M^{-1}cm^{-1}. Urocanic acid inhibits *Lt*Lyase in a competitive model with TMH. Obtained kinetic data were fit to $K_i = \frac{K_M * [I]}{K_{M(app.)} - K_M}$. K_i (urocanic acid) = 74 ± 13.

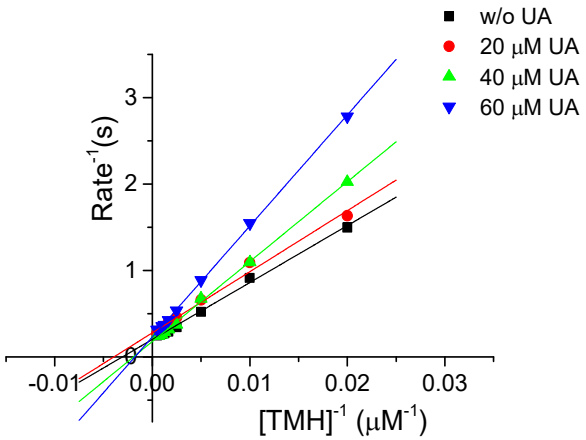

Figure 111. Lineweaver-Burk plot of the data used to examine *Lt*Lyase inhibition by urocanic acid (UA). *Lt*Lyase activity was monitored in the presence of 0, 20, 40, 60 μM additional urocanic acid. Michaelis-Menten plots are shown in Figure 110.

Table 23. Activity of *Lt*Lyase using TMH (2000 μM or 200 μM) as substrate in the presence of $ZnCl_2$ (0 – 50 μM) in phosphate buffer at pH 7.5. Formation of the product was monitored using the spectrophotometer (Variant Cary 300 UV-Vis spectrophotometer).

	v_{obs} [s^{-1}] **2000 μM TMH**	v_{obs} [s^{-1}] **200 μM TMH**
0 μM $ZnCl_2$	2.30 ± 0.04	0.73 ± 0.06
1 μM $ZnCl_2$	1.54 ± 0.25	0.84 ± 0.05
10 μM $ZnCl_2$	1.40 ± 0.16	0.95 ± 0.11
25 μM $ZnCl_2$	1.55 ± 0.20	0.76 ± 0.04
50 μM $ZnCl_2$	1.90 ± 0.28	0.74 ± 0.08

Substrate specificity. Substrate specificity was monitored in HEPES buffer at pH 7.5 using 2 mM of substrate by measuring the rate of product formation at 23 °C in a 1 cm quartz cuvette using a Variant Cary 300 UV-Vis spectrophotometer. If the activity was too low to determine Michaelis-Menten kinetics, enzyme concentration of 5 μM was used to follow turnover. ε_{311}.(thiourocanic acid) = 22500 $M^{-1}cm^{-1}$; ε_{295}.(urocanic acid, pH 7.5) = 38565 $M^{-1}cm^{-1}$, ε_{295}.(sulfono thiourocanic acid) = 15890 $M^{-1}cm^{-1}$; ε_{295}.(*S*-methyl thiourocanic acid) = 12170 $M^{-1}cm^{-1}$.

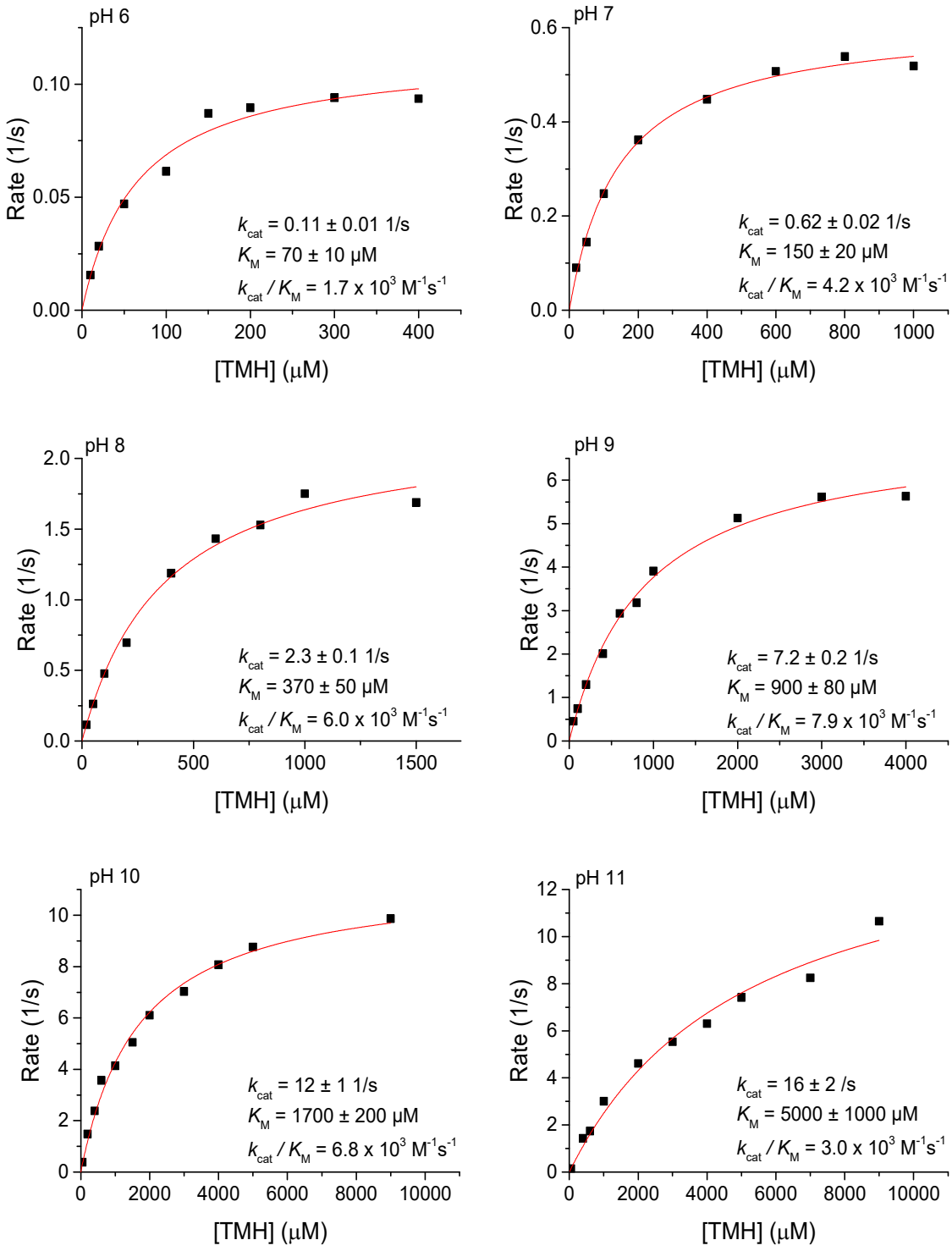

Figure 112. Michaelis-Menten Kinetics of *Lt*Lyase WT at pH 6 – pH 11. A buffer solution containing 40 mM acetic acid, 40 mM boric acid and 40 mM phosphoric acid (BR-buffer) was adjusted with NaOH to the desired pH. TMH substrate concentration was in between 10 µM and 10000 µM. Enzyme concentration was in between 0.1 µM and 0.3 µM. Formation of the product urocanic acid at 23 °C was monitored using the spectrophotometer (Variant Cary 300 UV-Vis spectrophotometer). $\varepsilon_{295\ nm}$ (urocanic acid, pH 6) = 26470 $M^{-1}cm^{-1}$; $\varepsilon_{295\ nm}$ (urocanic acid, pH 7) = 38680 $M^{-1}cm^{-1}$; $\varepsilon_{295\ nm}$ (urocanic acid, pH 8) = 38450 $M^{-1}cm^{-1}$; $\varepsilon_{295\ nm}$ (urocanic acid, pH 9) = 41680 $M^{-1}cm^{-1}$; $\varepsilon_{295\ nm}$ (urocanic acid, pH 10) = 42480 $M^{-1}cm^{-1}$; $\varepsilon_{295\ nm}$ (urocanic acid, pH 11) = 46230 $M^{-1}cm^{-1}$.

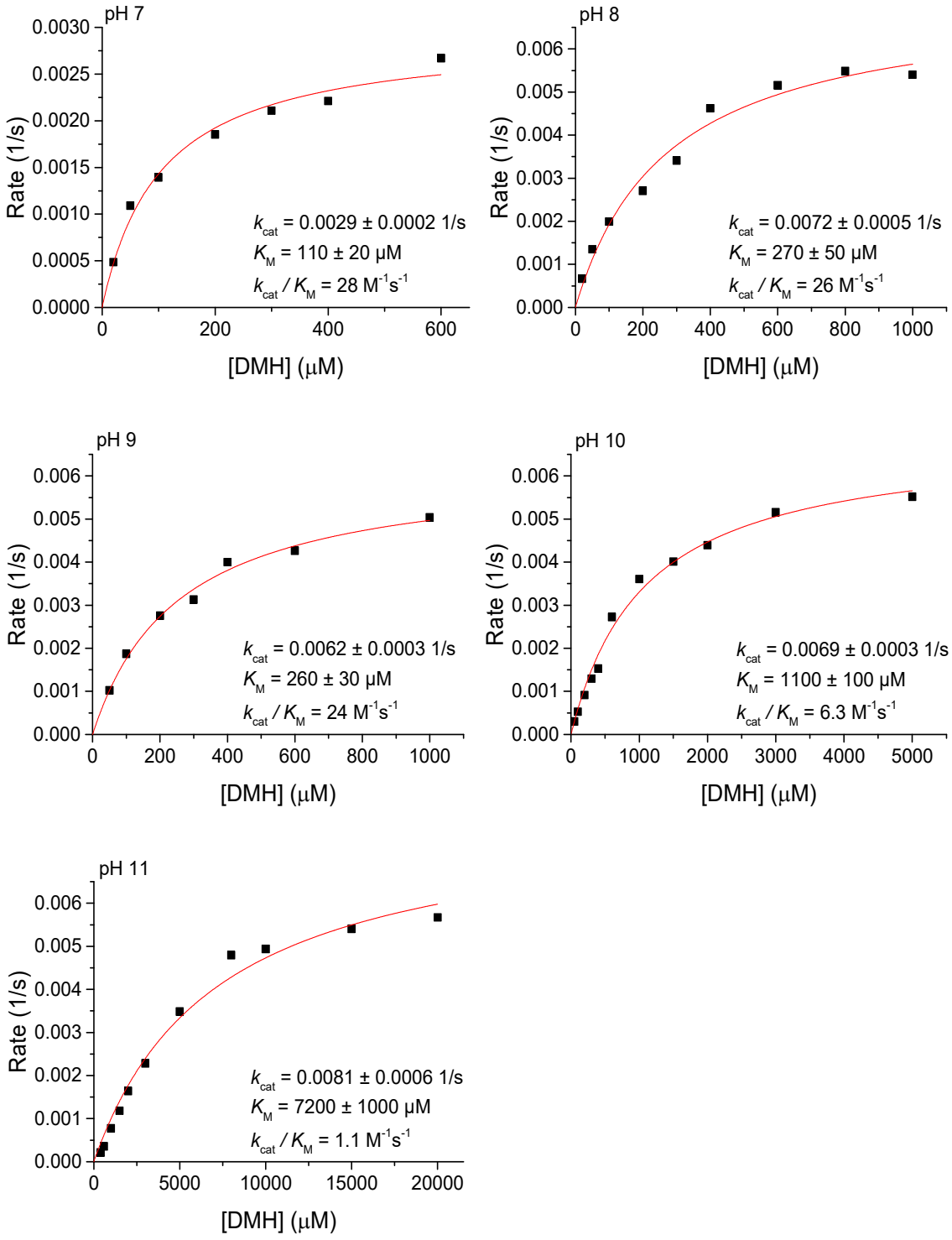

Figure 113. Michaelis-Menten Kinetics of *Lt*Lyase WT at pH 7 – pH 11. A buffer solution containing 40 mM acetic acid, 40 mM boric acid and 40 mM phosphoric acid (BR-buffer) was adjusted with NaOH to the desired pH. DMH substrate concentration was in between 25 µM and 20000 µM. Enzyme concentration was 1 µM. Formation of the product urocanic acid at 23 °C was monitored using the spectrophotometer (Variant Cary 300 UV-Vis spectrophotometer). $\varepsilon_{295\,nm}$ (urocanic acid, pH 6) = 26470 $M^{-1}cm^{-1}$; $\varepsilon_{295\,nm}$ (urocanic acid, pH 7) = 38680 $M^{-1}cm^{-1}$; $\varepsilon_{295\,nm}$ (urocanic acid, pH 8) = 38450 $M^{-1}cm^{-1}$; $\varepsilon_{295\,nm}$ (urocanic acid, pH 9) = 41680 $M^{-1}cm^{-1}$; $\varepsilon_{295\,nm}$ (urocanic acid, pH 10) = 42480 $M^{-1}cm^{-1}$; $\varepsilon_{295\,nm}$ (urocanic acid, pH 11) = 46230 $M^{-1}cm^{-1}$.

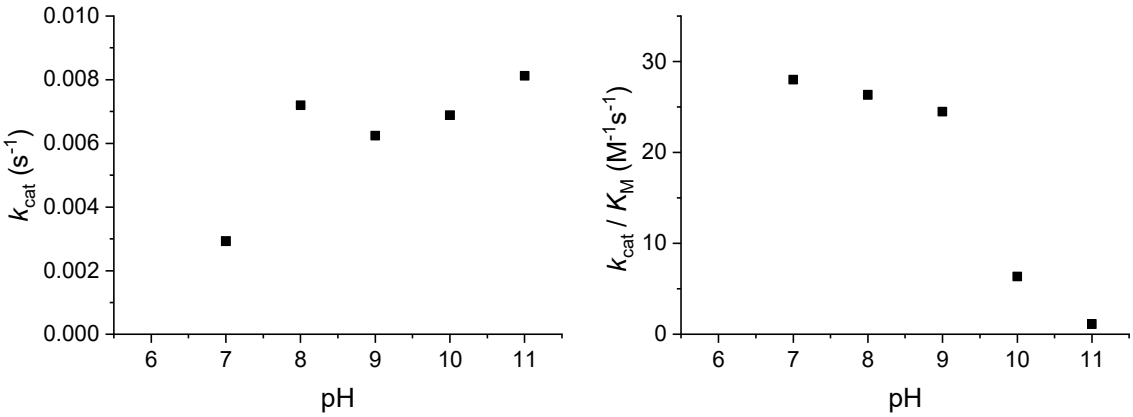

Figure 114. Summary of the observed pH-dependent kinetic parameters of *Lt*Lyase WT using DMH as substrate (Kinetic data is shown in Figure 113).

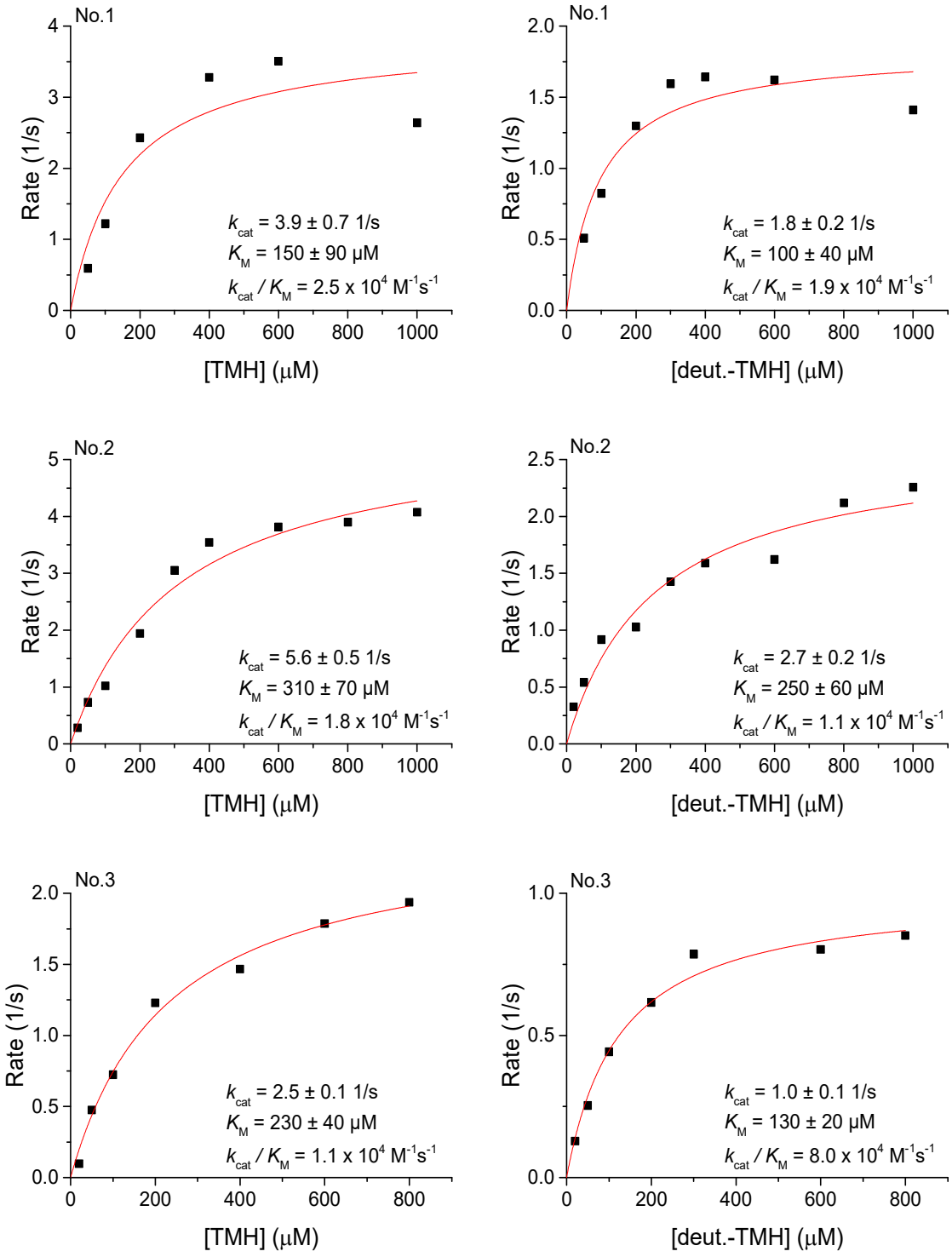

Figure 115. Michaelis-Menten Kinetics of *Lt*Lyase WT in HEPES buffer at pH 7.5 using TMH (left figures) or deuterated N-α-trimethyl histidine (deut.-TMH, right figures) as substrate. Deuterated histidine (D_5, 98%; $^{15}N_3$, 98%; ReseaChem GmbH) was converted to deuterated N-α-trimethyl histidine according to the published protocol.[158] TMH Substrate concentration was in between 25 µM and 800 µM. Enzyme concentration was 0.1 µM. Formation of the product urocanic acid at 23 °C was monitored using the spectrophotometer (Variant Cary 300 UV-Vis spectrophotometer). ε_{295}.(urocanic acid, pH 7.5) = 38565 $M^{-1}cm^{-1}$. KIE (k_{cat}) = 2.2 ± 0.2; KIE (k_{cat}/K_M) = 1.4 ± 0.2.

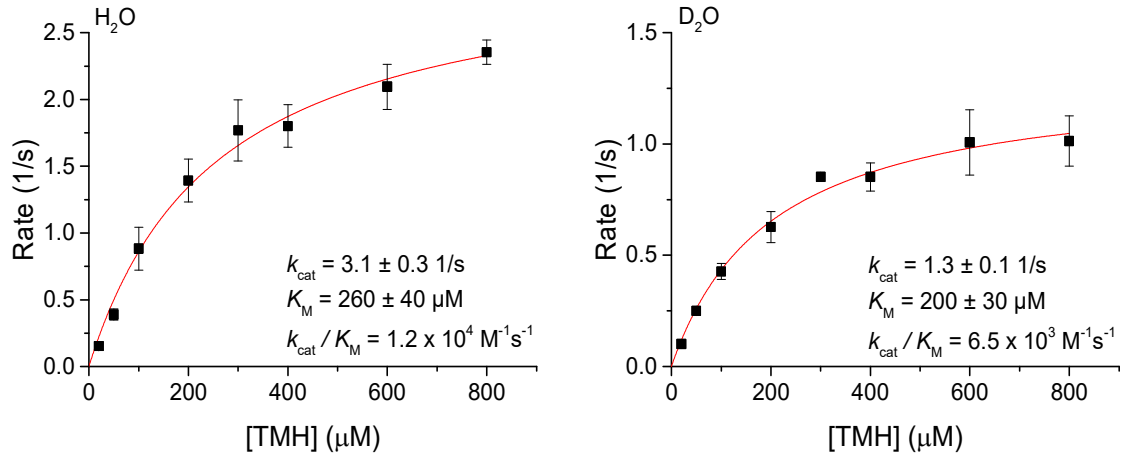

Figure 116. Michaelis-Menten Kinetics of *Lt*Lyase WT at pH 7.5 using HEPES buffer in H_2O (left graph) or D_2O (right graph). The pH of the buffer was adjusted to 7.5 for the reaction in H_2O and to 7.10 for the reaction in D_2O. Both buffers were lyophilized and dissolved in H_2O or D_2O, respectively. TMH substrate concentration was in between 25 µM and 800 µM. Enzyme concentration was 0.1 µM. Formation of the product urocanic acid at 23 °C was monitored using the spectrophotometer (Variant Cary 300 UV-Vis spectrophotometer). ε_{295}.(urocanic acid, pH 7.5) = 38565 $M^{-1}cm^{-1}$. KSIE (k_{cat}) = 2.3 ± 0.2; KSIE (k_{cat}/K_M) = 1.8 ± 0.1.

Substrate kinetic isotope effect in D_2O. To determine the substrate kinetic isotope effect in D_2O turnover of *Lt*Lyase WT at pH 7.5 in HEPES buffer in D_2O using TMH or deuterated TMH as substrate was followed. Substrate concentration was 1 mM. Deuterated histidine (D_5, 98%; $^{15}N_3$, 98%; ReseaChem GmbH) was converted to deuterated TMH according to the published protocol.[158] The pH of the buffer was adjusted to 7.10, lyophilized and dissolved in D_2O (final pD 7.5). The reaction rates were determined by following product formation at 23 °C using the spectrophotometer (Variant Cary 300 UV-Vis spectrophotometer). ε_{295}.(urocanic acid, pH 7.5) = 38565 $M^{-1}cm^{-1}$. The ratio $\frac{rate\ (TMH)}{rate\ (deut.\ TMH)}$ presents the substrate isotope effect. KIE (in D_2O) = 1.6 ± 0.1.

Kinetic solvent isotope effect using deuterated TMH as substrate. To determine the kinetic solvent isotope effect of *Lt*Lyase WT using deuterated TMH as substrate turnover at pH 7.5 in HEPES buffer in H_2O or D_2O was followed. The pH of the buffer was adjusted to 7.5 for the reaction in H_2O and to 7.10 for the reaction in D_2O. Both buffers were lyophilized and dissolved in H_2O or D_2O, respectively. 1 mM deuterated TMH was used as substrate. Deuterated histidine (D_5, 98%; $^{15}N_3$, 98%; ReseaChem GmbH) was converted to deuterated TMH according to the published protocol.[158] The reaction rates were determined by following product formation at 23 °C using the spectrophotometer (Variant Cary 300

UV-Vis spectrophotometer). ε_{295}.(urocanic acid, pH 7.5) = 38565 $M^{-1}cm^{-1}$. The ratio $\frac{rate\ in\ H_2O}{rate\ in\ D_2O}$ presents the kinetic solvent isotope effect. KSIE (deut. TMH) = 1.5 ± 0.2.

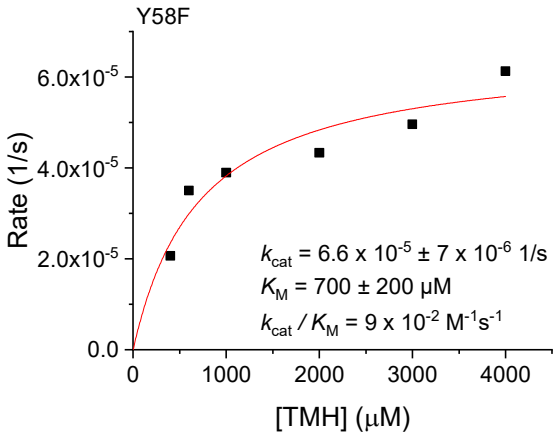

Figure 117. Michaelis-Menten Kinetics of *Lt*Lyase Y58F in BR-Buffer at pH 9. TMH substrate concentration was in between 400 µM and 4000 µM. Enzyme concentration was 3 µM. Formation of the product urocanic acid at 23 °C was monitored using the spectrophotometer (Variant Cary 300 UV-Vis spectrophotometer). $\varepsilon_{295\ nm}$ (urocanic acid, pH 9) = 41680 $M^{-1}cm^{-1}$.

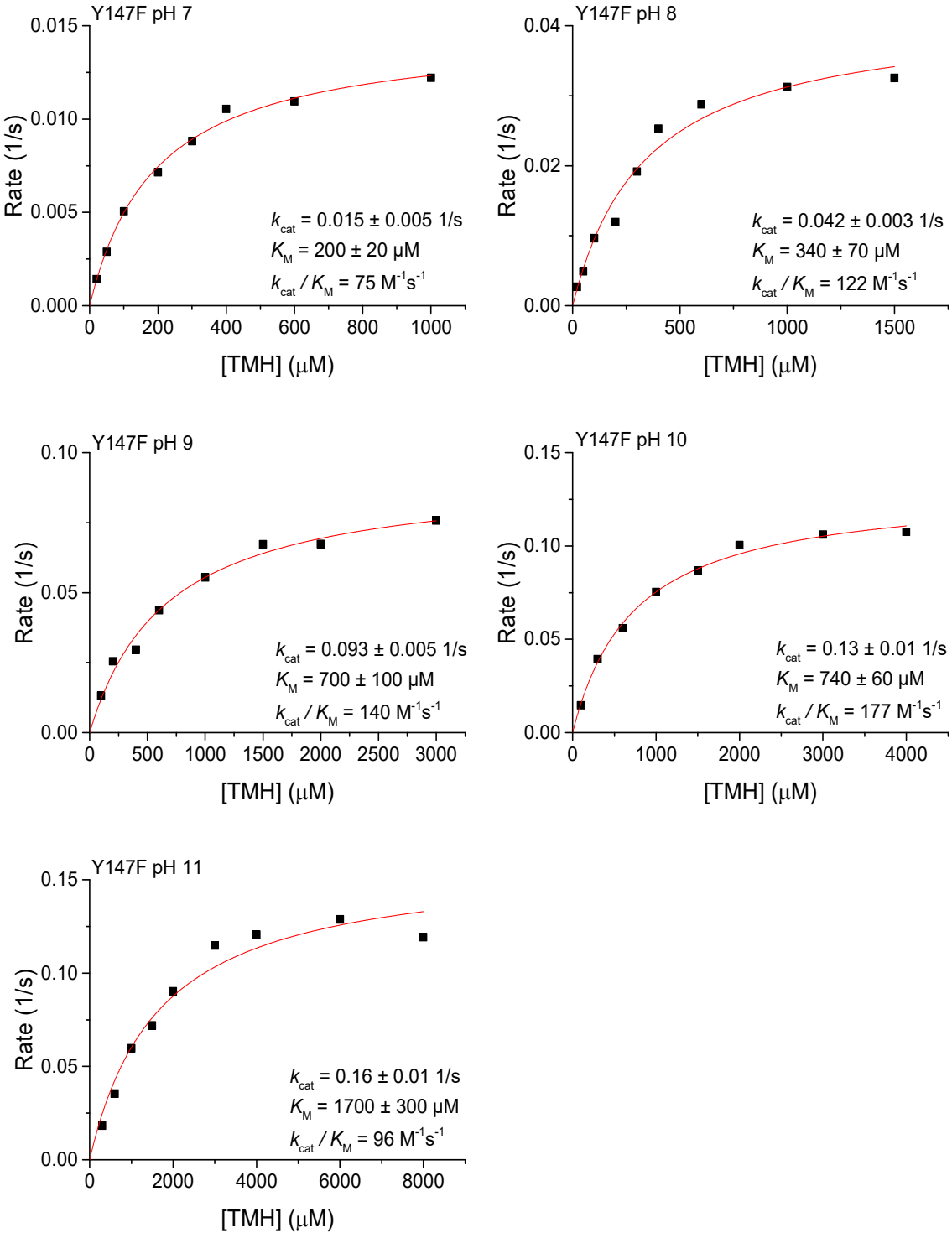

Figure 118. Michaelis-Menten Kinetics of *Lt*Lyase Y147F at pH 7 – pH 11. A buffer solution containing 40 mM acetic acid, 40 mM boric acid and 40 mM phosphoric acid (BR-buffer) was adjusted with NaOH to the desired pH. TMH substrate concentration was in between 25 µM and 8000 µM. Enzyme concentration was 0.5 µM. Formation of the product urocanic acid at 23 °C was monitored using the spectrophotometer (Variant Cary 300 UV-Vis spectrophotometer). $\varepsilon_{295\ nm}$ (urocanic acid, pH 7) = 38680 $M^{-1}cm^{-1}$; $\varepsilon_{295\ nm}$ (urocanic acid, pH 8) = 38450 $M^{-1}cm^{-1}$; $\varepsilon_{295\ nm}$ (urocanic acid, pH 9) = 41680 $M^{-1}cm^{-1}$; $\varepsilon_{295\ nm}$ (urocanic acid, pH 10) = 42480 $M^{-1}cm^{-1}$; $\varepsilon_{295\ nm}$ (urocanic acid, pH 11) = 46230 $M^{-1}cm^{-1}$.

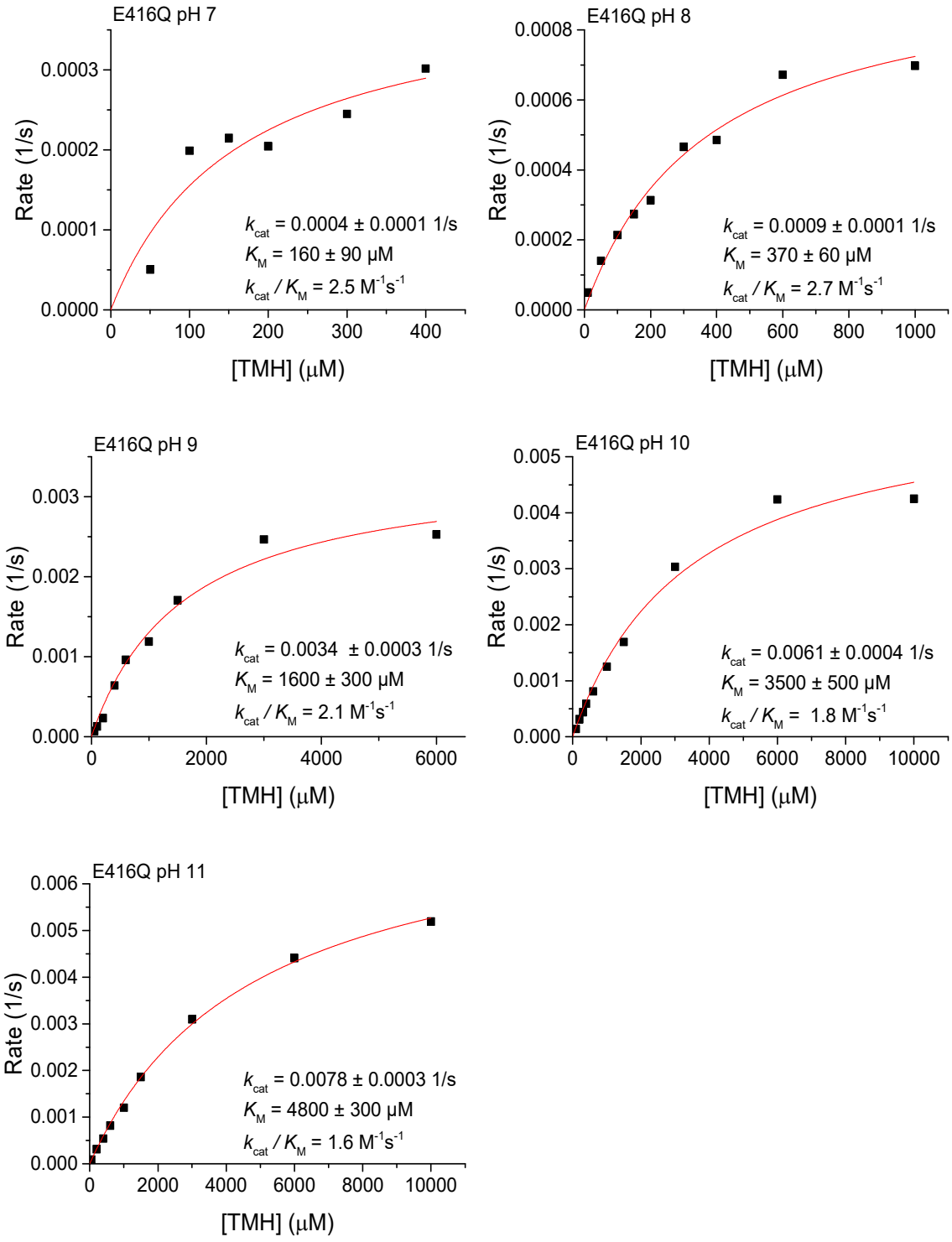

Figure 119. Michaelis-Menten Kinetics of *Lt*Lyase E416Q at pH 7 – pH 11. A buffer solution containing 40 mM acetic acid, 40 mM boric acid and 40 mM phosphoric acid (BR-buffer) was adjusted with NaOH to the desired pH. TMH substrate concentration was in between 25 µM and 10000 µM. Enzyme concentration was in between 0.5 µM – 1 µM. Formation of the product urocanic acid at 23 °C was monitored using the spectrophotometer (Variant Cary 300 UV-Vis spectrophotometer). $\varepsilon_{295\,nm}$ (urocanic acid, pH 7) = 38680 $M^{-1}cm^{-1}$; $\varepsilon_{295\,nm}$ (urocanic acid, pH 8) = 38450 $M^{-1}cm^{-1}$; $\varepsilon_{295\,nm}$ (urocanic acid, pH 9) = 41680 $M^{-1}cm^{-1}$; $\varepsilon_{295\,nm}$ (urocanic acid, pH 10) = 42480 $M^{-1}cm^{-1}$; $\varepsilon_{295\,nm}$ (urocanic acid, pH 11) = 46230 $M^{-1}cm^{-1}$.

***Ortho*-Hydroxy Benzyl Histidine as MIO-Mimetic.** In order to test if the elimination reaction catalyzed by an ortho-hydroxy group as acid is possible from a chemical perspective, the compound *ortho*-hydroxy benzyl histidine was synthesized by David Lim. The idea was that incubation of this compound might lead to formation of urocanic acid, which would then show that the enol of MIO could indeed function as catalytic acid for the elimination reaction. However, due to solubility problems at neutral pH, we had to run this experiment at pH 9 which then caused degradation to histidine (Figure 120, Figure 121).

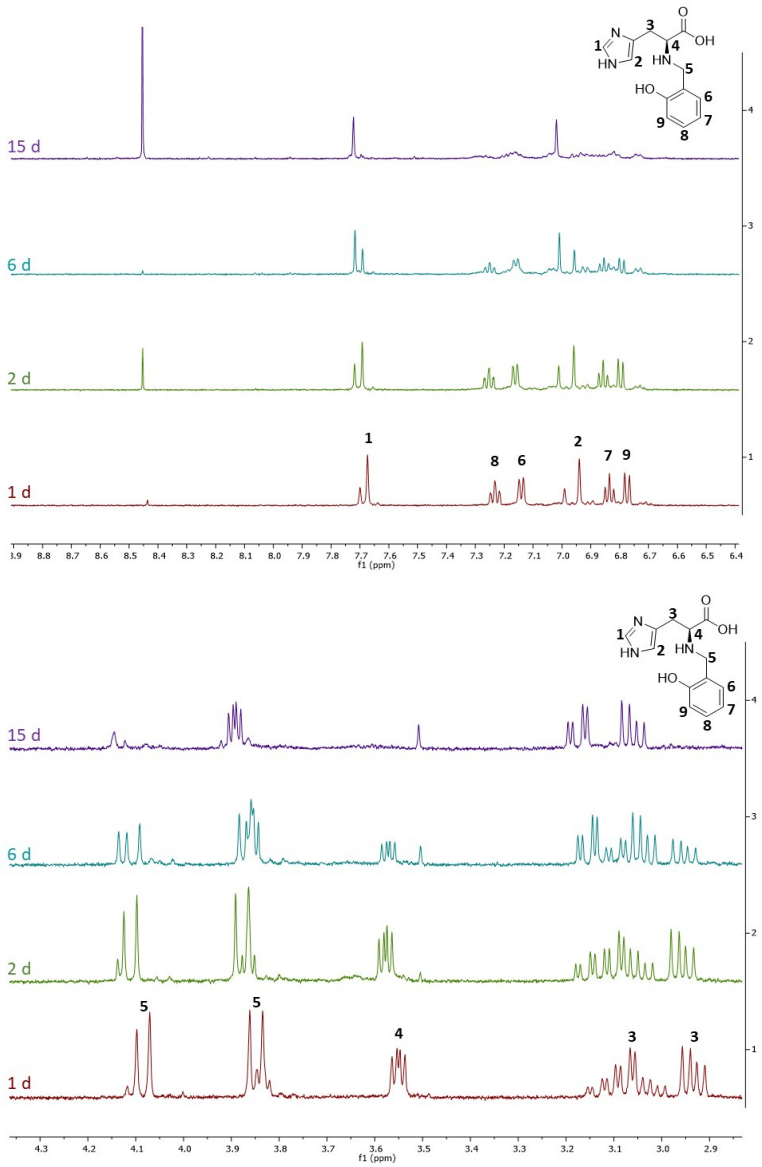

Figure 120. ^{1}H-NMR of *o*-hydroxy-benzyl-histidine (top: 8.8 – 6.4 ppm; bottom: 4.3 – 2.9 ppm). The compound (1 mM) was incubated in BR-buffer at pH 9 (BR-buffer) for 1 (red), 2 (green), 6 (blue), 15 (purple) days.

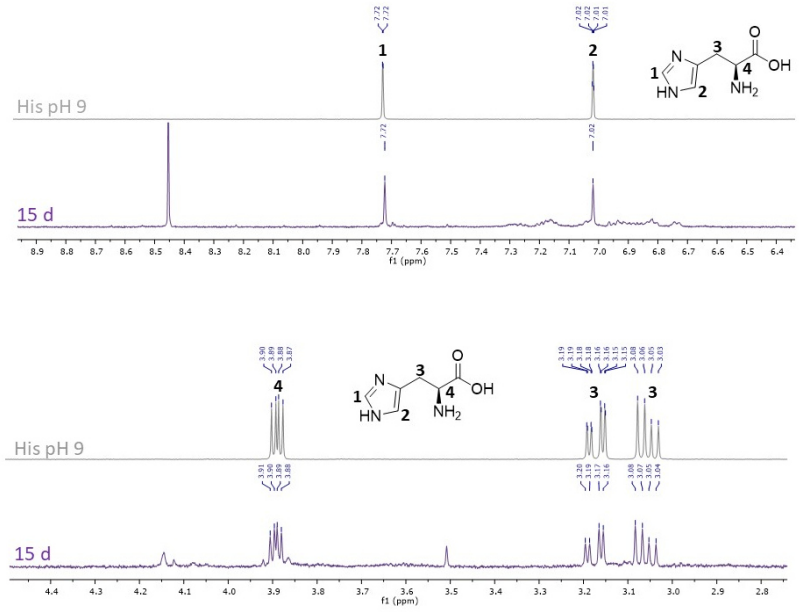

Figure 121. ^{1}H-NMR of histidine at pH 9 (light blue) and the degradation product of *o*-hydroxy-benzyl-histidine after 15 days incubation at 60 °C at pH 9 (top: 8.9 – 6.4 ppm; bottom: 4.4 – 2.8 ppm). We suggest that *o*-hydroxy-benzyl-histidine decomposed to histidine.

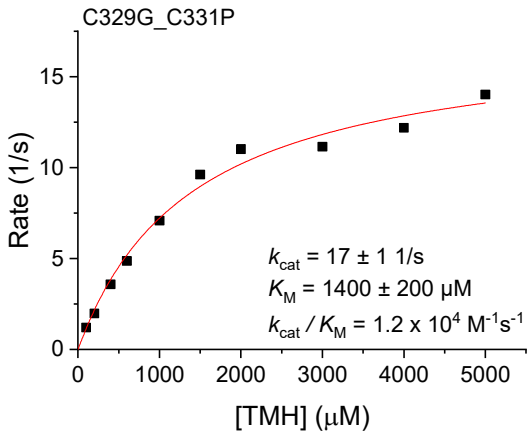

Figure 122. Michaelis-Menten Kinetics of *Lt*Lyase C329G_C331P in BR-Buffer at pH 9. TMH substrate concentration was in between 100 µM and 5000 µM. Enzyme concentration was in between 0.2 µM. Formation of the product urocanic acid at 23 °C was monitored using the spectrophotometer (Variant Cary 300 UV-Vis spectrophotometer). $\varepsilon_{295\ nm}$ (urocanic acid, pH 9) = 41680 $M^{-1}cm^{-1}$.

***Td*ETL Variants to Simulate MIO-Formation.** Formation of the Mio-moiety should give absorbance at 308 nm.(Röther *et al.*, *Angew. Chem. Int. Ed Engl.* **39**, 2462–2464 (2000) Therefore, the UV-spectra of variant 1 – 5 and the wild type were recorded. The corresponding difference-spectra are shown in Figure 123. MIO-Formation includes two times elimination of H_2O. Therefore, successful MIO-formation causes a mass decrease of 32 Da. In order to investigate if the *Td*ETL variants are able to form MIO, a chymotryptic digest was run. Subsequently, the resulting peptides were analyzed by UHPLC-MS (Agilent 1290 Infinity system coupled to Agilent 6130 quadrupol-MS). We did not detect a loss in mass of 32 Da (Table 24).

*Td*ETL variant-1 x144S
*Td*ETL variant-2 E143T x144S
*Td*ETL variant-3 E143A x144S
*Td*ETL variant-4 E143A_x144S_S195N
*Td*ETL variant-5 E143A_x144S_S195N_L278Y

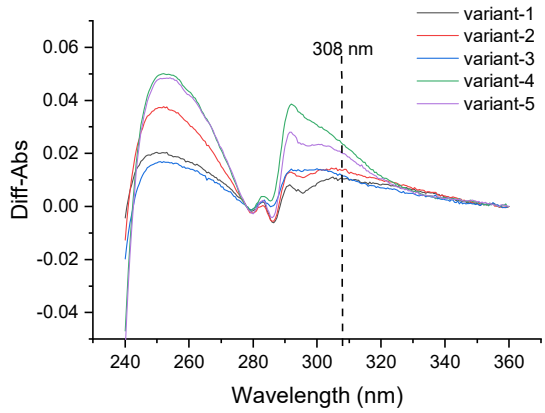

Figure 123. Difference UV-spectra of the *Td*ETL variants measured against *Td*ETL WT. Protein concentration was 0.6 mg/mL. The maxima at around 250 nm and 290 nm are a result of unproper protein folding. Formation of a MIO-moiety should increase absorbance at 308 nm.

Table 24. Overview of the calculated and observed masses of the chymotryptic peptide fragment of *Td*ETL WT and variants. 0.8 mg/mL protein was digested by 0.1 mg/mL chymotrypsin for 4 h. Subsequently peptides were analyzed by UHPLC/MS.

	Chymotryptic peptide fragment	**m/z $_{calc}$ (without modification)**	**m/z $_{calc}$ (after MIO-formation)**	**m/z $_{obs}$**
***Td*ETL WT**	RSSIGEGDITTL	1248.6	--	1249
***Td*ETL variant_1**	RSSIGESGDITTL	1335.7	1303.7	1336
***Td*ETL variant_2**	RSSIGTSGDITTL	1307.7	1275.7	1308
***Td*ETL variant_3**	RSSIGASGDITTL	1277.7	1245.7	1278

***Td*ETL variant_4**	RSSIGASGDITTL	1277.7	1245.7	1278
***Td*ETL variant_5**	RSSIGASGDITTL	1277.7	1245.7	1278

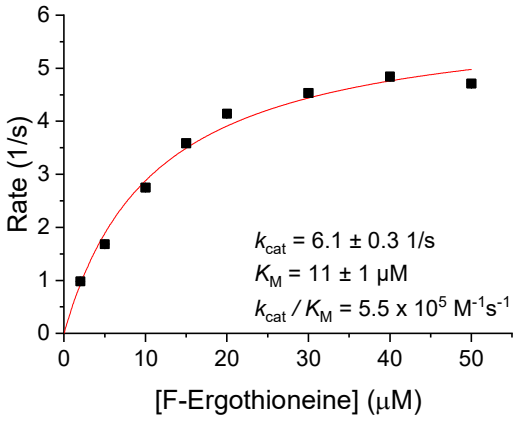

Figure 124. Michaelis-Menten kinetics of *Td*ETL using F-ergothioneine as substrate in HEPES buffer (50 mM, pH 7.5). Formation of the product thiourocanic acid was monitored Variant Cary 300 UV-Vis spectrophotometer). $\varepsilon_{311\ nm}$ (thio urocanic acid) = 22500 $M^{-1}cm^{-1}$

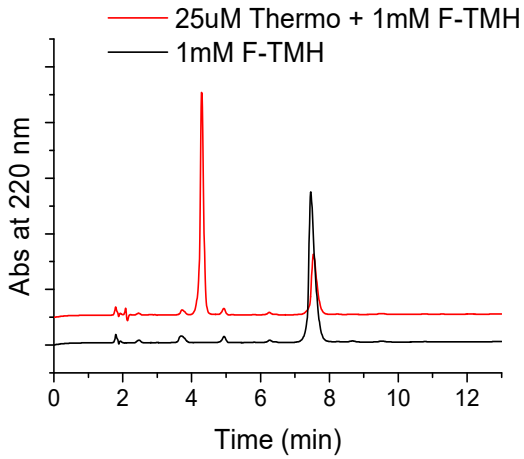

Figure 125. Ion-Exchange HPLC chromatogram of 1 mM F-TMH (black) and 1 mM F-TMH incubated in the presence of 25 µM *Lt*Lyase (red) 24h. The signal at 7.45 min shows F-TMH. The signal at 4.28 min shows Urocanic acid. Calculated turnover v_{obs} = 2.7 x 10^{-4} s^{-1}.

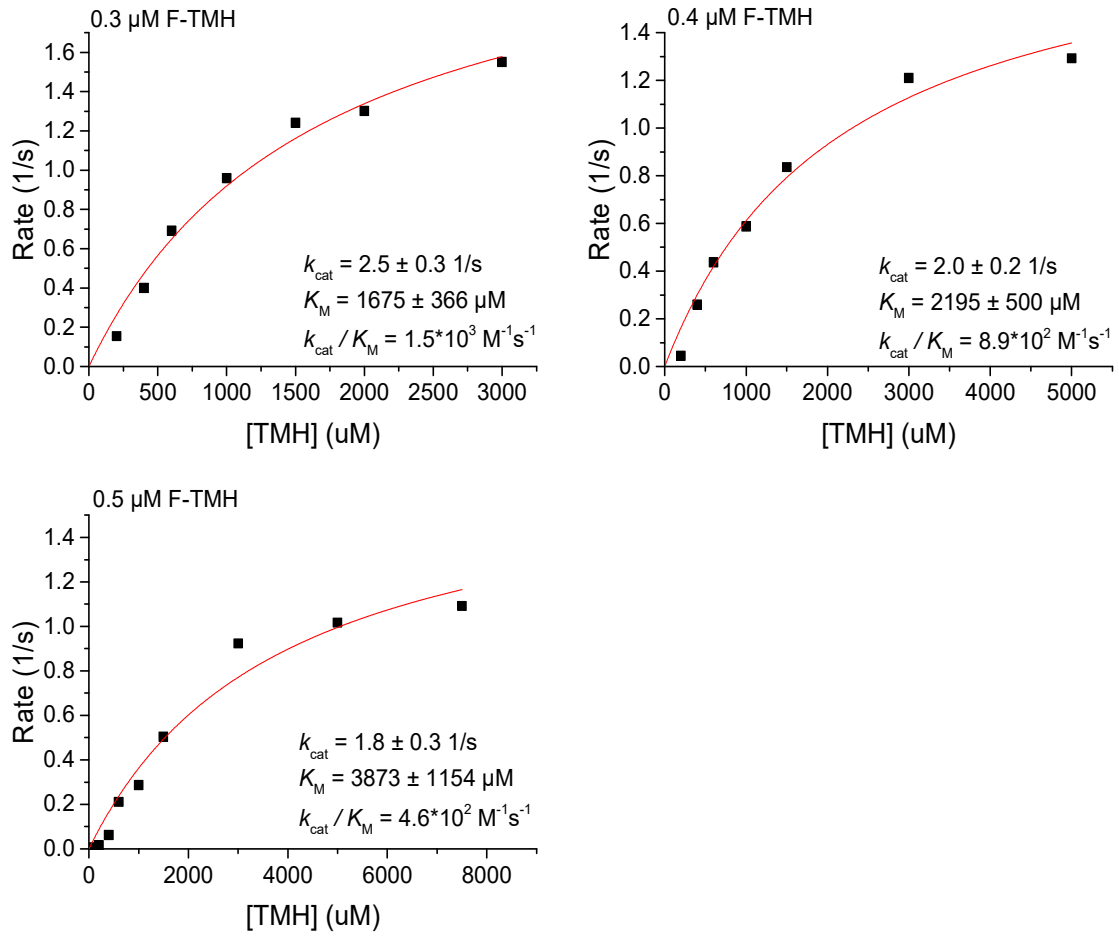

Figure 126. Michaelis-Menten kinetic of *Lt*Lyase WT in HEPES buffer at pH 7.5 using TMH as substrate in the presence of 0.3, 0.4, 0.5 µM F-TMH. Product formation at 23 °C was monitored using the spectrophotometer (Variant Cary 300 UV-Vis spectrophotometer). ε_{295}.(urocanic acid, pH 7.5) = 38565 $M^{-1}cm^{-1}$. Obtained kinetic data were fit to $K_i = \frac{K_M * [I]}{K_{M(app.)} - K_M}$. K_i (F-TMH) = 0.09 µM.

Time-dependent inhibition. To determine time dependent inhibition 0.2 µM *Lt*Lyase$_{\text{wild type}}$ or 0.5 µM *Lt*Lyase$_{Y147F}$ were incubated in the presence of 0.3 µM F-TMH in HEPES buffer (50 mM, pH 7.5). After t = 1, 5, 10, 15, 20, 45 min 1 mM TMH was added to start the reaction. For the first time point, t = 0 min, 1 mM TMH was added prior addition of the enzyme. The same experiment was run in the absence of F-TMH. Product formation was followed at 23 °C in a 1 cm quartz cuvette using a Variant Cary 300 UV-Vis spectrophotometer. ε_{295}.(urocanic acid, pH 7.5) = 38565 $M^{-1}cm^{-1}$.

Tryptic digest. 60 µM *Lt*Lyase was incubated for 5 min in the presence of 30 µM F-TMH in HEPES buffer (50 mM, pH 7.5). Subsequently, the protein was digested by 2 µM trypsin for 16 h. The digested fragments were analysed by UPLC-HR-ESI-MS (Bruker, maXis II ESI-TOF).

^{19}F-NMR. 1 mM F-TMH was incubated in the presence of 100 µM *Lt*Lyase in phosphate buffer (50 mM, pH 7.5). In addition, 1 mM F-TMH was incubated in the same buffer without enzyme. As a control to determine the chemical shift of fluoride, NaF (50 µM) was analyzed (Figure 127). Each NMR sample contained an insert glass tube containing trifluoracetic acid (1 mM) as reference (-76.5 ppm). NMR spectra were obtained on a Bruker Ascend™ 500 (500 MHz) spectrometer.

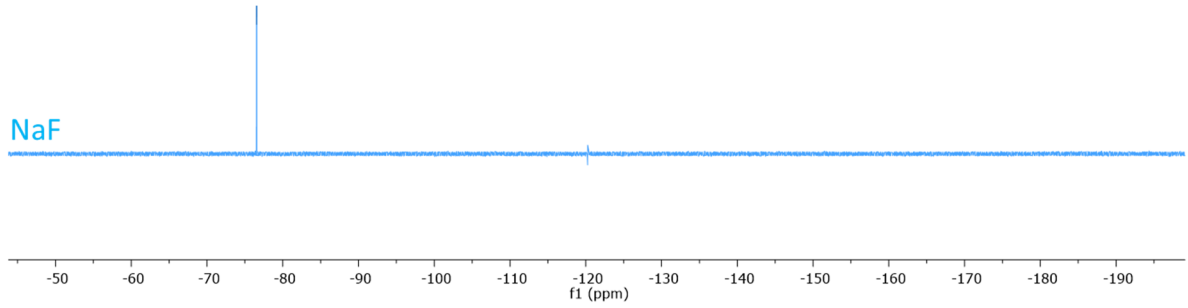

Figure 127. ^{19}F-NMR of NaF (-123.7 ppm) using trifluoracetic acid (-76.5 ppm) as reference.

5 Examination of EgtD Regulation

The *S*-adenosyl methionine (SAM)-dependent methyltransferase EgtD (EC 2.1.1.44) catalyzes the formation of TMH from histidine and represents the first enzyme in the biosynthetic pathway for ergothioneine production (section 1.4.1).[121] EgtD possesses both a Rossmann-fold domain that is typical for SAM-dependent methyltransferases and a substrate binding domain that is unique to EgtD.[168] The binding site for histidine and SAM is located in the cleft between both domains. EgtD can be classified as part of the methyltransf_33 protein family.[169]

As typical for SAM-dependent methyltransferases, EgtD proceeds methylation via a classic S_N2 reaction.[168] Kinetic and structural investigations provide evidence for an ordered sequential binding mechanism in which EgtD binds the substrate histidine first, followed by SAM binding. After one methylation has occurred, both the methylated substrate and *S*-adenosyl homocysteine (SAH) leave the binding site prior to re-binding of the mono-methylated substrate and SAM to run the subsequent methylation reaction, which is again followed by unbinding and renewed binding to proceed the third and final methylation.[170]

A remarkable processivity of EgtD reactivity was found: one equivalent of both SAM and histidine produces less than 1% of mono-methylated histidine, 13 ± 9% of di-methylated histidine but 88 ± 4% of TMH.[169] Kinetic investigations revealed that this processivity does not originate from an increased k_{cat} for the methylated histidine derivatives, rather an increased affinity of EgtD for the methylated variants. Detailed inspection of the crystal structure further corroborated this finding: the *N*-α-amino moiety of histidine hydrogen bonds to two active site residues (Gly161 and Asn166). In contrast, DMH only hydrogen bonds to Asn166; however, this single hydrogen bond becomes shorter and stronger, resulting in a 100-fold stronger binding of DMH in comparison to histidine.[170] In order to accommodate the growing size of substrate upon successive methylations, the active site of EgtD expands through the repositioning of Gly161 and Asn166. Interestingly, TMH is found to be a good ligand (K_i = 39 ± 6 µM), despite not forming any hydrogen bonds from the *N*-α-amino moiety; however, two methyl groups of TMH have attractive interactions with the carbonyl moieties of Gly161 and Asn166. The strong binding of TMH results in distinct product feedback inhibition of EgtD.[170]

The efficient and irreversible trimethylation in addition to product inhibition, which derives from specific evolutionary optimization, is important to circumvent wastage of intracellular histidine, as any methylated histidine leads to ergothioneine production. Ergothioneine biosynthesis produces an inherent energy cost for mycobacteria. In addition to histidine and three equivalents of SAM, cysteine, glutamate, ATP and pyridoxalphosphate is required.[121] For this reason, regulation of the first enzyme

of this biosynthesis pathway, EgtD, is important to regulate the whole ergothioneine biosynthetic pathway. The $K_{i,TMH}$= 39 ± 6 µM of EgtD is similar to the $K_{M,TMH}$= 43 ± 12 µM of EgtB,[171] the next enzyme of the ergothioneine biosynthetic pathway.[170] This helps to avoid accumulation of TMH, and thus adjusts the supply of TMH to ergothioneine biosynthesis which might be of significant value for regulation.

In 2015, Richard-Greenblatt *et al.* postulated that EgtD activity in *Mycobacterium tuberculosis* is under phosphorylation control.[172] Reversible post-translational phosphorylation is a dominant form of protein regulation.[173] Phosphorylation introduces a negative charge on the targeted amino acid and introduces the capacity to form a hydrogen network, both of which can strongly affect the overall activity of a protein.[174] Beside controlling protein activity, phosphorylation also affects protein localization and can induces changes in the secondary, tertiary or quaternary structure. In their publication, Richard-Greenblatt *et al.* claim that introduction of a phosphate on the EgtD active site residue Thr213 hidners interaction between the enzyme and substrate, and thus inhibits EgtD activity.[172] They proposed that the kinase PknD is responsible for this phosphorylation event. In the following chapter we reexamine the possible phosphorylation of EgtD from *M. tuberculosis* (*Tb*EgtD). The goal is to investigate the influence of PknD on *Tb*EgtD activity, to analyze PknD activity *in vitro,* and thus determine if the proposed phosphorylation on *Tb*EgtD occurs.

5.1 Importance of Residue Thr213

Richard-Greenblatt *et al.* reported that the active site residue Thr213 of *Tb*EgtD is target for a phosphorylation reaction.[172] Therefore, we were curious to investigate the localization and function of this residue. The previously published crystal structure of EgtD from *Mycobacterium smegmatis* (*Sm*EgtD) in complex with DMH and SAH (PDB: 4PIO) provided a thorough structural description of *Sm*EgtD active site residues.[169] In *Sm*EgtD, Thr213 is located on a α-helix in the active site that forms part of the pocket in which the imidazole ring of the substrate binds (Figure 128).[169] Nτ of the imidazole ring hydrogen bonds to a water molecule that anchors to Thr213 and Ala205. While Nπ of the imidazole ring shares a proton with the side chain of Glu282. Glu282 was stated to be highly important for substrate binding, with the $K_{M,\ His}$ for the E282A mutation increases 200-fold. The hydrogen bond of Thr213 to the active site water is reported to be essential for the substrate specificity of EgtD as tyrosine and phenylalanine cannot hydrogen bond to Thr213 and are therefore rejected as substrates.[169] As *Sm*EgtD shares >70% sequence identity with *Tb*EgtD we can assume that both proteins adopt a similar structure. Therefore, we hypothesized that Thr213 may also be important for catalysis in *Tb*EgtD and expect a decrease in activity of the T213A variant.

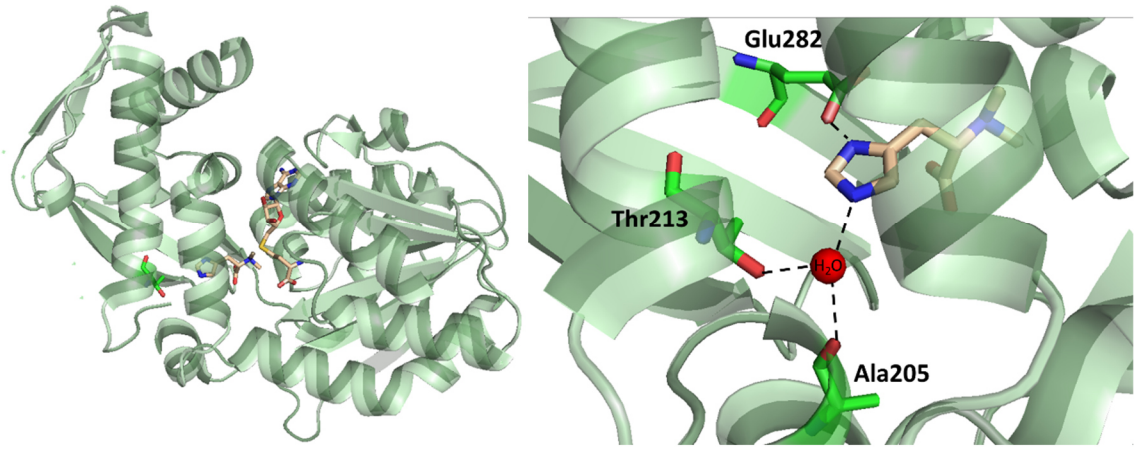

Figure 128. Crystal structure of *Sm*EgtD in complex with DMH and SAH (PDB: 4PIO). Overall structure (left) and close up view of the active site (right). Nπ of DMH hydrogen bonds with Glu282; Nτ hydrogen bonds via a water molecule to Thr213 and Ala205.

Indeed, our investigation into *Tb*EgtD T213A revealed a 300-fold decrease in activity (3.7×10^{-5} s^{-1}) towards the wild type (1.2×10^{-2} s^{-1}), underlining the importance of Thr213 for catalysis (Table 25). We further examined the variant T213E, however, the mutation to glutamate resulted in an unstable protein. Based on these data, we can conclude that Thr213 is essential for *Tb*EgtD activity. Any changes at this position, such as phosphorylation, would impact enzyme activity. However, we have to consider that Thr213 is located on an α-helix within the EgtD structure, approximately 8 Å away from the protein surface, making this threonine residue an unlikely kinase substrate. Large scale conformational changes would be required to make Thr213 accessible to the kinase.

Table 25. Observed activity of *Tb*EgtD WT and T213A using histidine as substrate. The reaction conditions are described in the experimental section.

	Rate [s^{-1}]
***Tb*EgtD WT**	1.2×10^{-2}
***Tb*EgtD T213A**	3.7×10^{-5}

We further tested the activity of the T213A variant with 1-methyl histidine (Figure 129) as substrate. Thereby, we observed an 8-fold increase in activity ($3.0 \times 10^{-4} \pm 5 \times 10^{-5}$ s^{-1}) in comparison to the histidine substrate, likely due to an improved binding affinity between the small hydrophobic Ala-moiety and the methylated imidazole moiety of 1-methyl histidine.

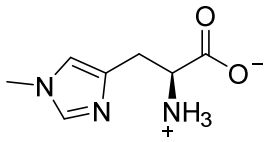

Figure 129. Structure of 1-methyl histidine.

5.2 Peptide Phosphorylation

While the importance of Thr213 for EgtD catalysis has been confirmed, its amenability for phosphorylation requires investigation. The kinase PknD is postulated to be responsible for EgtD phosphorylation in *M. tuberculosis*.[172] PknD is among 10 other kinases part of the group of Ser/Thr protein kinases (STPK) that produce stable phosphor-esters that require a phosphatase to be reversed.[175] STPKs are involved in many cellular processes like regulation of development, stress response and pathogenicity.[176]

In order to analyze PknD activity *in vitro*, we first investigated its ability for peptide phosphorylation. Therefore, we synthesized a peptide (peptide A, Abz- GRDDEA**T**SAVELTEA), reported to be a good substrate for PknD.[177]. We decorated the peptide with a N-terminal amino benzoic acid (Abz) to enable UV-based detection. The subsequent phosphorylation assay showed 41 ± 4 % phosphorylated peptide A after 1 h incubation with PknD (Figure 130). Therefore, we concluded that PknD is an active enzyme that is able to transfer phosphor groups. Knowing that PknD is active under our experimental conditions, we set to explore our main question: Is PknD able to phosphorylate EgtD? To address this question, we constructed a peptide (peptide B, Abz- AYDDPGGV**T**AQFNR) with the EgtD sequence containing the postulated phosphorylation target Thr213. Utilizing the same assay as for peptide A, we observed 43 ± 2 % phosphorylation of peptide B (Figure 130). This study provides evidence that the Thr213 containing protein sequence of *Tb*EgtD is a target for PknD. Next, we wanted to investigate if PknD-driven phosphorylation can occur on the native protein as well.

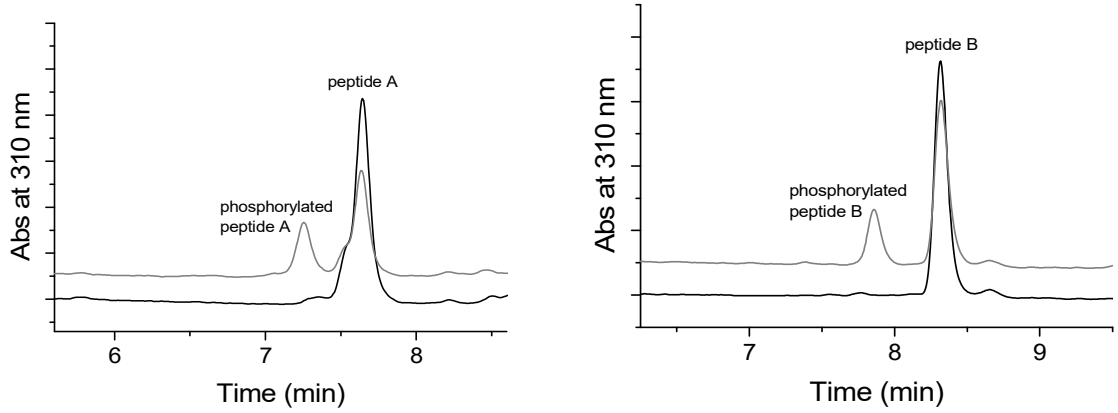

Figure 130. HPLC-chromatograms of PknD-mediated peptide phosphorylation of peptide A (left) and peptide B (right). Both peptides possess the aminobenzoic acid precursor to show absorbance at 310 nm. The control reaction without PknD is shown in black. The reaction containing PknD is shown in grey. The reaction conditions are described in the experimental section.

5.3 Examination on Protein Phosphorylation

5.3.1 High-Resolution ESI-MS Analysis of Phosphorylation of Native *Tb*EgtD

Using high-resolution ESI-MS, we are able to determine the exact mass of native proteins. Phosphorylation of a protein residue results in a mass increase of 80 Da, and is therefore telling if phosphorylation has occurred or not. In order to explore the possible phosphorylation of *Tb*EgtD, we incubated *Tb*EgtD in the presence of PknD under the conditions which resulted in the successful phosphorylation of peptide A and peptide B (section 5.2). We ran the same experiment without PknD or without ATP as negative controls. Afterwards, the protein mixtures were analyzed using high-resolution ESI-MS. In the phosphorylation experiment the mass of unmodified *Tb*EgtD and *Tb*EgtD with a mass increase of 178 Da, due to gluconylation of the N-terminal his-tag was found (Table 26).[178] Furthermore, we detected the mass of self-phosphorylated PknD (Table 26). However, we were not able to observe phosphorylation of *Tb*EgtD. This finding suggests that PknD is not able to phosphorylate the native folded form of *Tb*EgtD. To further support this finding, we ran a tryptic digest of *Tb*EgtD to screen the resulting peptide fragments for phosphorylation.

Table 26. Overview of the calculated and observed masses of the native proteins in the protein phosphorylation assay. The reaction conditions are described in the experimental section.

	***Tb*EgtD [Da]**		**PknD [Da]**		**Phosphorylated *Tb*EgtD [Da]**	
	$m/z_{calc.}$	$m/z_{obs.}$	$m/z_{calc.}$	$m/z_{obs.}$	$m/z_{calc.}$	$m/z_{obs.}$
***Tb*EgtD + PknD + ATP**	37436.2	37436.1 37613.1*[1]	40124.1	40770.0*[2] 40848.8 40929.5 41010.1 41089.9 41170.0 41249.9 41329.6	37516.2	not detected
***Tb*EgtD + PknD**	37436.2	37435.8 37612.8*[1]	40124.1	40291.0*[2] 40371.1 40454.8 40535.5 40615.5 40697.0 40774.3 40856.4	37516.2	not detected
***Tb*EgtD + ATP**	37436.2	37435.3 37614.7*[1]	40124.1	not detected	37516.2	not detected

*[1] Gluconylated form of TbEgtD.[178] *[2] Multiple self-phosphorylation of PknD.

5.3.2 LC-MS Analysis of Tryptic Digests

Based on the data achieved by high resolution MS, we suggest that native *Tb*EgtD is not phosphorylated by PknD *in vitro*. In order to further confirm this finding experimentally, we incubated *Tb*EgtD in the presence of PknD followed by trypsin digestion. Subsequently, we screened the resulting peptides for the phosphorylated variants by UPLC-MS. The advantage of this method was that we were able to analyze the tryptic digested peptides by both their mass and their chromatographic separation. The extracted ion chromatogram allowed us to plot signal intensity of a selected m/z value as a function of retention time. For this purpose, we selected (I) the mass of the unmodified tryptic digested *Tb*EgtD fragment (1510 m/z) and (II) the mass of the phosphorylated *Tb*EgtD fragment (1590 m/z)

(Figure 131). In addition to the reaction mixture containing *Tb*EgtD and PknD (blue), we also digested and analyzed controls containing only *Tb*EgtD (red) or PknD (green). Analysis of this experiment required care because a tryptic fragment of PknD (residues 45 to 57; sequence: LISPQYSDNAVFR) resulted in the same mass (1510 m/z) as the Thr213 containing *Tb*EgtD fragment of interest. Furthermore, the PknD-fragment contains a serine residue that is target of auto-phosphorylation. Accordingly, the resulting phosphorylated PknD-fragment would possess the same mass as a phosphorylated *Tb*EgtD-fragment (1590 m/z). In the reaction mixture containing both *Tb*EgtD and PknD, we observed a signal with 1590 m/z; however, the control reaction provides evidence that this signal derives from the phosphorylated PknD fragment. This indicates that Thr213 of *Tb*EgtD is not phosphorylated by PknD *in vitro*. As mentioned above (section 5.1) Thr213 is not surface exposed which makes a phosphorylation of this residue unlikely.

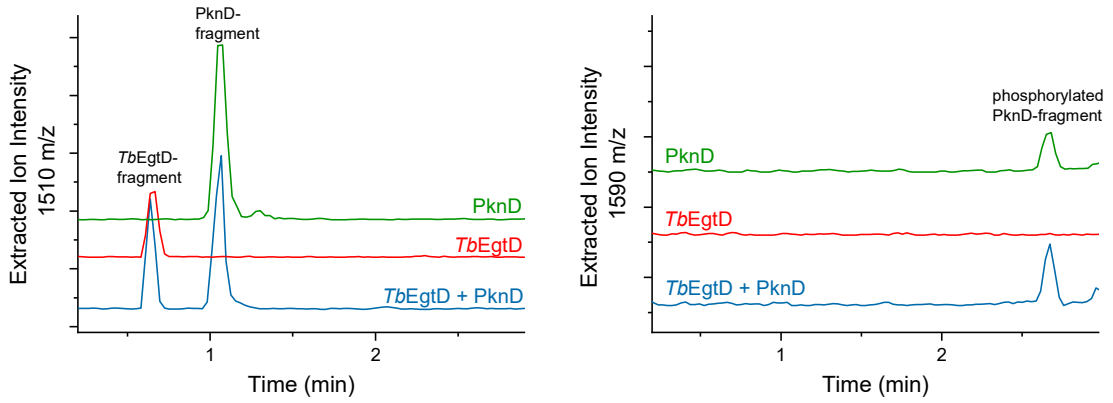

Figure 131. Extracted ion-chromatogram of the phosphorylation reaction of *Tb*EgtD after trypsin digestion. The extracted ion chromatograms are shown for 1510 m/z (left, expected mass of the *Tb*EgtD-derived fragment and the PknD derived fragment), for 1590 m/z (right, expected mass of the phosphorylated *Tb*EgtD- and PknD-derived fragment). The reaction containing both *Tb*EgtD and PknD is shown in blue, *Tb*EgtD alone is shown in red, PknD alone is shown in green. The reaction conditions are described in the experimental section.

In order to further validate this method for finding phosphorylated peptides, we ran a control reaction using peptide B as phosphorylation target (Figure 132). Peptide B is a synthetic tryptic fragment of *Tb*EgtD that contains Thr213 with an *ortho*-amino benzoic acid at the N-terminus. From our previous experiment we can confidentially conclude that PknD is able to phosphorylate peptide B (section 5.2). Therefore, the extracted ion chromatogram also shows that the signal of the phosphorylated peptide B (1709 m/z) is derived only in presence of PknD. In order to screen for the tryptic PknD-fragment, which we observed in the previous study, we recorded the extracted ion chromatogram for the corresponding mass (1510 m/z) and the corresponding phosphorylated fragment mass (1590 m/z).

Surprisingly, we detected a signal for peptide B with the mass of 1510 m/z and the corresponding phosphorylated peptide B (1590 m/z). These signals derive from the reductive elimination of the N-terminal amino benzoic acid (Abz) under ESI conditions (Figure 133) and therefore have the same retention time as their Abz-containing precursors. As expected, we further detected the signal of the PknD-fragment in both non-phosphorylated (1510 m/z) and phosphorylated (1590 m/z) form. In conclusion, this positive control showed that we are able to detect phosphorylation using this assay; confirming that we did not observe phosphorylation on *Tb*EgtD.

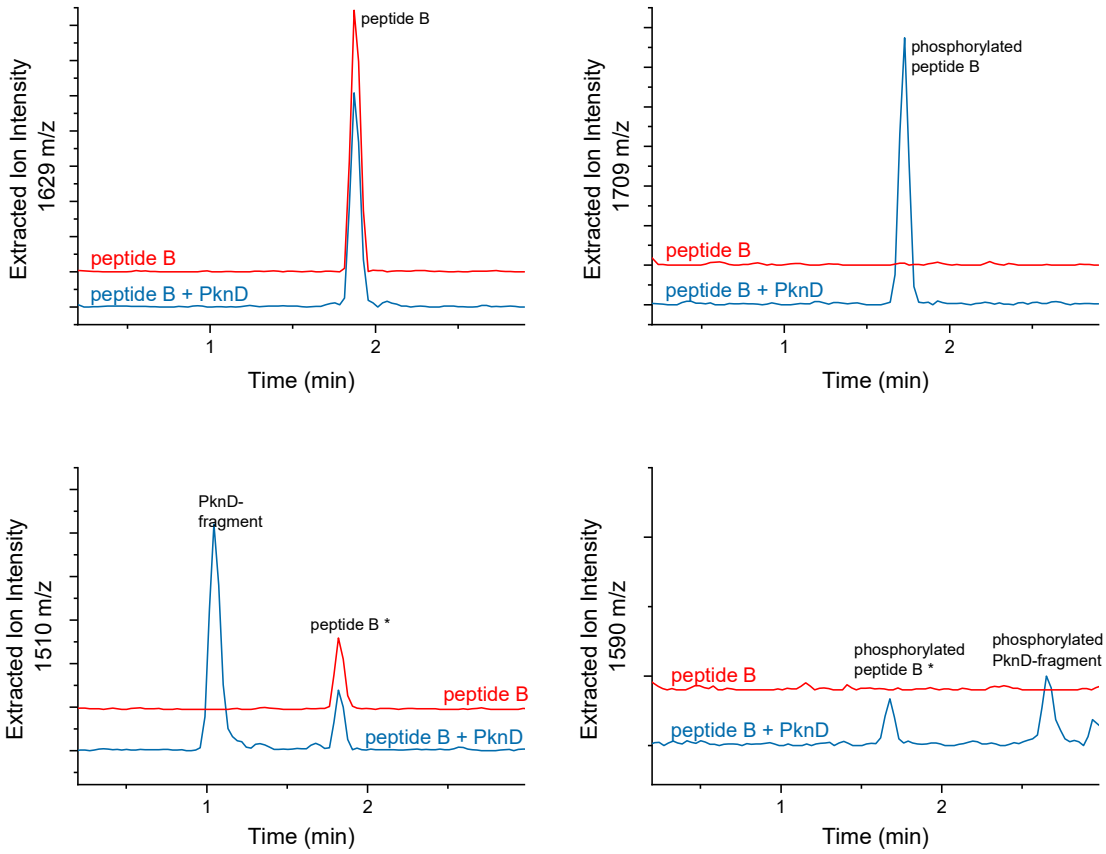

Figure 132. Extracted ion-chromatogram of the phosphorylation reaction of peptide B after trypsin digestion. The extracted ion chromatograms are shown for 1629 m/z (top left, expected mass of peptide B), 1709 m/z (top right, expected mass of phosphorylated peptide B), 1510 m/z (bottom left, expected mass of the PknD derived fragment and expected mass of peptide B after reductive elimination of the N-terminal amino benzoic acid, labeled as peptide B*), for 1590 m/z (bottom right, expected mass of the phosphorylated PknD fragment and expected mass of phosphorylated peptide B after reductive elimination of the N-terminal amino benzoic acid, labeled as phosphorylated peptide B*). The reaction containing both peptide B and PknD is shown in blue, peptide B alone is shown in red. The reaction conditions are described in the experimental section.

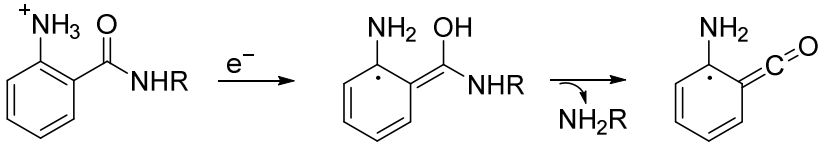

Figure 133. Reductive elimination of the N-terminal aminobenzoic acid under ESI conditions.

5.4 Activity of EgtD in the Presence of PknD

Previously, we showed that PknD does not phosphorylate *Tb*EgtD; however, we were interested to examine if PknD influences *Tb*EgtD activity. Therefore, we developed an *in vitro* assay where we studied methyltransferase activity with and without incubation for 1 h, both in the presence and in the absence of kinase. Firstly, *Tb*EgtD activity with an excess of substrate was measured giving an observed rate of $1.2 \times 10^{-2} \pm 3 \times 10^{-3}$ s^{-1}, which is consistent with the published activity of *Tb*EgtD (1.3×10^{-2} s^{-1}) (Table 27).[172] Next, we incubated *Tb*EgtD in the presence of PknD. After one hour of incubation we tested methyltransferase activity and observed a drastic decrease in *Tb*EgtD activity ($6.5 \times 10^{-4} \pm 1 \times 10^{-5}$ s^{-1}). As a control, we ran the same experiment in the absence of PknD; however again, we observed the same diminished activity rate ($8.4 \times 10^{-4} \pm 4 \times 10^{-5}$ s^{-1}). We deduced that after one hour of incubation *Tb*EgtD loses activity; 95 ± 4 % activity loss in the presence of PknD, and 93 ± 1 % activity loss in the absence of PknD. This finding indicates that activity loss is independent of the presence of kinase and therefore not a result of any phosphorylation event. What remains is the observation of a general lack of stability of *Tb*EgtD after one hour of incubation.

Table 27. Observed activity of *Tb*EgtD catalyzed formation of TMH. The reaction conditions are described in the experimental section.

	Rate [s^{-1}]
published[172]	1.3×10^{-2}
***Tb*EgtD**	$1.2 \times 10^{-2} \pm 3 \times 10^{-3}$
***Tb*EgtD + 1 h incubation**	$8.4 \times 10^{-4} \pm 4 \times 10^{-5}$
***Tb*EgtD + 1 h incubation + PknD**	$6.5 \times 10^{-4} \pm 7 \times 10^{-5}$

It was published previously that PknD (I) is part of the osmosensory pathway that enables adaption to osmotic stress,[179] (II) downregulates the malate dehydrogenase in the TCA cycle,[180] (III) influences cell division by phosphorylation of proteins that are key components of the bacterial chromosome segregation apparatus,[181] (IV) phosphorylates SAH-hydrolase, an enzyme that maintains cellular SAH concentration.[182] The later role might provide an alternative in which PknD-mediated phosphorylation

may indirectly influence EgtD activity in *M. tuberculosis in vivo*. SAH-hydrolase catalyzes the NAD^+ dependent degradation of SAH to adenosine and homocysteine. Reduction of SAH-hydrolase activity after phosphorylation would result in an increase in cellular SAH-concentration.[182] As SAH stabilizes the EgtD-TMH complex,[170] an increase in cellular SAH concentration would consequently downregulate ergothioneine biosynthesis. However, further experiments are required to confirm a possible SAH-hydrolase phosphorylation

5.5 Conclusion

The presented data suggests that phosphorylation of EgtD by PknD does not occur *in vitro*. The observed loss in activity of EgtD is not related to the presence of PknD and a subsequent phosphorylation. Our control experiment in the absence of PknD rationalizes that any reduction in activity is due to the instability of EgtD. The kinase PknD was confirmed to be active and was able to phosphorylate a peptide sequence that originates from EgtD, however the tertiary fold of the EgtD structure prevents phosphorylation of its native folded form. Furthermore, we showed that Thr213, the postulated target for phosphorylation, is indeed an important residue for EgtD activity. However, we could not observe phosphorylation of Thr213 by analysis of native protein or peptide analysis after tryptic digest. Based on this data, we conclude that methyltransferase activity is *in vitro* not regulated by phosphorylation of EgtD.

5.6 Experimental

Protein production. The pET28 plasmids containing genes coding for *Tb*EgtD WT, *Tb*EgtD T213A and PknD were kindly shared by Dr. Richard-Greenblatt and Av-Gay. Proteins were produced as described in section 3.8. The extinction coefficients 36565 $M^{-1}cm^{-1}$ for *Tb*EgtD, 21890 $M^{-1}cm^{-1}$ for PknD were calculated to determine protein concentration by UV at 280 nm (Nanodrop2000, Thermo Scientific). Protein homogeneity was assessed by SDS-PAGE (Figure 134). The mass was confirmed by high resolution mass spectroscopy (micrOTOF ESI-TOF, Bruker).

*Tb*EgtD WT: m/z_{calc} = 37436 Da, m/z_{obs} = 37436 Da

*Tb*EgtD T213A: m/z_{calc} = 37406 Da, m/z_{obs} = 37406 Da

PknD: m/z_{calc} = 40124 Da, m/z_{obs} = 40770 Da; 40849 Da; 40930 Da; 41010 Da; 41090 Da; 41170 Da; 41250 Da; 41330 Da (Δ x80 Da due to self-phosphorylation)

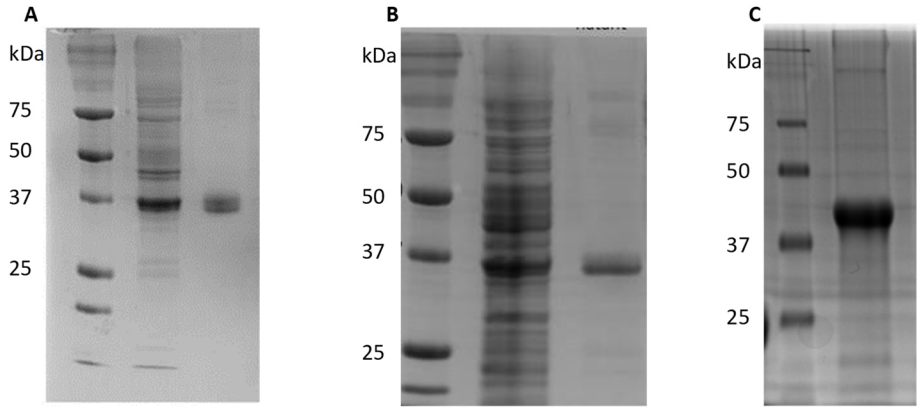

Figure 134. SDS-PAGE of (A) *Tb*EgtD WT (lane 2 shows the pellet fraction, lane 3 shows the purified protein), (B) *Tb*EgtD T213A (lane 2 shows the pellet fraction, lane 3 shows the purified protein), (C) PknD (lane 2 shows the purified protein).

>*Tb*EgtD wildtype (Accession number: WP_003419799.1)
GSSHHHHHHSSGLVPRGSHMRVSVANHLGEDAGHLALRRDVYSGLQKTPKSLPPKWFYDTVGSELFDQITRLPEY
YPTRAEAEILRARSAEVASACRADTLVELGSGTSEKTRMLLDALRHRGSLRRFVPFDVDASVLSATATAIQREYS
GVEINAVCGDFEEHLTEIPRGGRRLFVFLGSTIGNLTPGPRAQFLTALAGVMRPGDSLLLGTDLVKDAARLVRAY
DDPGGV**T**AQFNRNVLAVINRELEADFDVDAFQHVARWNSAEERIEMWLRADGRQRVRVGALDLTVDFDAGEEMLT
EVSCKFRPQAVGAELAAAGLHRIRWWTDEAGDFGLSLAAK

>PknD (Accession number: WP_031717884.1)
GSSHHHHHHSSGLVPRGSHMSDAVPQVGSQFGPYQLLRLLGRGGMGEVYEAEDTRKHRVVALKLISPQYSDNAVF
RARMQREADTAGRLTEPHIVPIHDYGEINGQFFVEMRMIDGTSLRALLKQYGPLTPARAVAIVRQIAAALDAAHA
NGVTHRDVKPENILVTASDFAYLVDFGIARAASDPGLTQTGTAVGTYNYMAPERFTGDEVTYRADIYALACVLGE

CLTGAPPYRADSVERLIAAHLMDPAPQPSQLRPGRVPPALDQVIAKGMAKNPAERFMSAGDLAIAAHDALTTSEQ
HQATTILRRGDNATLLATPADTGLSQSESGIAGAGTGPPTPGAARWSPGDSATVTPRPPDRRKPVANPSQTVRSH
P

Methyltransferase Activity Assay. Methyltransferase activity was analyzed under the following conditions: *Tb*EgtD WT or *Tb*EgtD T213A (25 µM or 100 µM), histidine (4 mM) or 1-methyl histidine (4 mM), SAM (0.5 mM), adenine deaminase and adenosylhomocysteine nucleosidase (10 µM), DTT (2 mM), Tris-HCl (pH 7.6, 100 mM), $MnCl_2$ (0.5 mM), NaCl (5 mM), $Mg(OAc)_2$ (1 mM) were incubated at 37 °C. Aliquots of the reaction were quenched using 1% TFA and analyzed by cation exchange HPLC (Buffer A: 20 mM phosphoric acid pH 2; Buffer B: 20 mM phosphoric acid pH 2 with 1 M NaCl). Formation of the tri-methylated product was followed at 220 nm and the concentration was determined by using a calibration for the product peak area. The slope of the linear function of product formation against time was used to calculate enzyme activity (Figure 135, Figure 136).

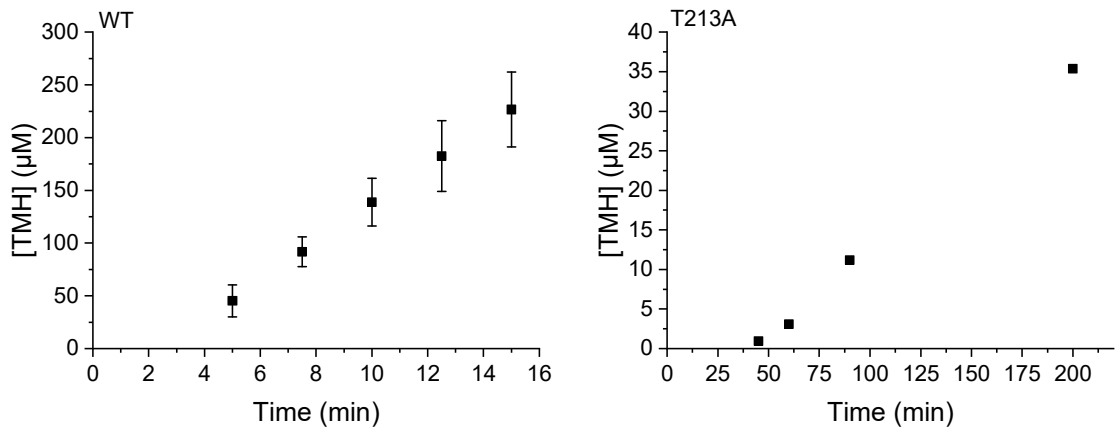

Figure 135. Product formation in the reaction of *Tb*EgtD WT (left) and *Tb*EgtD T213A (right). The rate of enzyme catalysis was calculated from the linear function of product formation against time. The observed activity was 0.012 ± 0.003 s^{-1} for *Tb*EgtD WT and 3.7 x 10^{-5} s^{-1} for *Tb*EgtD T213A.

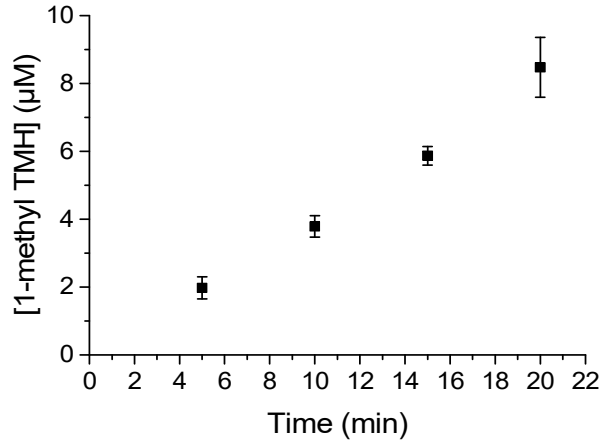

Figure 136. Product formation in the reaction of *Tb*EgtD T213A using 1-methyl histidine as substrate. The rate of enzyme catalysis was calculated by the linear function of product formation against time. The observed activity was $3.0 \times 10^{-4} \pm 5 \times 10^{-5}$ s^{-1}.

In order to determine influence of PknD, we incubated *Tb*EgtD (25 µM), w/o and w/ PknD (25 µM), ATP (100 µM), $MgSO_4$ (10 mM), $MnCl_2$ (10 mM) in Tris-HCl (pH 7.4, 50 mM). After 1 h methyltransferase activity was analyzed as described above (Figure 137).

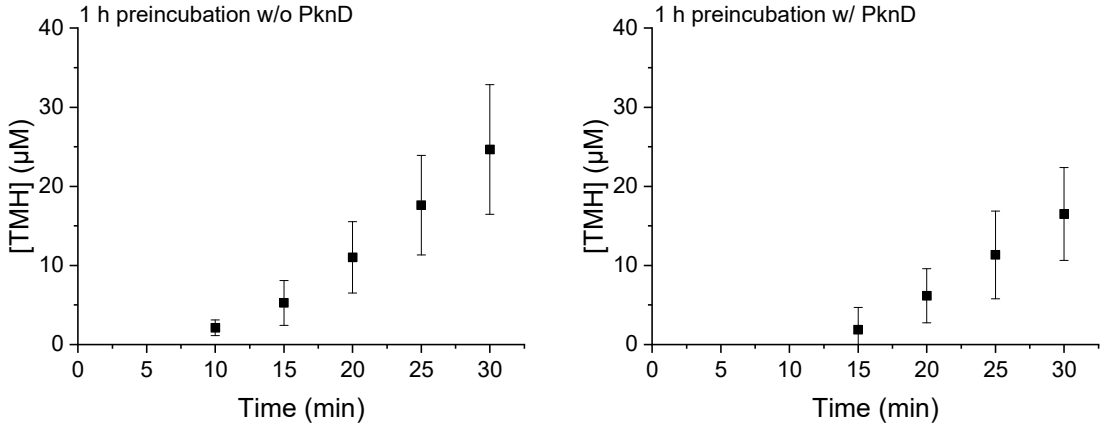

Figure 137. Product formation in the reaction of *Tb*EgtD WT after 1 h preincubation of *Tb*EgtD WT in the absence of PknD (left), or in the presence of PknD (right). The rate of enzyme catalysis was calculated by the linear function of product formation against time. The observed activity was $8.4 \times 10^{-4} \pm 4 \times 10^{-5}$ s^{-1} (left) and $6.5 \times 10^{-4} \pm 7 \times 10^{-5}$ s^{-1} (right).

Peptide Synthesis. Peptides (peptide A, published by Prisic to be a good substrate for PknD: ABZ-GRDDEATSAVELTEA;[177] peptide B, tryptic digested part of TbEgtD: ABZ-AYDDPGGVTAQFNR) were synthesized using standard protocols for Fmoc solid phase peptide synthesis using the synthesis robot (Syro I, MultiSynTech). Peptides were cleaved from the rink amid resin (0.41 mmol/g) (Novabiochem), deprotected and washed using TFA: EDT: TIPS: DCM (94: 2.5: 2.5: 1) for 4 h. Ice-cold diethylether was

used for resuspension the peptides and afterwards removed by centrifugation. The pellet was dried using N_2.

Afterwards, the peptides were dissolved in acetonitrile: water (1:1) and purified by preparative HPLC (Buffer A: H_2O, 1% acetonitrile, 0.1% TFA; Buffer B: acetonitrile, 0.085% TFA; Flowrate: 20 mL/min; column: 10 µm particles, 250x12, C18, Gemini Phenominics). After lyophilization the peptides were dissolved in acetonitrile: water (1:1) and analyzed by analytical RP-HPLC (Buffer A: Acetonitrile; 0.1% TFA; Buffer B: H_2O, 1% Acetonitrile; 0.1% TFA) at 310 nm. The concentration was determined using a standard of free amino benzoic acid. The mass was determined by ESI-MS (Bruker Esquire3000plus).

Peptide A: $M_{calc.}$ = 1681.7 Da; $[M+H]^+$= 1683.1

Peptide B: M_{calc} = 1627.7 Da, $[M+H]^+$= 1629.0

Peptide Phosphorylation. Peptide phosphorylation was analyzed under the following conditions: peptide A or peptide B (25 µM), PknD (25 µM), ATP (100 µM), Buffer: Tris-HCl (pH 7.4, 50 mM); $MgSO_4$ (10 mM); $MnCl_2$ (10 mM), incubated for 1 h at 30 °C. To quantify peptide phosphorylation, we used RP-HPLC at 310 nm (Buffer A: Acetonitrile; 0.1% TFA; Buffer B: H_2O, 1% Acetonitrile; 0.1% TFA). The mass of the phosphorylated peptides was analyzed by UHPLC/MS on Agilent 1290 Infinity system with Zorbax Eclipse Plus C-18-column (2.1 x 50 mm; 1.8 µm) coupled to Agilent 6130 quadrupol-MS (Eluent A: water/ acetonitrile/ TFA (1000: 10: 1); Eluent B: acetonitrile/ water/ TFA (1000 : 10 : 1)).

Phosphorylated peptide A: MW_{calc} = 1761.7 Da; $[M+H]^+$ = 1763.0

Phosphorylated peptide B: MW_{calc} = 1707.7 Da; $[M+H]^+$ = 1709.0

High-Resolution ESI-MS Analysis of Native Proteins. The following conditions were used to examine protein phosphorylation: *Tb*EgtD WT (25-100 µM), PknD (2-100 µM), ATP (100 µM), Buffer: Tris-HCl (pH 7.4, 50 mM); $MgSO_4$ (10 mM); $MnCl_2$ (10 mM), incubated for 1-6 h. We run the same assay without ATP or PknD as negative controls. Protein mass was analyzed by LC/MS-TOF on Agilent 1100 Series instrument coupled to microTOF ESI-TOF (Bruker) using a Jupiter C4 300A column (50 x 2 mm, 5 Microns, Phenomenex).

LC-MS Analysis of Tryptic Digests. We incubated phosphorylation reactions containing one equivalent of *Tb*EgtD and/or peptide B and PknD in the presence of ATP (100 µM), $MgSO_4$ (10 mM); $MnCl_2$ (10 mM) for 1.5 h in Tris-HCl (pH 7.4, 50 mM). The phosphorylation reaction was heat-inactivated (98 °C, 10 min) and subsequently digested with 4 µM trypsin for 1.5 h at 25 °C. These samples were heat inactivated and submitted to UHPLC/MS Agilent 1290 Infinity system with Zorbax Eclipse Plus C-18-column (2.1 x 50 mm; 1.8 µm) coupled to Agilent 6130 quadrupol-MS (Eluent A: water/ acetonitrile/ TFA (1000: 10: 1); Eluent B: acetonitrile/ water/ TFA (1000 : 10 : 1)). The extracted ion chromatogram of the expected m/z values for the peptides of interest were analyzed (Table 28).

Table 28. Overview of the observed m/z values in the analysis of tryptic digests.

1510 m/z	*Tb*EgtD derived fragment PknD derived fragment Peptide B after reductive elimination of ABZ-precursor
1590 m/z	Phosphorylated PknD derived fragment Phosphorylated peptide B after reductive elimination of ABZ-precursor
1629 m/z	Peptide B
1709 m/z	Phosphorylated peptide B

6 References

[1] B. Alberts, A. Johnson, J. Lewis, M. Raff, K. Roberts, P. Walter, *Molecular Biology of the Cell*, Garland Science, **2002**.

[2] IUBMB Nomenclature Home Page, can be found under https://www.qmul.ac.uk/sbcs/iubmb/, **2020**.

[3] R. E. Viola, *Crit. Rev. Biochem. Mol. Biol.* **2019**, *54*, 467–483.

[4] V. Puthan Veetil, G. Fibriansah, H. Raj, A.-M. W. H. Thunnissen, G. J. Poelarends, *Biochemistry* **2012**, *51*, 4237–4243.

[5] F. Parmeggiani, N. J. Weise, S. T. Ahmed, N. J. Turner, *Chem. Rev.* **2018**, *118*, 73–118.

[6] J. H. Quastel, B. Woolf, *Biochem. J.* **1926**, *20*, 545–555.

[7] S. H. Fisher, *Mol. Microbiol.* **1999**, *32*, 223–232.

[8] S. A. Woods, S. D. Schwartzbach, J. R. Guest, *Biochim. Biophys. Acta* **1988**, *954*, 14–26.

[9] H. A. Krebs, W. A. Johnson, *Biochem. J.* **1937**, *31*, 645–660.

[10] W. Shi, J. Dunbar, M. M. Jayasekera, R. E. Viola, G. K. Farber, *Biochemistry* **1997**, *36*, 9136–9144.

[11] T. Weaver, L. Banaszak, *Biochemistry* **1996**, *35*, 13955–13965.

[12] M. Y. Yoon, K. A. Thayer-Cook, A. J. Berdis, W. E. Karsten, K. D. Schnackerz, P. F. Cook, *Arch. Biochem. Biophys.* **1995**, *320*, 115–122.

[13] G. Fibriansah, V. P. Veetil, G. J. Poelarends, A.-M. W. H. Thunnissen, *Biochemistry* **2011**, *50*, 6053–6062.

[14] G. M. Stuttgen, J. D. Grosskopf, C. R. Berger, J. F. May, B. Bhattacharyya, T. M. Weaver, *FEBS Lett.* **2020**, *594*, 337–357.

[15] D. J. Porter, H. J. Bright, *J. Biol. Chem.* **1980**, *255*, 4772–4780.

[16] I. I. Nuiry, J. D. Hermes, P. M. Weiss, C. Y. Chen, P. F. Cook, *Biochemistry* **1984**, *23*, 5168–5175.

[17] T. Fujii, H. Sakai, Y. Kawata, Y. Hata, *J. Mol. Biol.* **2003**, *328*, 635–654.

[18] V. P. Veetil, H. Raj, W. J. Quax, D. B. Janssen, G. J. Poelarends, *FEBS J.* **2009**, *276*, 2994–3007.

[19] J. S. Blanchard, W. W. Cleland, *Biochemistry* **1980**, *19*, 4506–4513.

[20] H. A. Barker, R. D. Smyth, R. M. Wilson, H. Weissbach, *J. Biol. Chem.* **1959**, *234*, 320–328.

[21] Y. Kato, Y. Asano, *Arch. Microbiol.* **1997**, *168*, 457–463.

[22] M. Khomyakova, Ö. Bükmez, L. K. Thomas, T. J. Erb, I. A. Berg, *Science* **2011**, *331*, 334–337.

[23] S. K. Goda, N. P. Minton, N. P. Botting, D. Gani, *Biochemistry* **1992**, *31*, 10747–10756.

[24] M. Asuncion, W. Blankenfeldt, J. N. Barlow, D. Gani, J. H. Naismith, *J. Biol. Chem.* **2002**, *277*, 8306–8311.

[25] C. W. Levy, P. A. Buckley, S. Sedelnikova, Y. Kato, Y. Asano, D. W. Rice, P. J. Baker, *Structure* **2002**, *10*, 105–113.

[26] C. H. Archer, N. R. Thomas, D. Gani, *Tetrahedron Asymmetry* **1993**, *4*, 1141–1152.

[27] H. Raj, B. Weiner, V. P. Veetil, C. R. Reis, W. J. Quax, D. B. Janssen, B. L. Feringa, G. J. Poelarends, *ChemBioChem* **2009**, *10*, 2236–2245.

[28] H. Goldfine, E. R. Stadtman, *J. Biol. Chem.* **1960**, *235*, 2238–2245.

[29] G. Herrmann, T. Selmer, H. J. Jessen, R. R. Gokarn, O. Selifonova, S. J. Gort, W. Buckel, *FEBS J.* **2005**, *272*, 813–821.

[30] A. Heine, G. Herrmann, T. Selmer, F. Terwesten, W. Buckel, K. Reuter, *Proteins Struct. Funct. Bioinforma.* **2014**, *82*, 2041–2053.
[31] I.-M. Jeng, H. A. Barker, *J. Biol. Chem.* **1974**, *249*, 6578–6584.
[32] H. A. Barker, J. M. Kahn, S. Chew, *J. Bacteriol.* **1980**, *143*, 1165–1170.
[33] T. Nagasawa, K. Tanizawa, T. Satoda, H. Yamada, *J. Biol. Chem.* **1988**, *263*, 958–964.
[34] T. Uo, T. Yoshimura, T. Nishiyama, N. Esaki, *Biosci. Biotechnol. Biochem.* **2002**, *66*, 2639–2644.
[35] F. Khan, V. R. Jala, N. A. Rao, H. S. Savithri, *Biochem. Biophys. Res. Commun.* **2003**, *306*, 1083–1088.
[36] S. Bisht, V. Rajaram, S. R. Bharath, J. N. Kalyani, F. Khan, A. N. Rao, H. S. Savithri, M. R. N. Murthy, *J. Biol. Chem.* **2012**, *287*, 20369–20381.
[37] G. Deka, S. Bisht, H. S. Savithri, M. R. N. Murthy, *J. Struct. Biol.* **2018**, *202*, 118–128.
[38] J. N. Kalyani, N. Ramachandra, A. H. Kachroo, S. Mahadevan, H. S. Savithri, *J. Bacteriol.* **2012**, *194*, 5604–5612.
[39] C. Bradbeer, *J. Biol. Chem.* **1965**, *240*, 4669–4674.
[40] C. Bradbeer, *J. Biol. Chem.* **1965**, *240*, 4675–4681.
[41] T. Toraya, *Chem. Rev.* **2003**, *103*, 2095–2128.
[42] N. Shibata, H. Tamagaki, N. Hieda, K. Akita, H. Komori, Y. Shomura, S. Terawaki, K. Mori, N. Yasuoka, Y. Higuchi, T. Toraya, *J. Biol. Chem.* **2010**, *285*, 26484–26493.
[43] R. J. O'Brien, J. A. Fox, M. G. Kopczynski, B. M. Babior, *J. Biol. Chem.* **1985**, *260*, 16131–16136.
[44] D. A. Garsin, *Nat. Rev. Microbiol.* **2010**, *8*, 290–295.
[45] R. N. Costilow, L. Laycock, *J. Biol. Chem.* **1971**, *246*, 6655–6660.
[46] L. E. Khaw, G. A. Böhm, S. Metcalfe, J. Staunton, P. F. Leadlay, *J. Bacteriol.* **1998**, *180*, 809–814.
[47] J. L. Goodman, S. Wang, S. Alam, F. J. Ruzicka, P. A. Frey, J. E. Wedekind, *Biochemistry* **2004**, *43*, 13883–13891.
[48] W. L. Muth, R. N. Costilow, *J. Biol. Chem.* **1974**, *249*, 7463–7467.
[49] Gatto Gregory J., M. T. Boyne, N. L. Kelleher, C. T. Walsh, *J. Am. Chem. Soc.* **2006**, *128*, 3838–3847.
[50] K. Min, H.-J. Yoon, A. Matsuura, Y. H. Kim, H. H. Lee, *Mol. Cells* **2018**, *41*, 331–341.
[51] H. A. Cooke, C. V. Christianson, S. D. Bruner, *Curr. Opin. Chem. Biol.* **2009**, *13*, 460–468.
[52] R. N. Kumavath, C. V. Ramana, C. Sasikala, D. Barh, A. P. Kumar, V. Azevedo, *Curr. Protein Pept. Sci.* **2015**, *16*, 775–781.
[53] L. Poppe, J. Rétey, *Angew. Chem. Int. Ed.* **2005**, *44*, 3668–3688.
[54] H. Morrison, C. Bernasconi, G. Pandey, *Photochem. Photobiol.* **1984**, *40*, 549–550.
[55] J. C. Calabrese, D. B. Jordan, A. Boodhoo, S. Sariaslani, T. Vannelli, *Biochemistry* **2004**, *43*, 11403–11416.
[56] G. V. Louie, M. E. Bowman, M. C. Moffitt, T. J. Baiga, B. S. Moore, J. P. Noel, *Chem. Biol.* **2006**, *13*, 1327–1338.
[57] T. F. Schwede, J. Rétey, G. E. Schulz, *Biochemistry* **1999**, *38*, 5355–5361.
[58] Y. Zhao, F. G. Bordwell, *J. Org. Chem.* **1995**, *60*, 3932–3933.
[59] J. Rétey, *Biochim. Biophys. Acta BBA - Proteins Proteomics* **2003**, *1647*, 179–184.
[60] R. B. Wickner, *J. Biol. Chem.* **1969**, *244*, 6550–6552.
[61] L. Poppe, *Curr. Opin. Chem. Biol.* **2001**, *5*, 512–524.
[62] B. Schuster, J. Rétey, *Proc. Natl. Acad. Sci. U. S. A.* **1995**, *92*, 8433–8437.
[63] K. R. Hanson, E. A. Havir, *Arch. Biochem. Biophys.* **1970**, *141*, 1–17.
[64] L. Poppe, J. Rétey, *Angew. Chem. Int. Ed Engl.* **2005**, *44*, 3668–3688.

[65] I. L. Givot, T. A. Smith, R. H. Abeles, *J. Biol. Chem.* **1969**, *244*, 6341–6353.
[66] C. V. Christianson, T. J. Montavon, G. M. Festin, H. A. Cooke, B. Shen, S. D. Bruner, *J. Am. Chem. Soc.* **2007**, *129*, 15744–15745.
[67] L. Wang, A. Gamez, H. Archer, E. E. Abola, C. N. Sarkissian, P. Fitzpatrick, D. Wendt, Y. Zhang, M. Vellard, J. Bliesath, S. M. Bell, J. F. Lemontt, C. R. Scriver, R. C. Stevens, *J. Mol. Biol.* **2008**, *380*, 623–635.
[68] A.-L. Seff, S. Pilbák, I. Silaghi-Dumitrescu, L. Poppe, *J. Mol. Model.* **2011**, *17*, 1551–1563.
[69] L. Feng, U. Wanninayake, S. Strom, J. Geiger, K. D. Walker, *Biochemistry* **2011**, *50*, 2919–2930.
[70] S. Pilbák, Ö. Farkas, L. Poppe, *Chem. – Eur. J.* **2012**, *18*, 7793–7802.
[71] T. Tosa, T. Sato, T. Mori, I. Chibata, *Appl. Microbiol.* **1974**, *27*, 886–889.
[72] A. Liese, K. Seelbach, A. Buchholz, J. Haberland, in *Ind. Biotransformations*, John Wiley & Sons, Ltd, **2006**, pp. 447–503.
[73] B. Weiner, G. J. Poelarends, D. B. Janssen, B. L. Feringa, *Chem. – Eur. J.* **2008**, *14*, 10094–10100.
[74] A. Vogel, R. Schmiedel, U. Hofmann, K. Gruber, K. Zangger, *ChemCatChem* **2014**, *6*, 965–968.
[75] C. Han, P. Yao, J. Yuan, Y. Duan, J. Feng, M. Wang, Q. Wu, D. Zhu, *J. Mol. Catal. B Enzym.* **2015**, *115*, 113–118.
[76] M. de Villiers, V. Puthan Veetil, H. Raj, J. de Villiers, G. J. Poelarends, *ACS Chem. Biol.* **2012**, *7*, 1618–1628.
[77] M. Akhtar, B. Nigel P., C. Mark A., D. Gani, *Tetrahedron* **1987**, *43*, 5899–5908.
[78] H. Raj, W. Szymański, J. de Villiers, H. J. Rozeboom, V. P. Veetil, C. R. Reis, M. de Villiers, F. J. Dekker, S. de Wildeman, W. J. Quax, A.-M. W. H. Thunnissen, B. L. Feringa, D. B. Janssen, G. J. Poelarends, *Nat. Chem.* **2012**, *4*, 478–484.
[79] P. S. Spencer, D. N. Roy, A. Ludolph, J. Hugon, M. P. Dwivedi, H. H. Schaumburg, *Lancet Lond. Engl.* **1986**, *2*, 1066–1067.
[80] H. Ying, S. Tao, J. Wang, W. Ma, K. Chen, X. Wang, P. Ouyang, *Microb. Cell Factories* **2017**, *16*, 52.
[81] G. E. Tsotsou, F. Barbirato, *Biochimie* **2007**, *89*, 591–604.
[82] T. Shibatani, N. Nishimura, K. Nabe, T. Kakimoto, I. Chibata, *Appl. Microbiol.* **1974**, *27*, 688–694.
[83] Z. Zhang, *Tetrahedron Lett.* **2008**, *49*, 6468–6470.
[84] J. H. Bartha-Vári, M. I. Toşa, F.-D. Irimie, D. Weiser, Z. Boros, B. G. Vértessy, C. Paizs, L. Poppe, *ChemCatChem* **2015**, *7*, 1122–1128.
[85] I. Rowles, B. Groenendaal, B. Binay, K. J. Malone, S. C. Willies, N. J. Turner, *Tetrahedron* **2016**, *72*, 7343–7347.
[86] B. de Lange, D. J. Hyett, P. J. D. Maas, D. Mink, F. B. J. van Assema, N. Sereinig, A. H. M. de Vries, J. G. de Vries, *ChemCatChem* **2011**, *3*, 289–292.
[87] M. Li, K. R. Kildegaard, Y. Chen, A. Rodriguez, I. Borodina, J. Nielsen, *Metab. Eng.* **2015**, *32*, 1–11.
[88] H. L. Levy, C. N. Sarkissian, C. R. Scriver, *Mol. Genet. Metab.* **2018**, *124*, 223–229.
[89] R. A. Bender, *Microbiol. Mol. Biol. Rev. MMBR* **2012**, *76*, 565–584.
[90] R. G. Taylor, M. A. Lambert, E. Sexsmith, S. J. Sadler, P. N. Ray, D. J. Mahuran, R. R. McInnes, *J. Biol. Chem.* **1990**, *265*, 18192–18199.
[91] D. Kessler, J. Rétey, G. E. Schulz, *J. Mol. Biol.* **2004**, *342*, 183–194.
[92] J. Klepp, A. Fallert-Müller, K. Grimm, W. E. Hull, J. Rétey, *Eur. J. Biochem.* **1990**, *192*, 669–676.

[93] G. R. Smith, Y. S. Halpern, B. Magasanik, *J. Biol. Chem.* **1971**, *246*, 3320–3329.
[94] D. C. Hagen, S. L. Gerson, B. Magasanik, *J. Bacteriol.* **1975**, *121*, 583–593.
[95] B. J. Leidigh, M. L. Wheelis, *Mol. Gen. Genet. MGG* **1973**, *120*, 201–210.
[96] B. Magasanik, *J. Biol. Chem.* **1955**, *213*, 557–569.
[97] F. C. Neidhardt, B. Magasanik, *J. Bacteriol.* **1957**, *73*, 253–259.
[98] C. Tanret, *Compt.Rend.* **1909**, *149*, 222–224.
[99] B. M. Cumming, K. C. Chinta, V. P. Reddy, A. J. C. Steyn, *Antioxid. Redox Signal.* **2017**, *28*, 431–444.
[100] P. E. Hartman, *Methods Enzymol.* **1990**, *186*, 310–318.
[101] P. C. Jocelyn, *Biochemistry of the SH Group: The Occurrence, Chemical Properties, Metabolism and Biological Function of Thiols and Disulphides*, Academic Press, **1972**.
[102] D. Akanmu, R. Cecchini, O. I. Aruoma, B. Halliwell, *Arch. Biochem. Biophys.* **1991**, *288*, 10–16.
[103] F. Franzoni, R. Colognato, F. Galetta, I. Laurenza, M. Barsotti, R. Di Stefano, R. Bocchetti, F. Regoli, A. Carpi, A. Balbarini, L. Migliore, G. Santoro, *Biomed. Pharmacother. Biomedecine Pharmacother.* **2006**, *60*, 453–457.
[104] I. K. Cheah, B. Halliwell, *Biochim. Biophys. Acta* **2012**, *1822*, 784–793.
[105] R. Burn, L. Misson, M. Meury, F. P. Seebeck, *Angew. Chem. Int. Ed.* **2017**, *56*, 12508–12511.
[106] Q. Zhao, M. Wang, D. Xu, Q. Zhang, W. Liu, *Nature* **2015**, *518*, 115–119.
[107] J. B. Wolff, *J. Biol. Chem.* **1962**, *237*, 874–881.
[108] B. Halliwell, I. K. Cheah, C. L. Drum, *Biochem. Biophys. Res. Commun.* **2016**, *470*, 245–250.
[109] D. S. Genghof, *J. Bacteriol.* **1970**, *103*, 475–478.
[110] D. S. Genghof, E. Inamine, V. Kovalenko, D. B. Melville, *J. Biol. Chem.* **1956**, *223*, 9–17.
[111] A. Ramirez-Martinez, N. Wesolek, J.-C. Yadan, M. Moutet, A.-C. Roudot, *Hum. Ecol. Risk Assess. Int. J.* **2016**, *22*, 667–677.
[112] D. Gründemann, S. Harlfinger, S. Golz, A. Geerts, A. Lazar, R. Berkels, N. Jung, A. Rubbert, E. Schömig, *Proc. Natl. Acad. Sci. U. S. A.* **2005**, *102*, 5256–5261.
[113] Y. Kato, Y. Kubo, D. Iwata, S. Kato, T. Sudo, T. Sugiura, T. Kagaya, T. Wakayama, A. Hirayama, M. Sugimoto, K. Sugihara, S. Kaneko, T. Soga, M. Asano, M. Tomita, T. Matsui, M. Wada, A. Tsuji, *Pharm. Res.* **2010**, *27*, 832–840.
[114] S. Tokuhiro, R. Yamada, X. Chang, A. Suzuki, Y. Kochi, T. Sawada, M. Suzuki, M. Nagasaki, M. Ohtsuki, M. Ono, H. Furukawa, M. Nagashima, S. Yoshino, A. Mabuchi, A. Sekine, S. Saito, A. Takahashi, T. Tsunoda, Y. Nakamura, K. Yamamoto, *Nat. Genet.* **2003**, *35*, 341–348.
[115] V. D. Peltekova, R. F. Wintle, L. A. Rubin, C. I. Amos, Q. Huang, X. Gu, B. Newman, M. Van Oene, D. Cescon, G. Greenberg, A. M. Griffiths, P. H. St George-Hyslop, K. A. Siminovitch, *Nat. Genet.* **2004**, *36*, 471–475.
[116] B. Halliwell, I. K. Cheah, R. M. Y. Tang, *FEBS Lett.* **2018**, *592*, 3357–3366.
[117] B. N. Ames, *Proc. Natl. Acad. Sci. U. S. A.* **2018**, *115*, 10836–10844.
[118] Y. Ishikawa, S. E. Israel, D. B. Melville, *J. Biol. Chem.* **1974**, *249*, 4420–4427.
[119] Y. Ishikawa, D. B. Melville, *J. Biol. Chem.* **1970**, *245*, 5967–5973.
[120] D. B. Melville, S. Eich, M. L. Ludwig, *J. Biol. Chem.* **1957**, *224*, 871–877.
[121] F. P. Seebeck, *J. Am. Chem. Soc.* **2010**, *132*, 6632–6633.
[122] G. W. Jones, S. Doyle, D. A. Fitzpatrick, *Gene* **2014**, *549*, 161–170.
[123] A. M. Gamage, C. Liao, I. K. Cheah, Y. Chen, D. R. X. Lim, J. W. K. Ku, R. S. L. Chee, M. Gengenbacher, F. P. Seebeck, B. Halliwell, Y.-H. Gan, *FASEB J.* **2018**, *32*, 6395–6409.

[124] A. R. Stampfli, K. V. Goncharenko, M. Meury, B. N. Dubey, T. Schirmer, F. P. Seebeck, *J. Am. Chem. Soc.* **2019**, *141*, 5275–5285.
[125] W. Hu, H. Song, A. Sae Her, D. W. Bak, N. Naowarojna, S. J. Elliott, L. Qin, X. Chen, P. Liu, *Org. Lett.* **2014**, *16*, 5382–5385.
[126] T. Pluskal, M. Ueno, M. Yanagida, *PLOS ONE* **2014**, *9*, e97774.
[127] F. Leisinger, R. Burn, M. Meury, P. Lukat, F. P. Seebeck, *J. Am. Chem. Soc.* **2019**, *141*, 6906–6914.
[128] A. R. Stampfli, W. Blankenfeldt, F. P. Seebeck, *Curr. Opin. Struct. Biol.* **2020**, *65*, 1–8.
[129] C. Liao, F. P. Seebeck, *Chembiochem Eur. J. Chem. Biol.* **2017**, *18*, 2115–2118.
[130] D. Yanasugondha, M. D. Appleman, *J. Bacteriol.* **1957**, *74*, 381–385.
[131] B. Kelly, M. D. Appleman, *J. Bacteriol.* **1961**, *81*, 715–720.
[132] H. Muramatsu, H. Matsuo, N. Okada, M. Ueda, H. Yamamoto, S. Kato, S. Nagata, *Appl. Microbiol. Biotechnol.* **2013**, *97*, 5389–5400.
[133] A. Maurer, F. Leisinger, D. Lim, F. P. Seebeck, *Chem. Eur. J.* **2019**, *25*, 10298-10303.
[134] H. Muramatsu, H. Miyaoku, S. Kurita, H. Matsuo, T. Kashiwagi, C.-S. Kim, M. Hayashi, H. Yamamoto, S.-I. Kato, S. Nagata, *J. Biochem. (Tokyo)* **2020**, *167*, 333–341.
[135] D. Limmathurotsakul, N. Golding, D. A. Dance, J. P. Messina, D. M. Pigott, C. L. Moyes, D. B. Rolim, E. Bertherat, N. P. Day, S. J. Peacock, S. I. Hay, *Nat. Microbiol.* **2016**, *1*, 15008.
[136] D. Smets, M. S. Loos, S. Karamanou, A. Economou, *Protein J.* **2019**, *38*, 262-273
[137] M. N. Sela, *Crit. Rev. Oral Biol. Med.* **2001**, *12*, 399–413.
[138] F. P. Seebeck, D. Hilvert, *J. Am. Chem. Soc.* **2003**, *125*, 10158–10159.
[139] B. Stanovnik, M. Tišler, *Anal. Biochem.* **1964**, *9*, 68–74.
[140] H. Ritter, G. E. Schulz, *Plant Cell* **2004**, *16*, 3426–3436.
[141] H. A. Cooke, S. D. Bruner, *Biopolymers* **2010**, *93*, 802–810.
[142] D. Röther, L. Poppe, S. Viergutz, B. Langer, J. Rétey, *Eur. J. Biochem.* **2001**, *268*, 6011–6019.
[143] F. M. Menger, *Pure Appl. Chem.* **2005**, *77*, 1873–1886.
[144] R. Das, E. A. Vázquez-Montelongo, G. A. Cisneros, J. Wu, **2019**, *141*, 13739–13743.
[145] L. Servillo, D. Castaldo, R. Casale, N. D'Onofrio, A. Giovane, D. Cautela, M. L. Balestrieri, *Free Radic. Biol. Med.* **2015**, *79*, 228–236.
[146] L. Servillo, N. D'Onofrio, R. Casale, D. Cautela, A. Giovane, D. Castaldo, M. L. Balestrieri, *Free Radic. Biol. Med.* **2017**, *108*, 8–18.
[147] P. F. Cook, W. W. Cleland, *Enzyme Kinetics and Mechanism*, Garland Science, **2007**.
[148] S. Pilbák, A. Tomin, J. Rétey, L. Poppe, *FEBS J.* **2006**, *273*, 1004–1019.
[149] M. C. Moffitt, G. V. Louie, M. E. Bowman, J. Pence, J. P. Noel, B. S. Moore, *Biochemistry* **2007**, *46*, 1004–1012.
[150] L. Wang, A. Gamez, C. N. Sarkissian, M. Straub, M. G. Patch, G. W. Han, S. Striepeke, P. Fitzpatrick, C. R. Scriver, R. C. Stevens, *Mol. Genet. Metab.* **2005**, *86*, 134–140.
[151] M. M. Heberling, M. F. Masman, S. Bartsch, G. G. Wybenga, B. W. Dijkstra, S. J. Marrink, D. B. Janssen, *ACS Chem. Biol.* **2015**, *10*, 989–997.
[152] D. L. Nelson, M. M. Cox, *Lehninger Principles of Biochemistry*, Macmillan Education, **2005**.
[153] S. Rath, B. Heidrich, D. H. Pieper, M. Vital, *Microbiome* **2017**, *5*, 54.
[154] W. H. W. Tang, D. Y. Li, S. L. Hazen, *Nat. Rev. Cardiol.* **2019**, *16*, 137–154.
[155] S. H. Zeisel, M. Warrier, *Annu. Rev. Nutr.* **2017**, *37*, 157–181.
[156] N. Rascio, N. La Rocca, in *Ref. Module Earth Syst. Environ. Sci.*, Elsevier, **2013**.
[157] M. R. Wilkins, E. Gasteiger, A. Bairoch, J. C. Sanchez, K. L. Williams, R. D. Appel, D. F. Hochstrasser, *Methods Mol. Biol. Clifton NJ* **1999**, *112*, 531–552.

[158] P. L. Khonde, A. Jardine, *Org. Biomol. Chem.* **2015**, *13*, 1415–1419.
[159] J. A. Gerlt, J. T. Bouvier, D. B. Davidson, H. J. Imker, B. Sadkhin, D. R. Slater, K. L. Whalen, *Biochim. Biophys. Acta BBA - Proteins Proteomics* **2015**, *1854*, 1019–1037.
[160] C. B. Klee, *J Biol Chem* **1972**, 1398–1406.
[161] T. Furuta, H. Takahashi, H. Shibasaki, *J Biol Chem* **1992**, *267*, 6.
[162] M. Baedeker, G. E. Schulz, *Struct. Lond. Engl. 1993* **2002**, *10*, 61–67.
[163] A. Peterkofsky, *J. Biol. Chem.* **1962**, *237*, 787–795.
[164] P. A. Sánchez-Murcia, J. A. Bueren-Calabuig, M. Camacho-Artacho, Á. Cortés-Cabrera, F. Gago, *Biochemistry* **2016**, *55*, 5854–5864.
[165] M. Baedeker, G. E. Schulz, *Eur. J. Biochem.* **2002**, *269*, 1790–1797.
[166] D. A. Morrison, *Int. J. Parasitol.* **1996**, *26*, 589–617.
[167] X.-X. Zhang, P. B. Rainey, *Genetics* **2007**, *176*, 2165–2176.
[168] J.-H. Jeong, H. J. Cha, S.-C. Ha, C. Rojviriya, Y.-G. Kim, *Biochem. Biophys. Res. Commun.* **2014**, *452*, 1098–1103.
[169] A. Vit, L. Misson, W. Blankenfeldt, F. P. Seebeck, *ChemBioChem* **2015**, *16*, 119–125.
[170] L. Misson, R. Burn, A. Vit, J. Hildesheim, M. A. Beliaeva, W. Blankenfeldt, F. P. Seebeck, *ACS Chem. Biol.* **2018**, *13*, 1333–1342.
[171] K. V. Goncharenko, A. Vit, W. Blankenfeldt, F. P. Seebeck, *Angew. Chem. Int. Ed Engl.* **2015**, *54*, 2821–2824.
[172] M. Richard-Greenblatt, H. Bach, J. Adamson, S. Peña-Diaz, W. Li, A. J. C. Steyn, Y. Av-Gay, *J. Biol. Chem.* **2015**, *290*, 23064–23076.
[173] H. Nishi, A. Shaytan, A. R. Panchenko, *Front. Genet.* **2014**, *5*, 270.
[174] L. N. Johnson, R. J. Lewis, *Chem. Rev.* **2001**, *101*, 2209–2242.
[175] M. Richard-Greenblatt, Y. Av-Gay, *Microbiol. Spectr.* **2017**, *5*, 2.
[176] Y. Av-Gay, M. Everett, *Trends Microbiol.* **2000**, *8*, 238–244.
[177] S. Prisic, S. Dankwa, D. Schwartz, M. F. Chou, J. W. Locasale, C.-M. Kang, G. Bemis, G. M. Church, H. Steen, R. N. Husson, *Proc. Natl. Acad. Sci. U. S. A.* **2010**, *107*, 7521–7526.
[178] K. F. Geoghegan, H. B. Dixon, P. J. Rosner, L. R. Hoth, A. J. Lanzetti, K. A. Borzilleri, E. S. Marr, L. H. Pezzullo, L. B. Martin, P. K. LeMotte, A. S. McColl, A. V. Kamath, J. G. Stroh, *Anal. Biochem.* **1999**, *267*, 169–184.
[179] S. K. Hatzios, C. E. Baer, T. R. Rustad, M. S. Siegrist, J. M. Pang, C. Ortega, T. Alber, C. Grundner, D. R. Sherman, C. R. Bertozzi, *Proc. Natl. Acad. Sci. U. S. A.* **2013**, *110*, E5069-5077.
[180] X. M. Wang, K. Soetaert, P. Peirs, M. Kalai, V. Fontaine, J. P. Dehaye, P. Lefèvre, *PLOS ONE* **2015**, *10*, e0123327.
[181] G. Baronian, K. Ginda, L. Berry, M. Cohen-Gonsaud, J. Zakrzewska-Czerwińska, D. Jakimowicz, V. Molle, *PLOS ONE* **2015**, *10*, e0119907.
[182] R. M. Corrales, J. Leiba, M. Cohen-Gonsaud, V. Molle, L. Kremer, *Biochem. Biophys. Res. Commun.* **2013**, *430*, 858–864.

Acknowledgement

I would like to express my gratitude to Prof. Florian Seebeck for giving me the opportunity to work in his research group on this interesting project. Furthermore, I would like to thank him for providing guidance and constant feedback throughout my PhD. His scientific enthusiasm and creativity were always inspiring and motivating.

I would like to thank Prof. Michael Müller for accepting the co-examination and for reading my thesis.

Thank you to all current and former group-members of the Seebeck-Group: Laetitia, Matthias, Roxana, Kristina, Pascal, Marcel, Sebastian, Reto, Liao, Davey, Anja, Dima, Florian, Mariia, Jiaming, Xiaojin, Egor and Camille. I really enjoyed the cheerful and helpful atmosphere in our lab, and all the coffee breaks and beer o'clocks we have spent together – you have been great colleagues. Special thanks to Flo who crystallized my enzymes and to Anja and Davey for proof-reading my thesis.

I would also like to thank Dr. Heinz Nadig for his introduction to mass spectroscopy and Dr. Michael Pfeffer for the productive operations and time we spend together in front of the machine.

Furthermore, I would like to thank the Werkstatt-Team and the Secretary for keeping the Departement running.

I am grateful to my parents, for believing in my abilities, and their huge interest they bring towards my work and every step in my life.

Special thanks to Paula, for the pregnancy free of any complaints, which allowed me to finish up my experiments; and now for being such a great little girl that brings so much joy and happiness to our daily routine.

My deepest gratitude goes to Daniel, for all the unconditional support, patience and encouragement that you give to me every day. I am looking forward to our common future!

Curriculum vitae

Personal Data

Alice Maurer

Konviktstraße 10
79098 Freiburg
alice.maurer@posteo.de

Date of birth 21.09.89 in Aachen, Germany

Education

2016 – 2020	PhD student in Biochemistry in the group of Prof. Dr. F.P.Seebeck, University of Basel, Switzerland
2013 – 2015	Albert- Ludwigs- University Freiburg, Germany Master of Science: Pharmaceutical Science
2009 – 2013	Albert- Ludwigs- University Freiburg, Germany Bachelor of Science: Pharmaceutical Science

Professional Experience

11.2014 – 02.2015	Internship in Peptide Biology Laboratory with Dr. W. Fischer Salk Institute La Jolla, California, USA
06.2013 – 01.2014	Student assistant in the group of Jun.-Prof.Dr. J.N. Andexer Albert- Ludwigs- University Freiburg, Germany
08.2011 – 10.2011	Internship QA-Laboratory Novartis, Wehr, Germany

Publications

Maurer A.; Seebeck, F. P.''Reexamination of the ergothioneine biosynthetic methyltransferase EgtD from Mycobacterium tuberculosis as a protein kinase substrate'' ChemBioChem. 2020, 21, 2908 – 2911.

Maurer, A; Leisinger, F.; Lim, D.; Seebeck, F. P. "Structure and mechanism of ergothionase from Treponema denticola." Chem. Eur. J., 2019, 25, 10298 - 10303.

Mordhorst S.; Maurer A.; Popadic D.; Brech J.; Andexer J.N. "A Flexible Polyphosphate-Driven Regeneration System for Coenzyme A Dependent Catalysis" ChemCatChem 2017, 9, 4164 - 4168.